Characterization of extra-column peak broadening in capillary high-performance liquid chromatography

Dissertation

zur Erlangung des akademischen Grades eines
Doktors der Naturwissenschaften
– Dr. rer. nat. –

vorgelegt von
Tobias Werres
geboren in
Haan

Fakultät für Chemie
der
Universität Duisburg-Essen

2022

Die vorliegende Arbeit wurde im Zeitraum von April 2018 bis April 2022 im Arbeitskreis von Prof. Dr. Torsten C. Schmidt in der Fakultät für Chemie im Bereich Instrumentelle Analytische Chemie der Universität Duisburg-Essen durchgeführt.

Tag der Disputation: 20.03.2023

Gutachter: Prof. Dr. Torsten C. Schmidt

Prof. Dr. Oliver J. Schmitz

Vorsitzender: Prof. Dr. Eckhard Spohr

DOI: 10.17185/duepublico/78273
URN: urn:nbn:de:hbz:465-20230503-122419-9

Danksagung

Einer der Hauptgründe, warum die Menschheit trotz der kurzen Existenz bereits die dominierende Spezies auf dem Planeten Erde werden konnte, lässt sich darauf zurückführen, dass wir von Natur aus sehr soziale Lebewesen sind. Dies ermöglichte die effektive Zusammenarbeit einzelner Individuen, um gemeinsam Größeres zu schaffen. Schlussfolgernd lässt sich dies auch auf kleinere, wenn auch umfangreiche Projekte, wie diese Promotion anwenden, welche in einer Einzelleistung nicht zu bewältigen gewesen wäre. Deshalb möchte ich an dieser Stelle einigen Personen danken.

In erster Instanz danke ich meinem Doktorvater Prof. Dr. Torsten C. Schmidt und Forschungsbetreuer Dr. Thorsten Teutenberg für ihre fachkundige und professionelle Begleitung sowie für ihre Ermutigungen, das entgegengebrachte Vertrauen und Engagement während unserer Zusammenarbeit, es war stets ertragreich und eine Freude.

Bei Herrn Professor Oliver J. Schmitz bedanke ich mich für die bereitwillige Übernahme des Zweitgutachtens.

Besonderer Dank gilt Kjell Kochale und Lars Reinders, die mir gezeigt haben, dass man das Tal der Tränen nicht allein durchschreiten muss, dies hat maßgeblich dazu beigetragen die Ziellinie nie aus dem Auge zu verlieren.

Ich bedanke mich bei allen Koautoren für die Zusammenarbeit. Christian Thoben danke ich für seine unkomplizierte Art, die dazu beigetragen hat, die langen und frustreichen, aber durchaus ertragreichen Laborwochen in Hannover zu einem freudigen Ereignis zu machen. Martin Klaßen in der Rolle des Bindegliedes der Generation danke ich für die zahlreichen Gespräche, die häufig einen anderen Blickwinkel auf Probleme ermöglichten und dazu beitrugen als Wissenschaftler zu wachsen.

Mathias und Maria danke ich für ihre herzliche und offene Art. Ihr habt euch innerhalb kürzester Zeit zu einem wichtigen Anker in meinem Leben entwickelt, der mir ebenfalls geholfen hat die Promotion zu einem erfolgreichen Abschluss zu führen.

Meiner Lebenspartnerin Anna danke für die bedingungslose Unterstützung. Du hast mir gezeigt, wie großartig es ist eine Person im Leben zu haben, bei der man vollständig authentisch sein kann.

Zu Guter Letzt danke ich jedem Steuerzahler dessen Gelder dazu beigetragen haben die Forschungsvorhaben zu finanzieren, in deren Rahmen diese Promotionsschrift entstanden ist.

Summary

Ensuring reasonable energy prices, establishing reliable supply chains, ensuring the availability of resources and, last but not least, taking environmental protection into account are global challenges of the future. Corresponding challenges also play an increasingly central role in everyday analytical laboratory work. The search for countermeasures to these challenges is also becoming increasingly prevalent in the analytical laboratory. Miniaturization as one of the cornerstones of Green Analytical Chemistry (GAC) can help save resources in the form of solvents, energy and laboratory space, especially in the field of capillary liquid chromatography (cLC), without reducing the integrity of analytical data and even increasing sample throughput in the process. Despite advances in cLC development and research in recent years, and the disruptive nature of the technology, market penetration has still not been achieved. This is partly because there is a persistent assumption that the systems are unsuitable for routine operation due to a lack of robustness. In addition, although the number of commercial systems is increasing, current research is often not consistently implemented for example by sticking to the modular concept. This creates unnecessary capillary paths, increases the extra-column volume, which results in peak band broadening and thus poorer chromatographic efficiency. Therefore, the aim of this work is to investigate the influence of different factors on the extra-column band broadening in cLC, to lower barriers for the implementation of cLC and to develop a new system.

The first part of the PhD thesis was mainly devoted to quantifying the influence of different extra-column volumes on peak band broadening and served to answer open questions in the current literature. To start, the influence of injection volume and pre-column volume was investigated for both isocratic and gradient elution as a function of retention factor. Subsequently, the focus was shifted to the influence of the post-column volume. For this purpose, different commercially available concentration-dependent and mass flow-dependent detector systems were investigated. In addition, the ratio of the column inner diameter to the system volume on the band broadening during isocratic and gradient elution was compared. The knowledge gained from the previous research was used in the second part of the thesis to advance the development of new separation phases based on bead cellulose and a portable measurement system for on-site monitoring of contaminants in aqueous matrices based on on-line enrichment and cLC coupled with ion mobility spectrometry.

Zusammenfassung

Die Sicherstellung akzeptabler Energiepreise, die Etablierung zuverlässiger Lieferketten, die Verfügbarkeit von Ressourcen und nicht zuletzt die Berücksichtigung des Umweltschutzes sind globale Herausforderungen der Zukunft. Entsprechende Herausforderungen spielen auch im analytischen Laboralltag eine immer zentralere Rolle. Die Miniaturisierung ist einer der Eckpfeiler der Green Analytical Chemistry (GAC) und kann vor allem im Bereich der Kapillar-Flüssigkeitschromatographie (cLC) dazu beitragen, Ressourcen wie Lösemittel, Energie und Laborfläche zu sparen, dabei die Integrität der analytischen Daten beizubehalten und den Probendurchsatz zu steigern. Trotz der Fortschritte in Entwicklung und Forschung im Bereich cLC in den letzten Jahren und der disruptiven Natur der Technologie ist eine vollständige Marktdurchdringung immer noch nicht gelungen. Dies liegt zum einen daran, dass sich hartnäckig die Annahme hält, dass cLC aufgrund fehlender Robustheit für einen Routinebetrieb ungeeignet ist. Zum anderen nimmt die Anzahl kommerzieller Systeme zwar zu, häufig wird die aktuelle Forschung aber nicht konsequent umgesetzt und beispielsweise an modularen Konzepten festgehalten. Dadurch werden unnötige Kapillarwege geschaffen, das Außersäulenvolumen erhöht, welches wiederum zu Peak Bandenverbreiterung führt und damit geringerer chromatographischer Effizienz. Ziel der Arbeit ist es, die Einflussfaktoren auf die Außersäulenbandenverbreiterung in der cLC zu untersuchen sowie die Hürden zur Nutzung von cLC zu senken und ein neues System zu entwickeln.

Der erste Teil der Doktorarbeit widmete sich vor allem der Quantifizierung des Einflusses verschiedener Außer-Säulen Volumina auf die Peakbandenverbreiterung und diente der Beantwortung offener Fragestellungen in der aktuellen Literatur. Zu Beginn wurde der Einfluss des Injektionsvolumens und des Vorsäulenvolumens sowohl für die isokratische als auch die Gradientenelution in Abhängigkeit vom Retentionsfaktor untersucht. Im Anschluss lag der Fokus auf der Bestimmung des Einflusses des Nachsäulenvolumens. Hierzu wurden verschiedene kommerziell verfügbare konzentrationsabhängige und massenflussabhängige Detektorsysteme untersucht. Zusätzlich erfolgte der Vergleich des Verhältnisses des Säuleninnendurchmessers zum Systemvolumen auf die Bandenverbreiterung in Bezug zur isokratischen und Gradientenelution. Der Erkenntnisgewinn der vorangeschrittenen Forschung wurde im zweiten Teil der Doktorarbeit genutzt, um die Entwicklung neuer Trennphasen auf Basis von Perlcellulose voranzutreiben und ein portables Messystem für die vor Ort Überwachung von Kontaminanten in wässrigen Matrices auf Basis der Online-Anreicherung und cLC gekoppelt mit Ionenmobilitätsspektrometrie zu entwickeln.

Content

Chapter 1 General Introduction

Parts of this chapter were adapted from: T. Werres, J. Leonhardt, M. Jäger, T. Teutenberg, Critical Comparison of Liquid Chromatography Coupled to Mass Spectrometry and Three Different Ion Mobility Spectrometry Systems on Their Separation Capability for Small Isomeric Compounds, Chromatographia. 82 (2019) 251–260. https://doi.org/10.1007/s10337-018-3640-z.

1.1 History of Chromatography from Classical Antiquity via Modernity to Future

Chromatographic techniques are among the most fascinating, important, and flexible tools of the analytical chemist, capable of separating and analyzing the most complex mixtures into their individual components. Especially liquid chromatographic (LC) techniques are to be emphasized here. LC methods are used in almost all areas of chemical laboratory work and include forensic analysis [1–3], environmental analysis [4, 5], quality control [6, 7] and many more. The origin of LC is often dated back to ancient history. For example, in Exodus 15:22-25 Moses [8] is said to have used ion exchange chromatography to make undrinkable water drinkable [9]. Some readers believe that the first descriptions of chromatographic processes are also to be found in the writings called "Naturalis historia" by Pliny the Elder and Pliny the Younger, which were published from 77 AD onwards. But on closer examination the cases that were described can easily be identified as false and are based more on an interpretation clouded by today's experience or simple retellings of hearsay [10, 11].

The botanist Mikhail Semyonovich Zwet is considered the father of chromatography as it is known today [12]. In his publications from 1903 onwards, he laid the fundaments of chromatography. Thus, in the first publication of the series, he described the separation of chlorophyll a and chlorophyll b on the stationary phase inulin using the mobile phase ligroin. The work of Synge and Martin [13–15], published in the 1940s, significantly refined and expanded upon the basic principles [16], and their efforts were rewarded with the Nobel Prize in chemistry in 1952 [17]. The first commercially available instruments appeared in the form of gel permeation chromatography in 1964 by Dow chemical [18], the first high performance liquid chromatography system (HPLC) in 1967 by Waters [19], and an ion exchange chromatography system in 1975 by the Dionex group [20]. The triumph of this technology finally began with the establishment of reversed phase stationary phases [21], which made separations more robust and made it possible for the first time to separate very similar molecules [22, 23]. Since the 1980s, HPLC has been one of the standard analytical methods and it is hard to imagine an analytical laboratory without it.

The continuous development of hardware in pump technology as well as column technology since the establishment of HPLC as a standard method has enabled further milestones to be set.

Two trends have been observed around particle-based stationary phases. On the one hand, where at the beginning analytical separation columns were packed with particle diameters around 100 µm [13], the first commercial columns were packed with particles around 30 µm [24, 25]. Nowadays, sub 2 µm particles are becoming increasingly popular [26, 27]. In first publications, sub 1 µm particles are already being used [28]. On the other hand, with the reduction of the system volumes the inner diameter (ID) of the separation column has been continuously reduced, so that even 1.0 mm ID columns are used on optimized conventional HPLC [29, 30]. In addition, the selectivity of columns could be further increased by smaller particle size distributions [31, 32], manifold stationary phase modifications like hydrophilic interaction liquid chromatography (HILIC) [33] or mixed mode phases [34] and the growing understanding of the physical laws of column packing [35, 36]. Driven by these advances, pump technology also continued to develop. While in 1972 the M-6000, the first pump specifically designed for HPLC, was able to generate about 400 bars [37], around 2004 the capacity was increased to 1,000 bar and ultra-high performance liquid chromatography (UHPLC) was born [38]. Modern UHPLC systems can operate at up to 1,300 bar, some even reach specifications of 1,500 bar [39, 40]. A timeline of the discussed developments of HPLC can be found in Figure 1-1.

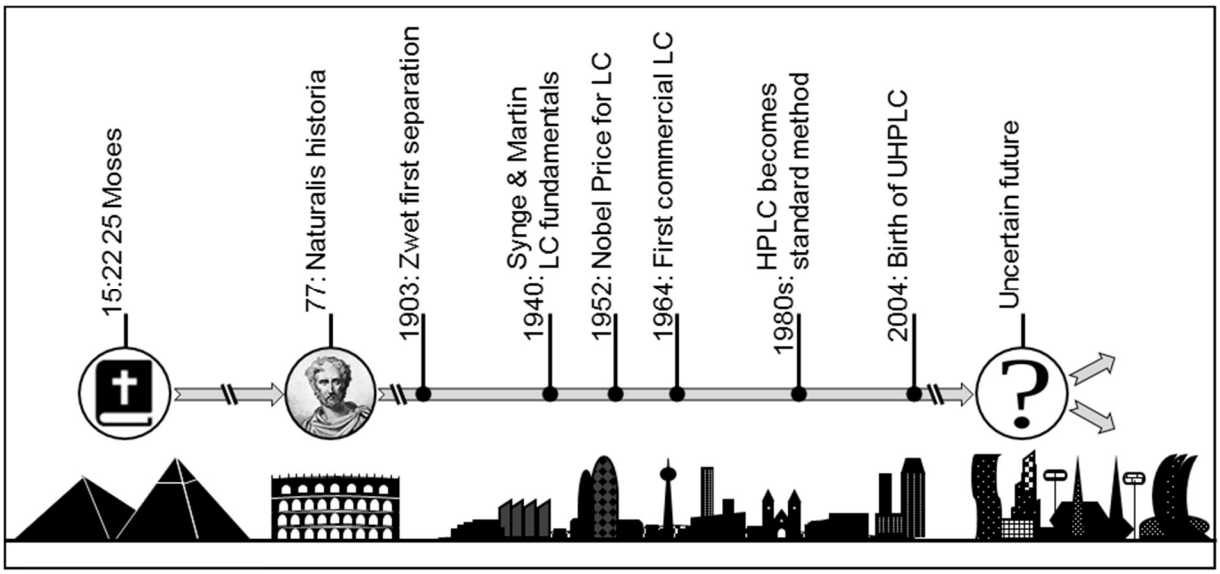

Figure 1-1: Timeline of the developments in chromatography described in chapter 1.1 beginning in antiquity and ending in current times.

Some research groups postulate an advancement of the maximum pressure for future HPLC systems up to 3,000 bars [41]. The arguments in favour of such systems are often faster analyses [42]. To ensure this, very high flow rates of up to 8 mL/min are used [43]. However, in addition to the high solvent consumption, other problems occur, such as frictional heating in the column

[44]. In addition, modern columns cannot withstand these pressures, and their operating lifetime is drastically reduced at pressures above 1,000 bar. It remains to be seen whether these predicted expectations for the future are realistic, especially since there is already technology available that offers a smarter way of performing rapid analysis without having to rely on ultra-high pressures or compromising resolution and peak capacity.

1.2 Miniaturized Liquid Chromatography: Infinite Potential but Unloved

Conventional LC is no more than a marginal note in this work and the spotlight belongs to its smaller siblings, the micro- (μLC) and nano-LC (nLC). These techniques make it possible to perform extremely fast, highly complex analyses. However, before miniaturized LC reached its current state, several hurdles had to be overcome. Which laws and dynamics apply to the diffusion-controlled mass transfer of solutes on a capillary scale? How must a column be dimensioned and how do you manufacture it? How must the periphery be designed to ensure sample application and detection while reducing band broadening?

In 1966 Pretorius and Smuts proposed the first time the use of columns with small ID for fast analysis [45]. In 1967, the pioneering work of Horvath et al. followed [46]. They investigated peak broadening in columns without stationary phase and an inner diameter of about 0.3 mm and for separation they used particle packed capillaries of 1.0 mm ID. Only nearly a decade later, further developments picked up again, mainly due to the contributions of Tsuda and Novotny, who modified an LC system and detector to minimize band broadening [47]. In 1978-79, publications appeared on band broadening of packed columns [48, 49], band broadening [47] and fabrication of open tubular (OT) columns [50], and applications of these achievements [51]. In 1983, Jorgenson and Guthrie proposed the theory that smaller ID will lead to more efficient columns [52]. The theory was supported by experimental data from Folestad et al. in 1978 [53]. Thereafter in 1988, efficiency studies on miniaturized columns followed [54], and in the following year, a paper on the fabrication of packed capillary columns [55]. With these two publications it could be proven that a reproducibility is given, and fabrication of miniaturized separation columns was possible. The technology was ready for commercial use. At the latest with the invention of electrospray ionization (ESI) [56] and the first concepts of miniaturized ESI interfaces [57], the interest in a continuous development of the technique increased.

The most important achievements that enable extremely fast analysis with miniaturized LC are the combination of very small tubing diameters and the reduction of the column and particle diameter [58]. This allows high peak capacities and peak capacity production rates to be

achieved even with short analytical separation columns and with fast gradients as shown in Figure 1-2 [59]. Thanks to modern µLC systems with small extra-column volumes, columns with an inner diameter of 1.0 mm form the link between conventional and miniaturized LC. Classically, 0.1-0.3 mm ID separation columns are used in µLC with flow rates between 1-100 µL/min. The term nLC is used for column ID < 0.1 mm and flow rates < 1 µL/min [60, 61]. The term capillary liquid chromatography (cLC) can be used as an umbrella term for µLC and nLC.

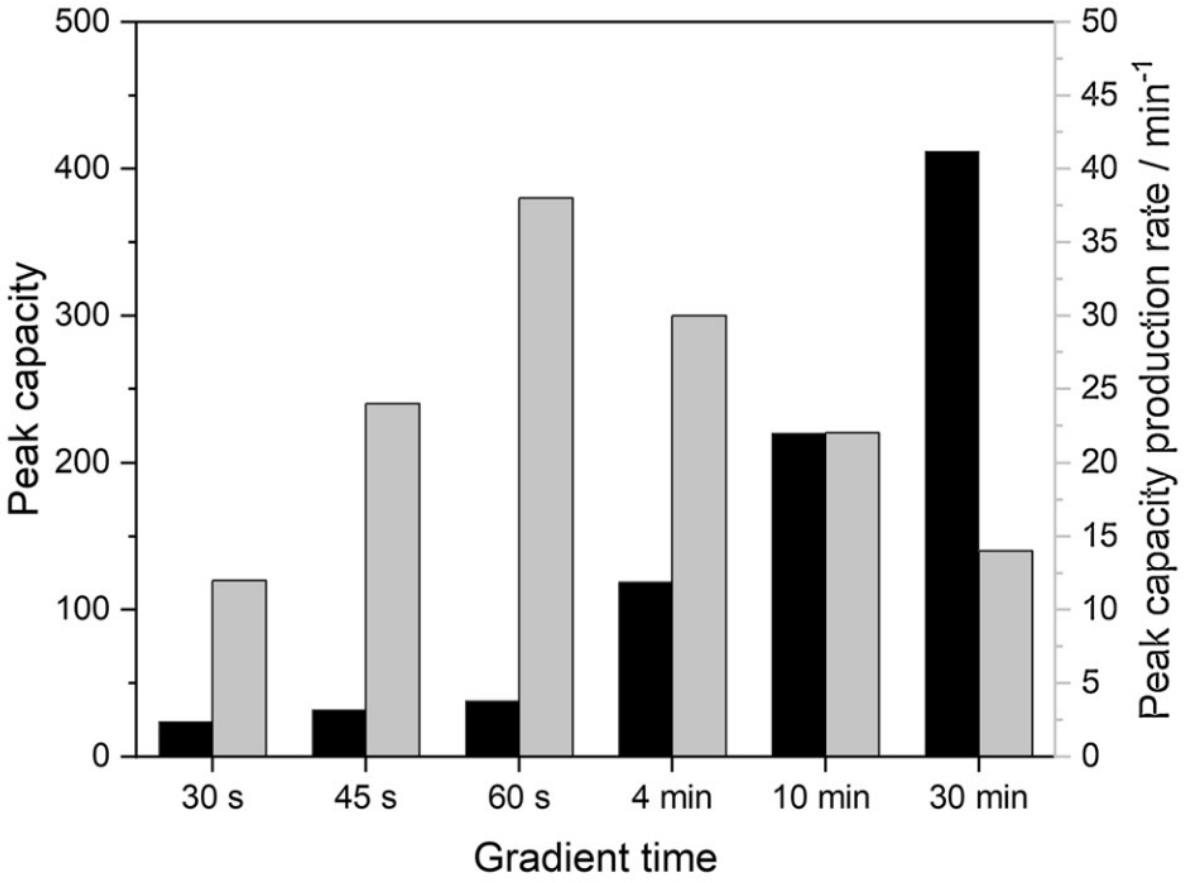

Figure 1-2: Comparison of peak capacity (black) and peak capacity production rate (light grey). Characteristically, the peak capacity increases with longer gradient times. The peak capacity production rate reaches a maximum at around 60 s. Data were generated on a microbore C18 column with dimensions of 50 x 0.3 mm. Redrafted from [59].

Optimized µLC systems nowadays have gradient dwell volumes in the low µL range [62–64]. As a result, gradients arrive on the column practically with the injection of the sample plug, cycle times are reduced and band broadening due to isocratic plateaus is avoided. By reducing the column ID, high linear flow rates at low absolute flow rates can be achieved with significantly lower solvent consumption [64]. This can be illustrated very well by an example calculation comparing a typical pharmaceutical method with the equivalent of a µLC and nLC

method. Equation 1-1 can be used to calculate a constant linear flow rate, and thus reproducible chromatography, between two columns with different ID and constant length.

$$\left(\frac{column\ ID_{new}}{column\ ID_{old}}\right)^2 * F_{old} = F_{new} \qquad \text{Equation 1-1}$$

Where F_{old} is the flow rate of the current method and F_{new} the flow rate for the transferred method. Even today, separation columns with an ID of 4.6 mm with a flow rate of 1 mL/min are still applied [65–67]. Assuming a full utilization of the system (24/7), this corresponds to a solvent consumption of 10,080 mL per week. To generate the same sample throughput at an identical linear flow rate with a 0.3 mm ID column, a flow rate of 4 µL/min would have to be used. The weekly consumption of solvent is thus 42.9 mL. With the solvent consumption of the conventional method, the µLC could be operated for 235 weeks or 4.5 years. If the comparison is made between LC and nLC, where columns with 0.075 mm ID are widely used the results are even more impressive [68–70]. At a flow rate of 0.2 µL/min, the weekly consumption would be 2.7 mL. To reach the solvent consumption of the conventional method, such a system would have to be operated continuously for 3,762 weeks or 72 years. The comparison between HPLC techniques and solvent consumption is illustrated in Figure 1-3. This low solvent consumption also has the advantage that the use of specially formulated and expensive solvents, e.g. deuterated solvents, is a viable option.

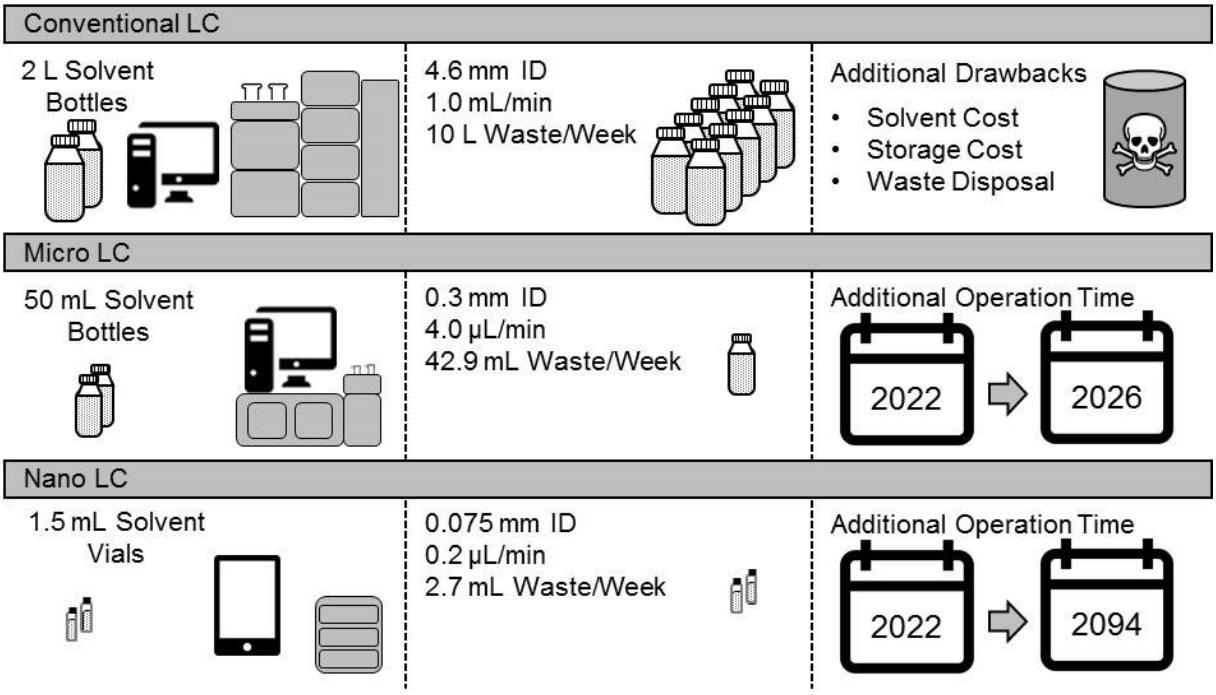

Figure 1-3: Visual comparison of solvent consumption and possible operating time of conventional HPLC, µLC and nLC.

The reduction of the column dimension brings two further advantages. The development of new separation phases can be very time-consuming and cost intensive. Depending on the synthesis protocol, only a few grams of the new phase remain for the packing process after preparation. By reducing the ID of the column from 2.1 to 0.5 mm, the amount of phase material required to pack a column can be reduced by a factor of 17. This is shown in Table 1-1 on the example of the preparation of cellulose bead columns used in Chapter 6. Miniaturization thus enables the comparison of several approaches and modifications when synthesising new stationary phases. In addition, the heat generated through friction at high linear flow velocities and high pressures can be better dissipated by the small dimensions of cLC columns [71, 72]. Thus, the so-called frictional heating plays only a minor role on the miniaturized scale [73]. In conventional LC, the resulting temperature gradients in the column bed have a negative effect on performance [74]. The mitigation of this phenomenon is the subject of many publications and the reason for new technical developments [75–77]. This fact also speaks against the further development of systems with higher pressure resistances up to 3,000 bars.

Table 1-1: Comparison of the required amount bead cellulose for packing a separation column with a porosity of 0.7 as a function of ID and length.

Length	Inner diameter	Volume column	Mass cellulose beads
cm	mm	mm^3	mg
5	2.10	173.2	157.6
5	0.75	22.1	20.1
5	0.50	9.8	8.9

Despite these advantages, cLC is only widely used in the fields of life sciences because these techniques are necessary due to the limited sample volume [78–80]. In other fields, the German proverb applies: "Was der Bauer nicht kennt, frisst er nicht!" which roughly translates to "What the farmer doesn't know he doesn't eat! “. Thus, similar to the time of Zwet in 1903, users are not open to innovations and prefer applying methods and techniques they are familiar with. However, a paradigm shift might be foreseen. A large part of the user’s reticence can be traced back to the propagated disadvantages of the technology.

1.3 Drawbacks of Miniaturized Systems

The technology of cLC does not only offer advantages. However, many disadvantages of cLC have been overcome and some of the frequently recited disadvantages can be written off as prejudices. Among the classically recited disadvantages are: the poor quality of the packed bed, a significantly reduced column loadability, reduced sensitivity, lack of robustness and the

generally difficult manual handling of the systems as well as the vulnerability to band broadening due to increased influence of extra-column volume.

1.3.1 Packing Quality of Miniaturized Columns

The frequently criticized quality of packed miniaturized columns is a prejudice. By the end of the 1980s it was proven that reproducible production of miniaturized columns is possible [54, 55]. Since then, the understanding of the packing process has steadily improved, extensive research on the fabrication of capillary columns has been done and methods for the evaluation of the columns are available [35]. Using confocal laser scanning microscopy, the quality of the column beds of columns with ID of 75-10 µm was evaluated in detail, showing that the porosity of the packing at the wall increases with increasing IDs, leading to lower performance in this zone [81, 82]. The influence of different frits for capillary columns was also investigated. For example, the studies by Franc et. al. showed that the choice of frit already has a significant influence on the separation efficiency [83]. This is an underestimated factor especially for self-produced columns. Nowadays, columns are commercially available from various manufacturers which are characterized by excellent performance and reproducibility.

The opposite is more likely to be the case. cLC opens the possibility of applying completely new column technologies that are not feasible on a conventional scale and could lead to massive efficiency increases in the future. In the early days of cLC, OT columns were used but due to lack of suitable LC systems were quickly replaced by packed columns [58]. With technological advances in detection techniques and sample injection, this technology is making a comeback in the form of Porous Layer Open Tubular (PLOT) and Wall Coated Open Tubular Columns (WCOT). A major advantage of OT columns is that they do not exhibit eddy diffusion, normally accounting for a large portion in column band broadening [84, 85]. Furthermore, OT columns theoretically achieve 10 times higher plate counts than packed columns when considering kinetic limits [85]. Currently, PLOTs are more suitable for liquid chromatographic applications because they have a larger usable ID range of 5-100 µm and a larger surface area for analyte retention due to the porous stationary phase layer [86]. PLOTs have a higher permeability than monolithic columns, allowing even higher flow rates and longer columns to increase efficiency [87]. For example, in the work of Forster et. al. separations have been successfully performed with PLOT columns that achieved a plate number of 170,000 [86]. In work by Hara, plate counts for an unretained substance of 1,000,000 were achieved for a 2.6 m x 0.05 mm column [88]. WCOTs have very low sample loadability due to their non-porous, thin liquid film, but in theory have the potential to be the most efficient column technology currently known [89]. But

it is only when extremely small ID of 2 µm are used that the true potential of the OT columns is revealed. Extremely fast analyses are possible, e.g., the separation of 6 amino acids in 700 ms and of a protein digestion in one minute [90]. High-efficiency columns with 10 million plates per meter were also described [91]. However, both OT variants are still far away from being ready for the market, mainly due to the low loadability, the high demands on the HPLC systems and lack of protocols for manufacturing.

The situation is different for micro pillar array columns (µPAC), which are already commercially available and are mainly used for proteomics, lipidomic, metabolomics and the analysis of biopharmaceuticals [71, 92, 93]. The design of µPAC is fundamentally different from the classical column and leaning to a chip approach. The technique is characterized by the fact that pillars on which a layer of the porous stationary phase is located are arranged perpendicular to the flow in perfectly spaced rows. The 200 cm µPAC™ has a dimension of 2 m x 0.315 mm x 0.018 mm, the pillars have a diameter of 5 µm and are spaced at 2.5 µm resulting in a bed channel porosity of 59%. Again, no eddy diffusion takes place and plate numbers of 400,000 per column can be achieved [94]. Baca et al. coupled 4 of these columns and achieved a maximum plate number of 1.2 x 10^6 and a peak capacity of 1,815 at a gradient time of 2,050 min [95]. This technique is therefore particularly suitable for the analysis of highly complex samples and less so for rapid analysis.

1.3.2 Loadability of Miniaturized Columns

With downsizing of column dimensions, the amount of available stationary phase also decreases. Therefore, the poor loadability of the columns applied in cLC is indeed a disadvantage. A clear distinction must be made between volume overloading and mass overloading. The latter occurs when too much substance is introduced to the column and the equilibrium between mobile and stationary phase is disturbed [96, 97]. Depending on the type of isotherm, either a peak with reduced retention time and significant tailing occurs or the retention of the peak increases but shows significant fronting [98]. Depending on the circumstances there are only two valid options to prevent mass overload. If the mass overloading problem exists in relation to the target analyte, the sample can be diluted [99]. If the problem persists in the ultra-trace analysis, the matrix must be specifically depleted and the target enriched. This can be done offline using solid phase extraction methods (SPE) e.g., for the analysis of hormones in water with highly specialized materials like molecular imprinted polymers (MIP) [100]. Alternatively, online methods are also available, such as the use of trapping columns [101].

Volume overload occurs when the injection volume is set too high [63]. Unlike mass overload this only affects the band broadening and not the peak shape. According to a rule of thumb, the injection volume for packed columns should not exceed 10% of the effective column volume [102]. The effective column volume (V_{eff}) can be calculated according to Equation 1-2.

$$V_{eff} = r^2 * \pi * L * \epsilon \qquad \text{Equation 1-2}$$

Where r is the radius of the column, L the length of the column and ϵ the porosity of the stationary phase. The equation shows that the injection volume depends to the square on the ID. However, in many real applications, the injection volume must be chosen > 10% of the V_{eff} to achieve a sufficient response in the detector [102]. Different methods for band focusing were developed, which also allows large volume injection for cLC columns. The simplest way is to choose an injection solution that is weaker than the mobile phase [63]. Like what is described for mass overloading, online enrichment can also be performed on different stationary phases. In the column-in-valve approach, such concentration steps can already be obtained in the switching valve before the transfer to the analytical separation column [103, 104]. Due to the compact dimensions of the cLC columns, temperature can also be used for focusing. In this case, the column is cooled down to a few degrees at the inlet and then heated up very fast within a few seconds to release the analytes [105]. Through the work in Chapter 3, an extensive investigation of the loading capacity of cLC columns was carried out. Here, it was highlighted which factors should be fulfilled in order to enable large volume injection without loss of efficiency.

1.3.3 Low Sensitivity of Miniaturized Systems

Due to the low injection volume, it is automatically assumed that the sensitivity of cLC systems must be inferior. However, quite in contrast, under certain conditions, the sensitivity of cLC systems can even be significantly higher than that of conventional LC [106]. Especially in combination with mass spectrometry (MS), cLC is “a marriage in heaven” that meets the sensitivity requirements in bioanalytical applications. Today, ESI is a gentle and universal method for the ionization of a wide range of analytes. However, the main weaknesses of this technique are competing ionization reactions in the ion source and the dependence of desolvation on ionization yield. Both drawbacks are mitigated by cLC.

Due to the low column ID there is less radial dilution of the molecules, the injection plug remains more concentrated, there is direct correlation between the column ID and the signal

intensity [107]. This also leads to a further reduction of the column ID in conventional LC. The extent to which this approach can be implemented was investigated in Chapter 5. Due to the small injection volume, less matrix is introduced into the mass spectrometer, competing ionization is reduced, the ionization efficiency increases, the signal to noise ratio increases and limits of detection improve [108–110]. In addition, the low introduction of matrix also increases the operating time of the system, and the cleaning intervals of the ion source and the quadrupoles can be extended [111]. Due to the low flow rates, a complete desolvation of the solvent can be guaranteed, lower gas flow temperatures can be used, and thus temperature-labile substances will not undergo in-source fragmentation [112]. A further promising approach in the coupling of cLC and MS is the possibility to position the column directly at the source, post-column band broadening is thereby significantly reduced. In one very promising approach, the emitter itself was packed with the stationary phase [113, 114].

1.3.4 Robustness and Handling of Miniaturized Systems

The frequently criticized lack of robustness and the generally difficult handling of cLC can be traced back to a common source of error, the untrained user. Unlike in conventional LC, careless handling, such as poorly cut capillaries, unclean connections, or the use of incorrect method parameters, can contribute to a measurable loss of chromatographic efficiency and a significant lack of robustness. Classic factors attributed to lack of robustness, such as clogging, can also be eliminated by simple changes in behavior.

If tubing is manufactured in-house from fused silica capillaries, two main factors need to be considered. Cutting should be done with special diamond cutters to obtain an acceptable cut edge. This edge should then be polished to ensure a dead volume free joint [115]. Alternatively, pre-cut, and polished capillaries can be purchased. Connections must be made with great care, double sleeves should be avoided. If capillaries are not screwed properly, dead volumes can occur where the mobile phase is stagnant. In addition, turbulence can occur on the bad connection. Both effects contribute negatively to the overall band broadening [115, 116]. If unions are used to connect individual components, the bore should correspond to the capillary diameter used.

The robustness of cLC systems can also be significantly improved by simple measures. To prevent clogging of the capillaries and especially the column inlet frit, samples and solvents should be filtered [117]. To prevent outgassing and thus spike signals in the detector, solvents must be degassed [118]. Injection volumes must be adjusted to the respective column

dimensions. The ideal injection volume of a 2.1 mm column corresponds to a loading of a 0.3 mm column of 480%. If these ratios were mirrored on the 2.1 mm column, the injection volume would be 576 µL and would also lead to significantly less robust measurements. To avoid clogged emitter tips, the temperature of the source should be cooled down to room temperature before the flow is stopped.

In summary, working with miniaturized systems is more demanding but far from impossible. New developments in peripherals make it possible to eliminate a large part of the sources of error. In addition, it can be assumed that with increasing market share, handling will also be significantly simplified.

1.3.5 Band Broadening and Extra-Column Volume in Miniaturized Systems

Band broadening due to increased influence of extra-column volume is a well-known challenge in cLC [119, 120]. Reducing the extra-column volume is the most effective method to significantly increase chromatographic performance [121]. All system components contribute to band broadening [63, 115, 122, 123]. Since there is a linear correlation between peak variance and band broadening for a Gaussian peak, the peak variance has been accepted as a general parameter in the literature and is frequently used applying different methods [63, 115, 124–130]. Provided that the individual system components do not influence each other, the total system variance (σ^2_{system}) can be represented as a simple sum equation as shown in Equation 1-3 [122, 131].

$$\sigma^2_{system} = \sigma^2_{inj} + \sigma^2_{con} + \sigma^2_{tub} + \sigma^2_{frit} + \sigma^2_{column\ bed} + \sigma^2_{detector} \qquad \text{Equation 1-3}$$

Here σ^2_{inj} is the influence of the injector on the band broadening, σ^2_{con} the influence of the connectors consisting of unions and fittings, σ^2_{tub} the influence of the tubing and $\sigma^2_{detector}$ the influence of the detector. Unlike usually presented, the variance of the column σ^2_{column} was deliberately divided into the single factors σ^2_{frit} of the column frit and $\sigma^2_{column\ bed}$ for the column bed. As already described the choice of the frit and the corresponding swept volume can have a significant impact on the separation efficiency [83]. Several methods are available to determine the influence of the frits [132–134]. Even though it would be more correct to speak of the extra-column bed variance, the methods are very complex, therefore σ^2_{column} is usually used and all other factors are defined as the extra-column variance.

The simplest method to reduce the influence of σ^2_{tub} can be achieved by reducing the ID of the connecting capillaries [122]. However, this also increases the backpressure and thus the demand

on the system. A reduction of the band broadening by σ_{inj}^2 can already be achieved by the choice of the right injection method [63]. Many investigations have shown that a metered injection is preferable to a full loop injection [63, 119, 135]. For σ_{con}^2 reduction of unions should be the first priority, if their use cannot be avoided dead volume free connectors should be used [136]. If their use is necessary, the bore should be chosen to match the ID of the tubing [115]. For bores and fittings applies, the closer to the tubing outer diameter the better, as this minimizes the negative influence on the separation efficiency in case of unclean connections [136]. Through the comprehensive study of commercially available detectors as presented in Chapter 4, factors were identified which, when optimized, significantly minimize the influence of $\sigma_{detector}^2$. Nowadays, all known detector types have now been downscaled to the dimensions of cLC [115]. Also, conventional detectors can be made usable with cLC systems by special interfaces, e.g., the exchange of the emitter capillary in many MS systems is sufficient to make the technique compatible with µLC [59, 115]. In addition, methods for on-column and on-capillary detection are available that do not contribute to band broadening and can be used, for example, as an additional source of information before coupling with other means of detection [137, 138].

1.3.6 The Interplay of Progress and Regress

The described influences have been the subject of many publications since the 1970s. Nevertheless, the knowledge is not consistently implemented in the commercially available systems. As a result, modern commercial cLC systems often have the same dimensions as their conventional counterparts. In comparison, the miniaturization of transistors and the modular design of integrated circuits in microchips in electronics show the potential that consistent implementation has for steadily increasing efficiency and user acceptance. This approach has been so successful that there will be an estimated 7.69 billion smartphone subscriptions by 2027 [141]. A stringent realization and implementation of miniaturization has so far failed to materialize in the field of instrumental analytics. For example, threads in valves of column hardware for cLC have been optimized to 1/32" threads in order to reduce the influence of improper connections; the new systems rely on 1/16" threads again. This makes the use of special dead volume free fittings necessary and prevents a miniaturization of the valve interfaces due to the need of bigger bores and fittings.

Another example is the optimization of the tubing pathways. With the new systems, the post-column volume has been reduced to an absolute minimum, making it possible, e.g., to place the

column in an oven directly in front of the MS interface [142]. However, this progress has come at the cost of increasing the pre-column volume by the same amount, making modern systems unsuitable for isocratic measurements or analytes with little retention on the stationary phase. The main problem of these developments is that miniaturization is not thought through. Usually only the flow path is miniaturized, the dimensions of the systems hardly differ from the conventional systems or even exceed them in some cases. Design takes precedence over function with clear disadvantages for chromatographic efficiency and acceptance of the systems by the end user. The introduction of modular system components starting in 1968 with stand-alone UV detector and pumps is considered a milestone in the history of HPLC [143, 144]. However, this basic idea stands in the way of modern, future-oriented miniaturization. Modular thinking in individual modules for pumps, autosamplers, column ovens and detectors leads to unnecessarily long capillary paths between the individual modules, which in turn leads to an increase in the extra-column volume, resulting in additional band broadening [119, 145].

In conclusion, the industry's preference to use “standard” HPLC and UHPLC, as well as the trend in conventional LC to shorten columns and reduce particle diameters to advertise faster analysis without real efficiency gains, is the main reason why miniaturized systems have not yet become the new gold standard.

1.4 With Miniaturization into a More Efficient and Greener Future

One of the greatest challenges of modern times is to cope with the hunger for resources driven by constant economic growth. The annually published Earth Overshoot Day of the Global Footprint Network allows an estimation of the resource consumption, it indicates when the annually naturally regenerable resources of the planet Earth are exhausted [146]. The data show a clear trend, the available resources are consumed increasingly faster, the Earth Overshoot Day is reached sooner every year, and this pattern is only broken by global crises such as the recent Corona pandemic as illustrated in Figure 1-4. What the Corona pandemic also showed clearly is that an economic standstill leads to a significant reduction in resource consumption, but the socio-economic consequences are serious, so innovation should be the means of choice [147, 148]. Already today, modern processes in industry need to be resource-saving, sustainable, cost-optimized and still offer high efficiency, and sooner or later this trend will also have to be reflected in the analytical laboratory. Miniaturization is the tool to fully meet these requirements.

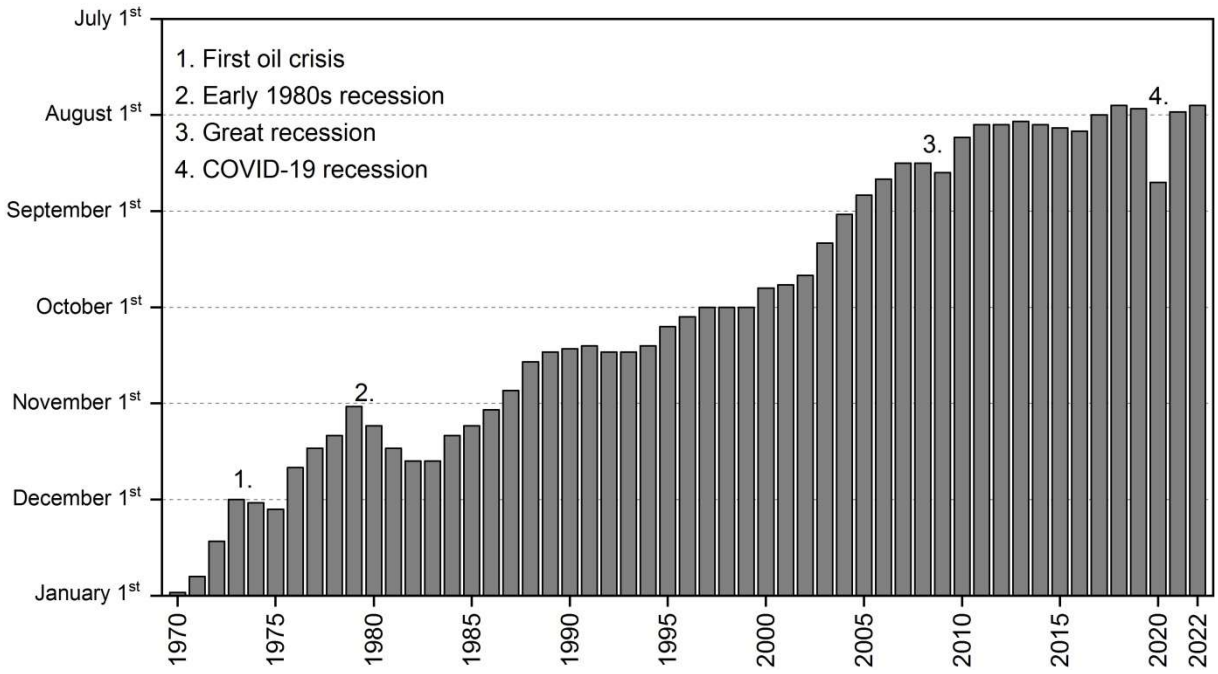

Figure 1-4: Representation of the Earth Overshoot Day from 1970 to 2022. The various crises that have led to a significant reduction in resource consumption are marked.

Over the past quarter century, understanding of the massive impact of human actions on the environment has grown and is undisputed in the scientific community [149–152]. Environmental issues are also at the top of the list of concerns among the general population [153, 154]. For Generation Z in particular, issues such as renewable energy, abandoning fossil fuels, and climate change are of utmost importance, as demonstrated by the protests called Fridays for Future that have occurred in over 150 countries since 2018 [155, 156]. With the definition of the 12 principles of green chemistry by Anastas and Warner in 1998, the development of sustainable methods was initiated [157]. In 2013, the 12 principles of green analytical chemistry (GAC) were defined, which are also known as SIGNIFICANCE [158]. The principles of waste avoidance, energy conservation, user protection and miniaturization are inherently covered by cLC [101]. Figure 1-5 shows the results of an "exact match" search in the web of science core collection for "green analytical method", "environmentally friendly method" and "green analytical chemistry" and illustrates the increased research interest in GAC.

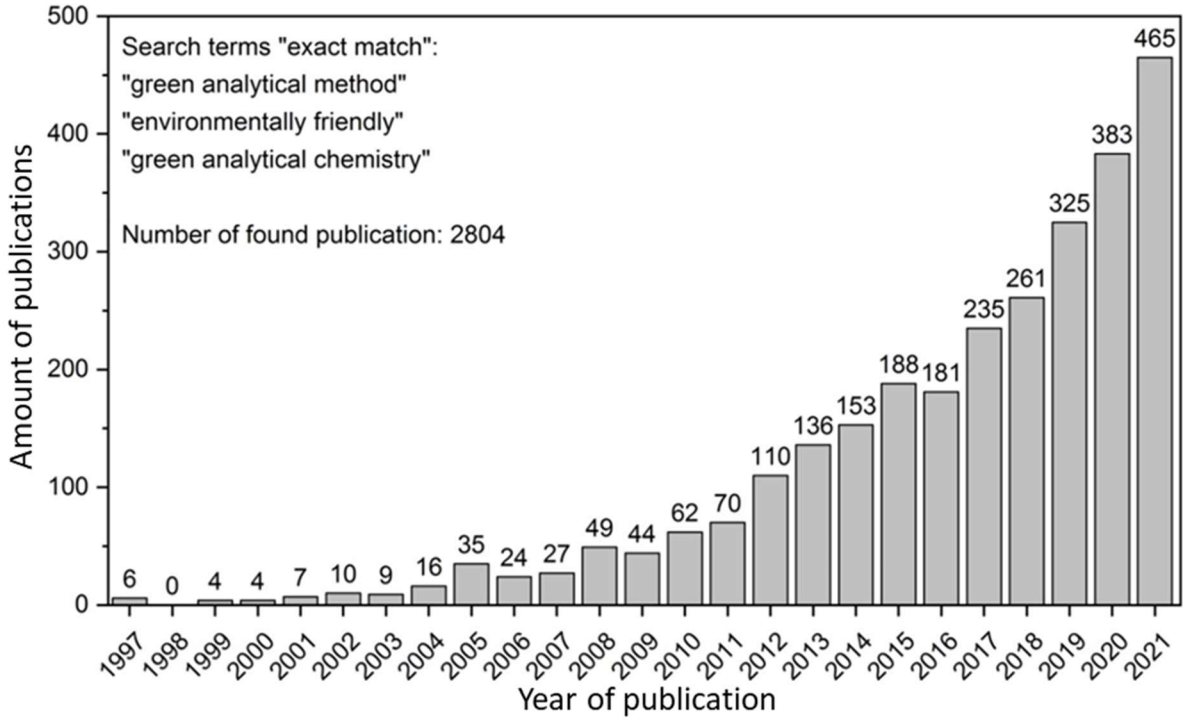

Figure 1-5: "exact match" analysis for the words "green analytical method", "environmentally friendly method" or "green analytical chemistry" in the web of science core collection. Data is illustrated for the last 25 years.

As already mentioned, cLC contributes to a massive reduction in solvent consumption and can therefore also mitigate the consequences of geopolitical events [64]. The first major acetonitrile crisis occurred in 2009, which also drove research into alternatives in instrumental analytics [159–161]. A similar effect is also looming in 2022, driven primarily by the continuing supply bottlenecks of the Corona pandemic and the Ukraine war leading to reduced acetonitrile availability on the world market. For example, the price of natural gas has increased fivefold within a year based on Title Transfer Facility (TTF) prices [162]. Acetonitrile can be produced from propene by the SOHIO process [163]. Among other things, propene is obtained by steam cracking of natural gas with an approximate yield of 15%. From 1 t of natural gas, 150 kg of propene are obtained, which in turn yields 15 kg or 19 L of acetonitrile [164].

Particularly in view of the fact that the cost of wholesale electricity on the stock exchange has increased fourfold in quarter four of 2021 compared to the average from 2015-2020 and has continued to rise since then [165]. Complete miniaturization reduces energy consumption and can also be of economic interest [101]. This can be vividly illustrated by the often underestimated costs of laboratory air [166]. The German Federal Institute for Occupational Safety and Health (BAuA) recommends an air exchange rate in the laboratory of 25 m^3/m^2h, which is equivalent to approximately 8 changes per hour for a ceiling height of 3 m [167]. If we now imagine a small HPLC laboratory with a ground area of 60 m^2 and an operating time

of 24/7/365 and assume that the costs for the exchange of 1,000 m^3 are 2 €, the costs for the laboratory air per year alone amount to 26,280 €. Replacing conventional HPLC systems with cLC systems opens up two options.

Option 1: If the laboratory space is maintained, more systems can be accommodated in the same space with complete miniaturization. Although this does not reduce the cost of laboratory air, it can significantly increase the productivity of the laboratory by parallelizing analyses and increasing sample throughput.

Option 2: Alternatively, by changing to miniaturized systems, laboratory space could be reduced while maintaining the same productivity. This would have two economic advantages: the cost of laboratory air could be reduced accordingly and the maintenance costs, which are 5-8 times higher than for office space, would be eliminated. If the freed-up space is now converted into recreation rooms for employees and the laboratory workplaces are moved to the cloud, employee satisfaction can be increased. Studies have shown that this is associated with reduced sick leave, increased productivity and fewer resignations [168, 169]. The discussed options are shown in Figure 1-6 as an example of a classic HPLC laboratory.

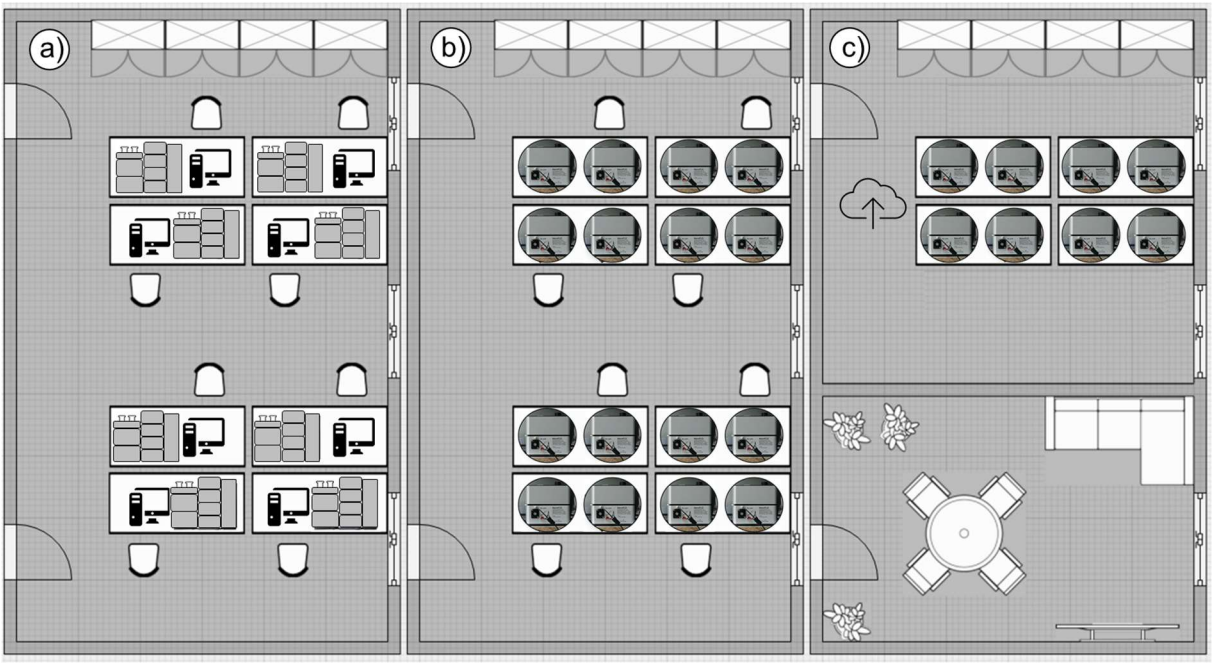

Figure 1-6: a) A classic HPLC laboratory with workstations for data evaluation on the individual systems. b) Illustration of option 1: significant increase in possible processing through parallelization. c) Illustration of option 2: laboratory space can be significantly reduced through the use of fully miniaturized cLC systems with equal sample processing rates and elimination of laboratory workstations through data analysis in the cloud. Free space can be used for recreation areas or additional office space.

Regardless of the option chosen, the BAuA states that the air exchange rate can also be reduced or natural ventilation can be used if a risk assessment is available [167]. Since cLC is operated with only minimal amounts of solvent, such measures are realistic, potentially reducing the cost for laboratory air further. Other economic factors that have not yet been taken into account are the reduced costs of waste disposal, lower electricity consumption and savings in air conditioning due to lower waste heat from the systems.

1.5 The Future is (Almost) Now.

The final sub-chapter could easily be found in a well-stocked bookstore in the science fiction section. This is mainly due to the difficulty of extrapolating current trends and developments into the future. Nevertheless, two developments can currently be observed which, in combination, could lead to fully miniaturized total analysis systems (μTAS) in the coming years. Firstly, the continuing developments of Lab-on-Chip systems (LOC) which miniaturize individual laboratory functions and transfer them to a microfluidic chip. Secondly, the increasing use of additive manufacturing in the chromatographic field. This is also supported by the increasing number of publications on portable HPLC systems.

A major concern with classical laboratory HPLC analysis is the time gap between sample collection and analysis. The classical approach involves sampling in the field followed by preparation and analysis in the laboratory [170]. During this time, samples can change chemically, or the target can be degraded, in addition there is a delay in reaction and action [101]. To reduce response times, special trucks are used, which are equipped with full laboratory equipment and allow on-site monitoring [171]. However, these are expensive solutions that cannot be implemented on a large scale. Based on this context, intensive work is being done on the development of portable HPLC systems [172]. In particular, the development of UV LEDs based on AlGaN with a peak output of 341 nm, first described in 2001, and the work of Adivarahan et al. on a 278 nm deep-UV LED, as well as the further development in the Semiconductor Ultraviolet Optical Sources (SUVOS) Program of the American military, have laid the foundations and contributed to the establishment of small battery-operated UV detectors [173–175]. Several systems applying such deep-UV LEDs are reported [115, 138, 176]. Furthermore, considerable progress has been made in miniaturization to meet the requirements of pressure stability, reproducibility, and freedom from pulsation resulting in e.g. high pressure electroosmotic pumps, piston pumps and even zero electrical power pumps [138, 177, 178]. All these developments in detail have led to a number of miniaturized systems being developed for field use like the hand-portable HPLC with broadband spectral detection from

Chatzimichail et al. [172, 179]. In the meantime, the first fully miniaturized HPLC systems have become commercially available [180, 181]. Our own efforts to develop a new system that takes advantage of on-site sample preparation and analytics are detailed in Chapter 7.

LOC systems are the next step in miniaturization and are considered the most important trend in the miniaturization of chromatographic systems [90]. In the past, some impressive performances have used LOC techniques. Piendl et al. created an FS chip for multiple heart-cutting HPLC/MS. With the developed chip transfer cross a particularly dead volume free connection between both separation phases was possible [182]. In another publication of the same group, the coupling of an HPLC chip with a miniaturized IMS and the separation of a mixture of four antidepressants succeeded in complete resolution in a 2D-plot in less than 20 s [183]. Furthermore, first proposes for creating 3D HPLC LOCs with ultra-high peak capacities and peak production rates were made in 2015 [184]. The development of LOCs with classical manufacturing approaches is costly and complex and requires expensive equipment. For chromatographic applications, it is important that the materials used are resistant to organic solvents to prevent dissolution or destruction of the chip structures [185]. Today mainly quartz and fused silica are used in LOC, due to the good light transmission and mechanical stability as well the resistance against the most common organic solvents. However, one of the main disadvantages is that these materials are very fragile. The production of LOC in polymers is also taking place, the dominant substrate here is polydimethylsiloxane (PDMS). The main drawback of this substrate is the low-pressure stability and the hydrophobicity causes nonspecific absorption [186, 187]. Regardless of the material, the systems are mainly manufactured using classical production methods. Microfluidic channels are milled, etched, or drilled into a base body [188]. These channels are then sealed with a lid using a complex bonding process. A further disadvantage of this approach is that several months can elapse between design and production. Another difficulty is the introduction of the stationary phase; for particulate phases, auxiliary channels are usually used, which then must be sealed afterwards. Monolithic phases can be synthesized on chip or are fabricated offline in a mould and afterwards integrated into the chip prior to the bonding process. Another difficulty is the implementation of the chip-to-world connection which allows connecting the chip with further peripherals like pumps or detectors [189, 190]. To reduce the problems described above, LOC systems are increasingly being manufactured using 3D printing [191].

Additive manufacturing is experiencing a noticeable surge in the chromatographic community [192]. Due to the low access hurdles and the comparatively low acquisition costs, the technology also enables small workgroups to manufacture new systems. Hardly any field

experiences such a rapid development as 3D printing in the last years, new techniques like Computed Axial Lithography (CAL) are developed at regular intervals [193, 194]. Also in the chromatographic community, the field is becoming increasingly important. Additive manufacturing is given its own sessions at the most important conferences. Large European funded projects combining chromatography and 3D printing such as the recently completed Separation Technology for A Million Peaks (STAMP) project of the University of Amsterdam are being funded [195]. In the meantime, all system components of an HPLC can be manufactured by 3D printing. For example, pneumatic switching valves and pumps as well as valves for fluidic circuits have already been manufactured. Various experiments on printing columns have also been carried out. The studies of Salmean et al. dealt with the optimal bed formation and geometries of the stationary phase and could show that additive manufacturing is not limited by the complexity of the design, and more efficient beds based on regular monolithic architectures are possible [196]. As already mentioned, 3D printing is also used in LOC, the dominating technology is stereolithography, which is a layer-by-layer photopolymerization of liquid resins. The problem with this method is that the resin used is difficult to remove from the printed cavities. In addition, there is the risk of incomplete polymerization and thus contamination of samples. The bottleneck holding back 3D printing in analytical chemistry is the problem of resolution vs. time. To address the described problems of current LOCs, a flexible additively manufactured LOC system is developed in an own research project which is introduced in Chapter 8.

1.6 References

[1] Y. Boumrah, W. Kermouche, B. Zarita, E.D. Drardja, S. Bouanani, Hashish seizures in Algeria over the 2019–2020 period: The rise of potent hashish hybrids, J. Forensic Sci. 67 (2022) 889–898. https://doi.org/https://doi.org/10.1111/1556-4029.15001.

[2] L. Lin, P. Amaratunga, J. Reed, P. Huang, B.L. Lemberg, D. Lemberg, Quantitation of Δ8-THC, Δ9-THC, Cannabidiol and 10 Other Cannabinoids and Metabolites in Oral Fluid by HPLC-MS-MS, J. Anal. Toxicol. 46 (2022) 76–88. https://doi.org/10.1093/jat/bkaa184.

[3] L. Rivier, Criteria for the identification of compounds by liquid chromatography-mass spectrometry and liquid chromatography-multiple mass spectrometry in forensic toxicology and doping analysis, Anal. Chim. Acta. 492 (2003) 69–82. https://doi.org/10.1016/S0003-2670(03)00889-4.

[4] F. Itzel, N. Baetz, L.L. Hohrenk, L. Gehrmann, D. Antakyali, T.C. Schmidt, J. Tuerk, Evaluation of a biological post-treatment after full-scale ozonation at a municipal wastewater treatment plant, Water Res. 170 (2020) 115316. https://doi.org/10.1016/j.watres.2019.115316.

[5] F. Itzel, L. Gehrmann, T. Teutenberg, T.C. Schmidt, J. Tuerk, Recent developments and concepts of effect-based methods for the detection of endocrine activity and the importance of antagonistic effects, TrAC - Trends Anal. Chem. 118 (2019) 699–708. https://doi.org/10.1016/j.trac.2019.06.030.

[6] L.M.H. Reinders, M.D. Klassen, C. vom Eyser, T. Teutenberg, M. Jaeger, T.C. Schmidt, J. Tuerk, Quality control of cytostatic drug preparations—comparison of workflow and performance of Raman/UV and high-performance liquid chromatography coupled with diode array detection (HPLC-DAD), Anal. Bioanal. Chem. 413 (2021) 2587–2596. https://doi.org/10.1007/s00216-021-03223-9.

[7] K.A. Lippa, J.J. Aristizabal-Henao, R.D. Beger, J.A. Bowden, C. Broeckling, C. Beecher, W. Clay Davis, W.B. Dunn, R. Flores, R. Goodacre, G.J. Gouveia, A.C. Harms, T. Hartung, C.M. Jones, M.R. Lewis, I. Ntai, A.J. Percy, D. Raftery, T.B. Schock, J. Sun, G. Theodoridis, F. Tayyari, F. Torta, C.Z. Ulmer, I. Wilson, B.K. Ubhi, Reference materials for MS-based untargeted metabolomics and lipidomics: a review by the metabolomics quality assurance and quality control consortium (mQACC), Metabolomics. 18 (2022) 1–29. https://doi.org/10.1007/s11306-021-01848-6.

[8] New International Version of the Holy Bible, Exodus 15:22-27, 1984.

[9] C.A. Lucy, Evolution of ion-exchange: From Moses to the Manhattan Project to Modern Times, J. Chromatogr. A. 1000 (2003) 711–724. https://doi.org/10.1016/S0021-9673(03)00528-4.

[10] L.S. Ettre, Chromatography in the ancient world?, J. High Resolut. Chromatogr. 18 (1995) 277–278. https://doi.org/10.1002/jhrc.1240180502.

[11] L.S. Ettre, Was Moses the first chromatographer?: Chromatography in the ancient world, LCGC North Am. 24 (2006) 1280–1283.

[12] E.P. Altova, I. Hargittai, Mikhail S. Tsvet—pioneer of chromatography—150 years from his birth, Struct. Chem. 33 (2022) 1–3. https://doi.org/10.1007/s11224-021-01804-z.

[13] A.J.P. Martin, R.L.M. Synge, A new form of chromatogram employing two liquid phases, Biochem. J. 35 (1941) 1358–1368. https://doi.org/10.1016/0968-0004(77)90204-3.

[14] A.H. Gordon, A.J. Martin, R.L. Synge, Partition chromatography in the study of protein constituents, Biochem. J. 37 (1943) 79–86. https://doi.org/10.1042/bj0370079.

[15] A.H. Gordon, A.J. Martin, R.L. Synge, Technical notes on the partition chromatography of acetamino-acids with silica gel, Biochem. J. 38 (1944) 65–68. https://doi.org/10.1042/bj0380065.

[16] M. Lippmann, A.T. Kirk, M. Hitzemann, S. Zimmermann, IMS Instrumentation I: Isolated data acquisition for ion mobility spectrometers with grounded ion sources, Int. J. Ion Mobil. Spectrom. 23 (2020) 69–74. https://doi.org/10.1007/s12127-020-00260-5.

[17] Royal Society: Awards of Medals, Nature. 170 (1952) 826. https://doi.org/10.1038/170826a0.

[18] J.C. Moore, Gel permeation chromatography. I. A new method for molecular weight distribution of high polymers, J. Polym. Sci. Part A Gen. Pap. 2 (1964) 835–843. https://doi.org/10.1002/pol.1964.100020220.

[19] P.D. McDonald, James Waters and his Liquid Chromatography People: A Personal Perspective, Golden Jubil. Year Chromatogr. Soc. (2006) 12–16.

[20] H. Small, T.S. Stevens, W.C. Bauman, Novel Ion Exchange Chromatographic Method Using Conductimetric Detection, Anal. Chem. 47 (1975) 1801–1809. https://doi.org/10.1021/ac60361a017.

[21] J.J. Kirkland, High speed liquid-partition chromatography with chemically bonded organic stationary phases, J. Chromatogr. Sci. 9 (1971) 206–214. https://doi.org/10.1093/chromsci/9.4.206.

[22] J.G. Dorsey, K.A. Dill, The Molecular Mechanism of Retention in Reversed-Phase Liquid Chromatography, Chem. Rev. 89 (1989) 331–346. https://doi.org/10.1021/cr00092a005.

[23] T. Greibrokk, The contributions of Csaba Horváth to liquid chromatography, J. Sep. Sci. 27 (2004) 1249–1254. https://doi.org/10.1002/jssc.200401909.

[24] J.J. Kirkland, Superficially Porous Supports for Chromatography, 1970. https://www.google.de/patents/US3505785A.

[25] J.J. Kirkland, Performance of zipax® controlled surface porosity support in high-speed liquid chromatography, J. Chromatogr. Sci. 10 (1972) 129–137. https://doi.org/10.1093/chromsci/10.3.129.

[26] S. Fekete, J.L. Veuthey, D. Guillarme, Comparison of the most recent chromatographic approaches applied for fast and high resolution separations: Theory and practice, J. Chromatogr. A. 1408 (2015) 1–14. https://doi.org/10.1016/j.chroma.2015.07.014.

[27] C. Luo, J.J. DeStefano, T.J. Langlois, B.E. Boyes, S.A. Schuster, J.M. Godinho, Fundamental to achieving fast separations with high efficiency: A review of chromatography with superficially porous particles, Biomed. Chromatogr. 35 (2021). https://doi.org/10.1002/bmc.5087.

[28] F. Ali, A.R. Malik, W.J. Cheong, N.U. Rehman, Demonstration of high separation efficiency for polystyrene-modified sub-1 μm particles originating from silica monolith under isocratic elution mode in liquid chromatography, J. Liq. Chromatogr. Relat. Technol. 42 (2019) 662–672. https://doi.org/10.1080/10826076.2019.1665539.

[29] S. Fekete, A. Murisier, G.L. Losacco, J. Lawhorn, J.M. Godinho, H. Ritchie, B.E. Boyes, D. Guillarme, Using 1.5 mm internal diameter columns for optimal compatibility with current liquid chromatographic systems, J. Chromatogr. A. 1650 (2021) 462258. https://doi.org/10.1016/j.chroma.2021.462258.

[30] F. Lestremau, D. Wu, R. Szücs, Evaluation of 1.0mm i.d. column performances on ultra high pressure liquid chromatography instrumentation, J. Chromatogr. A. 1217 (2010) 4925–4933. https://doi.org/10.1016/j.chroma.2010.05.044.

[31] D. Cabooter, A. Fanigliulo, G. Bellazzi, B. Allieri, A. Rottigni, G. Desmet, Relationship between the particle size distribution of commercial fully porous and superficially porous high-performance liquid chromatography column packings and their chromatographic performance, J. Chromatogr. A. 1217 (2010) 7074–7081. https://doi.org/10.1016/j.chroma.2010.09.008.

[32] C. Dewaele, M. Verzele, Influence of the particle size distribution of the packing material in reversed-phase high-performance liquid chromatography, J. Chromatogr. A. 260 (1983) 13–21. https://doi.org/10.1016/0021-9673(83)80002-8.

[33] B. Buszewski, S. Noga, Hydrophilic interaction liquid chromatography (HILIC)-a powerful separation technique, Anal. Bioanal. Chem. 402 (2012) 231–247. https://doi.org/10.1007/s00216-011-5308-5.

[34] K. Zhang, X. Liu, Reprint of "Mixed-mode chromatography in pharmaceutical and biopharmaceutical applications," J. Pharm. Biomed. Anal. 130 (2016) 19–34. https://doi.org/10.1016/j.jpba.2016.09.013.

[35] M.F. Wahab, D.C. Patel, R.M. Wimalasinghe, D.W. Armstrong, Fundamental and Practical Insights on the Packing of Modern High-Efficiency Analytical and Capillary Columns, Anal. Chem. 89 (2017) 8177–8191. https://doi.org/10.1021/acs.analchem.7b00931.

[36] J. Kirkland, J. Destefano, The art and science of forming packed analytical high-performance liquid chromatography columns, J. Chromatogr. A. 1126 (2006) 50–57. https://doi.org/10.1016/j.chroma.2006.04.027.

[37] L. Abrahams, H.M. Burleigh, J.L. Waters, Novel pumpin apparatus, 1974.

[38] M.E. Swartz, UPLCTM: An Introduction and Review, J. Liq. Chromatogr. Relat. Technol. 28 (2005) 1253–1263. https://doi.org/10.1081/JLC-200053046.

[39] J. De Vos, K. Broeckhoven, S. Eeltink, Advances in Ultrahigh-Pressure Liquid Chromatography Technology and System Design, Anal. Chem. 88 (2016) 262–278. https://doi.org/10.1021/acs.analchem.5b04381.

[40] J. De Vos, D. Stoll, S. Buckenmaier, S. Eeltink, J.P. Grinias, Advances in ultra-high-pressure and multi-dimensional liquid chromatography instrumentation and workflows, Anal. Sci. Adv. 2 (2021) 171–192. https://doi.org/10.1002/ansa.202100007.

[41] K. Broeckhoven, G. Desmet, Advances and Challenges in Extremely High-Pressure Liquid Chromatography in Current and Future Analytical Scale Column Formats, Anal. Chem. 92 (2020) 554–560. https://doi.org/10.1021/acs.analchem.9b04278.

[42] D.T.T. Nguyen, D. Guillarme, S. Rudaz, J.L. Veuthey, Fast analysis in liquid chromatography using small particle size and high pressure, J. Sep. Sci. 29 (2006) 1836–1848. https://doi.org/10.1002/jssc.200600189.

[43] D.C. Patel, M.F. Wahab, T.C. O'Haver, D.W. Armstrong, Separations at the Speed of Sensors, Anal. Chem. 90 (2018) 3349–3356. https://doi.org/10.1021/acs.analchem.7b04944.

[44] I. Halász, R. Endele, J. Asshauer, L. Pl, I. Clrwric, ultimate limits in HPLC, 2 (1975) 37–60. https://ac.els-cdn.com/S0021967300999412/1-s2.0-S0021967300999412-main.pdf?_tid=d67638cb-69fa-4491-8515-c7c7acf889f0&acdnat=1547646315_3e01e4f38af378f66e5fc8b3fabdf2f3.

[45] V. Pretorius, T.W. Smuts, Turbulent Flow Chromatography: A New Approach to Faster Analysis, Anal. Chem. 38 (1966) 274–281. https://doi.org/10.1021/ac60234a030.

[46] C.G. Horvath, B.A. Preiss, S.R. Lipsky, Fast Liquid Chromatography: An Investigation of Operating Parameters and the Separation of Nucleotides on Pellicular Ion Exchangers, Anal. Chem. 39 (1967) 1422–1428. https://doi.org/10.1021/ac60256a003.

[47] T. Tsuda, M. Novotny, Band-Broadening Phenomena in Microcapillary Tubes under the Conditions of Liquid Chromatography, Anal. Chem. 50 (1978) 632–634. https://doi.org/10.1021/ac50026a023.

[48] M. Novotny, T. Tsuda, Packed Microcapillary Columns in High Performance Liquid Chromatography, Anal. Chem. 50 (1978) 271–275. https://doi.org/10.1021/ac50024a026.

[49] Y. Hirata, M. Novotny, T. Tsuda, D. Ishii, Packed Microcapillary Columns with Different Selectivities for Liquid Chromatography, Anal. Chem. 51 (1979) 1807–1809. https://doi.org/10.1021/ac50047a046.

[50] K. Hibi, D. Ishii, I. Fujishima, T. Takeuchi, T. Nakanishi, Studies of open tubular micro capillary liquid chromatography. 1. The development of open tubular micro capillary liquid chromatography, J. High Resolut. Chromatogr. 1 (1978) 21–27. https://doi.org/10.1002/jhrc.1240010106.

[51] T. Tsuda, K. Hibi, T. Nakanishi, T. Takeuchi, D. Ishii, Studies of open-tubular micro-capillary liquid chromatography. II. Chemically bonded octadecylsilane stationary phase, J. Chromatogr. A. 158 (1978) 227–232. https://doi.org/10.1016/S0021-9673(00)89969-0.

[52] J.W. Jorgenson, E.J. Guthrie, Liquid chromatography in open-tubular columns. Theory of column optimization with limited pressure and analysis time, and fabrication of chemically bonded reversed-phase columns on etched borosilicate glass capillaries, J. Chromatogr. A. 255 (1983) 335–348. https://doi.org/10.1016/S0021-9673(01)88293-5.

[53] S. Folestad, B. Josefsson, M. Larsson, Performance and preparation of immobilized polysiloxane stationary phases in 5-55 μm I.D. open-tubular fused silica columns for liquid chromatography, J. Chromatogr. A. 391 (1987) 347–372. https://doi.org/10.1016/S0021-9673(01)94338-9.

[54] K. E. Karlsson, M. Novotny, Separation Efficiency of Slurry-Packed Liquid Chromatography Microcolumns with Very Small Inner Diameters, Anal. Chem. 60 (1988) 1662–1665. https://doi.org/10.1021/ac00168a006.

[55] R.T. Kennedy, J.W. Jorgenson, Preparation and Evaluation of Packed Capillary Liquid Chromatography Columns with Inner Diameters from 20 to 50 μm, Anal. Chem. 61 (1989) 1128–1135. https://doi.org/10.1021/ac00185a016.

[56] M. Dole, L.L. Mack, R.L. Hines, D.O. Chemistry, R.C. Mobley, L.D. Ferguson, M.B. Alice, Molecular beams of macroions, J. Chem. Phys. 49 (1968) 2240–2249. https://doi.org/10.1063/1.1670391.

[57] M.T. Davis, D.C. Stahl, S.A. Hefta, T.D. Lee, A Microscale Electrospray Interface for Online, Capillary Liquid Chromatography/Tandem Mass Spectrometry of Complex Peptide Mixtures, Anal. Chem. 67 (1995) 4549–4556. https://doi.org/10.1021/ac00120a019.

[58] M. V. Novotny, Development of capillary liquid chromatography: A personal perspective, J. Chromatogr. A. 1523 (2017) 3–16. https://doi.org/10.1016/j.chroma.2017.06.042.

[59] T. Werres, J. Leonhardt, M. Jäger, T. Teutenberg, Critical Comparison of Liquid Chromatography Coupled to Mass Spectrometry and Three Different Ion Mobility Spectrometry Systems on Their Separation Capability for Small Isomeric Compounds, Chromatographia. 82 (2019) 251–260. https://doi.org/10.1007/s10337-018-3640-z.

[60] A. Claessens, C.A. Cramers, J.R.C. Vlssers, Microcolumn liquid chromatography : instrumentation , detection and applications, J. Chromatogr. A. 779 (1997) 1–28.

[61] J.P. Chervet, M. Ursem, J.P. Salzmann, Instrumental requirements for nanoscale liquid chromatography, Anal. Chem. 68 (1996) 1507–1512. https://doi.org/10.1021/ac9508964.

[62] T. Hetzel, C. Blaesing, M. Jaeger, T. Teutenberg, T.C. Schmidt, Characterization of peak capacity of microbore liquid chromatography columns using gradient kinetic plots, J. Chromatogr. A. 1485 (2017) 62–69. https://doi.org/10.1016/j.chroma.2017.01.018.

[63] T. Werres, T.C. Schmidt, T. Teutenberg, The influence of injection volume on efficiency of microbore liquid chromatography columns for gradient and isocratic elution, J. Chromatogr. A. 1641 (2021) 461965. https://doi.org/10.1016/j.chroma.2021.461965.

[64] J. Šesták, D. Moravcová, V. Kahle, Instrument platforms for nano liquid chromatography, J. Chromatogr. A. 1421 (2015) 2–17. https://doi.org/https://doi.org/10.1016/j.chroma.2015.07.090.

[65] I. Bulduk, HPLC-UV method for quantification of favipiravir in pharmaceutical formulations, Acta Chromatogr. 33 (2021) 209–215. https://doi.org/10.1556/1326.2020.00828.

[66] K. Soliman, F. Jirjees, R. Sonawane, R. Sheshala, Y. Wang, D. Jones, T.R.R. Singh, Latanoprost quantification in ocular implants and tissues: HPLC-fluorescence vs HPLC-UV, J. Chromatogr. Sci. 59 (2021) 64–70. https://doi.org/10.1093/chromsci/bmaa078.

[67] G. Jîtcă, E. Fogarasi, B.E. Ősz, C.E. Vari, A. Tero-Vescan, A. Miklos, M.G. Bătrînu, C.M. Rusz, M.D. Croitoru, M.T. Dogaru, A simple hplc/dad method validation for the quantification of malondialdehyde in rodent's brain, Molecules. 26 (2021) 1–10. https://doi.org/10.3390/molecules26165066.

[68] B.G. Cho, W. Peng, Y. Mechref, Separation of permethylated o-glycans, free oligosaccharides, and glycosphingolipid-glycans using porous graphitized carbon (Pgc) column, Metabolites. 10 (2020) 1–12. https://doi.org/10.3390/metabo10110433.

[69] S. Zhang, H. Xiao, R. Molden, H. Qiu, N. Li, Rapid Polysorbate 80 Degradation by Liver Carboxylesterase in a Monoclonal Antibody Formulated Drug Substance at Early Stage Development, J. Pharm. Sci. 109 (2020) 3300–3307. https://doi.org/https://doi.org/10.1016/j.xphs.2020.07.018.

[70] M. Jansons, D. Fedorenko, R. Pavlenko, Z. Berzina, V. Bartkevics, Nanoflow liquid chromatography mass spectrometry method for quantitative analysis and target ion screening of pyrrolizidine alkaloids in honey, tea, herbal tinctures, and milk, J. Chromatogr. A. 1676 (2022) 463269. https://doi.org/https://doi.org/10.1016/j.chroma.2022.463269.

[71] G. Rozing, Micropillar array columns for advancing nanoflow HPLC, Microchem. J. 170 (2021) 106629. https://doi.org/10.1016/j.microc.2021.106629.

[72] F. Gritti, T. McDonald, M. Gilar, Intrinsic advantages of packed capillaries over narrow-bore columns in very high-pressure gradient liquid chromatography, J. Chromatogr. A. 1451 (2016) 107–119. https://doi.org/10.1016/j.chroma.2016.05.035.

[73] K.D. Patel, A.D. Jerkovich, J.C. Link, J.W. Jorgenson, In-depth characterization of slurry packed capillary columns with 1.0-μm nonporous particles using reversed-phase isocratic ultrahigh-pressure liquid chromatography, Anal. Chem. 76 (2004) 5777–5786. https://doi.org/10.1021/ac049756x.

[74] A. de Villiers, H. Lauer, R. Szucs, S. Goodall, P. Sandra, Influence of frictional heating on temperature gradients in ultra-high-pressure liquid chromatography on 2.1 mm I.D. columns, J. Chromatogr. A. 1113 (2006) 84–91. https://doi.org/10.1016/j.chroma.2006.01.120.

[75] L. Nováková, J.L. Veuthey, D. Guillarme, Practical method transfer from high performance liquid chromatography to ultra-high performance liquid chromatography: The importance of frictional heating, J. Chromatogr. A. 1218 (2011) 7971–7981. https://doi.org/10.1016/j.chroma.2011.08.096.

[76] F. Gritti, G. Guiochon, Optimization of the thermal environment of columns packed with very fine particles, J. Chromatogr. A. 1216 (2009) 1353–1362. https://doi.org/10.1016/j.chroma.2008.12.072.

[77] R.S. Plumb, T. McDonald, P.D. Rainville, J. Hill, L.A. Gethings, K.A. Johnson, I.D. Wilson, High-Throughput UHPLC/MS/MS-Based Metabolic Profiling Using a Vacuum Jacketed Column, Anal. Chem. 93 (2021) 10644–10652. https://doi.org/10.1021/acs.analchem.1c01982.

[78] K.L. Sanders, J.L. Edwards, Nano-liquid chromatography-mass spectrometry and recent applications in omics investigations, Anal. Methods. 12 (2020) 4404–4417. https://doi.org/10.1039/d0ay01194k.

[79] J. Gleba, J. Kim, Determination of Morphine, Fentanyl and Their Metabolites in Small Sample Volumes Using Liquid Chromatography Tandem Mass Spectrometry, J. Anal. Toxicol. 44 (2020) 325–330. https://doi.org/10.1093/jat/bkz104.

[80] J.B. Langford, I.S. Lurie, Use of micro, capillary, and nano liquid chromatography for forensic analysis, J. Sep. Sci. 45 (2022) 38–50. https://doi.org/https://doi.org/10.1002/jssc.202100631.

[81] S. Bruns, U. Tallarek, Physical reconstruction of packed beds and their morphological analysis: Core-shell packings as an example, J. Chromatogr. A. 1218 (2011) 1849–1860. https://doi.org/10.1016/j.chroma.2011.02.013.

[82] S. Bruns, J.P. Grinias, L.E. Blue, J.W. Jorgenson, U. Tallarek, Morphology and separation efficiency of low-aspect-ratio capillary ultrahigh pressure liquid chromatography columns, Anal. Chem. 84 (2012) 4496–4503. https://doi.org/10.1021/ac300326k.

[83] M. Franc, J. Sobotníková, P. Coufal, Z. Bosáková, Comparison of different types of outlet frits in slurry-packed capillary columns, J. Sep. Sci. 37 (2014) 2278–2283. https://doi.org/10.1002/jssc.201400434.

[84] J. Billen, G. Desmet, Understanding and design of existing and future chromatographic support formats, J. Chromatogr. A. 1168 (2007) 73–99. https://doi.org/10.1016/j.chroma.2007.07.069.

[85] G. Desmet, S. Eeltink, Fundamentals for LC Miniaturization, Anal. Chem. 85 (2013) 543–556. https://doi.org/10.1021/ac303317c.

[86] S. Forster, H. Kolmar, S. Altmaier, Synthesis and characterization of new generation open tubular silica capillaries for liquid chromatography, J. Chromatogr. A. 1265 (2012) 88–94. https://doi.org/https://doi.org/10.1016/j.chroma.2012.09.054.

[87] W. Zhou, X. Yu, Y. Liu, W. Sun, Z. Chen, Porous layer open-tubular column with styrene and itaconic acid-copolymerized polymer as stationary phase for capillary electrochromatography–mass spectrometry, Electrophoresis. 42 (2021) 2664–2671. https://doi.org/10.1002/elps.202100148.

[88] T. Hara, S. Futagami, S. Eeltink, W. De Malsche, G. V. Baron, G. Desmet, Very High Efficiency Porous Silica Layer Open-Tubular Capillary Columns Produced via in-Column Sol-Gel Processing, Anal. Chem. 88 (2016) 10158–10166. https://doi.org/10.1021/acs.analchem.6b02713.

[89] K. Mejía-Carmona, J. Soares da Silva Burato, J.V.B. Borsatto, A.L. de Toffoli, F.M. Lanças, Miniaturization of liquid chromatography coupled to mass spectrometry: 1. Current trends on miniaturized LC columns, TrAC - Trends Anal. Chem. 122 (2020) 115735. https://doi.org/10.1016/j.trac.2019.115735.

[90] P. Xiang, Y. Yang, Z. Zhao, M. Chen, S. Liu, Ultrafast gradient separation with narrow open tubular liquid chromatography, Anal. Chem. 91 (2019) 10738–10743. https://doi.org/10.1021/acs.analchem.9b02190.

[91] H. Chen, Y. Yang, Z. Qiao, P. Xiang, J. Ren, Y. Meng, K. Zhang, J. Juan Lu, S. Liu, A narrow open tubular column for high efficiency liquid chromatographic separation, Analyst. 143 (2018) 2008–2011. https://doi.org/10.1039/c7an02065a.

[92] A. Gęgotek, A. Moniuszko-Malinowska, M. Groth, S. Pancewicz, P. Czupryna, J. Dunaj, S. Atalay, P. Radziwon, E. Skrzydlewska, Plasma Proteomic Profile of Patients with Tick-Borne Encephalitis and Co-Infections, Int. J. Mol. Sci. 23 (2022). https://doi.org/10.3390/ijms23084374.

[93] B.G. Cho, P. Jiang, M. Goli, S. Gautam, Y. Mechref, Using micro pillar array columns (μPAC) for the analysis of permethylated glycans, Analyst. 146 (2021) 4374–4383. https://doi.org/10.1039/d1an00643f.

[94] S. Koen, J. Vandenbussche, R. ’t Kindt, B. Claerebout, J. Op De Beeck, W. De Malsche, G. Desmet, P. Sandra, Evaluation of Micro-Pillar Array Columns (μPAC) Combined with High Resolution Mass Spectrometry for Lipidomics, LC-GC Eur. 30 (2017) 6–13.

[95] M. Baca, G. Desmet, H. Ottevaere, W. De Malsche, Achieving a Peak Capacity of 1800 Using an 8 m Long Pillar Array Column, Anal. Chem. 91 (2019) 10932–10936. https://doi.org/10.1021/acs.analchem.9b02236.

[96] S.M.C. Buckenmaier, D. V. McCalley, M.R. Euerby, Overloading study of bases using polymeric RP-HPLC columns as an aid to rationalization of overloading on silica-ODS phases, Anal. Chem. 74 (2002) 4672–4681. https://doi.org/10.1021/ac0202381.

[97] J. Dai, P.W. Carr, D. V. McCalley, A new approach to the determination of column overload characteristics in reversed-phase liquid chromatography, J. Chromatogr. A. 1216 (2009) 2474–2482. https://doi.org/10.1016/j.chroma.2009.01.036.

[98] D. Stoll, Essentials of LC Troubleshooting, Part III: Those Peaks Don’t Look Right, LCGC North Am. 40 (2022) 244–247. https://cdn.sanity.io/files/0vv8moc6/chroma/a7cf53ca3dda905e53ceda130c31ada43ea0a722.pdf.

[99] T. Hetzel, C. vom Eyser, J. Tuerk, T. Teutenberg, T.C. Schmidt, Micro-liquid chromatography mass spectrometry for the analysis of antineoplastic drugs from wipe samples, Anal. Bioanal. Chem. 408 (2016) 8221–8229. https://doi.org/10.1007/s00216-016-9932-y.

[100] A. Mpupa, S.K. Selahle, B. Mizaikoff, P.N. Nomngongo, Recent advances in solid-phase extraction (Spe) based on molecularly imprinted polymers (mips) for analysis of hormones, Chemosensors. 9 (2021). https://doi.org/10.3390/chemosensors9070151.

[101] C. Thoben, T. Werres, I. Henning, P.R. Simon, S. Zimmermann, T.C. Schmidt, T. Teutenberg, Towards a miniaturized on-site nano-high performance liquid chromatography electrospray ionization ion mobility spectrometer with online enrichment, Green Anal. Chem. 1 (2022) 100011. https://doi.org/10.1016/j.greeac.2022.100011.

[102] F. Busetti, W.J. Backe, N. Bendixen, U. Maier, B. Place, W. Giger, J.A. Field, Trace analysis of environmental matrices by large-volume injection and liquid chromatography-mass spectrometry, Anal. Bioanal. Chem. 402 (2012) 175–186. https://doi.org/10.1007/s00216-011-5290-y.

[103] V. Pepermans, M.T. Rerick, B. Degreef, S. Eeltink, S.G. Weber, G. Desmet, Column-in-valve designs to minimize extra-column volumes, J. Chromatogr. A. 1637 (2021) 461779. https://doi.org/https://doi.org/10.1016/j.chroma.2020.461779.

[104] J.B. Quintana, M. Miro, J.M. Estela, V. Cerdà, Automated on-line renewable solid-phase extraction-liquid chromatography exploiting multisyringe flow injection-bead injection lab-on-valve analysis, Anal. Chem. 78 (2006) 2832–2840. https://doi.org/10.1021/ac052256z.

[105] R.E. Wilson, S.R. Groskreutz, S.G. Weber, Improving the Sensitivity, Resolution, and Peak Capacity of Gradient Elution in Capillary Liquid Chromatography with Large-Volume Injections by Using Temperature-Assisted On-Column Solute Focusing, Anal. Chem. 88 (2016) 5112–5121. https://doi.org/10.1021/acs.analchem.5b04793.

[106] R.E. Kopec, R.M. Schweiggert, K.M. Riedl, R. Carle, S.J. Schwartz, Comparison of high-performance liquid chromatography/tandem mass spectrometry and high-performance liquid chromatography/photo-diode array detection for the quantitation of carotenoids, retinyl esters, α-tocopherol and phylloquinone in chylomicron-rich fr, Rapid Commun. Mass Spectrom. 27 (2013) 1393–1402. https://doi.org/10.1002/rcm.6576.

[107] M. Dams, J.L. Dores-Sousa, R.J. Lamers, A. Treumann, S. Eeltink, High-Resolution Nano-Liquid Chromatography with Tandem Mass Spectrometric Detection for the Bottom-Up Analysis of Complex Proteomic Samples, Chromatographia. 82 (2019) 101–110. https://doi.org/10.1007/s10337-018-3647-5.

[108] H. Wang, P. Bennett, Performance assessment of microflow LC combined with high-resolution MS in bioanalysis, Bioanalysis. 5 (2013) 1249–1267. https://doi.org/10.4155/bio.13.93.

[109] J. Alcántara-Durán, D. Moreno-González, B. Gilbert-López, A. Molina-Díaz, J.F. García-Reyes, Matrix-effect free multi-residue analysis of veterinary drugs in food samples of animal origin by nanoflow liquid chromatography high resolution mass spectrometry, Food Chem. 245 (2018) 29–38. https://doi.org/https://doi.org/10.1016/j.foodchem.2017.10.083.

[110] A.A.M. Heemskerk, J.M. Busnel, B. Schoenmaker, R.J.E. Derks, O. Klychnikov, P.J. Hensbergen, A.M. Deelder, O.A. Mayboroda, Ultra-low flow electrospray ionization-mass spectrometry for improved ionization efficiency in phosphoproteomics, Anal. Chem. 84 (2012) 4552–4559. https://doi.org/10.1021/ac300641x.

[111] T. Hetzel, Characterization of micro liquid chromatography - theoretical performance limits and practical aspects for routine analysis on the example of cytotoxic drugs, 2017.

[112] J. Alexander Harrison, A. Pruška, I. Oganesyan, P. Bittner, R. Zenobi, Temperature-Controlled Electrospray Ionization: Recent Progress and Applications, Chem. - A Eur. J. 27 (2021) 18015–18028. https://doi.org/10.1002/chem.202102474.

[113] S. Vainauskas, H. Guntz, E. McLeod, C. McClung, C. Ruse, X. Shi, C.H. Taron, A Broad-Specificity O-Glycoprotease That Enables Improved Analysis of Glycoproteins and Glycopeptides Containing Intact Complex O-Glycans, Anal. Chem. 94 (2022) 1060–1069. https://doi.org/10.1021/acs.analchem.1c04055.

[114] N. Wanner, G. Andrieux, P. Badia-i-Mompel, C. Edler, S. Pfefferle, M.T. Lindenmeyer, C. Schmidt-Lauber, J. Czogalla, M.N. Wong, Y. Okabayashi, F. Braun, M. Lütgehetmann, E. Meister, S. Lu, M.L.M. Noriega, T. Günther, A. Grundhoff, N. Fischer, H. Bräuninger, D. Lindner, D. Westermann, F. Haas, K. Roedl, S. Kluge, M.M. Addo, S. Huber, A.W. Lohse, J. Reiser, B. Ondruschka, J.P. Sperhake, J. Saez-Rodriguez, M. Boerries, S.S. Hayek, M. Aepfelbacher, P. Scaturro, V.G. Puelles, T.B. Huber, Molecular consequences of SARS-CoV-2 liver tropism, Nat. Metab. 4 (2022) 310–319. https://doi.org/10.1038/s42255-022-00552-6.

[115] T. Werres, T.C. Schmidt, T. Teutenberg, Peak broadening caused by using different micro–liquid chromatography detectors, Anal. Bioanal. Chem. (2022) 6107–6114. https://doi.org/10.1007/s00216-022-04170-9.

[116] J.J. Stankovich, F. Gritti, P.G. Stevenson, G. Guiochon, The impact of column connection on band broadening in very high pressure liquid chromatography, J. Sep. Sci. 36 (2013) 2709–2717. https://doi.org/10.1002/jssc.201300175.

[117] M. Noga, F. Sucharski, P. Suder, J. Silberring, A practical guide to nano-LC troubleshooting, J. Sep. Sci. 30 (2007) 2179–2189. https://doi.org/10.1002/jssc.200700225.

[118] J.W. Dolan, Mobile-Phase Degassing: What, Why, and How, LCGC North Am. 32 (2014) 482–487.

[119] A. Prüß, C. Kempter, J. Gysler, T. Jira, Extracolumn band broadening in capillary liquid chromatography, J. Chromatogr. A. 1016 (2003) 129–141. https://doi.org/https://doi.org/10.1016/S0021-9673(03)01290-1.

[120] J.J. Kirkland, W.W. Yau, H.J. Stoklosa, C.H. Dilks, Sampling and extra-column effects in high-performance liquid chromatography; influence of peak skew on plate count calculations, J. Chromatogr. Sci. 15 (1977) 303–316. https://doi.org/10.1093/chromsci/15.8.303.

[121] T. Hetzel, D. Loeker, T. Teutenberg, T.C. Schmidt, Characterization of the efficiency of microbore liquid chromatography columns by van Deemter and kinetic plot analysis, J. Sep. Sci. 39 (2016) 3889–3897. https://doi.org/10.1002/jssc.201600775.

[122] K. Vanderlinden, K. Broeckhoven, Y. Vanderheyden, G. Desmet, Effect of pre- and post-column band broadening on the performance of high-speed chromatography columns under isocratic and gradient conditions, J. Chromatogr. A. 1442 (2016) 73–82. https://doi.org/10.1016/j.chroma.2016.03.016.

[123] G. Desmet, K. Broeckhoven, Extra-column band broadening effects in contemporary liquid chromatography: Causes and solutions, TrAC - Trends Anal. Chem. 119 (2019) 115619. https://doi.org/10.1016/j.trac.2019.115619.

[124] F. Gritti, I. Leonardis, D. Shock, P. Stevenson, A. Shalliker, G. Guiochon, Performance of columns packed with the new shell particles, Kinetex-C18, J. Chromatogr. A. 1217 (2010) 1589–1603. https://doi.org/https://doi.org/10.1016/j.chroma.2009.12.079.

[125] J. Van Schoors, K. Maes, Y. Van Wanseele, K. Broeckhoven, A. Van Eeckhaut, Miniaturized ultra-high performance liquid chromatography coupled to electrochemical detection: Investigation of

system performance for neurochemical analysis, J. Chromatogr. A. 1427 (2016) 69–78. https://doi.org/https://doi.org/10.1016/j.chroma.2015.11.076.

[126] Y. Vanderheyden, K. Broeckhoven, G. Desmet, Comparison and optimization of different peak integration methods to determine the variance of unretained and extra-column peaks, J. Chromatogr. A. 1364 (2014) 140–150. https://doi.org/https://doi.org/10.1016/j.chroma.2014.08.066.

[127] A.J. Alexander, T.J. Waeghe, K.W. Himes, F.P. Tomasella, T.F. Hooker, Modifying conventional high-performance liquid chromatography systems to achieve fast separations with Fused-Core columns: A case study, J. Chromatogr. A. 1218 (2011) 5456–5469. https://doi.org/https://doi.org/10.1016/j.chroma.2011.06.026.

[128] A.C. Sanchez, J.A. Anspach, T. Farkas, Performance optimizing injection sequence for minimizing injection band broadening contributions in high efficiency liquid chromatographic separations, J. Chromatogr. A. 1228 (2012) 338–348. https://doi.org/https://doi.org/10.1016/j.chroma.2012.01.038.

[129] D. V McCalley, Instrumental considerations for the effective operation of short, highly efficient fused-core columns. Investigation of performance at high flow rates and elevated temperatures, J. Chromatogr. A. 1217 (2010) 4561–4567. https://doi.org/https://doi.org/10.1016/j.chroma.2010.04.070.

[130] F. Gritti, S.J. Shiner, J.N. Fairchild, G. Guiochon, Evaluation of the kinetic performance of new prototype 2.1mm×100mm narrow-bore columns packed with 1.6μm superficially porous particles, J. Chromatogr. A. 1334 (2014) 30–43. https://doi.org/https://doi.org/10.1016/j.chroma.2014.01.065.

[131] G. Desmet, K. Broeckhoven, Extra-column band broadening effects in contemporary liquid chromatography: Causes and solutions, TrAC Trends Anal. Chem. 119 (2019) 115619. https://doi.org/https://doi.org/10.1016/j.trac.2019.115619.

[132] F. Gritti, M. Gilar, Impact of frit dispersion on gradient performance in high-throughput liquid chromatography, J. Chromatogr. A. 1591 (2019) 110–119. https://doi.org/https://doi.org/10.1016/j.chroma.2019.01.021.

[133] S.M. Piraino, J.G. Dorsey, Comparison of frits used in the preparation of packed capillaries for capillary electrochromatography, Anal. Chem. 75 (2003) 4292–4296. https://doi.org/10.1021/ac026314h.

[134] A. Schultze-Jena, M.A. Boon, P.J.T. Bussmann, A.E.M. Janssen, A. van der Padt, The counterintuitive role of extra-column volume in the determination of column efficiency and scaling of chromatographic processes, J. Chromatogr. A. 1493 (2017) 49–56. https://doi.org/10.1016/j.chroma.2017.02.068.

[135] K. Vanderlinden, G. Desmet, K. Broeckhoven, Effect of the feed injection method on band broadening in analytical supercritical fluid chromatography, J. Chromatogr. A. 1630 (2020) 461525. https://doi.org/https://doi.org/10.1016/j.chroma.2020.461525.

[136] D.A. Vargas Medina, E.V.S. Maciel, A.L. de Toffoli, F.M. Lanças, Miniaturization of liquid chromatography coupled to mass spectrometry.: 2. Achievements on modern instrumentation for miniaturized liquid chromatography coupled to mass spectrometry, TrAC Trends Anal. Chem. 128 (2020) 115910. https://doi.org/https://doi.org/10.1016/j.trac.2020.115910.

[137] M.C. May, D.C. Pavone, I.S. Lurie, The separation and identification of synthetic cathinones by portable low microflow liquid chromatography with dual capillary columns in series and dual wavelength ultraviolet detection, J. Sep. Sci. 43 (2020) 3756–3764. https://doi.org/10.1002/jssc.202000767.

[138] Y. Li, P.N. Nesterenko, B. Paull, R. Stanley, M. Macka, Performance of a New 235 nm UV-LED-Based On-Capillary Photometric Detector, Anal. Chem. 88 (2016) 12116–12121. https://doi.org/10.1021/acs.analchem.6b02832.

[139] G.E. Moore, Cramming more components onto integrated circuits With unit cost, Electronics. 38 (1965) 114. https://newsroom.intel.com/wp-content/uploads/sites/11/2018/05/moores-law-electronics.pdf.

[140] J. Shalf, The future of computing beyond Moore ' s Law Subject Areas :, Philos. Trans. R. Soc. 378 (2020) 1–14.

[141] Ericsson Mobility Report June 2022, (2022).

[142] Microflow Liquid Chromatography Mass Spectrometry System Nexera Mikro, (2020) 6.

[143] C.A. Burtis, The determination of the base composition of rna by high-pressure cation-exchange chromatography, J. Chromatogr. A. 51 (1970) 183–194. https://doi.org/https://doi.org/10.1016/S0021-9673(01)96853-0.

[144] J.J. Kirkland, A High-Performance Ultraviolet Photometric Detector for Use with Efficient Liquid Chromatographic Columns, Anal. Chem. 40 (1968) 391–396. https://doi.org/10.1021/ac60258a024.

[145] M. Szumski, B. Buszewski, State of the Art in Miniaturized Separation Techniques, Crit. Rev. Anal. Chem. 32 (2002) 1–46. https://doi.org/10.1080/10408340290765434.

[146] Global Footprint Network, (n.d.). https://www.footprintnetwork.org/resources/glossary/.

[147] M. Grömling, T. Hentze, H. Schäfer, Wirtschaftliche Auswirkungen der Corona-Pandemie in Deutschland, IW-Trends. 49 (2022).

[148] K. Das, R.L. Behera, B. Paital, CHAPTER 8 - Socio-economic impact of COVID-19, in: D. Rawtani, C.M. Hussain, N.B.T.-C.-19 in the E. Khatri (Eds.), Elsevier, 2022: pp. 153–190. https://doi.org/https://doi.org/10.1016/B978-0-323-90272-4.00014-2.

[149] S. Dangendorf, C. Hay, F.M. Calafat, M. Marcos, C.G. Piecuch, K. Berk, J. Jensen, Persistent acceleration in global sea-level rise since the 1960s, Nat. Clim. Chang. 9 (2019) 705–710. https://doi.org/10.1038/s41558-019-0531-8.

[150] J. Hansen, M. Sato, R. Ruedy, P. Kharecha, A. Lacis, R. Miller, L. Nazarenko, K. Lo, G.A. Schmidt, G. Russell, I. Aleinov, S. Bauer, E. Baum, B. Cairns, V. Canuto, M. Chandler, Y. Cheng, A. Cohen, A. Del Genio, G. Faluvegi, E. Fleming, A. Friend, T. Hall, C. Jackman, J. Jonas, M. Kelley, N.Y. Kiang, D. Koch, G. Labow, J. Lerner, S. Menon, T. Novakov, V. Oinas, J. Perlwitz, J. Perlwitz, D. Rind, A. Romanou, R. Schmunk, D. Shindell, P. Stone, S. Sun, D. Streets, N. Tausnev, D. Threshe, N. Unger, M. Yao, S. Zhang, Dangerous human-made interference with climate: A GISS modelE study, Atmos. Chem. Phys. 7 (2007) 2287–2312. https://doi.org/10.5194/acp-7-2287-2007.

[151] J. Hansen, Defusing the Global Warming TIME BOMB, Sci. Am. 290 (2004) 68–77.

[152] J.Y. Fang, J.L. Zhu, S.P. Wang, C. Yue, H.H. Shen, Global warming, human-induced carbon emissions, and their uncertainties, Sci. China Earth Sci. 54 (2011) 1458–1468. https://doi.org/10.1007/s11430-011-4292-0.

[153] L. Whitmarsh, What's in a name? Commonalities and differences in public understanding of climate change and global warming, Public Underst. Sci. 18 (2009) 401–420. https://doi.org/10.1177/0963662506073088.

[154] B. Dahal, S.A.P. Kumar, Z. Li, Topic modeling and sentiment analysis of global climate change tweets, Soc. Netw. Anal. Min. 9 (2019) 1–20. https://doi.org/10.1007/s13278-019-0568-8.

[155] P. Beckh, A. Limmer, The Fridays for Future Phenomenon BT - Strategies for Sustainability of the Earth System, in: P.A. Wilderer, M. Grambow, M. Molls, K. Oexle (Eds.), Springer International Publishing, Cham, 2022: pp. 427–432. https://doi.org/10.1007/978-3-030-74458-8_28.

[156] C. Hickman, E. Marks, P. Pihkala, S. Clayton, R.E. Lewandowski, E.E. Mayall, B. Wray, C. Mellor, L. van Susteren, Climate anxiety in children and young people and their beliefs about government responses to climate change: a global survey, Lancet Planet. Heal. 5 (2021) e863–e873. https://doi.org/10.1016/S2542-5196(21)00278-3.

[157] P.T. Anastas, J.C. Warner, Green Chemistry: Theory and Practice, Oxford University Press, New York, 1998.

[158] A. Gałuszka, Z. Migaszewski, J. Namieśnik, The 12 principles of green analytical chemistry and the SIGNIFICANCE mnemonic of green analytical practices, TrAC Trends Anal. Chem. 50 (2013) 78–84. https://doi.org/https://doi.org/10.1016/j.trac.2013.04.010.

[159] M. Marinas, E. Sa, M.M. Rojas, M. Moalem, F.J. Urbano, C. Guillou, L. Rallo, Assessment of acetone as an alternative to acetonitrile in peptide analysis by liquid chromatography/mass spectrometry, Rapid Commun. Mass Spectrom. 23 (2010) 1457–1466. https://doi.org/10.1002/rcm.

[160] R.E. Majors, The Continuing Acetonitrile Shortage: How to Combat it or Live with It, LCGC North Am. 27 (2009) 458–471.

[161] F. Brettschneider, V. Jankowski, T. Günthner, S. Salem, M. Nierhaus, A. Schulz, W. Zidek, J. Jankowski, Replacement of acetonitrile by ethanol as solvent in reversed phase chromatography of biomolecules, J. Chromatogr. B. 878 (2010) 763–768. https://doi.org/https://doi.org/10.1016/j.jchromb.2010.01.029.

[162] International Energy Agency, Gas Market Report, 2022.

[163] D. Cespi, F. Passarini, E. Neri, I. Vassura, L. Ciacci, F. Cavani, Life Cycle Assessment comparison of two ways for acrylonitrile production: the SOHIO process and an alternative route using propane, J. Clean. Prod. 69 (2014) 17–25. https://doi.org/https://doi.org/10.1016/j.jclepro.2014.01.057.

[164] D.Y. Lee, A. Elgowainy, By-product hydrogen from steam cracking of natural gas liquids (NGLs): Potential for large-scale hydrogen fuel production, life-cycle air emissions reduction, and economic benefit, Int. J. Hydrogen Energy. 43 (2018) 20143–20160. https://doi.org/10.1016/j.ijhydene.2018.09.039.

[165] International Energy Agency, Electricity Market Report, 2022. https://www.iea.org/reports/electricity-market-report-january-2022.

[166] P. Rebehn, C. Lüttmann, Der unterschätzte Wert der Laborluft, (2020). https://www.laborpraxis.vogel.de/der-unterschaetzte-wert-der-laborluft-a-977652/.

[167] Bundesanstalt für Arbeitsschutz und Arbeitsmedizin, TRGS 526 Laboratorien, 2008.

[168] A.J. Oswald, E. Proto, D. Sgroi, Happiness and productivity, J. Labor Econ. 33 (2015) 789–822. https://doi.org/10.1086/681096.

[169] L. Fauver, M.B. McDonald, A.G. Taboada, Does it pay to treat employees well? International evidence on the value of employee-friendly culture, J. Corp. Financ. 50 (2018) 84–108. https://doi.org/https://doi.org/10.1016/j.jcorpfin.2018.02.003.

[170] A. Ishida, M. Fujii, T. Fujimoto, S. Sasaki, I. Yanagisawa, H. Tani, M. Tokeshi, A portable liquid chromatograph with a battery-operated compact electroosmotic pump and a microfluidic chip device with a reversed phase packed column, Anal. Sci. 31 (2015) 1163–1169. https://doi.org/10.2116/analsci.31.1163.

[171] M.A. Stravs, C. Stamm, C. Ort, H. Singer, Transportable Automated HRMS Platform "MS2field" Enables Insights into Water-Quality Dynamics in Real Time, Environ. Sci. Technol. Lett. 8 (2021) 373–380. https://doi.org/10.1021/acs.estlett.1c00066.

[172] F. Rahimi, S. Chatzimichail, A. Saifuddin, A.J. Surman, S.D. Taylor-Robinson, A. Salehi-Reyhani, A Review of Portable High-Performance Liquid Chromatography: the Future of the Field?, Springer Berlin Heidelberg, 2020. https://doi.org/10.1007/s10337-020-03944-6.

[173] J.P. Zhang, A. Chitnis, V. Adivarahan, S. Wu, V. Mandavilli, R. Pachipulusu, M. Shatalov, G. Simin, J.W. Yang, M. Asif Khan, Milliwatt power deep ultraviolet light-emitting diodes over sapphire with emission at 278 nm, Appl. Phys. Lett. 81 (2002) 4910–4912. https://doi.org/10.1063/1.1531835.

[174] T. Nishida, H. Saito, N. Kobayashi, Submilliwatt operation of AlGaN-based ultraviolet light-emitting diode using short-period alloy superlattice, Appl. Phys. Lett. 78 (2001) 399–400. https://doi.org/10.1063/1.1338964.

[175] J.C. Carrano, A.J. Maltenfort, Semiconductor ultraviolet optical sources for biological agent detection, in: Proc.SPIE, 2002. https://doi.org/10.1117/12.448517.

[176] S. Sharma, A. Plistil, H.E. Barnett, H.D. Tolley, P.B. Farnsworth, S.D. Stearns, M.L. Lee, Hand-Portable Gradient Capillary Liquid Chromatography Pumping System, Anal. Chem. 87 (2015) 10457–10461. https://doi.org/10.1021/acs.analchem.5b02583.

[177] S. Chatzimichail, D. Casey, A. Salehi-Reyhani, Zero electrical power pump for portable high-performance liquid chromatography, Analyst. 144 (2019) 6207–6213. https://doi.org/10.1039/c9an01302d.

[178] A. Chen, K.B. Lynch, X. Wang, J.J. Lu, C. Gu, S. Liu, Incorporating high-pressure electroosmotic pump and a nano-flow gradient generator into a miniaturized liquid chromatographic system for peptide analysis, Anal. Chim. Acta. 844 (2014) 90–98. https://doi.org/https://doi.org/10.1016/j.aca.2014.06.042.

[179] S. Chatzimichail, F. Rahimi, A. Saifuddin, A.J. Surman, S.D. Taylor-Robinson, A. Salehi-Reyhani, Hand-portable HPLC with broadband spectral detection enables analysis of complex polycyclic aromatic hydrocarbon mixtures, Commun. Chem. 4 (2021). https://doi.org/10.1038/s42004-021-00457-7.

[180] M. Pham, S.W. Foster, S. Kurre, R.A. Hunter, J.P. Grinias, Use of Portable Capillary Liquid Chromatography for Common Educational Demonstrations Involving Separations, J. Chem. Educ. 98 (2021) 2444–2448. https://doi.org/10.1021/acs.jchemed.1c00342.

[181] S.W. Foster, X. Xie, J.M. Hellmig, G. Moura-Letts, W.R. West, M.L. Lee, J.P. Grinias, Online monitoring of small volume reactions using compact liquid chromatography instrumentation, Sep. Sci. PLUS. 5 (2022) 213–219. https://doi.org/https://doi.org/10.1002/sscp.202200012.

[182] S.K. Piendl, D. Geissler, L. Weigelt, D. Belder, Multiple Heart-Cutting Two-Dimensional Chip-HPLC Combined with Deep-UV Fluorescence and Mass Spectrometric Detection, Anal. Chem. 92 (2020) 3795–3803. https://doi.org/10.1021/acs.analchem.9b05206.

[183] S.K. Piendl, C.R. Raddatz, N.T. Hartner, C. Thoben, R. Warias, S. Zimmermann, D. Belder, 2D in Seconds: Coupling of Chip-HPLC with Ion Mobility Spectrometry, Anal. Chem. 91 (2019) 7613–7620. https://doi.org/10.1021/acs.analchem.9b00302.

[184] B. Wouters, E. Davydova, S. Wouters, G. Vivo-Truyols, P.J. Schoenmakers, S. Eeltink, Towards ultra-high peak capacities and peak-production rates using spatial three-dimensional liquid chromatography, Lab Chip. 15 (2015) 4415–4422. https://doi.org/10.1039/C5LC01169H.

[185] X. Yuan, R.D. Oleschuk, Advances in Microchip Liquid Chromatography, Anal. Chem. 90 (2018) 283–301. https://doi.org/10.1021/acs.analchem.7b04329.

[186] P.N. Nge, C.I. Rogers, A.T. Woolley, Advances in Microfluidic Materials, Functions, Integration, and Applications, Chem. Phys. 113 (2013) 2550–2583.

[187] D. Bodas, C. Khan-Malek, Formation of more stable hydrophilic surfaces of PDMS by plasma and chemical treatments, Microelectron. Eng. 83 (2006) 1277–1279. https://doi.org/https://doi.org/10.1016/j.mee.2006.01.195.

[188] A.T. Giannitsis, Microfabrication of biomedical lab-on-chip devices. A review, Est. J. Eng. 17 (2011) 109–139. https://doi.org/10.3176/eng.2011.2.03.

[189] J. Liu, C. Hansen, S.R. Quake, Solving the "world-to-chip" interface problem with a microfluidic matrix, Anal. Chem. 75 (2003) 4718–4723. https://doi.org/10.1021/ac0346407.

[190] S. van den Driesche, F. Lucklum, F. Bunge, M.J. Vellekoop, 3D printing solutions for microfluidic chip-to-world connections, Micromachines. 9 (2018) 1–12. https://doi.org/10.3390/mi9020071.

[191] M. Carve, D. Wlodkowic, 3D-printed chips: Compatibility of additive manufacturing photopolymeric substrata with biological applications, Micromachines. 9 (2018). https://doi.org/10.3390/mi9020091.

[192] U. Kalsoom, P.N. Nesterenko, B. Paull, Current and future impact of 3D printing on the separation sciences, TrAC Trends Anal. Chem. 105 (2018) 492–502. https://doi.org/https://doi.org/10.1016/j.trac.2018.06.006.

[193] J. del Barrio, C. Sánchez-Somolinos, Light to Shape the Future: From Photolithography to 4D Printing, Adv. Opt. Mater. 7 (2019). https://doi.org/10.1002/adom.201900598.

[194] B. Kelly, I. Bhattacharya, M. Shusteff, R.M. Panas, H.K. Taylor, C.M. Spadaccini, Computed Axial Lithography (CAL): Toward Single Step 3D Printing of Arbitrary Geometries, (2017). http://arxiv.org/abs/1705.05893.

[195] European Research Council, Separation Technology for A Million Peaks, (2016) 1–4. https://doi.org/10.3030/694151.

[196] C. Salmean, S. Dimartino, 3D-Printed Stationary Phases with Ordered Morphology: State of the Art and Future Development in Liquid Chromatography, Chromatographia. 82 (2019) 443–463. https://doi.org/10.1007/s10337-018-3671-5.

Chapter 2 Aims & Scope

In the introduction, an overview of the current state of cLC was given, but at the same time existing shortcomings in the current literature were pointed out and reference was made to the own research of this thesis. Besides, it was made evident that there is a discrepancy between the manifold advantages of the technology and the actual range of application in present-day instrumental analytics. The thesis pursues three main aims: the characterization and quantification of the influence of different components of cLC on peak broadening, thereby a reduction of the entry barriers for the utilization of miniaturized systems and the application of the obtained knowledge for the development of new miniaturized separation systems and stationary phases. With the defined goals, the thesis can be differentiated into two main parts, the research consisting of Chapters 3-5 and the developments covered in Chapters 6-7.

In **Chapter 3**, the focus was on a major shortcoming of cLC, the loadability of the stationary phase. The investigation was conducted extensively for isocratic and gradient separations. The goal was to quantify the major influencing factor of pre-column band broadening and to derive simple guidelines to reduce the influence of the injection volume on the overall performance of the cLC.

While pre-column band broadening can be partially negated by focusing on the separation column, this is not the case for post-column band broadening. By defining the parameters in the previous chapter, a comprehensive investigation of commercial cLC detectors was carried out in **Chapter 4**. This enabled the quantification of the influence of detector designs on the band broadening, and thus one of the greatest negative factors influencing chromatographic efficiency.

Chapter 5 explores the influence of the relationship between extra-column volume and the effective-column volume on the efficiency. The focus of the investigations was on the 1.0 mm ID columns, which represent the cross-over between cLC and conventional LC.

Chapter 6 exploited the advantage that only small amounts of stationary phase are required for the preparation of a cLC separation column in order to promote the effective and cost-efficient development of new stationary separation phases based on bead cellulose.

Finally, the insights achieved in **Chapters 3-5** were used to develop a novel system in form of a portable device for on-site detection of pollutants in aqueous matrices based on online enrichment nano-HPLC ESI-IMS in **Chapter 7**. The scope and structure of the thesis is shown in Figure 2-1.

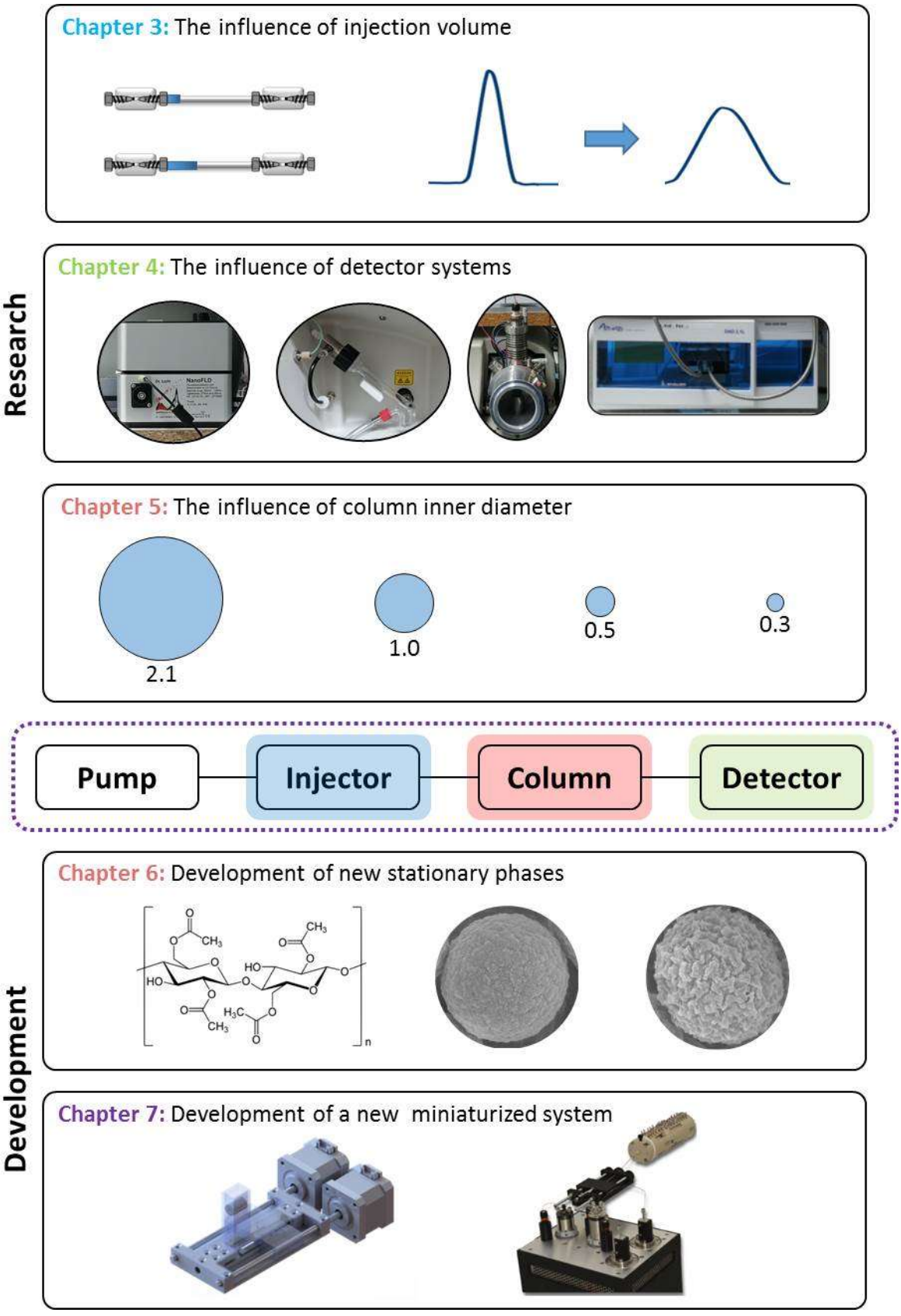

Figure 2-1: Graphical overview of the major content of this work.

Chapter 3 The influence of injection volume on efficiency of microbore liquid chromatography columns for gradient and isocratic elution

This chapter was adapted from: T. Werres, T.C. Schmidt, T. Teutenberg, The influence of injection volume on efficiency of microbore liquid chromatography columns for gradient and isocratic elution, J. Chromatogr. A. 1641 (2021) 461965. https://doi.org/10.1016/j.chroma.2021.461965.

Abstract: The injection volume and the associated column volume overload is one of the most common issues in miniaturized chromatography. The injection volume should not exceed 10% of the effective column volume. A further reduction of the injection volume leads to an increase in chromatographic efficiency. However, the signal intensity must be above a certain threshold to reach the ideal balance between chromatographic efficiency and sensitivity. This study examined the general influence of the injection volume for both isocratic and gradient elution, depending on the retention factor and peak standard deviation. For this purpose, substances of different polarity were selected to represent a broad elution spectrum. Besides the model analyte naphthalene, these were mainly pharmaceuticals. For all measurements a microbore column with an ID of 300 µm and packed with 1.9 µm fully porous particles was used. For isocratic elution, the injection volume was varied between 4 and 16% of the effective column volume. The retention factors were adjusted between 2 and 10. For gradient elution, the injection volume was varied between 4 and 160% of the effective column volume. The observed effects were further investigated using the gradient kinetic plot theory. In isocratic elution, a loss in plate height up to 50% was observed for components that elute near the void time. A significant reduction of the chromatographic efficiency was noticed up to a retention factor of 4. In gradient elution, a reduction in peak capacity could only be observed if the injection volume exceeded 40% of the effective column volume. For some substances, only a slight loss in peak capacity was noticed even with a volume overload of 160%.

3.1 Introduction

The requirements for chromatographic methods in analytical chemistry are becoming increasingly complex [1, 2]. The number of samples and substances to be analyzed is also increasing every year, pushing routine laboratories to their capacity limits. In environmental analysis, for example, multi-analyte methods are becoming a common practice as they enable a significant increase in time efficiency and productivity [3, 4]. For the analysis of complex samples, an optimization for all target analytes is virtually impossible. Therefore, the optimal balance between signal intensity, sensitivity, chromatographic resolution of the individual compounds and cycle time of the analysis method must be found.

One possibility to analyze many samples in a short period of time is the miniaturization of chromatographic systems [5, 6]. Besides the significant reduction of solvent consumption, there are other advantages of miniaturized systems that make them superior to UHPLC in conventional dimensions [7]. By reducing the inner diameter (ID) of the separation column, higher linear velocities can be achieved for a given flow rate. Moreover, the influence of frictional heating can be almost neglected for miniaturized separation systems [5]. In UHPLC and SFC, frictional heating is a topic that has received much attention for chromatographic separation at very high pressures and has led to the development of new products, such as vacuum jacketed columns [8–10].

Miniaturized HPLC is widely used in areas where only a small sample volume is available. This includes but is not limited to health science and forensic applications [7, 11–13]. Despite these advantages, miniaturized LC systems have not yet been established broadly in routine laboratories. Apart from the users' prejudices regarding stability and reproducibility of the systems, the argument that miniaturized columns cannot be packed reproducibly has long been refuted [14, 15]. Nevertheless, one of the major issues is the small effective column volume. Due to the smaller column IDs and the resulting reduced column volume, peak broadening quickly occurs by column volume or mass overloading [11]. While volume overloading leads to a symmetrical peak broadening, mass overloading leads to a deviation from the Gaussian peak shape by changing the distribution constant between mobile and stationary phase [16].

Although mass spectrometry is a technology widely available, UV detection is still most prevalent in the pharmaceutical industry. However, UV detection has lower sensitivity when compared to MS detection. To counteract this, the injection volume is increased to meet sensitivity requirements but this is detrimental for resolution [17]. This is especially true for applications in the field of pharmaceutical screening.

Therefore, the aim of this study was to determine the general influence of the injection volume in microbore columns with an ID of 300 µm for both isocratic as well as gradient elution depending on the retention factor and peak variance. The focus of this study is on RP, the technique most commonly used in contemporary HPLC practice. For this purpose, substances of different polarity were selected to represent a broad elution spectrum. The samples were dissolved in a mobile phase that corresponded precisely either to the isocratic mobile phase or the starting conditions of the solvent gradient to avoid solvent effects that could diminish the chromatographic performance. The data were further analysed using the gradient kinetic plot theory.

3.2 Materials and Methods

3.2.1 Experimental Setup

The experiments were carried out on an Eksigent ExpressLC Ultra system (Sciex, Dublin, CA, USA). The system is equipped with a binary pneumatic pump that is able to generate a maximum pressure of 690 bar with a total dwell volume of 1,500 nL, excluding the sample loop. For sample loading, an HTS PAL autosampler (CTC Analytics, Zwingen, Switzerland) was used. Sample injection onto the column was carried out by the integrated six-port-two-position-valve and via external sample loops. For the isocratic experiments, a PEEKSil sample loop with dimensions of 75 µm×10 cm was installed. For gradient elution, the sample loops were constructed using fused silica (FS) capillaries (Postnova Analytics, Germany) with an outer diameter of 360 µm and an inner diameter of 100 µm. With the help of a diamond cutter, the capillaries were cut to the length required for the desired injection volumes. For data acquisition a 1260 Infinity II diode array detector WR (Agilent Technologies, California, USA) with a cell volume of 100 nL was used. A data acquisition rate of 40 Hz and spectral band width of 4 nm was chosen. A YMC-Triart C18 column with a length of 50 mm and an ID of 0.3 mm packed with fully porous 1.9 µm particles with a pore size of 120 Å was chosen (YMC Europe GmbH, Dinslaken, Germany). The column was heated to 50 °C using the built-in static air oven of the Eksigent ExpressLC Ultra system. The connection between the HPLC system, the column and the DAD was done with the shortest possible pre-cut PEEKSil capillaries with an inner diameter of 50 µm which corresponded to a total length of 50 cm.

3.2.2 Chemicals

LC-MS grade water and acetonitrile (ACN) were used as mobile phases and were purchased from Th. Geyer (Chemsolute, Renningen, Germany). To adjust the pH, formic acid (Sigma-

Aldrich, Seelze, Germany) was added to a total volume concentration of 0.1% to the mobile phase solvents. Acetone (Sigma-Aldrich, Seelze, Germany) was used to determine the gradient dwell volume. The model compounds selected in this study are listed in Table 3-1. Uracil was used to determine the column void time. The stock solution for every compound was prepared in equal volume percentages of ACN/H_2O with a concentration of 1 g L^{-1}. Each standard was dissolved in a solvent that corresponded precisely to the isocratic mobile phase or the starting conditions of the solvent gradient. In order to eliminate the effects of column mass overloading, the concentrations of the analytes were adjusted to the injection volume.

Table 3-1: Achieved minimum plate heights depending on the injection volume and retention factor. Compounds sorted by retention factor (k) including organic volume fraction (φ) and the effective column volume in %. All measurements were performed in triplicate.

compound	CAS number	M g mol^{-1}	purity %	provider	Log P	Gradient β ng	Isocratic β ng
uracil	66-22-8	112.09	≥ 99	Fluka	0.86	0.13	0.13
metronidazole	443-48-1	171.16	≥ 99	Sigma	-0.02	0.50	0.50
sotalol	3930-20-9	272.36	≥ 99	Dr. Ehrenstorfer	0.24	0.10	x
etoposide	33419-42-0	588.56	≥ 99	Sigma	0.60	0.10	0.50
carbamazepine	298-46-4	236.27	≥ 98	Sigma	2.45	0.10	0.50
acetylsalicylic acid	50-78-2	180.16	≥ 99	Sigma	1.19	0.10	0.50
naphthalene	91-20-3	128.17	≥ 99	Sigma	3.30	0.10	0.10

3.2.3 Variation of the Injection Volume

As a rule of thumb, the applied injection volume should not exceed 10% of the effective column volume, which can be calculated according to Equation 3-1 [18].

$$V_{c,eff} = r^2 \cdot \pi \cdot L \cdot \varepsilon_T \qquad \text{Equation 3-1}$$

where r is the column radius, L the column length and ε_T the total porosity.

A total porosity of 0.7 can be assumed for the used column resulting in an effective column volume of 2.47 µL [19]. The injection was done by the integrated six-port-two-position-valve which was operated in two different modes.

Using the metered injection mode, the sample loop is completely filled. Afterwards, the sample loop is switched into the flow path of the column for a defined time, depending on the flow rate of the mobile phase. After the defined volume has been transferred to the column, the sample loop is taken out of the flow path and the chromatographic run is started. In this way, the injection volume can be adapted without changing the sample loop. For the injection volumes of 400, 300, 200 and 100 nL the metered injection was used. To verify the reproducibility of the metered injection method, a series of replicate measurements (n=12) at a flow rate of 25 µL/min and an injection volume of 100 nL was performed (See Figure 3-6).

In the first step of the full-loop injection mode, the entire sample loop is filled by the syringe of the autosampler. Afterwards, the sample loop is switched into the flow path by switching the six-port-two-position-valve. The chromatographic run starts and the entire sample volume is transferred to the column. During the chromatographic run the sample loop remains in the flow path and is continuously flushed by the mobile phase. Thereby, it contributes fully to the gradient dwell volume. For the injection volumes of 4000, 3000, 2000 and 1000 nL the full-loop injection mode was used.

3.2.4 Isocratic and Gradient Measurements

For the isocratic measurements, five separate experiments were carried out. The flow rate was varied between 2 and 25 µL min^{-1}. In order to investigate the influence of the injection volume on the plate height depending on the retention factor independent of the substance, naphthalene was selected as model analyte. The van Deemter analysis was performed for naphthalene at retention factors of 2, 4 and 10. The other analytes were measured in a mix solution with an organic volume fraction (φ) of 25% B. The minimum plate height of the very polar metronidazole was determined at an organic fraction of 5% B. The column void time (t_0) was determined using uracil at an organic fraction of 95% B. Afterwards, the column was replaced by a zero-dead volume (ZDV) union to correct for the system void time.

For the determination of the peak capacity, the flow rate was varied between 5 and 25 µL min^{-1} in 5-µL steps using a linear gradient from 5% to 95% B. In order to make use of the gradient kinetic plot theory, it is necessary to keep the t_g/t_0 -ratio as well as the ratio between the gradient dwell time (t_d) and t_0 constant. The t_0 values were determined as described for the isocratic measurements. To determine t_d a ZDV was installed and solvent B was replaced with H_2O + 0.1% acetone to record the gradient profile. The resulting t_d was corrected by the volume of the connection capillary after the ZDV and the detector cell volume. The t_g/t_0-ratio was set

to 20. To account for the change in the dwell volume due to the exchange of the sample loops an additional isocratic plateau was programmed at the beginning of the chromatographic run. For the investigated flow rate ranges, the resulting t_g were between 2.33 and 7.00 min. The specific timetables for the gradient measurements can be found in Table 3-3. Isocratic and gradient measurements were performed in triplicate at a column temperature of 50 °C.

3.2.5 Software

Data acquisition was performed using Open LAB CDS Rev.C.0107.SR3 (Agilent Technologies, California, USA). Further data processing was performed using OriginPro 2019b (64-bit) 9.6.5.169 (OriginLab, Massachusetts, USA) and Microsoft Office Excel 2010.

3.3 Results and Discussion

3.3.1 Isocratic Measurements

Sufficient retention is required to achieve separation. According to the Purnell equation retention factors > 5 no longer lead to a significant increase in resolution [20]. Against this background, the elution strength of the mobile phase was selected to adjust the retention factor between 2 and 10 for all components investigated. The retention factor (k) was calculated according to Equation 3-2.

$$k = \frac{t_R - t_0}{t_0} \qquad \text{Equation 3-2}$$

The retention time (t_R) of the unretained marker uracil was used to determine the void time (t_0). The t_0 times were corrected for the system void time by replacing the column by a ZDV. The plate height H was chosen to calculate the efficiency which can be derived from the van Deemter equation (Equation 3-3). The van Deemter equation is a hyperbolic function in whose vertex the highest efficiency is achieved.

$$H = A + \frac{B}{u_0} + C * u_0 \qquad \text{Equation 3-3}$$

here, A is the eddy diffusion, B the longitudinal diffusion, C the mass transfer and u_0 the linear velocity.

H can be directly calculated from each individual peak in the chromatogram. In this study, it was calculated using the peak width at half height. Table 3-2 summarizes the results for the isocratic experiments.

Table 3-2: Achieved minimum plate heights depending on the injection volume and retention factor. Compounds sorted by retention factor (k) including organic volume fraction (φ) and the effective column volume in %. All measurements were performed in triplicate.

Compound	k	φ	H_{min} / µm 400 nL 16%	300 nL 12%	200 nL 8%	100 nL 4%
naphthalene	2.0	0.61	11.2 ± 0.2	7.4 ± 0.2	6.3 ± 0.2	5.3 ± 0.2
metronidazole	2.2	0.05	8.8 ± 0.2	7.2 ± 0.3	6.1 ± 0.2	5.6 ±0.1
acetylsalicylic acid	2.2	0.25	9.8 ± 0.5	8.2 ± 0.2	6.9 ± 0.1	6.0 ± 0.1
naphthalene	4.0	0.50	8.6 ± 0.2	8.2 ± 0.2	7.6 ± 0.2	7.2 ±0.2
etoposide	6.2	0.25	5.0 ± 0.2	5.1 ± 0.1	5.1 ± 0.1	4.7 ± 0.2
carbamazepine	8.3	0.25	5.2 ± 0.2	4.9 ± 0.1	4.8 ± 0.1	4.9 ± 0.2
naphthalene	10.0	0.40	6.3 ± 0.2	6.3 ± 0.2	6.3 ± 0.2	6.3 ± 0.2

The maximum standard deviations over all measuring points of the corresponding van Deemter plot are given in Table 3-2. A comparison of the H_{min} immediately reveals different trends. Sotalol could not be determined isocratically under the given chromatographic conditions because the peak shape strongly deviated from a Gaussian shape (See Figure 3-7). Up to a retention factor of 6.2 for etoposide, a reduction of H_{min} was observed by reducing the injection volume to 100 nL. For an injection volume of 300 nL an increase in H_{min} is only noticed up to a retention factor of 4. For an injection volume of 200 nL, a loss of efficiency is still observed for retention near the void time. The reason is the insufficient focusing of the early eluting compounds at the column head. For naphthalene at $k = 2.0$ as well as metronidazole and acetylsalicylic acid at $k = 2.2$, the loss in efficiency due to an increase in injection volume is most pronounced. A visual comparison of the van Deemter plots of metronidazole and carbamazepine, which represent an early and a late eluting compound, is illustrated in Figure 3-1.

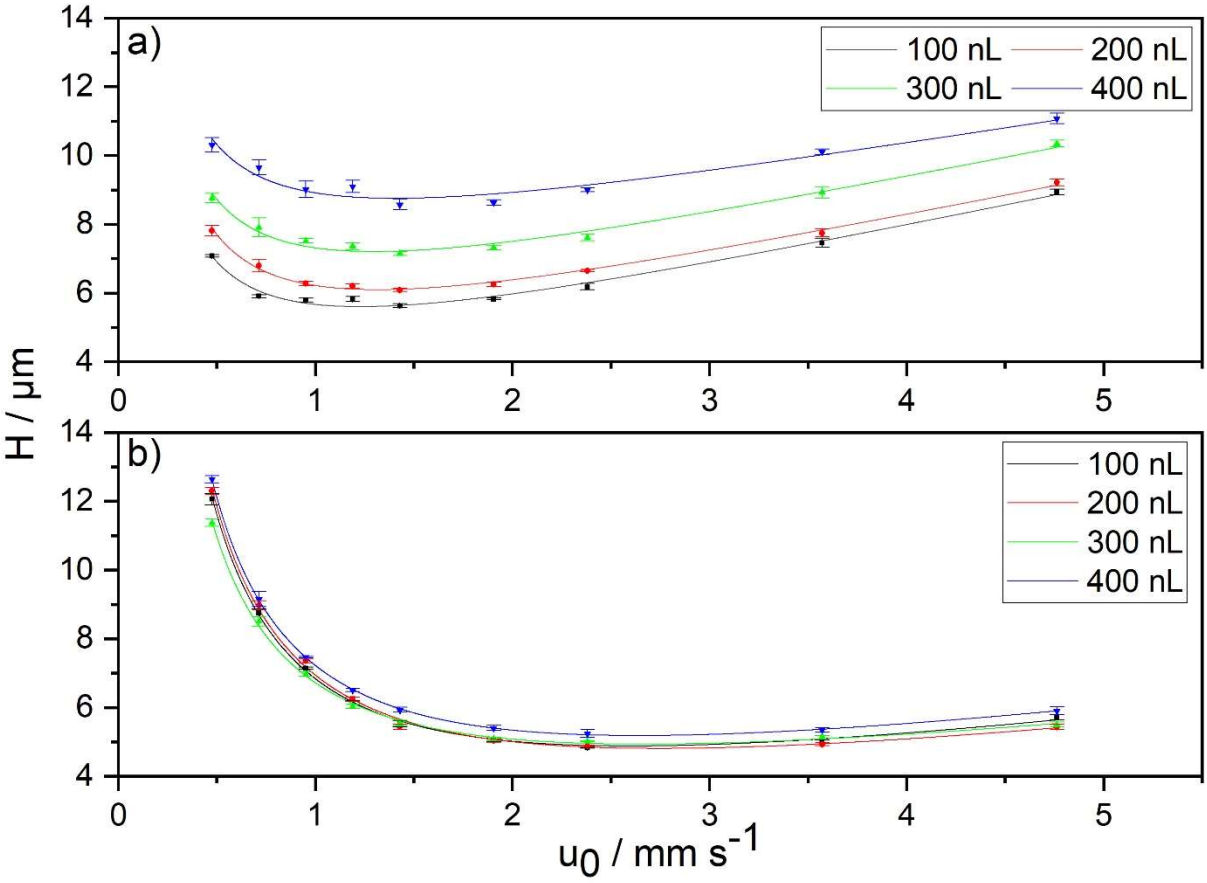

Figure 3-1: Van Deemter plots for A: metronidazole at a retention factor of 2.2 and B: carbamazepine at a retention factor of 8.3. Flow rate: 2 – 20 µL min^{-1}; mobile phase: 50% H2O + 0.1% FA; 50% ACN + 0.1% FA; column: YMC-Triart C18, 50 x 0.3 mm, 1.9 µm; temperature: 50 °C; detection: UV at 254 nm.

A reduction of H_{min} was observed for metronidazole with a retention factor of 2.2 if the injection volume is decreased from 400 nL to 100 nL. Furthermore, there is no linear relationship between the reduction of the injection volume and the reduction of H_{min} for metronidazole. The increase in efficiency is equivalent to a decrease in H_{min} of 22%, 18% and 9%, respectively. As mentioned above, carbamazepine only showed an increase by 6% at an injection volume of 400 nL. A reduction below 300 nL did not lead to a further increase in efficiency.

By examining the influence of the injection volume on the plate height at different retention factors for naphthalene, a substance-independent evaluation of the observed effect is possible. In Figure 3-2, the van Deemter curves for naphthalene are shown at a retention factor of 4 and 10.

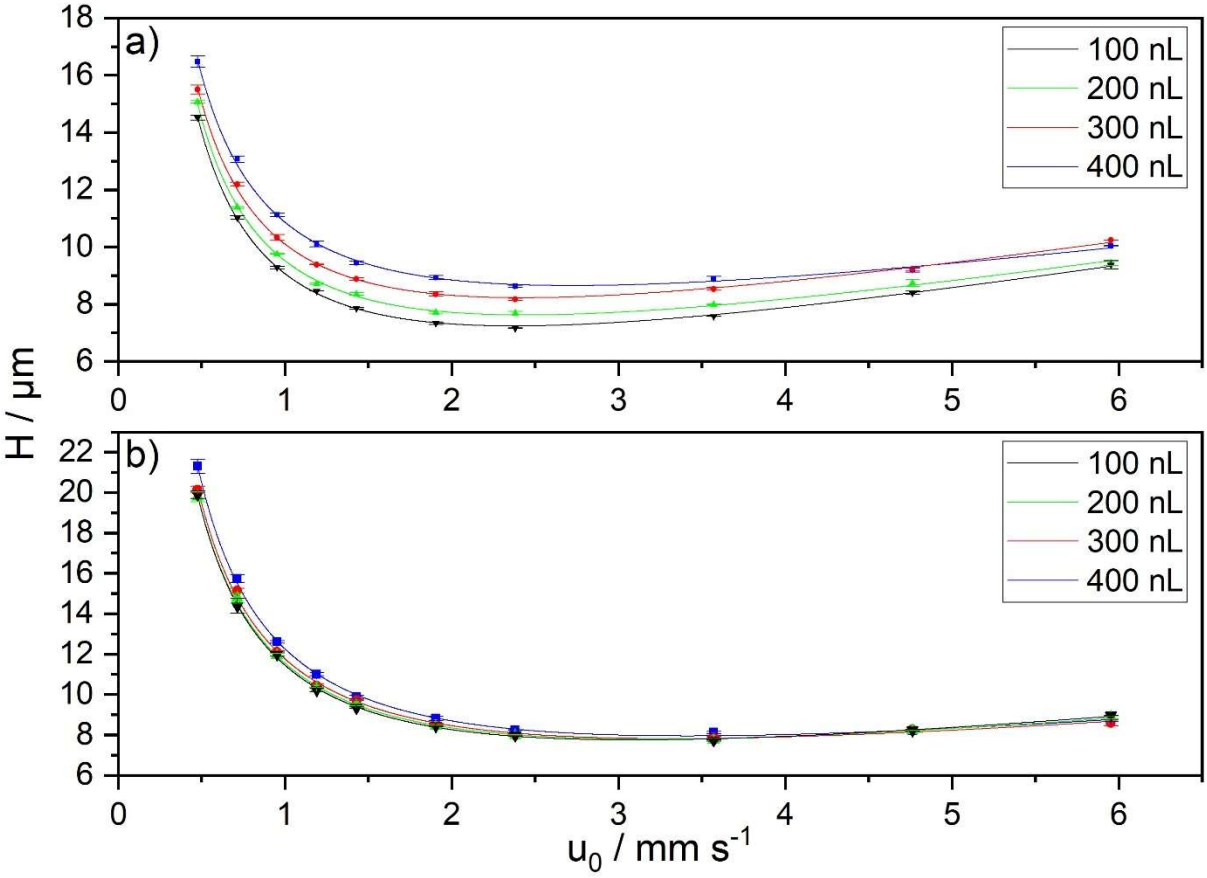

Figure 3-2: Van Deemter plots for a: naphthalene at a retention factor of 4.0 and b: naphthalene at a retention factor of 10.0. Flow rate: 2 – 25 µL min^{-1}; injection volume: 400 nL (blue); 300 nL (green); 200 nL (red); 100 nL (black); mobile phase: 75% H2O + 0.1% FA; 25% ACN + 0.1% FA; column: YMC-Triart C18, 50 x 0.3 mm, 1.9 µm; temperature: 50 °C; detection: UV at 254 nm.

The comparison of the van Deemter plots of naphthalene for $k = 4$ and $k = 10$ shows that the observed effect is independent of substance. For naphthalene, which was examined at three different retention factors, the resulting H_{min} varies greatly depending on the retention factor. For $k = 2$ the increase of the injection volume to 400 nL resulted in an increase of 111% compared to an injection volume of 100 nL, at $k = 4$ the increase of the injection volume only leads to an increase in H_{min} of 54%. At $k = 10$ an increase of H_{min} is no longer apparent. By comparing H_{min} of naphthalene for the three different retention factors at an injection volume of 100 nL, another aspect stands out. Here, an H_{min} of 5.3, 7.2 and 6.3 was achieved for naphthalene in ascending k order. The maximum in H_{min} at $k = 4$ can be explained by the different composition of the mobile phase and the resulting change viscosity. Similar effects can be observed by examining the increase of the C-term of the van Deemter plot. In addition to the retention factor, the composition of the mobile phase also has a significant influence on the plate height. This fact also illustrates that the determination of H_{min} without further data on the retention factor and mobile phase composition has only little significance.

For sub 2 µm particle packed stationary phases the generally accepted opinion is that the increase in the C-term of the van Deemter curve is less pronounced compared to larger particle diameters. Moreover, the optimal flow rate range of the column is shifted to higher flow rates. Therefore, the analysis time can be reduced without affecting the chromatographic efficiency. However, the measurements at φ=0.25 for the substances acetylsalicylic acid, etoposide and carbamazepine show that there is a pronounced increase of the C-term. The C-term decreases with increasing retention factor. From this it can be concluded that very fast analyses without significant loss of efficiency can only be performed if the retention factor is sufficiently high. This effect correlates with the retention factor and does not directly depend on the compound structure. This is evident from the comparison of the C-term for naphthalene at three different retention factors, where the slope of the C-term changes in the same way.

Although the plate height is an established performance parameter for the isocratic evaluation of a separation column, it does not allow a comparison of the overall peak dispersion. The reason is that H_{min} is not obtained at the same flow rate for different injection volumes and components. In order to get information about band broadening by increasing of the injection volume, the peak standard deviation (σ_h) was used. To calculate σ_h, the full width at half maximum (FWHM) of a peak (w_h) was divided by the factor 2.355 and multiplied by the flow rate. Figure 3 shows the variances for all investigated components.

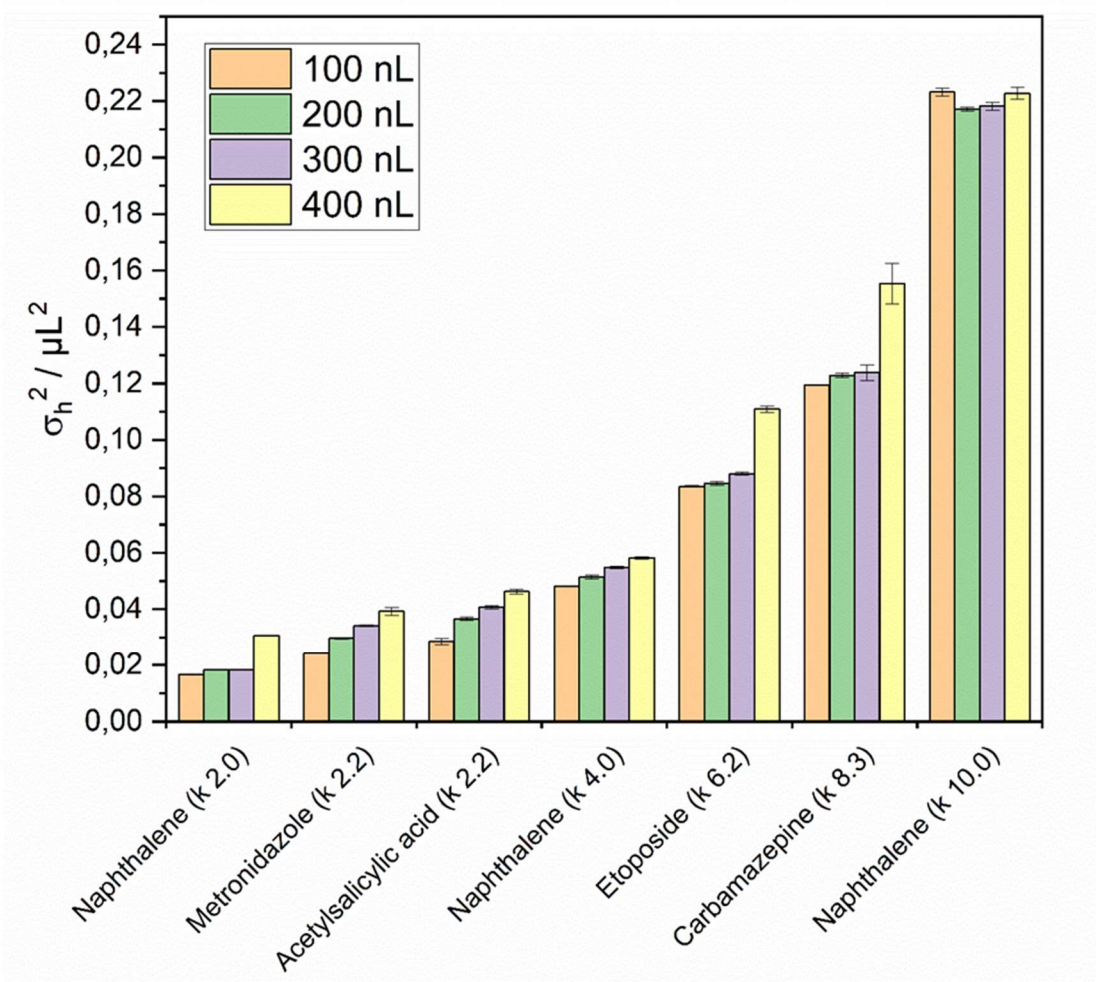

Figure 3-3: Effect of injection volume on peak variance at a flow rate of 10 µL min-1. Components are sorted by ascending retention factor. Error bars indicate the standard deviation calculated for n=3.

The comparison of the volume variances clearly shows that even for higher retention factors an effect on performance can be observed by the increase of the injection volume. Except for naphthalene ($k = 10.0$) every increase in injection volume leads to an incremental increase in σ_h. In the case of naphthalene ($k = 10.0$), the influence of the increase in injection volume is superimposed by diffusion, which is manifested in a stagnation of σ_h. In theory, a better column volume loading can be achieved by adjusting to higher retention factors, but only at the cost of a significant increase in width. Comparing the variances of naphthalene ($k = 10.0$) to that of carbamazepine ($k = 8.3$) for an injection volume of 100 nL, this corresponds to an increase of over 80%. The arrangement of the examined components by increasing retention factor indicates that despite different interactions with the stationary phase a clear trend to an increasing peak width with a higher retention factor can be observed. In combination with the van Deemter data it can be concluded that in addition to high injection volumes, high retention factors > 10 under isocratic conditions should be avoided in favor of lower peak width.

3.3.2 Gradient Experiments

3.3.2.1 Influence on Peak Capacity

The peak capacity (n_p) was determined individually for each component. The peak capacity describes how many compounds can be separated with a defined resolution. Therefore, n_p is a good measure of the efficiency of a column under gradient conditions. The peak capacity was calculated by Equation 3-4.

$$n_p = 1 + \frac{2{,}354 * t_G}{4 * w_h} \qquad \text{Equation 3-4}$$

where w_h is the FWHM of a peak and t_G is the gradient time. Figure 3-4 shows the obtained peak capacities for all components and injection volumes.

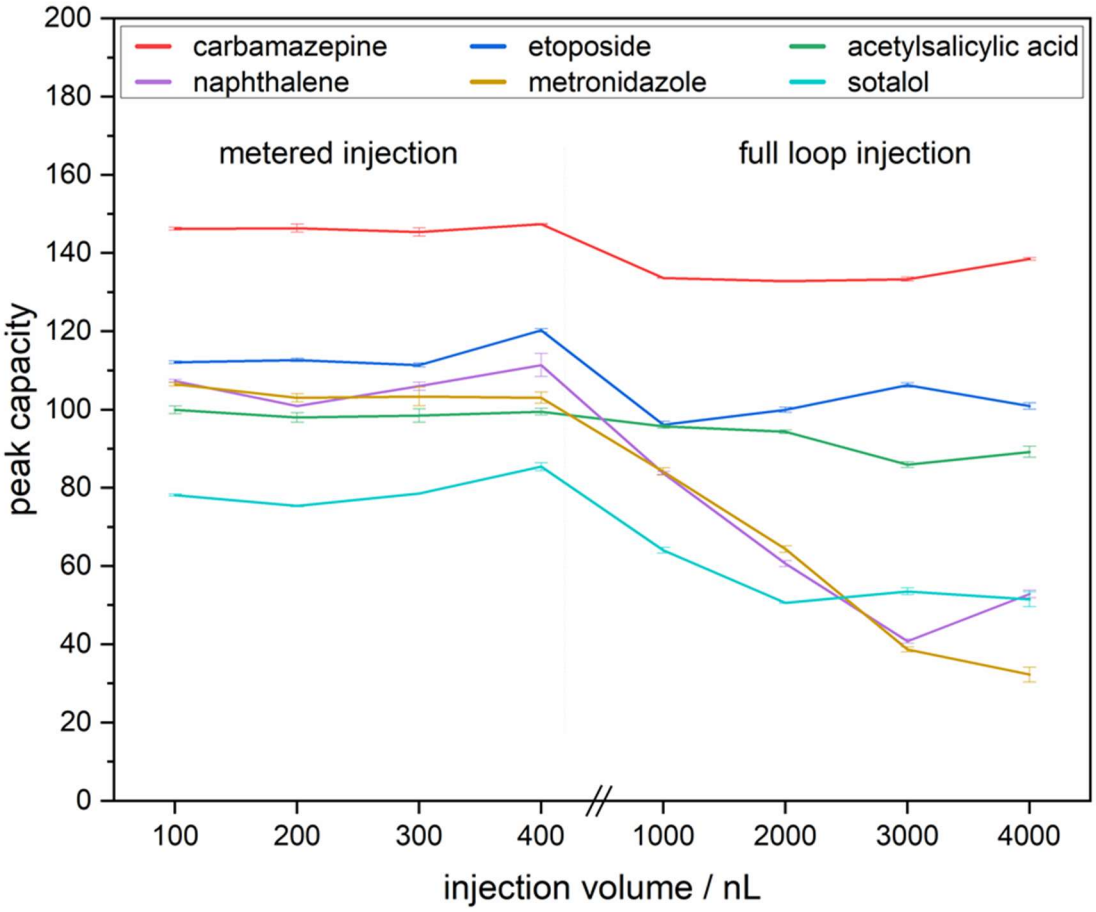

Figure 3-4: Dependence of peak capacity on injection volume for the selected compounds. Flow rate: 10 µL min-1; injection volume: 100-4000 nL; generic gradient elution from 5% to 95% B; column: YMC-Triart C18, 50 x 0.3 mm, 1.9 µm; temperature: 50 °C; detection: UV at 220 nm. All measurements were performed in triplicate.

It is particularly noticeable that for the majority of the compounds a decrease in the peak capacity is observed if the injection volume is increased from 400 nL to 1,000 nL. This decrease in peak capacity does not continue to the same extent for the other injection volumes

> 1,000 nL. The effect can be attributed to the overall increase in dwell time and the transfer of peak tail on the column with the switch of the injection mode. The injection volumes between 100 and 400 nL were performed by means of the metered injection. Here, the measurement starts by switching the valve after transfer of a defined sample volume from the loop to the column. Thus, the peak tail is cut off by the switching process and the gradient dwell volume is reduced by one port to port volume of the valve and the volume of the sample loop (See Figure 3-8) [21, 22]. The injection volumes between 1,000 and 4,000 nL were applied by full-loop injection. This is the most reproducible injection method available in chromatography. However, with increasing loop volume the gradient dwell volume and analysis time increases. In addition, there is no cut-off of the peak tail by full-loop injection. Furthermore, every change of the sample loop can potentially lead to an unclean connection in the system resulting in diminished chromatographic performance.

As expected, nonpolar substances were focused at the column head due to the aqueous starting conditions of the solvent gradient. While the plate height for isocratic analyses is strongly influenced by a small increase in injection volume, the peak capacity is constant for all selected analytes if the injection volume is varied between 100 nL and 400 nL. A reduction in peak capacity becomes visible for all compounds only when a four times higher injection volume than the recommended 10% effective column volume loading is reached. For carbamazepine, the peak capacity is reduced by 6% at an injection volume of 1,000 nL and remains constant for higher injection volumes. The reduction is due to the change of the injection method. Therefore, it can be concluded that with the full loop injection a loss in efficiency is already achieved due to increase in dwell volume and the transfer of the tailing part of the peak onto the separation column. Only a moderate drop in peak capacity was recorded for acetylsalicylic acid. Sotalol, naphthalene and metronidazole showed a constant drop in peak capacity if the injection volume is higher than 1,000 nL.

On the basis of our results, a metered injection should be preferred if applicable due to the described advantages. However, for high injection volumes that exceed the total system volume, this approach cannot be used for early eluting analytes. As described in metered injection the chromatographic run starts after the entire injection volume has been transferred to the column and the loop has been removed from the flow path. Consequently, it is possible that early eluting analytes are flushed through the column before the chromatographic run is started.

3.3.2.2 Gradient Kinetic Plots

For the application of the gradient kinetic plot theory a constant t_g/t_0 -ratio has to be maintained. This is the only way to ensure that all compounds experience the same mobile phase history when varying the injection volume [23]. Since t_0 is a column specific parameter, the gradient time was chosen to be constant for all injection volumes and only adapted to the flow rate. Due to the experimental setup, the gradient dwell volume changes depending on the injection mode and volume (see section 2.3 for a detailed explanation). To obtain a constant gradient dwell volume for all experiments, an isocratic plateau was programmed before the start of the gradient. The column length rescaling factor (λ) is used to transform the experimental data into kinetic plot limits (KPL) according to Equation 3-5 [25, 25]. The maximum experimental pressure during the gradient run (ΔP_{exp}) is used, which depends on the permeability of the column and the viscosity of the mobile phase.

$$\lambda = \frac{\Delta P_{max}}{\Delta P_{exp} - \Delta P_{ec}} \qquad \text{Equation 3-5}$$

where, ΔP_{max} is the maximum backpressure which was set to 1,000 bar, ΔP_{exp} the experimental pressure and ΔP_{ec} the extra column backpressure.

The column length rescaling factor enables the transformation of all other experimental data into KPL, according to Equation 3-6 to Equation 3-8.

$$n_{p,KPL} = 1 + \sqrt{\lambda} \cdot (n_{p,exp} - 1) \qquad \text{Equation 3-6}$$

$$t_{G,KPL} = \lambda \cdot t_{G,exp} \qquad \text{Equation 3-7}$$

$$L_{KPL} = \lambda \cdot L_{exp} \qquad \text{Equation 3-8}$$

where, $n_{p,KPL}$, is the maximum peak capacity, $t_{G,KPL}$ and L_{KPL} the corresponding gradient time and column length of the gradient kinetic plot limit. $n_{p,exp}$, $t_{G,exp}$ and L_{exp} are the experimentally determined peak capacity, gradient time and column length, respectively.

In order to obtain values for the extrapolation of peak capacities as accurately as possible, it is necessary that the extra column band broadening only makes a small contribution to overall system band broadening. In gradient elutions it is usually assumed that the extra column volume before the column can be neglected if a non-polar compound is focused on the head of the column. In order to determine the influence of the additional pre-column volume for carbamazepine and metronidazole, the volume in front of the column was extended with sample loops of 1000 – 4000 nL with an ID of 100 µm. The injection volume was kept constant (442 nL full-loop). For carbamazepine no effect of increasing pre-column volume on peak capacity was observed. An $\overline{n_p} = 131 \pm 1$ was achieved for all pre column volumes. For metronidazole a continuous decrease of n_p was observed. While an additional volume of 1000 nL resulted in $n_p = 91$, an increase to 4000 nL resulted in $n_p = 70$. For carbamazepine, KPL-data are only influenced by post-column band broadening. For metronidazole, the total extra column volume contributes to the dispersion. Therefore, the calculated peak capacities are lower than they would be if the experiments were performed with longer columns. The obtained gradient kinetic plot limits for carbamazepine and metronidazole are shown in Figure 3-5.

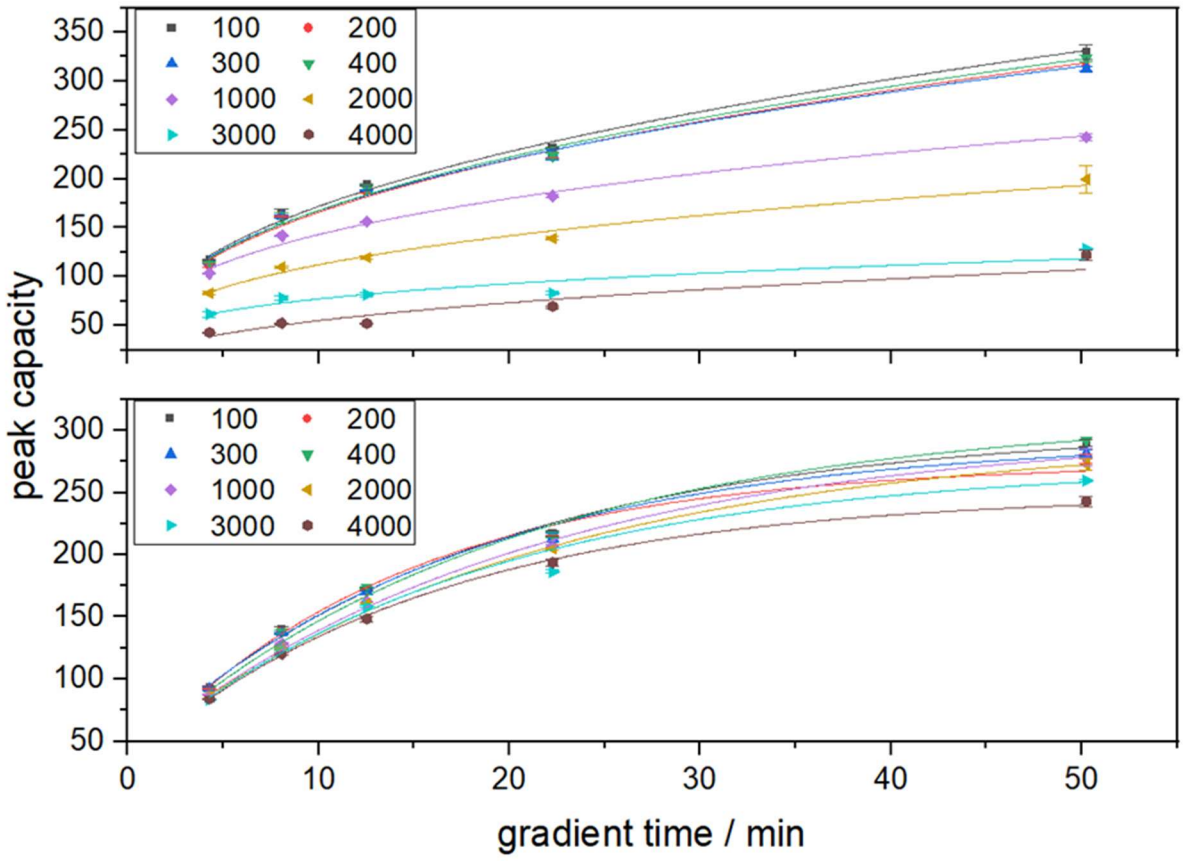

Figure 3-5: Influence of the injection volume on peak capacity. Obtained gradient kinetic plot limits for A: metronidazole and B: carbamazepine. Flow rate: 5 – 25 µL min^{-1}; injection volume: 4,000 nL (brown); 3,000 nL (turquoise); 2,000 nL (yellow); 1,000 nL (purple) 400 nL (green); 300 nL (blue); 200 nL (red); 100 nL (black). Mobile phase gradient: 1% ACN + 0.1% FA / 99% H_2O + 0.1% FA to 95% ACN / 0.1% FA; 5% H2O + 0.1%; column: YMC-Triart C18, 50 x 0.3 mm, 1.9 µm; temperature: 50 °C; detection: UV at 254 nm. Fit: power function.

For metronidazole, a clear trend can be observed if the injection volume is increased. For an injection volume between 100 nL and 400 nL and a gradient time of about 50 minutes at a flowrate of 10 µL min^{-1}, a maximum peak capacity of about 320 is obtained in each case. By further increasing the injection volume, a significant loss of peak capacity becomes visible as the injection volume increases. For an injection volume of 4,000 nL at 10 µL min^{-1} only a peak capacity of 120 is reached.

For short gradient times of about 4 min and a flow rate of 25 µL min^{-1}, an average peak capacity of about 110 is achieved if the injection volume is varied between 100 nL and 400 nL. A further increase of the injection volume also leads to a significant reduction of the peak capacity. A peak capacity of 100, 80, 60 and 40 is obtained for 25 µL min^{-1} and an injection volume of 1,000 nL, 2,000 nL, 3,000 nL and 4,000 nL, respectively. This corresponds to an average loss of $n_{p,KPL} = 20$ per 1,000 nL increase in the injection volume.

For carbamazepine no significant loss of the peak capacity was observed by varying the injection volume. Due to its higher hydrophobicity, a good focusing on the column head was achieved. When varying the injection volume between 100 and 400 nL for $t_{G,KPL} = 21\ min$, and $F = 10\ \mu L\ min^{-1}$ which corresponds to an $L_{KPL} = 34\ cm$, no change in peak capacity was observed. An average $n_{p,KPL} = 309 \pm 2$ was achieved. A further increase of the injection volume up to 160% of the effective column volume resulted in a reduction by $\Delta n_{p,KPL} = 28$ to $n_{p,KPL} = 281$. This corresponds to a decrease in efficiency of 10%. However, it should be noted that the metered injection creates a cut-off of the tailing part of the injection band [21, 22]. During full-loop injection, the whole volume including the tailing part of the injection band is transferred to the column. Since the full-loop injection was used for injection volumes between 1,000 and 4,000 nL, the difference can be attributed to this effect. For $F = 25\ \mu L\ min^{-1}$ and $t_{G,KPL} = 4\ min$ an average $n_{p,KPL} = 113$ was achieved.

3.4 Conclusion

The injection volume contributes significantly to band broadening. In order to reach the intrinsic separation efficiency of sub 2 µm particle packed microbore columns, the reduction of the injection volume is recommended. This is especially true in isocratic elution, where a pronounced decrease in plate height was observed for substances eluted near the void time of the column. Even by minimizing the injection volume to 4% of the effective column volume, a decrease in efficiency was observed. Only at high retention factors ≥ 8, the injection band can be sufficiently focused at the column head so that the injection volume can be increased. However, if the retention factor is further increased, the peak variance increases significantly. For real-world applications, enrichment for polar analytes, e.g. by off-line solid-phase extraction, is advantageous because it allows the injection volume to be reduced. For non-polar compounds, the advantages of a significantly higher injection volume can be used for direct large volume injection of the sample to achieve low limits of detection.

In gradient elution the influence of the injection plug is significantly reduced. Here, for non-polar analytes such as carbamazepine, only a slight decrease in peak capacity was observed even with an injection band occupying 160% of the effective column volume. In contrast to isocratic elution, a strong reduction of the peak capacity when increasing the injection volume was only observed for compounds eluting near the void time. With gradient elution, it is therefore possible to use large volume direct injection to achieve the lowest possible detection limits.

3.5 Supplementary Information

Figure 3-6 shows the overlay of 12 Injections of Naphthalene. The Injections were peformed to verify the reproducibility of the metered injection on the used LC-system. A flow rate of 25 µL/min was chosen which corresponds to a minimum switching time of the valve of 250 ms. A value of 1.455 ± 0.005 min was determined for the retention time. The deviation of the area was 876 ± 10 mAu*s and that of the height 254 mAU ± 3.

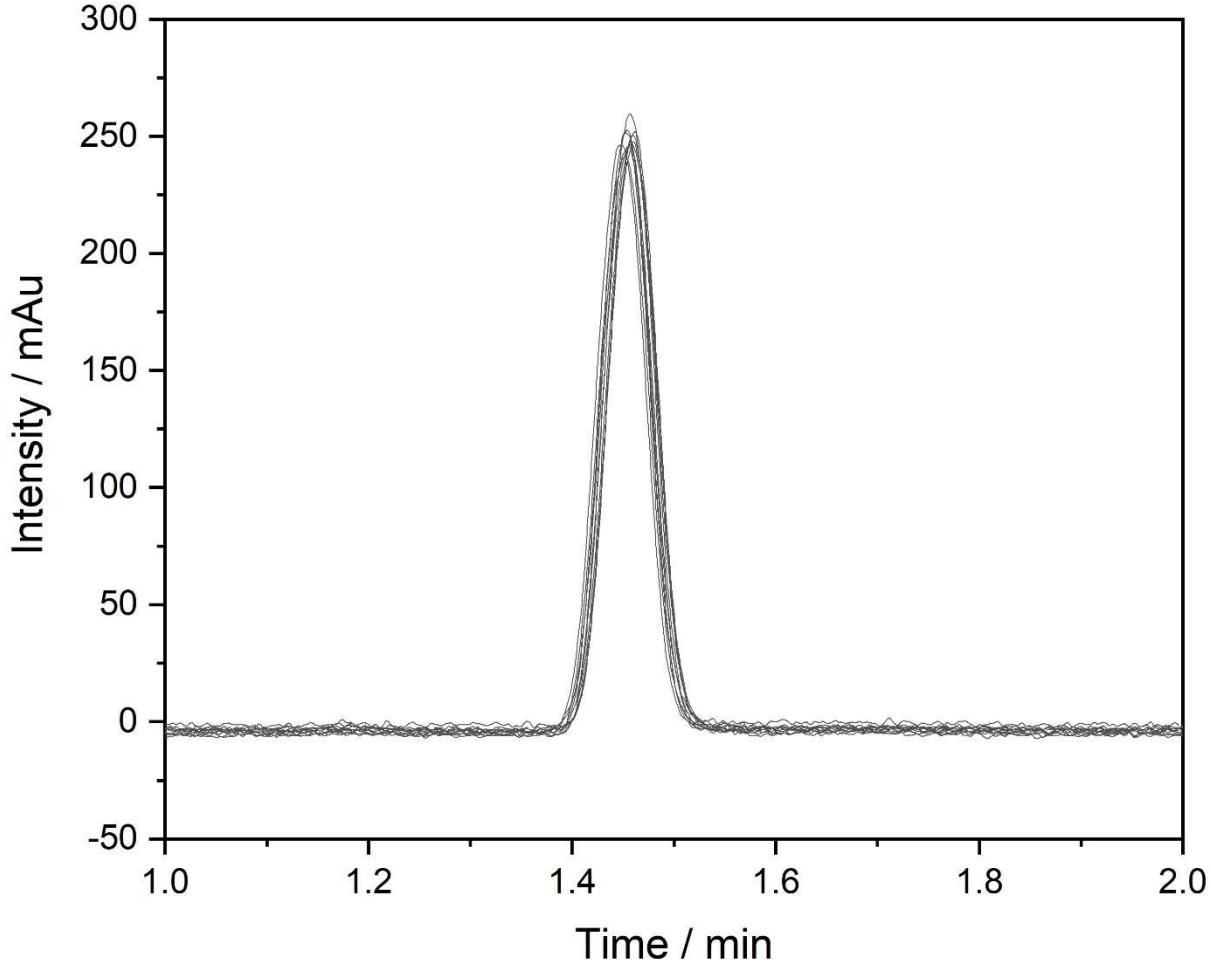

Figure 3-6: Twelve injections of naphthalene by metered injection. Injection volume: 100 nL; column: YMC-Triart C18, 50 x 0.3 mm, 1.9 µm; temperature: 50 °C; detection: UV at 254 nm.

Figure 3-7 shows the deviation of sotalol from the Gaussian peak shape. To illustrate this, a gauss fit was placed over both resulting peaks. Comparing the tailing factor and symmetry of both components according to the United States Pharmacopoeia (USP) method, it becomes clear why sotalol was not investigated under the isocratic experimental conditions used. For metronidazole a USP symmetry at 10% of 0.997 was achieved compared to 0.410 for sotalol. The USP tailing factor at a height of 5% was 0.998 for metronidazole and 2.334 for sotalol. To ensure a sufficient evaluation according to USP, the tailing factor should not exceed 1.2 and a symmetric peak should be present.

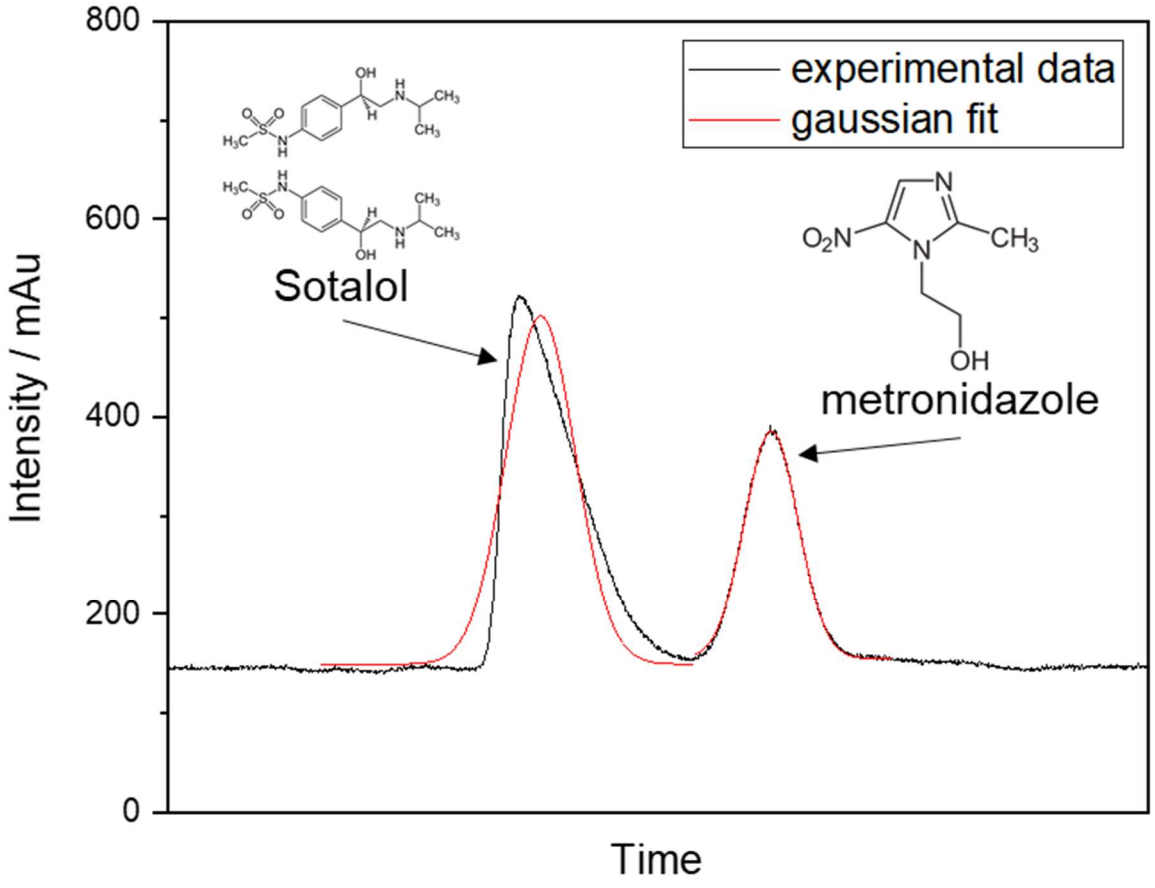

Figure 3-7: Comparison of the peak shapes of sotalol and metronidazole. Mobile phase: 95% H2O + 0.1% FA; 5% ACN + 0.1% FA; column: YMC-Triart C18, 50 x 0.3 mm, 1.9 µm; temperature: 50 °C; detection: UV at 254 nm.

Figure 3-8 shows the change in gradient dwell volume resulting from the use of the two injection methods. In full-loop injection the chromatographic run starts by switching the sample loop into the flow. In metered injection the chromatographic run begins after the sample loop is switched out of the flow after a defined time. Accordingly, the gradient dwell volume in metered injection is reduced by the volume of the sample loop and the port-to-port volume of the valve.

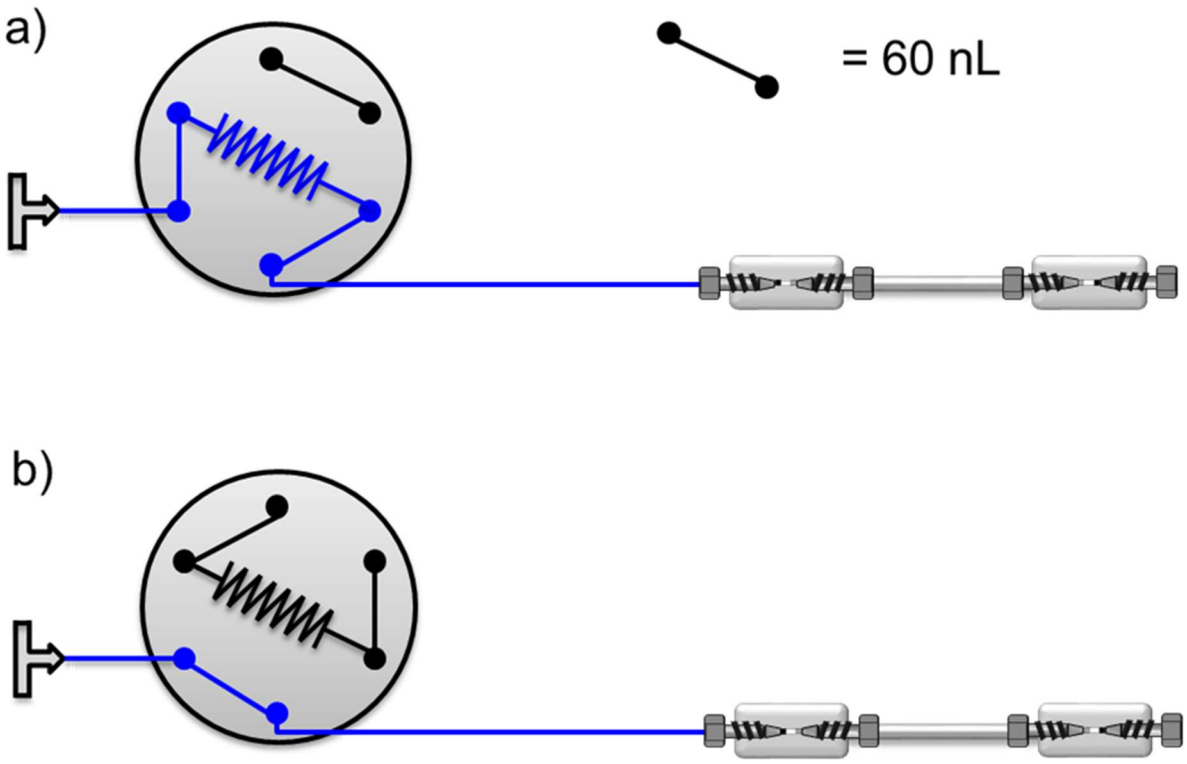

Figure 3-8: Resulting gradient dwell volumes (dark blue line) using a) full-loop injection and b) metered injection.

Table 3-3: Timetables for the gradient measurements.

F / µL min^{-1}	10	15	20	25	30	Gradient / %B
t_G / min	7.0	4.7	3.5	2.8	2.3	
start (100 – 400 nL)	0.00	0.00	0.00	0.00	0.00	1
t_p	0.15	0.10	0.08	0.06	0.05	1
t_G	7.15	4.80	3.58	2.94	2.35	95
hold	7.30	4.95	3.73	3.09	2.50	95
decrease	7.50	5.15	3.93	3.29	2.70	1
hold	7.60	5.25	4.03	3.39	2.80	1
start (1000 nL)	0.00	0.00	0.00	0.00	0.00	1
t_p	0.28	0.19	0.14	0.11	0.09	1
t_G	7.28	4.89	3.54	2.91	2.39	95
hold	7.43	5.04	3.69	3.06	2.54	95
decrease	7.63	5.24	3.89	3.26	2.74	1
hold	7.73	5.34	4.99	3.36	2.84	1
start (2000 nL)	0.00	0.00	0.00	0.00	0.00	1
t_p	0.37	0.27	0.19	0.15	0.12	1
t_G	7.37	4.97	3.69	2.95	2.42	95
hold	7.53	5.12	3.84	3.10	2.57	95
decrease	7.73	5.32	4.04	3.30	2.77	1
hold	7.83	5.42	4.14	3.40	2.87	1
start (3000 nL)	0.00	0.00	0.00	0.00	0.00	1
t_p	0.48	0.32	0.24	0.19	0.16	1
t_G	7.48	5.02	3.74	2.99	2.46	95
hold	7.63	5.17	3.89	3.14	2.61	95
decrease	7.83	5.37	4.09	3.34	2.81	1
hold	7.93	5.47	4.19	3.44	2.91	1
start (4000 nL)	0.00	0.00	0.00	0.00	0.00	1
t_p	0.57	0.38	0.29	0.23	0.19	1
t_G	7.57	5.08	3.79	3.03	2.49	95
hold	7.72	5.23	3.94	3.18	2.64	95
decrease	7.92	5.43	4.14	3.38	2.84	1
hold	8.02	5.53	4.24	3.48	2.94	1

3.6 References

[1] J. Leonhardt, T. Teutenberg, J. Tuerk, M.P. Schlüsener, T.A. Ternes, T.C. Schmidt, A comparison of one-dimensional and microscale two-dimensional liquid chromatographic approaches coupled to high resolution mass spectrometry for the analysis of complex samples, Anal. Methods. 7 (2015) 7697–7706. https://doi.org/10.1039/c5ay01143d.

[2] M. Sulyok, D. Stadler, D. Steiner, R. Krska, Validation of an LC-MS/MS-based dilute-and-shoot approach for the quantification of > 500 mycotoxins and other secondary metabolites in food crops: challenges and solutions, Anal. Bioanal. Chem. 412 (2020) 2607–2620. https://doi.org/10.1007/s00216-020-02489-9.

[3] A.M. Voigt, D. Skutlarek, C. Timm, C. Schreiber, C. Felder, M. Exner, H.A. Faerber, Liquid chromatography-tandem mass spectrometry as a fast and simple method for the determination of several antibiotics in different aqueous matrices, Environ. Chem. 17 (2020) 54–74. https://doi.org/10.1071/EN19115.

[4] P. Gago-Ferrero, A.A. Bletsou, D.E. Damalas, R. Aalizadeh, N.A. Alygizakis, H.P. Singer, J. Hollender, N.S. Thomaidis, Wide-scope target screening of >2000 emerging contaminants in wastewater samples with UPLC-Q-ToF-HRMS/MS and smart evaluation of its performance through the validation of 195 selected representative analytes, J. Hazard. Mater. 387 (2020) 121712. https://doi.org/10.1016/j.jhazmat.2019.121712.

[5] D.T.T. Nguyen, D. Guillarme, S. Rudaz, J.L. Veuthey, Fast analysis in liquid chromatography using small particle size and high pressure, J. Sep. Sci. 29 (2006) 1836–1848. https://doi.org/10.1002/jssc.200600189.

[6] H. Zhang, C. Liu, W. Hua, L.P. Ghislain, J. Liu, L. Aschenbrenner, S. Noell, K. Dirico, L.F. Lanyon, C.M. Steppan, D.W. Arnold, T.R. Covey, S.S. Datwani, M.D. Troutman, S. Sammy Datwani, Acoustic Ejection Mass Spectrometry for High-Throughput Analysis, (2020) 1–32. https://doi.org/10.1101/2020.01.28.923938.

[7] K. Mejía-Carmona, J. Soares da Silva Burato, J.V.B. Borsatto, A.L. de Toffoli, F.M. Lanças, Miniaturization of liquid chromatography coupled to mass spectrometry: 1. Current trends on miniaturized LC columns, TrAC - Trends Anal. Chem. 122 (2020) 115735. https://doi.org/10.1016/j.trac.2019.115735.

[8] F. Gritti, M. Gilar, J.A. Jarrell, Achieving quasi-adiabatic thermal environment to maximize resolution power in very high-pressure liquid chromatography: Theory, models, and experiments, J. Chromatogr. A. 1444 (2016) 86–98. https://doi.org/10.1016/j.chroma.2016.03.070.

[9] F. Gritti, M. Gilar, J.A. Jarrell, Quasi-adiabatic vacuum-based column housing for very high-pressure liquid chromatography, J. Chromatogr. A. 1456 (2016) 226–234. https://doi.org/10.1016/j.chroma.2016.06.029.

[10] N. Lambert, A. Felinger, The effect of the frictional heat on retention and efficiency in thermostated or insulated chromatographic columns packed with sub-2-µm particles, J. Chromatogr. A. 1565 (2018) 89–95. https://doi.org/10.1016/j.chroma.2018.06.038.

[11] D.A. Vargas Medina, E.V.S. Maciel, A.L. de Toffoli, F.M. Lanças, Miniaturization of liquid chromatography coupled to mass spectrometry.: 2. Achievements on modern instrumentation for miniaturized liquid chromatography coupled to mass spectrometry, TrAC - Trends Anal. Chem. 128 (2020) 115910. https://doi.org/10.1016/j.trac.2020.115910.

[12] M. Russo, F. Rigano, A. Arigò, D. Sciarrone, M.L. Calabrò, S. Farnetti, P. Dugo, L. Mondello, Rapid isolation, reliable characterization, and water solubility improvement of polymethoxyflavones from cold-pressed mandarin essential oil, J. Sep. Sci. 39 (2016) 2018–2027. https://doi.org/https://doi.org/10.1002/jssc.201501366.

[13] C. Tani, M. Stella, D. Donnarumma, M. Biagini, P. Parente, A. Vadi, C. Magagnoli, P. Costantino, F. Rigat, N. Norais, Quantification by LC-MSE of outer membrane vesicle proteins of the Bexsero® vaccine, Vaccine. 32 (2014) 1273–1279. https://doi.org/10.1016/j.vaccine.2014.01.011.

[14] E.V.S. Maciel, A.L. de Toffoli, F.M. Lanças, Current status and future trends on automated multidimensional separation techniques employing sorbent-based extraction columns, J. Sep. Sci. 42 (2019) 258–272. https://doi.org/10.1002/jssc.201800824.

[15] M.F. Wahab, D.C. Patel, R.M. Wimalasinghe, D.W. Armstrong, Fundamental and Practical Insights on the Packing of Modern High-Efficiency Analytical and Capillary Columns, Anal. Chem. 89 (2017) 8177–8191. https://doi.org/10.1021/acs.analchem.7b00931.

[16] F. Gritti, G. Guiochon, Overload behavior and apparent efficiencies in chromatography, J. Chromatogr. A. 1254 (2012) 30–42. https://doi.org/10.1016/j.chroma.2012.07.015.

[17] EMEA, ICH Topic Q 3 B (R2) - Impurities in New Drug Products, EMEA Eur. Med. Agency. (2006) 14.

[18] J. Šesták, D. Moravcová, V. Kahle, Instrument platforms for nano liquid chromatography, J. Chromatogr. A. 1421 (2015) 2–17. https://doi.org/https://doi.org/10.1016/j.chroma.2015.07.090.

[19] T. Hetzel, C. vom Eyser, J. Tuerk, T. Teutenberg, T.C. Schmidt, Micro-liquid chromatography mass spectrometry for the analysis of antineoplastic drugs from wipe samples, Anal. Bioanal. Chem. 408 (2016) 8221–8229. https://doi.org/10.1007/s00216-016-9932-y.

[20] E. Grushka, Chromatographic Peak Capacity and the Factors Influencing It, Anal. Chem. 42 (1970) 1142–1147. https://doi.org/10.1021/ac60293a001.

[21] J. Samuelsson, T. Fornstedt, Injection technique for generating accurate adsorption isotherm data using the elution by characteristic points method, Anal. Chem. 80 (2008) 7887–7893. https://doi.org/10.1021/ac8010999.

[22] J. Samuelsson, L. Edström, P. Forssén, T. Fornstedt, Injection profiles in liquid chromatography. I. A fundamental investigation, J. Chromatogr. A. 1217 (2010) 4306–4312. https://doi.org/10.1016/j.chroma.2010.04.045.

[23] G. Desmet, D. Cabooter, K. Broeckhoven, Graphical Data Representation Methods To Assess the Quality of LC Columns, Anal. Chem. 87 (2015) 8593–8602. https://doi.org/10.1021/ac504473p.

[24] A. Kurganov, A. Kanateva, E. Yakubenko, Application of kinetic plots in gas and liquid chromatography for the optimization of separation conditions, J. Sep. Sci. 39 (2016) 162–176. https://doi.org/10.1002/jssc.201500595.

[25] K. Broeckhoven, D. Cabooter, S. Eeltink, G. Desmet, Kinetic plot based comparison of the efficiency and peak capacity of high-performance liquid chromatography columns: theoretical background and selected examples., J. Chromatogr. A. 1228 (2012) 20–30. https://doi.org/10.1016/j.chroma.2011.08.003.

Chapter 4 Peak broadening caused by using different micro–liquid chromatography detectors

This chapter was adapted from: T. Werres, T.C. Schmidt, T. Teutenberg, Peak broadening caused by using different micro–liquid chromatography detectors, Anal. Bioanal. Chem. (2022) 6107–6114. https://doi.org/10.1007/s00216-022-04170-9.

Abstract: Advancements in column technology resulted in smaller particles and more efficient phases. In parallel, the use of columns with reduced dimensions is becoming more common. This means the effective column volume is also decreased, thereby making the systems more susceptible to effects of band broadening due to extra-column volume. Despite these trends and the fact that a growing number of miniaturized liquid chromatography systems are being offered commercially, manufacturers often stick to the modular concept with dedicated units for pumps, column oven, and detectors. This modular design results in long connection capillaries, which leads to extra-column band broadening and consequently prevents the exploitation of the intrinsic efficiency of state-of-the-art columns. In particular, band broadening post column has a considerable negative effect on efficiency. In this study, mass flow and concentration-dependent detectors were examined for their influence on band broadening using a micro-LC system. A mass spectrometric detector, an evaporative light scattering detector, two UV detectors, and a previously undescribed fluorescence detector were compared. The influence on efficiency is compared using plate height vs linear velocity data and peak variance. It is shown that an increase in the inner diameter after the post-column transfer capillary leads to significant loss in plate height. Comparing the UV detectors, it could be shown that the dispersion was reduced by 38% by the reduction of the post-column volume. The largest variance was found for the evaporative light scattering detector, which was 368% higher compared to the variance of the detector with the least effect on band broadening.

Grapical Abstract:

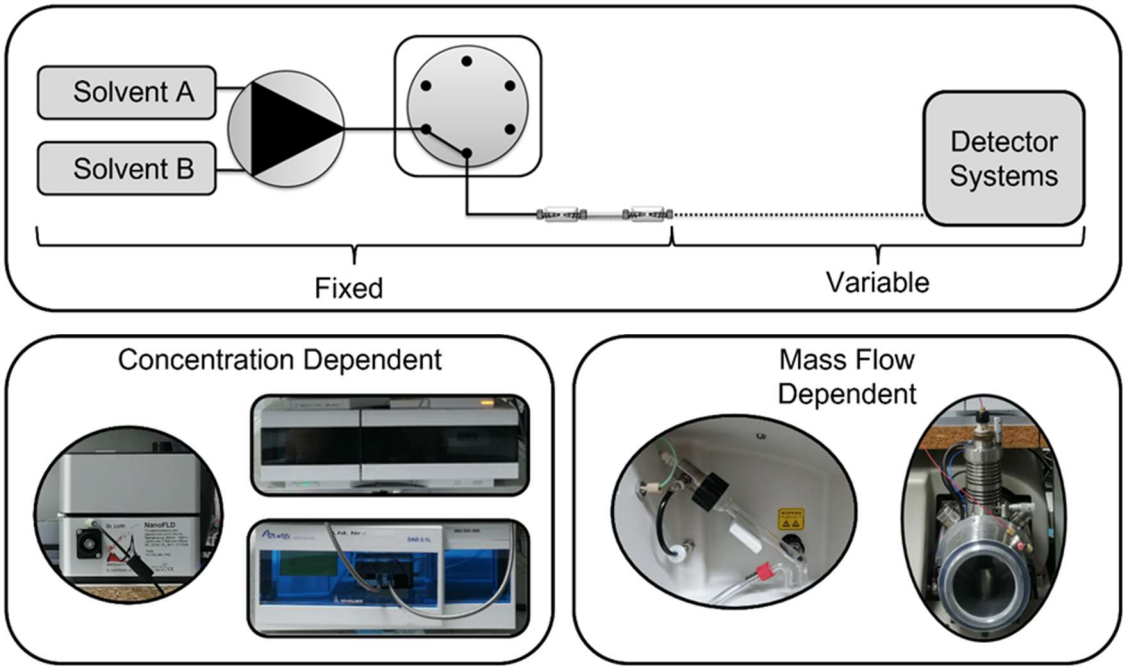

4.1 Introduction

Miniaturized LC systems are increasingly gaining both relevance and acceptance in industry [1, 2]. In addition to the increasing availability of commercial systems, this is mainly due to the increased environmental awareness of the users and factors of profitability [3, 4]. Above all, the benefits of high ionization efficiencies, reduced matrix influence, and the capability to analyze the smallest sample volumes make miniaturized LC coupled to mass spectrometry the main driving force behind the spread of the technology [1, 2, 5–7]. The modular design of classical HPLC systems is based on the "HiFi Tower" principle and offers above all the advantage of high flexibility. However, in the context of microflow systems, adherence to this concept has one major drawback. Due to the modular design, longer flow paths are required that inevitably lead to a high extra-column volume. As a consequence, the intrinsic efficiency of modern sub 2 µm separation phases cannot be fully utilized [8, 9]. However, in current research, it can be observed that the trend is moving further toward miniaturized compact systems. Such a compact design results in a reduction of the extra-column band broadening (ECBB). A growing number of these "suitcase systems" with focus on reduction of ECBB have been presented by several research groups [10-12]. Also, first approaches for ultra-low-cost miniaturized HPLC "for everybody" have already been proposed [13]. The rapid development of 3D printing will further accelerate this trend [14, 15].

While ECBB already has a significant effect on the resolving power of a separation in modern UHPLC systems using 2.1 mm ID columns, the effect is even more pronounced when using micro bore columns with an ID of 300 µm as employed in micro-LC systems [16, 17]. The mismatch will become particularly relevant in the light of ongoing improvements in the field of chromatographic separation phases, where new standards of efficiency are being set with increasingly smaller particle diameters and narrower particle size distributions [18]. Overall, the ECBB can be divided into three parts: the injection volume and injection method, tubing and connectors, and the detector.

In our previous work, the influence of the injection volume and the injection technique on the chromatographic efficiency and the extra-pre-column band broadening was investigated. It was found that a fixed loop in combination with metered injection generates the highest efficiency [19]. Thanks to Taylor and Aris the influence of tubing on the flow profile of the mobile phase is well understood and described at least for unbent, circular-profiled connection tubing under laminar flow conditions [20, 21]. However, tubing in real systems is often bent or shows other "irregularities." This can, for example, result in so-called racetrack effects [22]. Thus, the

determination of all possible factors that might cause significant band broadening in connecting tubing would have to be determined with, e.g., computational fluid dynamics (CFD) simulations [23]. Connections between individual HPLC components are potential sources for introducing ECBB but can nowadays be made with ultra-low dead volume connectors. Due to the diversity of detector designs and the associated changes in the inner diameters and turns of the flow path, no universal mathematical equation can be used for the prediction of the influence on the ECBB. The influence of the detector on the ECBB can only be determined by elaborate simulations or by experiments for each detector independently. Although miniaturized LC in combination with mass spectrometry is the preferred method for a variety of applications, there are no extensive studies on band dispersion using such a coupling.

Therefore, the aim of this investigation was to evaluate the influence of different detectors on the extra-post-column band broadening using sub 2 µm particles in columns with an ID of 300 µm. For this purpose, three concentration-dependent detectors and two mass flow–dependent detectors were investigated. Chromatographic performance was assessed by change in band spreading caused by the post-column connection tubing as well as the specific detector. Other variables were kept constant. These comprise the injector, the injection method, the injection volume, the pre-column tubing, and the column itself. Among the concentration-dependent detectors, two diode array detectors (DAD) and a fluorescence detector (FLD) were included. The mass flow–dependent detector was represented by an evaporative light scattering detector (ELSD) and an ESI–MS, where the influence of the emitter capillary ID on band broadening is discussed in detail.

4.2 Material and Methods

4.2.1 Chemicals and Reagents

Water and acetonitrile of LC–MS grade as well as acetone for the determination of the system dwell times were purchased from Th. Geyer (Chemsolute, Renningen, Germany). Formic acid (Sigma-Aldrich, Seelze, Germany) was added to a total volume concentration of 0.1% to the mobile-phase solvents. Uracil was used to determine the column void time and purchased from Sigma-Aldrich. Naproxen (Sigma-Aldrich) was chosen as the model analyte because it generated a sufficient signal for all investigated detectors.

4.2.2 HPLC Setup

All experiments were done on an Eksigent ExpressLC Ultra system (Sciex, Dublin, CA, USA). The system can be operated up to a maximum pressure of 690 bar. For sample loading, an HTS PAL autosampler (CTC Analytics, Zwingen, Switzerland) was used. Sample injection onto the column was carried out by the integrated six-port-two-position valve and via fixed sample loop (PEEKsil™ 75 µm × 10 cm) by means of metered injection. A YMC-Triart C18 column with a length of 50 mm and an ID of 0.3 mm packed with fully porous 1.9 µm particles with a pore size of 120 Å and 1/32″ connectors was used and operated at 50 °C (YMC Europe GmbH, Dinslaken, Germany). For connecting tubing, fused silica (FS) capillaries (Postnova Analytics, Germany) with an outer diameter of 360 µm and an inner diameter of 50 µm were used. The FS capillaries were cut to the required length using the Shortix™ Tubing Cutter (Supelco, Bellefonte, PA, USA). Furthermore, the cutting edges of the capillaries were further processed using the Capillary Polishing Station (ESI Source Solution, Woburn, MA, USA) using diamond lapping film with a 1 µm grade to obtain a mirror-smooth surface. Finally, the capillaries were rinsed to remove grinding residues. EXP®2 TI-LOK™ Hand-Tight Adapters (Optimize Technologies, Oregon City, OR, USA) were used to guarantee a dead volume free connection of the system components.

4.2.3 Detectors

Several detectors were used for comparison of the influence on the band broadening. Both DADs studied in this work had a U-shaped cell, but still differed in their conceptual implementation in some details. The first UV detector (DAD 1) was the AZURA DAD 2.1L (Knauer, Berlin, Germany) equipped with a nano UV flow cell with a volume of 6 nL and an effective light path of 3 mm. The cell consisted of a single continuous FS capillary with an inner diameter of 50 µm. The cell can be decoupled and placed directly behind the column using light wave guides. Therefore, this detector had the smallest post-column volume of about 200 nL. The absorbance was recorded with a sampling rate of 20 Hz and a wavelength of 275 nm was chosen. A spectral band width of 4 nm was selected. The second UV detector (DAD 2) with a cell volume of

80 nL and an effective light path of 6 mm was a 1260 Infinity II DAD WR (Agilent Technologies, CA, USA). The detector follows the classical “HiFi Tower” approach. The connection is made via a 400 mm × 0.05 mm pre-cut PEEKsil™ capillary, which can be connected to the cell without dead volume due to a special conical cut. The ID of the cell increased to 130 µm, resulting in a total detector post-column volume of 865 nL. The

absorbance was recorded with a data sampling rate of 20 Hz and a wavelength of 275 nm was chosen. A spectral band width of 4 nm was selected. As FLD, the NanoFLD (Dr. Licht GmbH, Nümbrecht, Germany, Art. LO116) was used. Recording of the signal was performed via the integrated single-board computer (Raspberry Pi 4) which resulted in sampling rates up to 10 Hz. For excitation of the sample, a UV-C LED with a wavelength of 275 nm was used. The emitted light was recorded using a photomultiplier equipped with a wide band filter that cuts all wavelengths < 305 nm. The flow cell consisted of a 6 cm long stripped FS capillary with an ID of 50 µm which resulted in the largest cell volume of 117 nL of the concentration-dependent detectors investigated. Two centimeters of the cell, corresponding to 39 nL, was located in the so-called Ulbricht sphere for efficient light collection. The total volume of the assembly is 530 nL without the swept volume of the T-pieces. Connection to the optical fibers and the column outlet is achieved using T-pieces (IDEX; U-428; swept volume of 0.57 µL). A description of this detector can be found in Chapter 4.5.

For the MS measurements, a QTrap 3200 mass spectrometer (Sciex, Dublin, CA, USA) was used. To characterize the band broadening, three different emitter capillaries with an ID of 65 (MS 65), 50 (MS 50), and 25 µm (MS 25) were used. While the 65 µm ID emitter capillary was made of stainless steel, the emitter capillaries with a smaller ID are based on a PEEKsil™ capillary with stainless steel tip. The signal intensity of naproxen was recorded by multiple reaction monitoring at *m/z* 229.0 – > 113.0 and a dwell time of 40 ms. The following source parameters were used: declustering potential, − 20 V; entrance potential, − 10 V; collision energy, − 30 V; collision cell exit potential, − 5 V; curtain gas, 10 psi; ion spray voltage, 4.2 kV; ion source gas 1, 20 psi; and temperature, off.

As an evaporative light scattering detector (ELSD), the ELSD 85LT (Knauer, Berlin, Germany) equipped with a special nebulizer and glassware chamber for the flow rate range of 5 to 40 µL/min was used. A sampling rate of 30 Hz with a gain of 12 and a filter time of 1 s was selected.

Since there is no classical cell volume in the mass flow–dependent detectors which influences the band broadening, it must be clearly differentiated which transport mechanism is used for the analytes after the transition into the gas phase. For ESI–MS, ions are generated from the analyte molecules which are subsequently transported through an electric field. An optimized ion source design has thus only influence on the sensitivity. When using an ELSD, a desolvation step is carried out after nebulization. Afterwards, the desolvated analyte particles are transported by a gas stream. During this process, further band broadening can take place.

Table 4-1 summarizes the most important dimensions and volumes of the individual detectors. The calculations were based on the nominal inner capillary diameters as specified by the manufacturers.

Table 4-1: Summary of the dimension and volume of additional connectors needed of the studied detectors and their acronym in the further document.

Detector	Acronym	Tubing mm x mm (nL)	Cell / Emitter / Desolvation mm x mm (nL)	Union / T-piecec amount (nL)	Total (nL)
AZURA DAD 2.1L	DAD 1	100 x 0.05 (196)	3 x 0.05 (6)	0/0	202
1260 Infinity II DAD WR	DAD 2	400 x 0.05 (785)	6 x 0.13 (80)	0/0	865
NanoFLD	FLD	210 x 0.05 (412)	60 x 0.05 (117)	0/2 (570)	1169
QTrap 3200	MS 25 µm	210 x 0.05 (412)	215 x 0.025 (105)	1/0	517
	MS 50 µm	210 x 0.05 (412)	215 x 0.05 (422)	1/0	834
	MS 65 µm	210 x 0.05 (412)	215 x 0.065 (713)	1/0	1125
ELSD 85LT	ELSD	250 x 0.05 (490)	-- (2570)	1/0	3060

Figure 4-1 shows the schematic of the cell detector geometries. Care was taken to maintain the ratio of the capillary diameters to each other.

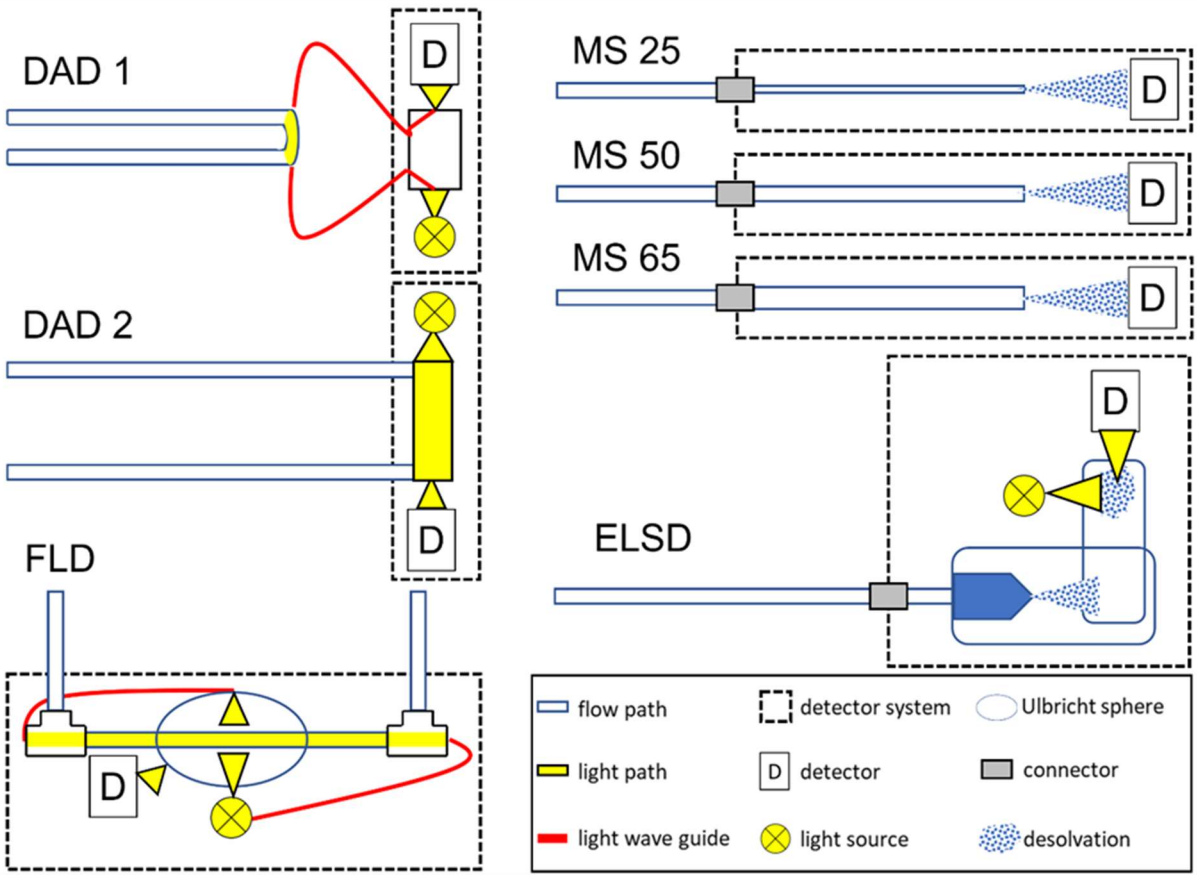

Figure 4-1: Schematic representation of the investigated detector configurations. Ratios of the capillary IDs were retained. A detailed explanation of the cell design of the FLD can be found in Chapter 4.5.

4.2.4 Determination of Plate Height and Peak Variance

For the determination of the plate height and peak variance (σ^2), the peak widths were measured at half height. This procedure is only valid if the peaks are symmetrical. Depending on the flow rate, a peak symmetry between 1.2 and 0.9 could be determined for all detectors investigated apart from the ELSD. To prevent peak dispersion due to volume overload, 100 nL of a 150 µg/mL naproxen sample was injected into the system. The mobile phase was set to 47% B to adjust the retention factor (k) of naproxen to 2. A retention factor of 2 was chosen because extra-column band broadening has a significant effect on weakly retained analytes. The flow rate was varied between 2 and 25 µL/min. All measurements were performed in triplicate.

4.2.5 Software and Data Processing

The micro-HPLC was controlled via Eksigent Control Software Version 4.2 Build 151,019–1321 (Sciex, Dublin, USA). Data acquisition for the Agilent detector was performed using Open LAB CDS Rev.C.0107.SR3 (Agilent Technologies, CA, USA). The detectors from Knauer were operated with Clarity Chrome® version 8.1.0.87 Build Mar 28 2019 (Knauer, Berlin, Germany). The FLD was controlled by means of a python script (Dr. Licht GmbH, Nümbrecht, Germany), and the MS data was acquired using Analyst® 1.6.3 Build 5095 (Sciex, Dublin, USA). Further data processing was performed using OriginPro 2019b (64-bit) 9.6.5.169 (OriginLab, MA, USA) and Microsoft Office Excel 2010. The peak widths were determined using the Peak Analyzer from OriginPro.

4.3 Results and Discussion

4.3.1 Comparison of the Influence of the Detectors on Extra-Post-Column Band Broadening

The visualization of the influence of the investigated detectors on the extra-post-column band broadening was done by volume peak dispersion [19, 24]. Here, the time-dependent peak widths are transformed into volume-dependent dispersion. The transformation was done using the following equation:

$$\sigma^2 = \left(\frac{w_h}{2.355} * F\right)^2 \qquad \text{Equation 4-1}$$

Where σ^2 is the peak variance, w_h the full width at half maximum (FWHM) of the peak, and F the flow rate.

Figure 4-2 shows the comparison of the different detectors on the efficiency of the system. Additionally, plate height (H) vs linear velocity (u_0) plots are shown to further discuss the observed effects [17, 25].

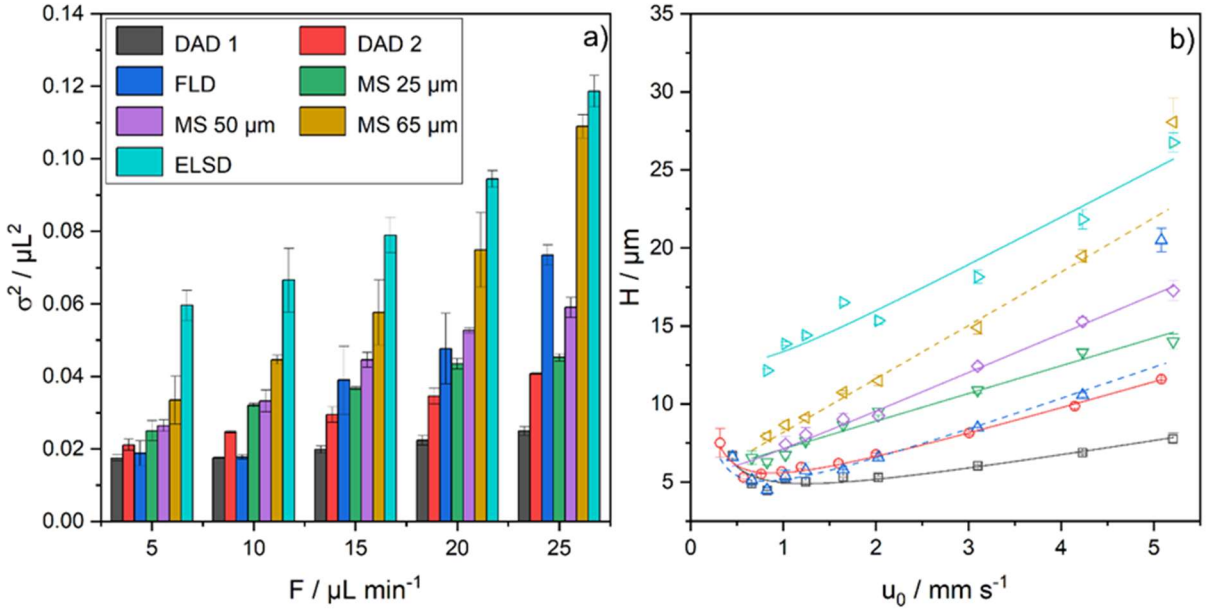

Figure 4-2: Comparison of the influence of the studied detectors on the extra-post-column band broadening in two visualizations. a) Dependence of the peak variance at different flow rates. b) Comparison of the resulting *H* versus u_0 plots. Solid lines represent the fit calculated by the residual sum of squares method for the experimental values. The dotted lines represent the fit if the last data point is omitted. Error bars indicate the standard deviation calculated for n = 3.

As Figure 4-2a shows, a significant increase in peak variance at the highest investigated flow rate of 25 µL min^{-1} was observed when the ESI–MS emitter capillary with an ID of 65 µm, the ELSD, or the FLD was used. The system configurations have in common that after the transfer capillary with an ID of 50 µm connecting the column outlet to the detector, there is a change to a larger ID of 65 µm for the ESI–MS emitter capillary and 500 µm for the T-piece of the FLD. When laminar flow occurs in a capillary, diffusion in the radial direction counteracts band spreading. When the ID of the capillary is increased, the linear flow velocity decreases. In addition, areas of stagnant mobile phase form at the transition to the larger ID. The molecules migrate into and out of the stagnant regions by diffusion. At high linear flow velocities, the analyte molecules near the center of the capillary move so fast in the longitudinal direction that the time for rediffusion is no longer sufficient and band broadening occurs. This has the consequence that an unfavorable flow path geometry can lead to significant losses in efficiency, especially at high linear flow velocities. These observations are consistent with the study of Filip et al. who, using CFD, were able to simulate similar effects on the peak broadening when changing to higher IDs at high linear flow velocities [23].

The lowest peak variance was found for DAD 1, with an overall increase from 0.018 µL^2 to 0.025 µL^2 (43%) in the observed flow rate range. The highest dispersion was found for the ELSD at a flow rate of 25 µL min^{-1} with 0.117 µL^2. The influence of the cell volumes for

DAD 2 and the ESI-MS emitter capillaries with an ID of 25 µm and 50 µm on the variance is comparable. The highest increase in peak broadening at a flowrate of 25 µL min^{-1} was found for the detectors with an increase of the inner diameter of the flow path after the transfer capillary. For the FLD and the ESI-MS emitter capillary with an ID of 65 µm, the increase was 290% and 225%, respectively.

The peak variance can be correlated with the post-column volume when the detectors are separated into concentration-dependent detectors and mass flow dependent-detectors. In the case of the FLD, the large change in variance can be explained by the significant increase in the inner diameter from 50 to 500 µm (see Figure 4-1). In conclusion it can be stated that a constant diameter of the flow path after the column as well as the reduction of the ID after the transfer capillary had no negative influence on the band broadening. By changing to a larger ID, deviations from the expected data patterns could be identified at high flow rates. For DAD 2, where the change to the larger ID only occurred within the detector cell, this effect was not observed.

Comparing the H vs u_0 plots for the concentration dependent detectors in Figure 4-2b there is no significant influence on H_{min}. The lowest $H_{min} = 4.9\ \mu m$ was achieved with the DAD 1. Considering all data points, an $H_{min} = 4.7\ \mu m$ was calculated for the FLD, which is explained by the overestimation of the C-term by the fit function. Examining the dotted plot line of the FLD, an intersection with the plotline of DAD 2 is observed at 2.2 mm s^{-1}. Excluding the last data point results in an $H_{min} = 5.0\ \mu m$. When using DAD 2 an $H_{min} = 5.5\ \mu m$ was achieved. With increasing ID of the ESI-MS emitter capillary, the post-column volume increases and the linear flow velocity in the emitter capillary decreases. As a result, due to spray instabilities, it was not possible to represent H_{min} when using the ESI-MS emitter capillaries with an ID of 50 µm and 65 µm, and the ELSD. When using the ESI-MS emitter capillary with an ID of 25 µm, an $H_{min} = 6.2$ was observed.

The general assumption that the dispersion is a function of the post-column volume only reflects reality to a limited extent. The 25 µm ID emitter capillary yields a comparable post-column volume as the detection cell of the FLD, and the emitter capillary with an ID of 50 µm has a comparable volume as the cell of the DAD 2, but the band broadening is clearly different. However, with increasing post-column volume, a correlation to an increase of the slope of the H versus u_0 plot at higher flow rates can be observed. As a result, only a small optimal flow rate range can be used despite the use of sub 2 µm particle packed stationary phases. The

specific choice of the detector can thus prevent the use of methods with a high flow rate if the chromatographic resolution needs to be optimized.

4.3.2 Comparison of Sensitivity and Signal-to-Noise Ratio

To allow a direct comparison between the different detectors, the concentration of the model analyte was chosen to generate a signal with a signal-to-noise ratio > 5. The resulting normalized chromatograms of the concentration dependent detectors are compared in Figure 4-3.

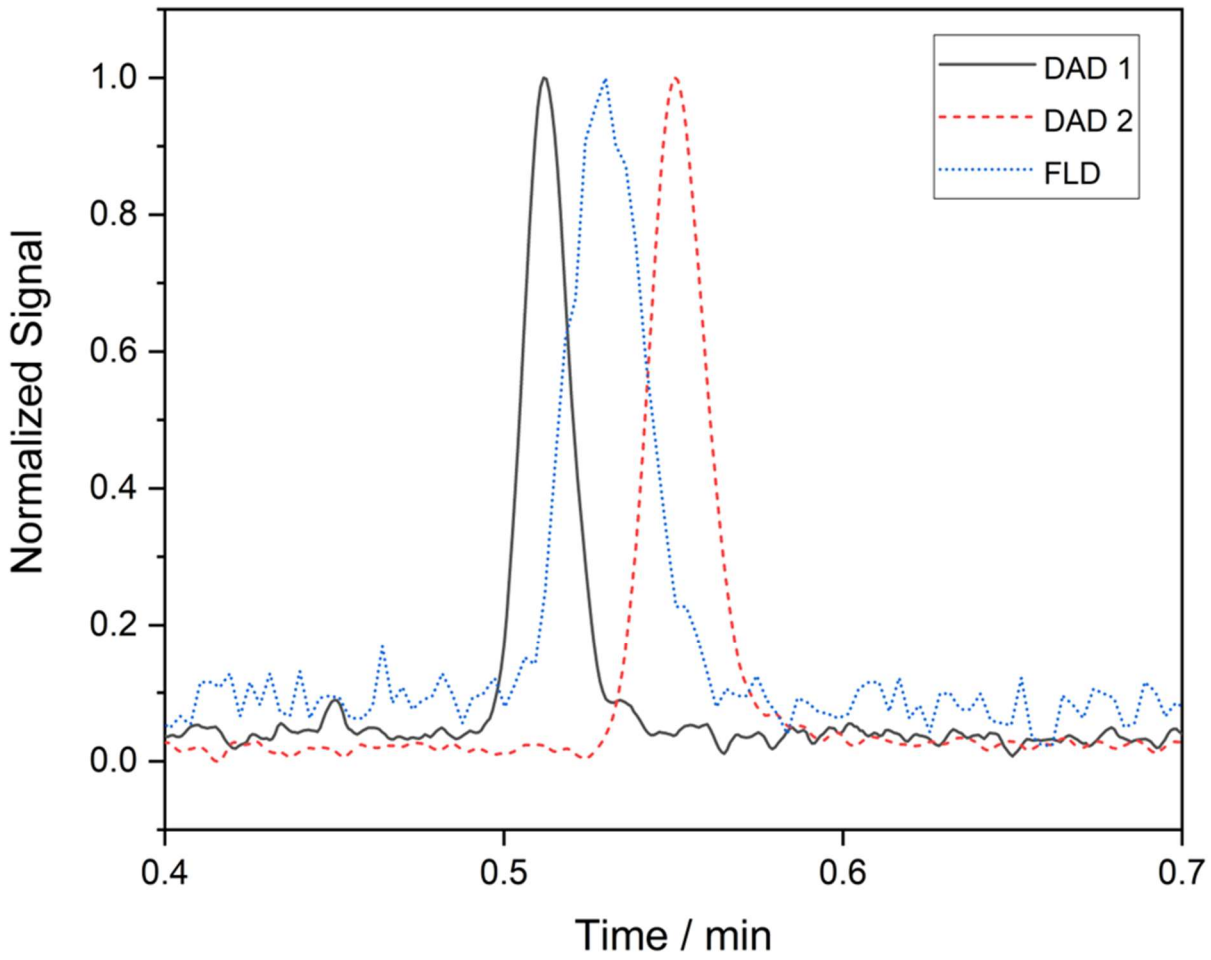

Figure 4-3: Normalized chromatogram of naproxen at k = 2 for the concentration-dependent detectors. Column: YMC-Triart C18, 50 × 0.3 mm, 1.9 µm; temperature: 50 °C; injection volume: 100 nL; F= 25 µL min^{-1}.

Only under the assumtion that turbulent mixing takes place in the detector cell can it be concluded that the sqauare of the cell volume is equal to peak variance [16]. In contrast, the inlets and outlets as well as the already discussed dead zones have a significant influence on the peak broadening. Based on the cell length of the DAD 1 being only half as long compared to the DAD 2, the signal intensity should be half as large. However, the resulting signal of DAD 1 is 8 times smaller, but at the same time the signal to noise ratio is only 1.5 times lower

(16 versus 24). On the other hand, the total dispersion of the system is reduced by 38% at a flow rate of 25 µL min^{-1}.

According to Lambert-Beer's law, the sensitivity of the UV detectors depends largely on the path length of the light beam through the sample. Nevertheless, other factors such as the light throughput play a decisive role. By increasing the ID of the cell, light coupling can be facilitated, but this increases the cell volume. Thus, while increasing the cell diameter has a positive effect on the detection limit, increasing the extra-post-column volume has a negative effect on band broadening and thus on the efficiency of the entire separation system. It is crucial to find the best balance between dispersion and sensitivity.

For the FLD, an S/N of only 6 was calculated under the same conditions. Comparing the total volumes of the concentration dependent detectors in Table 4-1, the retention time of naproxen using the FLD should be higher than for DAD 2. This only allows the conclusion that not the entire swept volume of the T-piece contributes to the total volume of the detector. The chromatogram of the FLD clearly shows the issue of the low data sampling rate at higher flow rates.The under sampling that occurs because of the lower data acquisition rate of the FLD can lead to electronic peak broadening. To eliminate the described weaknesses regarding sensitivity while maintaining portability, an active cooling of the LED by means of a heat sink and fan should be implemented. These modifications should substantially increase the utilizable intensity of the LED, thus increasing the detection limit and significantly reducing the noise. In addition, the installed T-pieces must be replaced by more suitable ones with a smaller bore to reduce the swept volume. The normalized peaks for the mass flow-dependent detectors are shown in Figure 4.

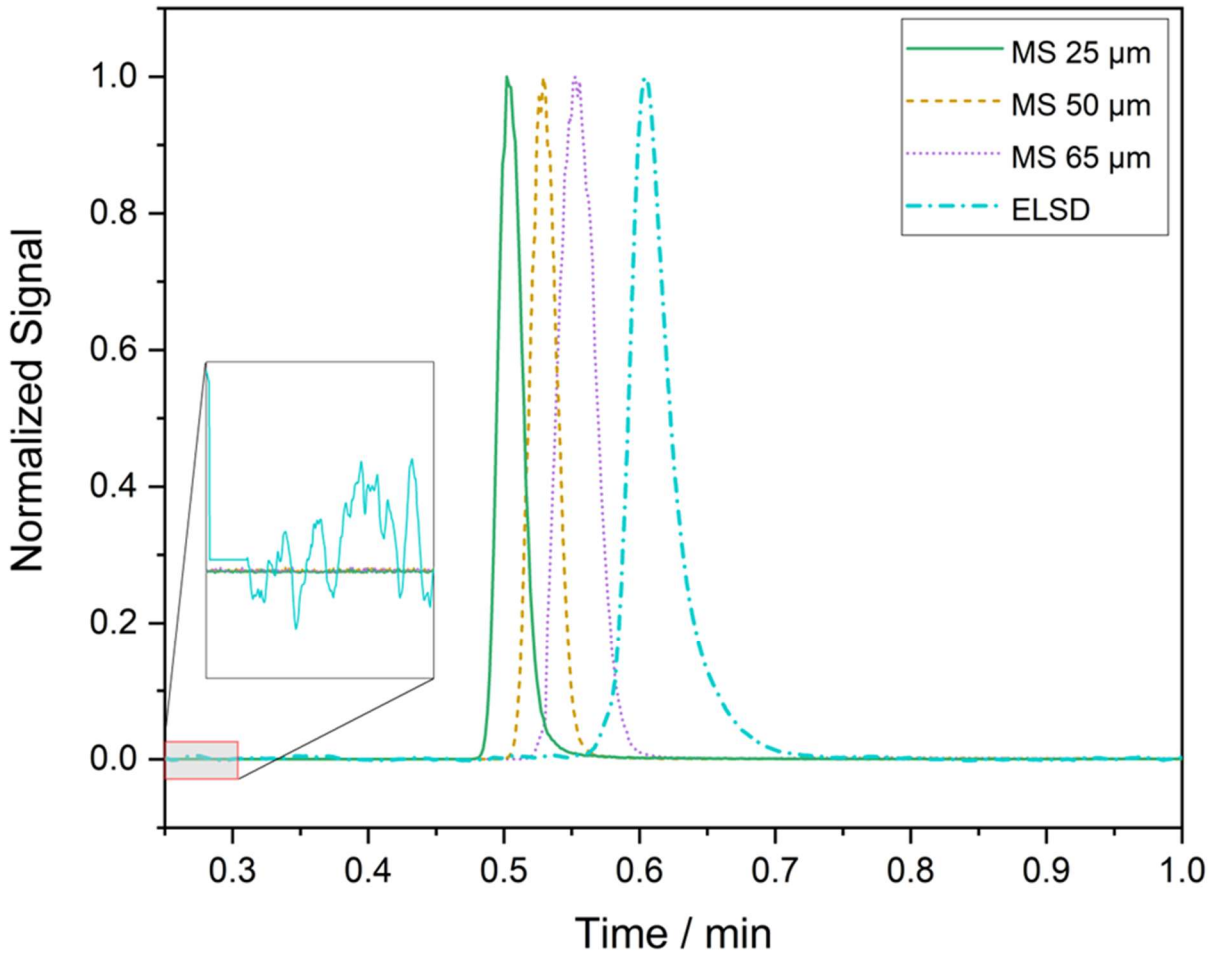

Figure 4-4: Normalized chromatogram of naproxen at k = 2 with zoom in on the baseline for the mass flow dependent detectors. Column: YMC-Triart C18, 50 × 0.3 mm, 1.9 µm; temperature: 50 °C; injection volume: 100 nL; F= 25 µL min^{-1}.

In the chromatogram of the ELSD, in addition to the peak broadening, a considerable tailing of the peak is evident. Using ESI-MS detection it can be assumed that after the spraying of the mobile phase the analyte peak does not experience any further dispersion [26]. In contrast to MS, in which ions are generated in the ion source and then transported through an electric field, in ELSD after nebulization in the micro flow chamber, molecules are transported through a gas stream in a heated spiral to get fully desolvated and subsequently detected. Because of the nature of the technology, it is not enough to modify only the periphery to utilize an ELSD for miniaturized applications; the components from nebulization to the optical detector must also be optimized.

For the different ESI-MS emitter tip capillaries, an S/N of $2{,}7 * 10^3$, $2{,}5 * 10^3$, and $3{,}0 * 10^3$ was determined with decreasing ID. Normally, at constant injection volume and constant concentration of the analyte, the S/N should decrease with increasing emitter ID due to higher extra-post-column volume and the resulting additional band broadening. This is not the case here and can be explained by the different surface roughness of the emitters. The ESI-MS

emitter with an ID of 65 µm is completely made of stainless steel while the other two emitters are made of PEEKsil™ and only the tip of these emitters is made of stainless steel. This in turn can lead to flow turbulences which influence the laminar flow at the wall region and have a negative effect on dispersion [16, 23]. In direct comparison of the ESI-MS emitter configurations no influence on the peak symmetry could be observed.

As expected, the mass flow–dependent detectors are, superior in direct S/N comparison to the concentration-dependent detector. It should also be noted that by simple modifications such as changing the nebulizer chamber of the ELSD or the simple change of the emitter tip ID of the ESI source, a successful coupling of conventional scale detector systems with MicroLC was achieved. This can contribute to the accelerating of the spread of miniaturized systems.

4.4 Conclusion

The assumption that only the cell volume of concentration-dependent detectors needs to be considered when determining the efficiency is a misconception. Due to the variety of detector designs, cell geometries, and the associated changes in the inner diameters and turns of the flow path, it can be concluded that there is no linear relationship between band broadening and extra-post-column volume. The comparison of the two UV detectors used in this study demonstrates that even if the modular design is retained, a reduction of the extra-post-column volume is possible using optical waveguides. If the volume is set in relation to the signal-to-noise ratio, it becomes clear that the efficiency gain outweighs the lower volume. In addition, it could be shown that a change to a larger capillary ID after the transfer capillary behind the column has a negative effect on the efficiency. This effect occurred especially at high flow rates as shown for the FLD and the ESI–MS emitter tip with an ID of 65 µm. In addition, the usable flow rate range can be shifted to lower flow rates by reducing the emitter tip ID. No negative influence was observed with a reduction of the diameter after the post-column transfer capillary ID. As assumed, the comparison of the MS setups clearly shows that by simply changing the ESI–MS emitter capillary, a conventional ion source can be used for miniaturized LC. This does not apply to the ELSD where, despite the use of a micro nebulizer, the evaporation area should also be optimized for the benefit of higher chromatographic efficiency. The investigated detector concepts also underline that the classical approach of “HiFi Tower” HPLC systems is no longer appropriate to fully utilize the intrinsic efficiency of sub 2 µm particle packed columns. Especially in the field of miniaturized HPLC, where the reduction of the extra-column volumes is of particular importance, systems should be used in which the individual components, e.g., pumps, valves, connecting tubing, and transfer capillaries, are fine-tuned to each other.

4.5 Supplementary Information

A previously undescribed portable FLD was used in this work. The emission spectrum of the LED shown in Figure 4-5 allows to draw conclusions about the general background noise of the system, the presence of parasitic emission, the emitted maximum wavelength, emission of higher order wavelength and the half-width of the emitted wavelength.

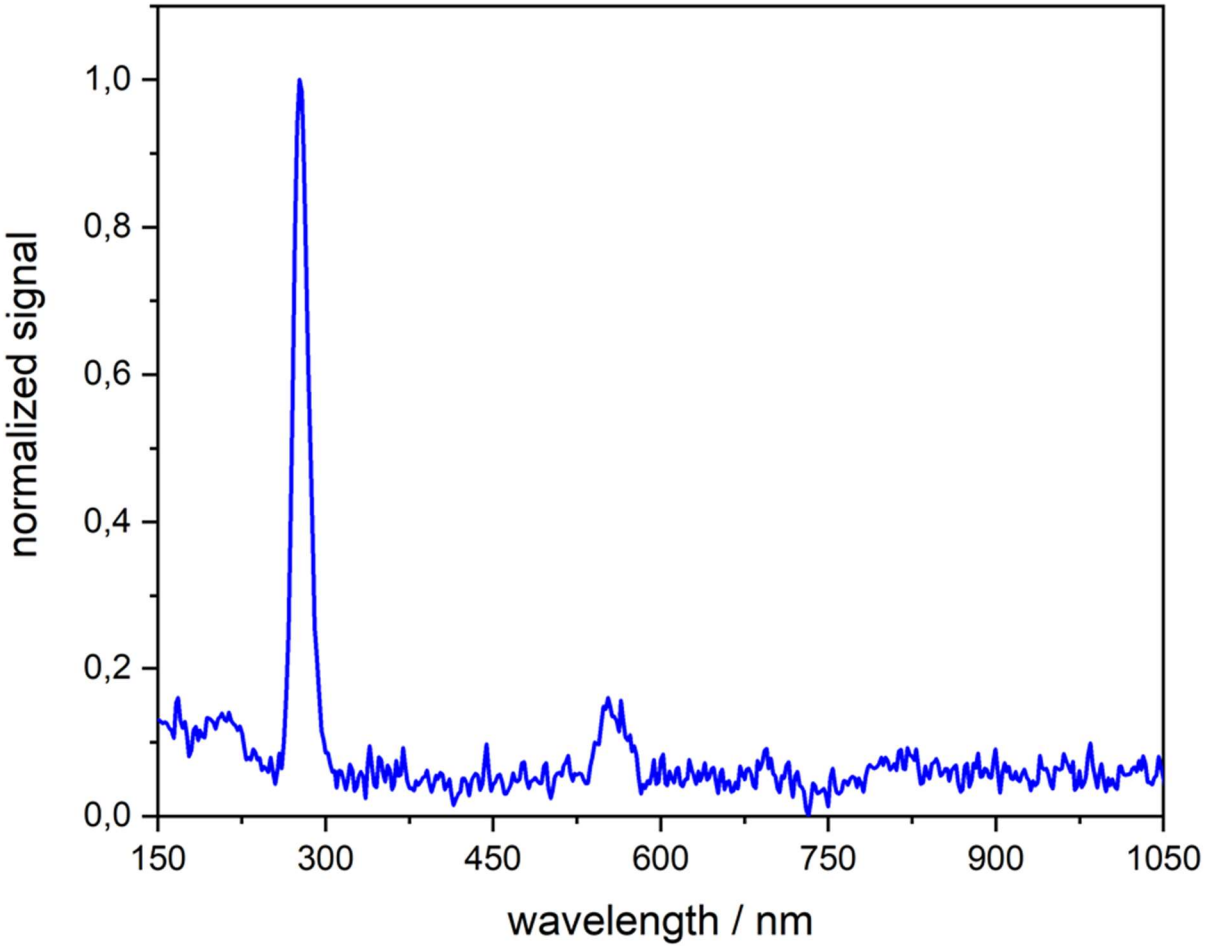

Figure 4-5: Emission spectrum of the UV-C-LED with a nominal wavelength of 275 nm. With an Emission band maximum at 276.5 nm and a band width at FWHM of 15.6 nm.

The maximum emission band measured was 276.5 nm. The slight shift of 1.5 nm in the wavelength of the LED can be attributed to temperature effects and the associated reduction in the band gap. The emission band width at half height was 15.6 nm. This allows the detection of analytes that are excitable at 250 – 300 nm. A significant background noise of 10% of the total signal can mainly be attributed to thermal effects due to the lack of active cooling [27, 28]. Despite the high background noise, a higher order band can be detected at twice the wavelength of the main emission band between 530-570 nm.

Another important factor affecting the sensitivity of the system is the ability of the LED to convert current into photons. Usually, the emission of photons is increased with an increase in

current, by recombination of electrons and holes. However, UV LEDs in particular have a low output optical power and therefore convert the current into thermal energy, which in turn leads to a decrease in the band gap and thus in the emission intensity [28, 29]. Figure 4-6 shows the influence between current, temperature and emission intensity.

An equidistant increase of the current did not lead to an equal increase of the emission intensity, as can be seen in Figure 4-6a. In addition, for an LED power > 50%, the additional power was largely converted into thermal energy. This can be clearly seen in the continuous drop in emission intensity. Furthermore, an increase in the background noise can also be observed. Figure 4-6b shows the influence of the heat buildup of the LED on the emission intensity. Figure 4-6c depicts the zoom of the first 250 seconds of the intensity drop. As early as 5 seconds after switching on the LED, 10% of the maximum intensity was lost. This was reduced to 80% after 100 seconds and after approximately 240 seconds, 30% of the emission intensity was lost. After 30 minutes the signal was constant, at this time only 45% of the initially detected radiation could still be observed.

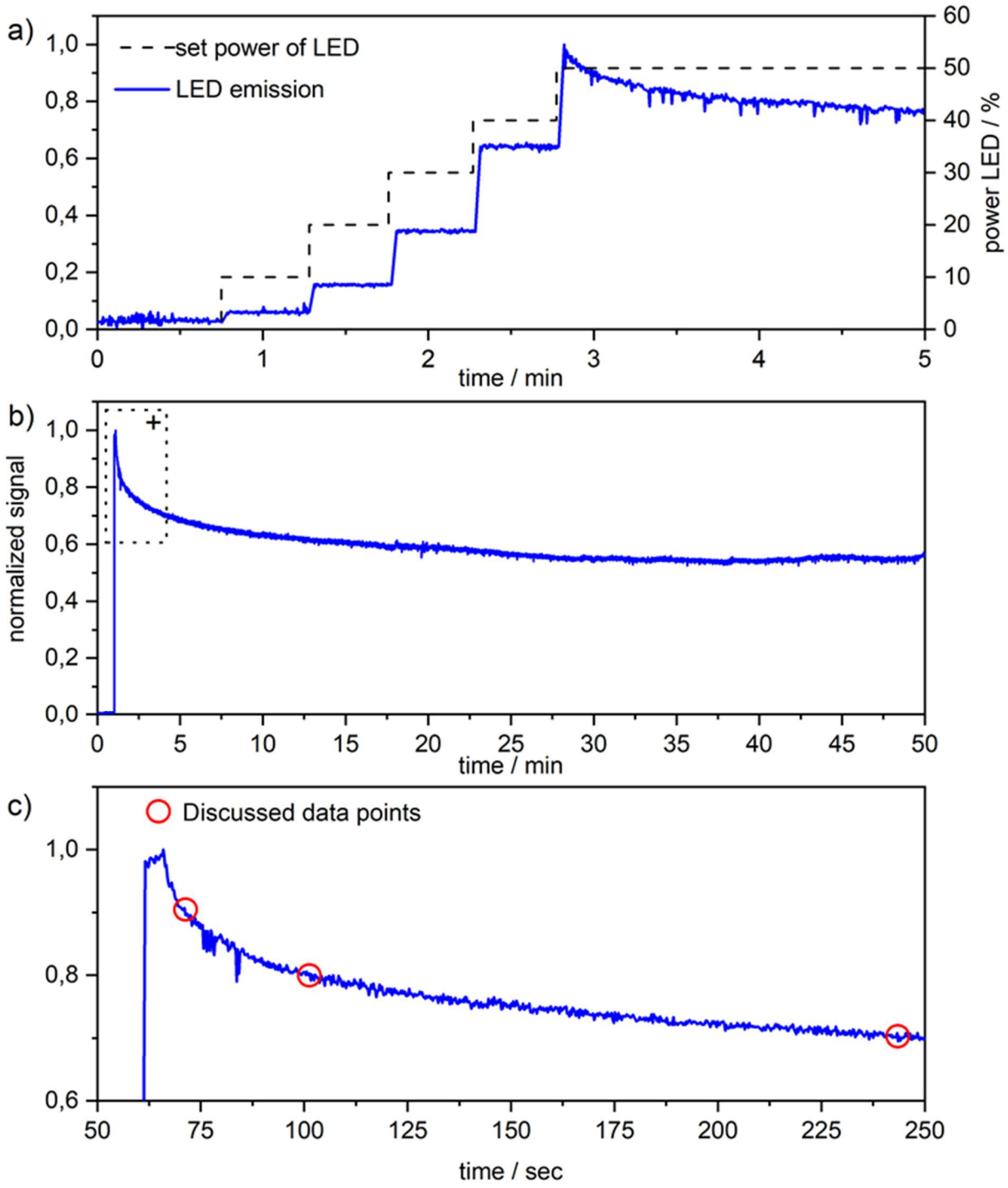

Figure 4-6: (a) Influence of the LED power on the signal intensity. (b) Decrease in signal intensity due to the heating of the LED. c) Enlargement of the section marked with a dotted rectangle in b), red circles mark the data points described in the text.

Figure 4-7 summarizes photos of the relevant components of the NanoFLD. The NanoFLD can excite the analyte in the measurement cell with different light sources in a wavelength range below 300 nm and detect the fluorescence signal of the sample components both as a spectrum in the wavelength range from 250 nm to 1050 nm and above 310 nm in sum from the whole solid angle.

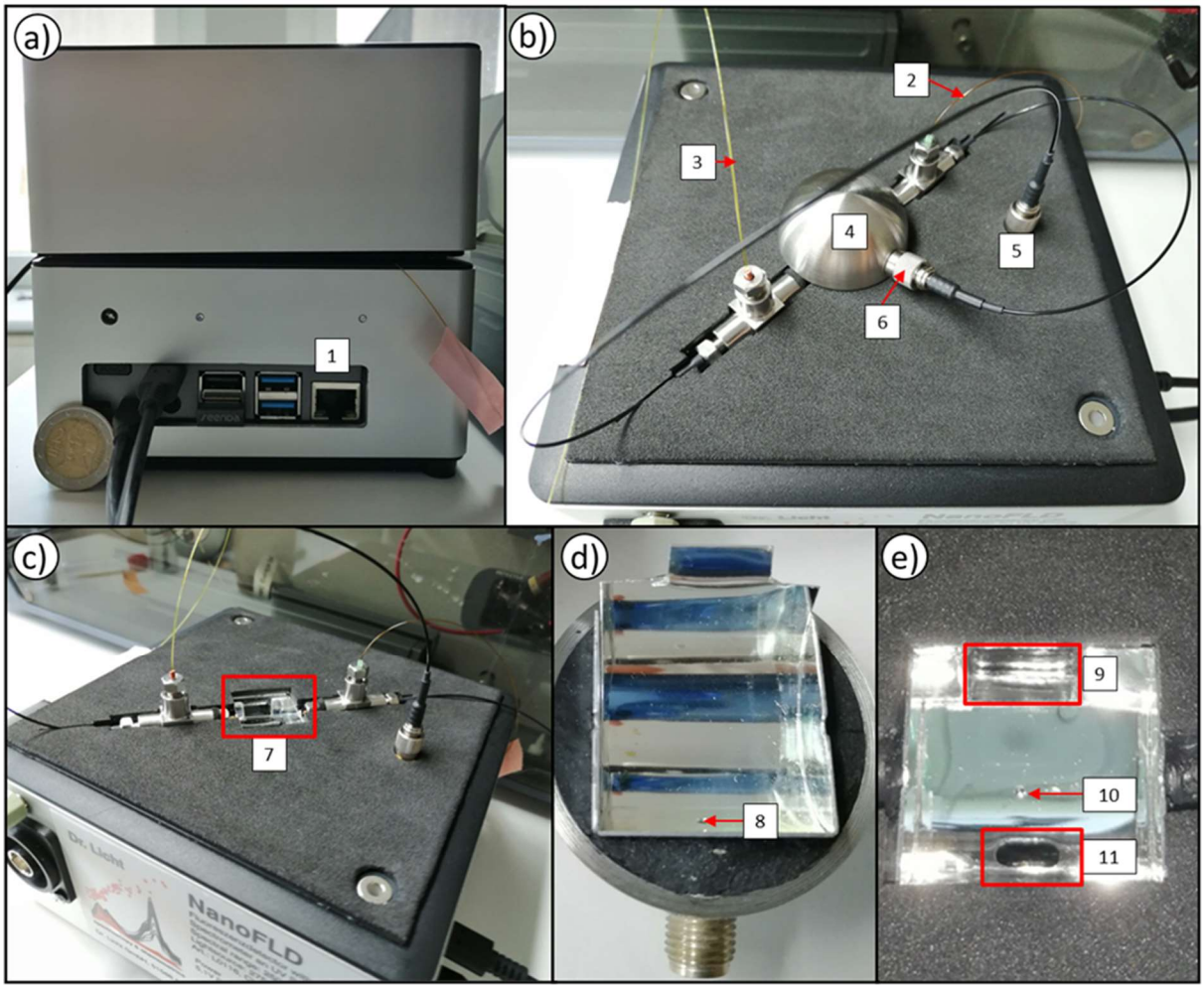

Figure 4-7: Photo documentation of the previously undescribed nanoFLD with front view, opened housing, opened detector cell, and detail shots of the upper and lower halves of the detector cell. Number description referenced in the text.

a) shows the front view of the detector with a 2-euro piece for size reference, the diameter of a 2-euro piece is 25.75 mm. 1: Besides the power input, the detector is equipped with 2x USB 2 sockets, 2x USB 3 sockets, 1x Gigabit Ethernet socket and a 4 pin audio port. On the side of the detector is a BNC socket with analog signal output in the range of 0-1500 mV and a 3.5 mm jack socket as TTL input for the external start signal.

b) The open housing allows a view of the entire cell design. 2 and 3 mark the flow from HPLC to waste. Under the dome in 4 is the heart of the measuring cell with mirrored interior, optical inputs and outputs, and the flow cell. At 5, the LED for excitation of the sample is coupled in the axial direction. at 6, the emitted fluorescence light is directed into the detector cell from the axial direction.

c) Interior view with detector cell open.7: In the area marked in red, the fixed lower part of the mirrored measuring cell can be seen. The flow cell the flow cell based on a stripped fused silica capillary can be seen in the center.

d) Interior view of the upper dome from 4. In the upper part of the mirrored cover, there is only the hole marked with 8 for the introduction of the emitted axial fluorescent light into the measuring cell.

e) Detail view of the lower part of the measuring cell. 9: Entrance to the photometer. 10: entrance to the photomultiplier 11: entrance for direct irradiation from the LED with filter window.

4.6 References

[1] D.A. Vargas Medina, E.V.S. Maciel, A.L. de Toffoli, F.M. Lanças, Miniaturization of liquid chromatography coupled to mass spectrometry.: 2. Achievements on modern instrumentation for miniaturized liquid chromatography coupled to mass spectrometry, TrAC - Trends Anal. Chem. 128 (2020) 115910. https://doi.org/10.1016/j.trac.2020.115910.

[2] K. Mejía-Carmona, J. Soares da Silva Burato, J.V.B. Borsatto, A.L. de Toffoli, F.M. Lanças, Miniaturization of liquid chromatography coupled to mass spectrometry: 1. Current trends on miniaturized LC columns, TrAC - Trends Anal. Chem. 122 (2020) 115735. https://doi.org/10.1016/j.trac.2019.115735.

[3] A. Agrawal, R. Keçili, F. Ghorbani-Bidkorbeh, C.M. Hussain, Green miniaturized technologies in analytical and bioanalytical chemistry, TrAC Trends Anal. Chem. 143 (2021) 116383. https://doi.org/https://doi.org/10.1016/j.trac.2021.116383.

[4] P.I. Napolitano-Tabares, I. Negrín-Santamaría, A. Gutiérrez-Serpa, V. Pino, Recent efforts to increase greenness in chromatography, Curr. Opin. Green Sustain. Chem. 32 (2021) 100536. https://doi.org/10.1016/j.cogsc.2021.100536.

[5] Y. Bian, R. Zheng, F.P. Bayer, C. Wong, Y.C. Chang, C. Meng, D.P. Zolg, M. Reinecke, J. Zecha, S. Wiechmann, S. Heinzlmeir, J. Scherr, B. Hemmer, M. Baynham, A.C. Gingras, O. Boychenko, B. Kuster, Robust, reproducible and quantitative analysis of thousands of proteomes by micro-flow LC–MS/MS, Nat. Commun. 11 (2020) 1–12. https://doi.org/10.1038/s41467-019-13973-x.

[6] T. Vehus, H. Roberg-Larsen, J. Waaler, S. Aslaksen, S. Krauss, S.R. Wilson, E. Lundanes, Versatile, sensitive liquid chromatography mass spectrometry-Implementation of 10 μm OT columns suitable for small molecules, peptides and proteins, Sci. Rep. 6 (2016) 1–10. https://doi.org/10.1038/srep37507.

[7] T. Hetzel, C. vom Eyser, J. Tuerk, T. Teutenberg, T.C. Schmidt, Micro-liquid chromatography mass spectrometry for the analysis of antineoplastic drugs from wipe samples, Anal. Bioanal. Chem. 408 (2016) 8221–8229. https://doi.org/10.1007/s00216-016-9932-y.

[8] K. Vanderlinden, K. Broeckhoven, Y. Vanderheyden, G. Desmet, Effect of pre- and post-column band broadening on the performance of high-speed chromatography columns under isocratic and gradient conditions, J. Chromatogr. A. 1442 (2016) 73–82. https://doi.org/10.1016/j.chroma.2016.03.016.

[9] K. Broeckhoven, G. Desmet, The future of UHPLC: Towards higher pressure and/or smaller particles?, TrAC Trends Anal. Chem. 63 (2014) 65–75. https://doi.org/https://doi.org/10.1016/j.trac.2014.06.022.

[10] F. Rahimi, S. Chatzimichail, A. Saifuddin, A.J. Surman, S.D. Taylor-Robinson, A. Salehi-Reyhani, A Review of Portable High-Performance Liquid Chromatography: the Future of the Field?, Springer Berlin Heidelberg, 2020. https://doi.org/10.1007/s10337-020-03944-6.

[11] S.C. Lam, L.J. Coates, M. Hemida, V. Gupta, P.R. Haddad, M. Macka, B. Paull, Miniature and fully portable gradient capillary liquid chromatograph, Anal. Chim. Acta. 1101 (2020) 199–210. https://doi.org/https://doi.org/10.1016/j.aca.2019.12.014.

[12] S. Sharma, A. Plistil, H.E. Barnett, H.D. Tolley, P.B. Farnsworth, S.D. Stearns, M.L. Lee, Hand-Portable Gradient Capillary Liquid Chromatography Pumping System, Anal. Chem. 87 (2015) 10457–10461. https://doi.org/10.1021/acs.analchem.5b02583.

[13] J. Lankelma, D.J. van Iperen, P.J. van der Sluis, Towards using high-performance liquid chromatography at home, J. Chromatogr. A. 1639 (2021) 461925. https://doi.org/10.1016/j.chroma.2021.461925.

[14] C.-K. Su, Review of 3D-Printed functionalized devices for chemical and biochemical analysis, Anal. Chim. Acta. 1158 (2021) 338348. https://doi.org/https://doi.org/10.1016/j.aca.2021.338348.

[15] H.K. Balakrishnan, E.H. Doeven, A. Merenda, L.F. Dumée, R.M. Guijt, 3D printing for the integration of porous materials into miniaturised fluidic devices: A review, Anal. Chim. Acta. (2021) 338796. https://doi.org/https://doi.org/10.1016/j.aca.2021.338796.

[16] G. Desmet, K. Broeckhoven, Extra-column band broadening effects in contemporary liquid chromatography: Causes and solutions, TrAC - Trends Anal. Chem. 119 (2019) 115619. https://doi.org/10.1016/j.trac.2019.115619.

[17] T. Hetzel, D. Loeker, T. Teutenberg, T.C. Schmidt, Characterization of the efficiency of microbore liquid chromatography columns by van Deemter and kinetic plot analysis, J. Sep. Sci. 39 (2016) 3889–3897. https://doi.org/10.1002/jssc.201600775.

[18] T.L. Chester, Recent developments in high-performance liquid chromatography stationary phases, Anal. Chem. 85 (2013) 579–589. https://doi.org/10.1021/ac303180y.

[19] T. Werres, T.C. Schmidt, T. Teutenberg, The influence of injection volume on efficiency of microbore liquid chromatography columns for gradient and isocratic elution, J. Chromatogr. A. 1641 (2021) 461965. https://doi.org/10.1016/j.chroma.2021.461965.

[20] G. Taylor, P.R.S.L. A, Dispersion of soluble matter in solvent flowing slowly through a tube, Proc. R. Soc. London. Ser. A. Math. Phys. Sci. 219 (1953) 186–203. https://doi.org/10.1098/rspa.1953.0139.

[21] R. Aris, P.R.S.L. A, On the dispersion of a solute in a fluid flowing through a tube, Proc. R. Soc. London. Ser. A. Math. Phys. Sci. 235 (1956) 67–77. https://doi.org/10.1098/rspa.1956.0065.

[22] B. He, N. Tait, F. Regnier, Fabrication of Nanocolumns for Liquid Chromatography, Anal. Chem. 70 (1998) 3790–3797. https://doi.org/10.1021/ac980028h.

[23] B. Filip, R. Bochenek, K. Baran, D. Strzałka, D. Antos, Influence of the geometry of extra column volumes on band broadening in a chromatographic system. Predictions by computational fluid dynamics, J. Chromatogr. A. 1653 (2021) 462410. https://doi.org/10.1016/j.chroma.2021.462410.

[24] C. Gunnarson, T. Lauer, H. Willenbring, E. Larson, M. Dittmann, K. Broeckhoven, D.R. Stoll, Implications of dispersion in connecting capillaries for separation systems involving post-column flow splitting., J. Chromatogr. A. 1639 (2021) 461893. https://doi.org/10.1016/j.chroma.2021.461893.

[25] G. Desmet, D. Cabooter, K. Broeckhoven, Graphical Data Representation Methods To Assess the Quality of LC Columns, Anal. Chem. 87 (2015) 8593–8602. https://doi.org/10.1021/ac504473p.

[26] D. Spaggiari, S. Fekete, P.J. Eugster, J.L. Veuthey, L. Geiser, S. Rudaz, D. Guillarme, Contribution of various types of liquid chromatography-mass spectrometry instruments to band broadening in fast analysis, J. Chromatogr. A. 1310 (2013) 45–55. https://doi.org/10.1016/j.chroma.2013.08.001.

[27] Y. Li, P.N. Nesterenko, B. Paull, R. Stanley, M. Macka, Performance of a New 235 nm UV-LED-Based On-Capillary Photometric Detector, Anal. Chem. 88 (2016) 12116–12121. https://doi.org/10.1021/acs.analchem.6b02832.

[28] S.C. Lam, V. Gupta, P.R. Haddad, B. Paull, 3D Printed Liquid Cooling Interface for a Deep-UV-LED-Based Flow-Through Absorbance Detector, Anal. Chem. 91 (2019) 8795–8800. https://doi.org/10.1021/acs.analchem.9b01335.

[29] M. Hemida, L.J. Coates, S. Lam, V. Gupta, M. Macka, H.J. Wirth, A.A. Gooley, P.R. Haddad, B. Paull, Miniature Multiwavelength Deep UV-LED-Based Absorption Detection System for Capillary LC, Anal. Chem. 92 (2020) 13688–13693. https://doi.org/10.1021/acs.analchem.0c03460.

Chapter 5 Interplay between extra-column volume and effective-column volume on efficiency: investigation of the column inner diameter in UHPLC and miniaturized LC

This chapter was adapted from: T. Werres, T.C. Schmidt, T. Teutenberg, Influence of the Column Inner Diameter on Chromatographic Efficiency in Miniaturized and Conventional Ultra-High-Performance Liquid Chromatography. Chromatographia 86 (2023) 143–151. https://doi.org/10.1007/s10337-023-04237-4.

Abstract: To reduce solvent consumption and cycle times of analyses, the inner diameters (ID) of separation columns are being reduced continuously in HPLC. In particular, 1.0 mm inner diameter columns seem to be the next logical step, as they represent a good compromise between resilience and speed. However, the necessary optimization of the extra-column volume is often not considered. The aim of the study was therefore to investigate the influence of the column inner diameter on the efficiency in the isocratic and gradient elution mode. Emphasis was placed on the relationship between extra-column volume and effective-column volume. The performance of 0.3, 0.5, 1.0 and 2.1 mm inner diameter columns were compared on a µ-HPLC and UHPLC system. To enable a fair comparison between the different columns the linear flowrate was kept constant. In isocratic mode the influence of the extra-column volume dispersion was assessed by the peak standard deviation and the reduced plate height. In gradient mode the separation of 7 antineoplastic drugs on the columns was used and rated based on the peak capacity and chromatographic resolution. Amongst other things it was shown that the ratio between extra-column volume and effective-column volume can be a simple parameter for choosing an appropriate column ID-HPLC combination. An unfavorable ratio between extra-column volume and effective-column volume led to a doubling of the minimum plate height in these investigations.

5.1 Introduction

As early as 1983, Jorgenson and Guthrie proposed the theory that smaller column inner diameters (ID) will lead to more efficient columns [1]. Today, the combination of very small capillary diameters and the reduction of column and particle diameters enable fast and efficient analyses in miniaturized LC without having to resort to high pressures [2, 3]. As a positive side effect by downsizing of the system components, a significant reduction in solvent consumption can be accomplished, making µ-HPLC an attractive alternative also in the context of Green Analytical Chemistry (GAC) [4–6]. While problems such as a poor packing quality of miniaturized separation columns are a bygone era, the reduced loading capability is an inherentdisadvantage [7]. However, especially when coupled with mass spectrometry, which is becoming increasingly important, this issue does not necessarily represent a disadvantage. Due to the reduced injection volume and lower flow rates, less matrix is introduced into the ion source. Therefore, competing ionization between the matrix and the target analytes is reduced, ionization efficiency increases, and the signal-to-noise ratio improves which in turn benefits the detection limits [8, 9]. This can also have a positive effect on the operating times and maintenance intervals, making the combination of MS with µ-HPLC a "marriage made in heaven" [10]. Furthermore, the reduction in column ID results in less radial dilution of molecules, the injection plug remains more concentrated, and there is a direct correlation between column ID and signal intensity [11]. Whereas miniaturized systems were previously used primarily in areas where sample volume is limited, they are now also increasingly being used in many other fields, such as process control [12].

With the introduction of UHPLC and the extended usable backpressure of modern systems, two trends towards the establishment of faster analyses have emerged in conventional HPLC. First, fast analyses are accomplished by extremely high flow rates, in some cases up to 8 mL/min [13]. However, in addition to high solvent consumption, other problems arise, such as frictional heating in the columns and generally poorer coupling capability to mass flow-dependent detector systems [14]. On the other hand, smaller column IDs are increasingly used in conventional HPLC in order to reduce analysis time through higher linear flow rates. Where 4.6 mm ID columns used to be the standard, 2.1 mm ID columns are now increasingly being used. Columns with an inner diameter of 1.0 mm are a good compromise between loadability and speed [15]. In this way, fast analyses with reduced resource consumption can also be achieved with UHPLC. However, in these column dimensions the extra-column volume starts to have a significant influence on the band broadening, so that optimization of the capillaries and peripheries becomes necessary [16].

Numerous investigations have focused on band broadening in HPLC. The majority of these rely on concentration-dependent detectors, primarily due to their simplicity [17–20]. It is true that the band broadening of various miniaturized detector systems has already been compared in the context of our own previous research studies, which also focused on mass flow-dependentdetectors [21]. Paradoxically, despite the increased importance of MS, band broadening studies performed in combination with this detection technique are scarce. This can be explained by the fact that especially the processes in the ionization source are strongly flow rate dependent. As a consequence, especially for large flow rate ranges parameters like needle position, voltages, gas flows or the ionization temperature have to be adjusted which makes direct correlations difficult but not impossible [22].

The aim of the study was therefore to investigate the influence of the column ID on the chromatographic efficiency in isocratic and gradient elution coupled with MS detection. For this purpose, the column ID was varied between 0.3-2.1 mm. For the performance of the experiments a µ-HPLC and a UHPLC system were used. The main focus was on the separation column with 1.0 mm ID as a bridge between both HPLC systems. In the isocratic range, band broadening was investigated using an already established sample mixture [7]. For the evaluation of the separation efficiency in gradient mode, a modified already published method for the determination of antineoplastic drugs in wipe samples was used [23].

5.2 Materials and Methods

5.2.1 Experimental Setup

The Nexera Mikros (Shimadzu Europa GmbH, Duisburg, Germany) was used as µ-HPLC in this study and consisted of the Mikros column oven, the LC Mikros pump, an SIL-30AC autosampler, a CBM-20A controller and a DGU-20A3R degassing unit. NanoViper™ fingertight fittings (Thermo Fisher Scientific, Waltham, Massachusetts, USA) with 50 µm ID were used for pre-column tubing. Post-column tubing was done via the UF-Link mechanism coupled directly to the Mikros emitter capillary.

An LC-40 system from Shimadzu was used as UHPLC and consisted of the Mikros column oven, two LC-40D X3 pumps, an SIL-40CX3 autosampler, an SCL-40 controller, and a DGU-40S degassing unit. A 20 µL static mixer was installed and tubing was done via 100 µm ID stainless steel tubing.

Both HPLC-systems were hyphenated to a Shimadzu 8060 triple quadrupole mass spectrometer equipped with the standard ESI ion source and fitted with a microESI capillary (225-12438-42). For the experiments with the Nexera Mikros the Micro-ESI source was installed.

The IDs investigated in the study were 0.3, 0.5, 1.0 and 2.1 mm. The columns with a length of 50 mm were packed with the YMC-Triart C18 fully porous 1.9 µm particles with a pore size of 120 Å (YMC Europe GmbH, Dinslaken, Germany). During measurements the column was heated to 40 °C.

5.2.2 Chemicals and Reagents

LC-MS grade water and acetonitrile (ACN) were used as mobile phases and were purchased from Th. Geyer (Chemsolute, Renningen, Germany). To adjust the pH, formic acid (Sigma-Aldrich, Seelze, Germany) was added to a total volume concentration of 0.1%.

Carbamazepine, acetylsalicylic acid (ASA), etoposide, gemcitabine, cyclophosphamide, ifosfamide, paclitaxel and Docetaxel were purchased from Sigma-Aldrich. Uracil was used to determine the column void time and methotrexate were bought from Honeywell Fluka (Thermo Fisher Scientific). For the experiments stock solutions for each compound were prepared in equal volume percentages of ACN/H_2O with a concentration of 1 g/L.

All stock solutions were diluted to their final concentration in a solvent that corresponded precisely to the isocratic mobile phase (φ=0.25) or the starting conditions of the solvent gradient (φ=0.10). For the isocratic experiments the standards were diluted to a final concentration of carbamazepine = 0.06 ng/mL, acetylsalicylic acid = 50 ng/mL, etoposide = 1.25 ng/mL, and uracil = 5 ng/mL. For the gradient elution the seven antineoplastic drugs were diluted to a final concentration of 10 ng/mL.

5.2.3 Experimental Conditions

All scaling within this work was performed based on the 0.3 mm ID column. To allow a fair comparison between different columns, the flow rate has to be adjusted so that the same linear flow rate prevails. This scaling was performed using the following equation.

$$F_2 = \left(\frac{ID_2}{ID_1}\right)^2 * F_1 \qquad \text{Equation 5-1}$$

Where F_1 and F_2 is the flow rate and ID_1 and ID_2 the inner diameter for the first and second column.

Because gradient elution offers the benefit of focusing of the injection plug on the column head two injection volumes of 1 µL and 5 µL were investigated in gradient elution. In isocratic elution, it is necessary to guarantee that an equivalent amount of compound and injection volume is introduced on the column in relation to the effective column volume (V_{eff}). To exclude the effects of volume overloading as far as possible, the injection volume was limited to 4% of V_{eff} in isocratic elution. V_{eff} was calculated according to Equation 5-2.

$$V_{eff} = r^2 * \pi * L * \epsilon \qquad \text{Equation 5-2}$$

Where r is the radius of the column, L the length of the column and ϵ the porosity of the stationary phase. For the material used an $\epsilon = 0.7$ can be assumed. Furthermore, the equation shows that the injection volume correlates to the square of the ID.

For gradient elution, after transferring the injection volume, the sample loop was removed from the flow path by switching the injection valve a second time. Thus, the gradient dwell volume that can contribute to extra-column band broadening (ECBB) can be reduced by the loop volume and a port-to-port volume of the valve. To avoid the additional pressure pulse, valve switching was omitted under isocratic conditions.

The visualization of the influence of column ID in relationship to the extra-column volume on the peak broadening calculations are based on the volume peak deviations (σ). The transformation of the peak widths (w_h) was done at the full width at half maximum (FWHM) using Equation 5-3:

$$\sigma = \frac{w_h}{2.355} * F \qquad \text{Equation 5-3}$$

Additionally, reduced plate height (h) versus linear velocity (u_0) plots were compared to further discuss the relationship between extra-column volume and effective-column volume.

The resolution R was also calculated at FWHM using Equation 5-4:

$$R = 1.18 * \left(\frac{t_{r1} - t_{r2}}{w_{h1} + w_{h2}}\right) \qquad \text{Equation 5-4}$$

Where t_{r1} is the retention time of the first and t_{r2} the retention time of the second component. The peak capacity (n_p) describes how many compounds can be separated with a defined resolution in a given gradient time (t_G). Therefore, n_p is a good measure of the efficiency of a column under gradient conditions. n_p was calculated using Equation 5-5.

$$n_p = 1 + \frac{2{,}354 * t_G}{4 * w_h}$$ Equation 5-5

In order to achieve a good spacing between the investigated components, a mobile phase composition of 25/75 (water/ACN) was chosen in the isocratic elution. The retention factors could now be adjusted between 2 and 8. The effective gradient time was 3.5 min. The programmed gradient in relation to water was as follows. 0.00-0.05 90%; 0.05-2.85 50%; 2.85-3.55 1%; 3.55-3.95 1%; 3.95-4.05 90; 4.05-6.00 90%.

Under ideal experimental conditions, the ion source parameters should be kept constant for all experiments. However, as already described in the introduction, these are strongly dependent on the flow rate. Overall, due to the scaling a flow range of 1.5-539 µL/min was investigated. Therefore, when changing to larger column IDs and thus higher flow rates, it was inevitable to resort to higher temperatures to ensure sufficient desolvation. The source parameters used are summarized in Table 5-1.

Table 5-1: Summary of the set ion source parameters.

Parameter	Value				Unit
Column ID	0.3	0.5	1.0	2.1	mm
Nebulizing gas flow rate	1.5	1.5	1.5	1.5	L/min
Interface temperature	3	3	3	3	°C
Desolvation line temperature	100	100	150	250	°C
Heat block temperature	400	400	400	400	°C
Drying gas flow	0	0	0	5	L/min

For MS data acquisition multiple reaction monitoring (MRM) was used. In the isocratic experimentation the following mass transitions were used: uracil *m/z* 113->96; etoposide *m/z* 589->229; carbamazepine *m/z* 237->194; and acetylsalicylic acid in negative mode *m/z* 179->137. The dwell time was 49 ms.

For gradient elution the following multiple transitions were usesd: gemcitabine, *m/z* 264-> 112; methotrexate *m/z* 455->175, 134; ifosfamide *m/z* 261->182, 154; cyclophosphamide *m/z* 261->106, 140; etoposide *m/z* 589->229; 185, paclitaxel *m/z* 854->569; 286; 7. Docetaxel as Na-adduct *m/z* 830->304;248.

5.2.4 Software and Data Processing

Data acquisition was performed using LabSolutions Version 5.109 (Shimadzu). Further data processing was performed using Origin 2022b (9.95) and Microsoft Office Excel 365 Version.

5.3 Results and Discussion

5.3.1 Isocratic Mode Evaluation

With decreasing column ID, the volume of the analyte peak is reduced to the same extent as the injection volume is adapted to the effective column volume. As a consequence, the band broadening in the connecting tubes can have a significant influence on the chromatographic performance. In isocratic mode, the relevant extra-column volume (V_{ex}) is composed of the injection volume (V_{inj}), the pre-column volume (V_{pre}) consisting of the inlet tubing and a port-to-port volume of the switching valve and the post-column volume (V_{post}) comprising the outlet tubing and the ESI-emitter capillary. All connection tubing or additional volume before the injection plug is irrelevant.

When comparing different column IDs it is necessary to perform the experiments on band broadening at the same linear flow velocity and to adjust the injection volume and substance mass in relation to the effective column volume. In this way, possible effects on peak dispersion due to mass or volume overloading of the column can be minimized. A direct correlation between the ECBB and the extra-column volume is not possible. Especially in miniaturized systems, various system components have an increasing influence on the peak dispersion. Nevertheless, a rough estimate of the expected band broadening of the investigated configurations can be made using the quotient of V_{eff}/V_{ex}. The assumptions used to determine this parameter are summarized in Table 5-2.

Table 5-2: System volumes of the investigated configurations used for the determination of V_{eff}/V_{ex}

System	ID	V_{eff}	V_{pre}	V_{post}	V_{inj}	V_{ex}	V_{eff}/V_{ex}
	mm	µL	µL	µL	µL	µL	
Mikros	0.3	2.5	1.5	0.3	0.1	1.9	1.3
Mikros	0.5	6.9	1.5	0.3	0.3	2.1	3.3
Mikros	1.0	27.5	1.5	0.3	1.1	2.9	9.4
LC-40	1.0	27.5	4.7	2.6	1.1	8.4	2.0
LC-40	2.1	121.1	4.7	2.6	5.0	13.5	9.0

The visualization of the band broadening was done by volume peak dispersion. This allows a correlation between the band broadening and the flow rate used. The results of the isocratic investigations are shown in Figure 5-1.

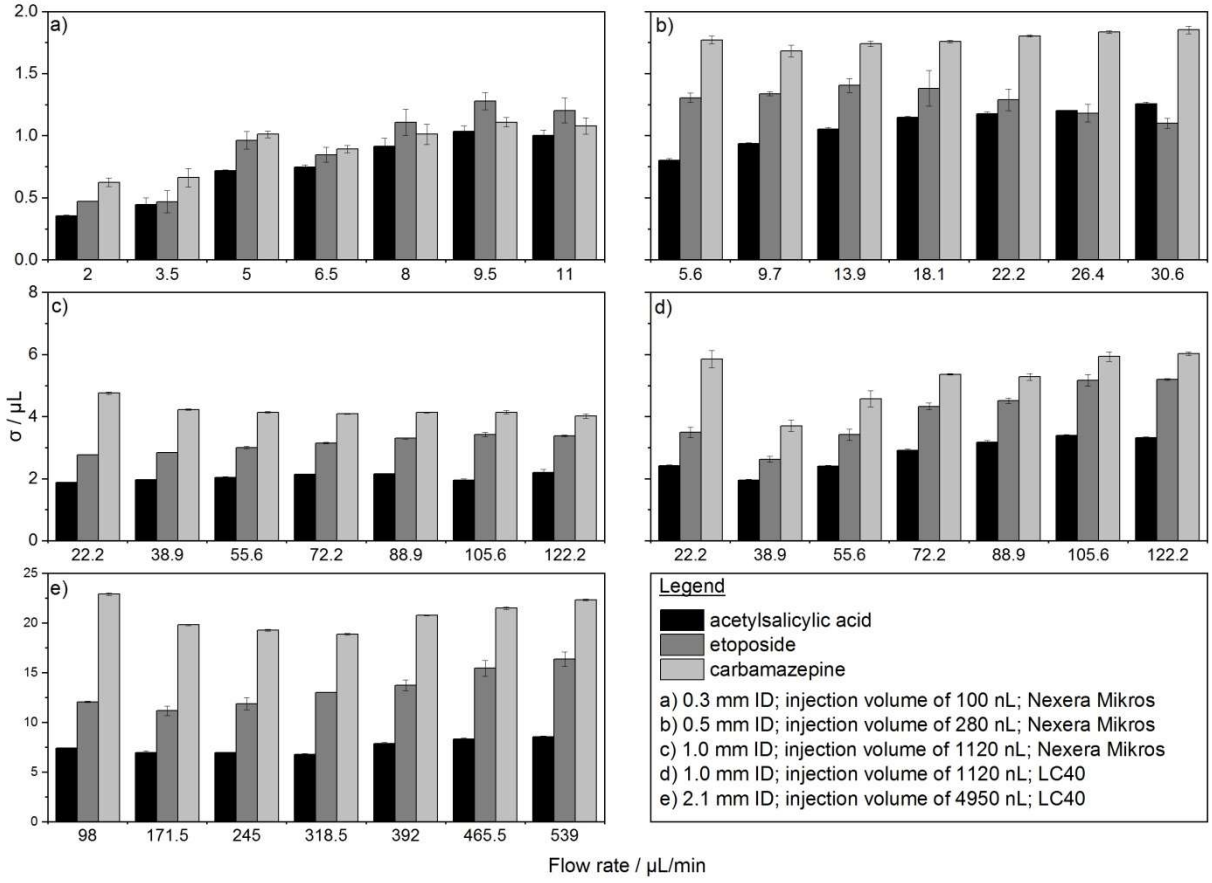

Figure 5-1: Effect of different column IDs and HPLC-systems on peak standard deviation. Injection volumes, sample concentrations and flow rates were proportional to column ID. The analytes are sorted by increasing retention factor from left to right. Error bars indicate the standard deviation calculated for n = 3.

It was shown that for all configurations investigated, an increase in dispersion can be observed with increasing retention factor. In addition, the flow rate and thus also σ increase with increasing ID. As expected, the lowest peak standard deviation of 0.35-1.08 µL was observed for the 0.3 mm ID column in Figure 5-1 a, but the unfavorable V_{eff}/V_{ex} ratio of 1.3 could be seen from the constant increase in σ with higher flow rates. A similarly distinct trend was also identified for the 1.0 mm ID column coupled to the LC-40 in Figure 5-1 d with a V_{eff}/V_{ex} of 2.0. Compared to the 0.5 mm ID column in b) with V_{eff}/V_{ex} of 3.0, a maximum increase for carbamazepine at a flow rate of 30.6 µL/min of 73% was evident. While for carbamazepine only a small fluctuation was observed over the flow range under investigation, the early eluting compound ASA with k=2 showed a similar pattern in respect to the increase of σ as when using the 0.3 mm ID column.

The experiments for Figure 5-1 c-d were performed on the identical column and thus allowed a direct correlation of the effects of both HPLC-systems investigated. In a direct comparison of both systems, V_{ex} was 2.9 times higher for the LC-40 than for the use of the Mikros system. The V_{eff}/V_{ex}ratio of 9.4 is 4.7 times worse on the LC-40 when compared to the Mikros system. This was also reflected in the considered peak standard deviation. The favorable V_{eff}/V_{ex} in Figure 5-1 c resulted in a small increase in σ for all analytes investigated. This amounted to a maximum of $\sigma = 0.3\ \mu L$ for ASA, $\sigma = 0.7\ \mu L$ for etoposide and $\sigma = 0.7\ \mu L$ for carbamazepine. In comparison, in the setup in figure 1 d, these were $\sigma = 1.4\ \mu L$ for ASA, $\sigma = 2.6\ \mu L$ for etoposide, and $\sigma = 2.9\ \mu L$ for carbamazepine. Thus, at the maximum, there was a 52% increase in σ for etoposide.

For the 2.1 mm ID column in Figure 5-1 e the highest peak standard deviation with $\sigma = 6.7 - 22.9\ \mu L$ was observed, which is mainly due to the comparatively high flow rates applied. The configuration had the second best ratio with V_{eff}/V_{ex} = 9.0. This was again reflected in the low increase of the early eluting compound ASA with a maximum increase of 16%. To further evaluate the interplay between extra-column volume and effective-column volume on efficiency, h versus u_0 analyses were performed which are shown in Figure 5-2.

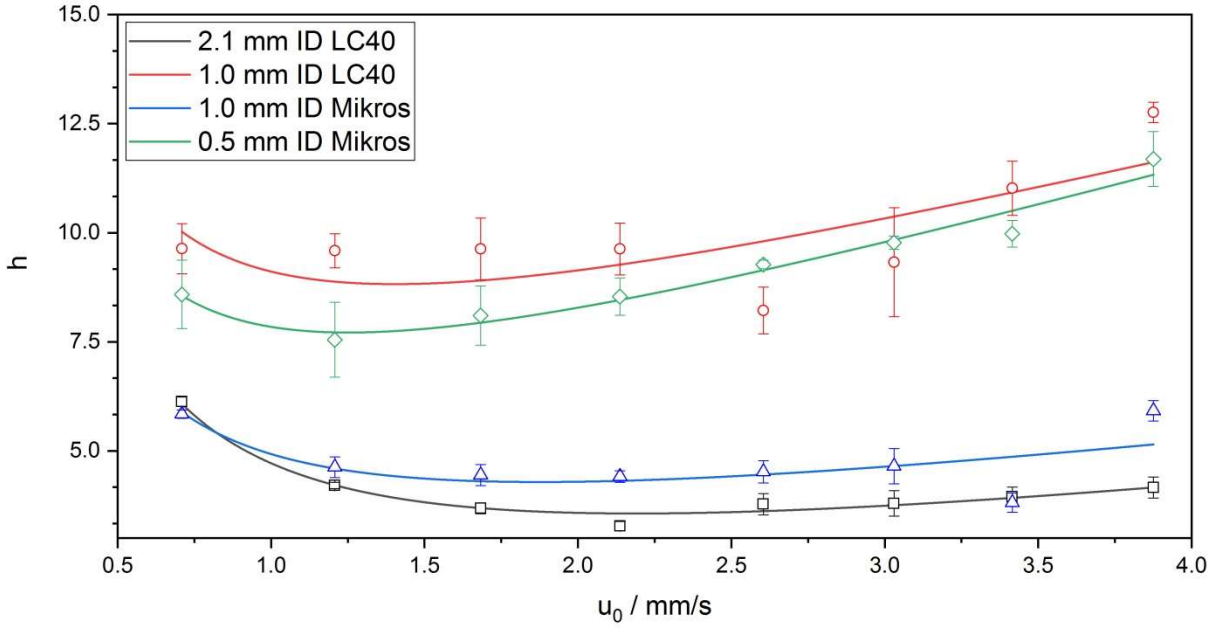

Figure 5-2:Comparison of the resulting h versus u_0 plots for carbamazepine. Solid lines represent the fit calculated by the residual sum of squares method for the experimental values. Injection volume: 100 nL (blue); 1,120 nL (green); 1,120 nL (red); 4,950 nL (black); mobile phase: 75% H_2O + 0.1% FA; 25% ACN + 0.1% FA; Error bars indicate the standard deviation calculated for n = 3.

The V_{eff}/V_{ex} ratio of the 0.3 mm ID column was too low to ensure a complete mapping of the h versus u_0 plot with h_{min} and $u_{0,opt}$. The determination of the V_{eff}/V_{ex} ratio is a simple way to estimate the expected efficiency. Two groups were formed consisting of the 2.1 mm ID LC-40 and 1.0 mm ID Mikros configuration and the 1.0 mm ID LC-40 and 0.5 mm ID Mikros configuration, which have comparable V_{eff}/V_{ex} ratios of 9.0 to 9.4 and 2.0 to 3.3, respectively. The resulting h_{min} were 3.6 for the black curve, 4.2 for the blue curve, 5.8 for the green curve, and 7.7 for the red curve. Therefore, comparing the 1.0 mm ID configurations, showed a doubling of h_{min} when switching to the LC-40 System. Furthermore, optimization of V_{eff}/V_{ex} showed higher $u_{0,opt}$ values. In the comparison of the 1.0 mm ID columns $u_{0,opt}$ was 1.9 for the Mikros configuration and 1.4 for the LC-40 configuration. As a consequence, for complex separation problems where maximum efficiency is required, sample throughput can be increased by a factor of 1.35 when opting for the miniaturized alternative. For the 2.1 mm ID column a $u_{0,opt} = 2.2$ and for the 0.5 mm ID column a $u_{0,opt} = 1.3$ was achieved.

The results showed that V_{ex} is too high for both systems to use small ID columns in isocratic mode. Further optimization of the system volumes would have to be carried

out in order to achieve a better utilization of the intrinsic efficiency of the separation column. Optimal and reproducible results were achieved from a V_{eff}/V_{ex} of approx. 9 onwards. A direct comparison of the configuration of the 1.0 mm ID column clearly showed that a reduction of the V_{ex} is essential for full utilization of the technology. Since the tubing lengths in LC-40 had already been optimized to the minimum length, a further reduction of V_{ex} would only be possible by using smaller tubing IDs, but this would lead to a significant increase in backpressure and thus prevent the use of high flow rates.

5.3.2 Gradient Mode Evaluation

In gradient elution, the extra-column volume is described by the gradient dwell volume V_{dwell} and V_{post}. V_{dwell} describes the volume from the mixture of the mobile phases to the column head. In general, it is assumed that especially the V_{post} has a negative influence on the band broadening in gradient mode. Therefore, manufacturers have started to reduce V_{post} to an absolute minimum. In the Mikros system this is achieved by positioning the column with the column oven directly in front of the ion source of the mass spectrometer and with a direct connection to the emitter capillary. The V_{dwell} for the Mikros was thus 2.8 µL for a $V_{inj} = 1\ \mu L$ and 7.8 µL for a $V_{inj} = 5\ \mu L$. For the LC-40 system, the values were $V_{dwell} = 30.4\ \mu L$ and $V_{dwell} = 34.4\ \mu L$. The values for V_{post} can be found in Table 5-2

If the ECBB is excluded it can be assumed that two columns of the same length, despite varying ID, provide the same resolution if the same linear flow velocity is maintained. This conclusion can thus also be applied to the chromatographic peak capacity. Especially when focusing of the analytes occurs on the column head, the influence of the V_{dwell} should thus become negligible. Since it was shown in previous studies that high injection volumes are also possible with microbore columns, V_{inj} was kept constant at 1 µL and 5 µL for all columns [7]. Figure 5-3 shows the resulting chromatograms for $V_{inj} = 5\ \mu L$.

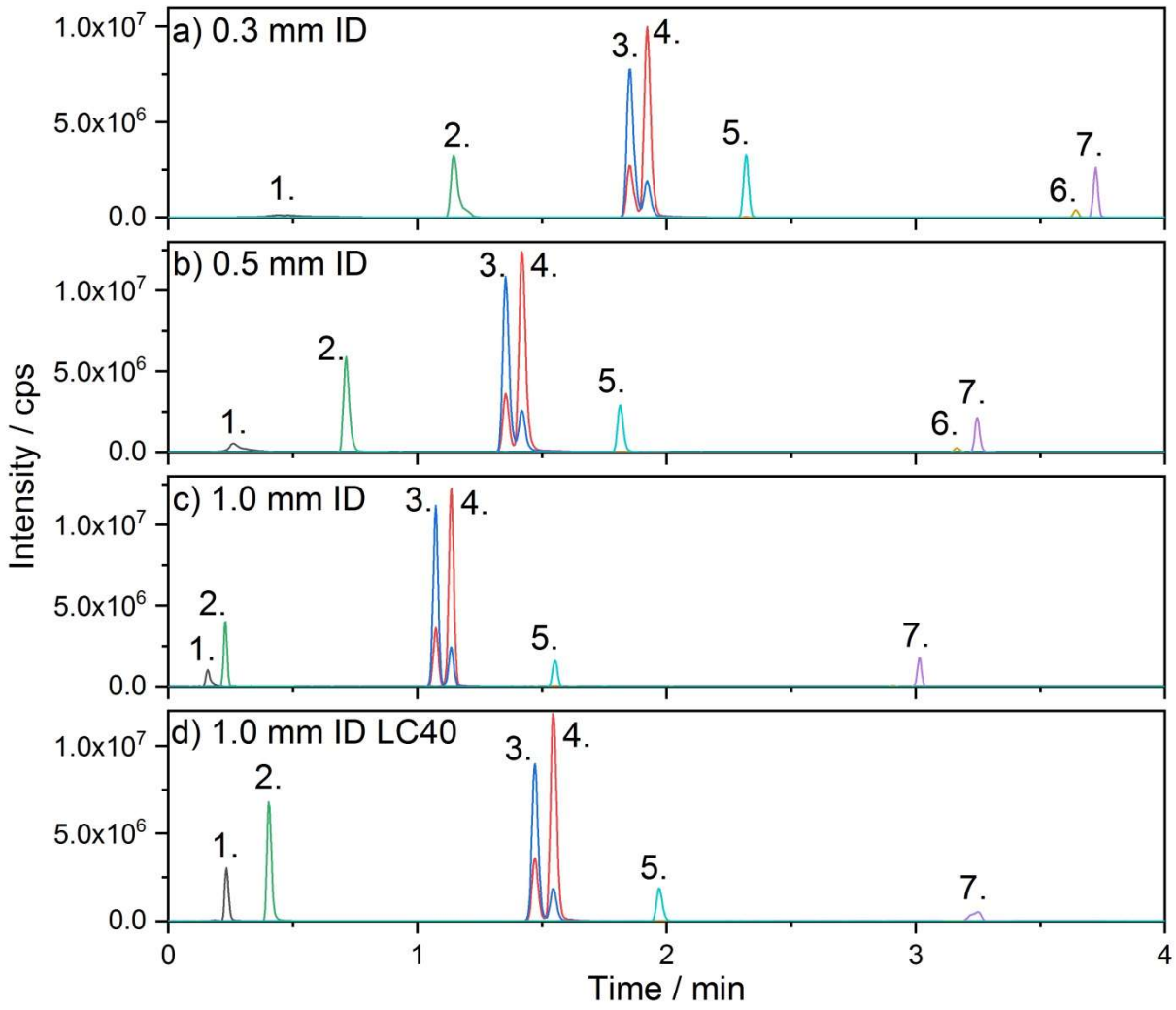

Figure 5-3: Chromatograms for the separation of the seven antineoplastic drugs on the different column IDs for a concentration of 10 ng/mL and an injection volume of 5 µL. Analytes: 1. gemcitabine, 2. methotrexate, 3. ifosfamide, 2. cyclophosphamide, 5. etoposide, 6. paclitaxel, 7. docetaxel. Flow rates: a) 25 µL/min b) 69 µL/min c) 278 µL/min.

What is obvious when looking at Figure 5-3 is that no analysis was performed on the 2.1 mm ID column. This is due to the fact that the method transfer was performed bottom up from the 0.3 mm ID column, to achieve an equivalent linear flow rate on the 2.1 mm ID column a flow rate of 1,225 µL/min would have had to be used. Thereby, the backpressure would have increased significantly above 1,000 bar, which was outside the specification of the phase material used. Furthermore, a significant shift in retention times can be observed. This can be explained by the fact that the influence of the V_{dwell} decreases in relation to the increased flow rate.

As described in the experimental part, one of the difficulties in using an MS detector to study band broadening is the influence of the ion source parameters on the ionization efficiency of

the analytes. Thus, when switching to the 1.0 mm ID column, the source temperature had to be increased by 50 °C, otherwise only incomplete desolvation was achieved. As a result, paclitaxel could no longer be detected when using the 1.0 mm ID column. A significant reduction in ionization efficiency was also observed for docetaxel. In addition, a strong deviation from the typical Gaussian peak shape for docetaxel was imminent when coupled with the LC-40.

As shown in Figure 5-3 a and b, a dependence of the V_{dwell} or V_{inj} on the peak shape was also observed for gemcitabine. While for the 0.3 mm ID column a tailing factor of 0.9 was determined for $V_{inj} = 1\ \mu L$, an increase in V_{inj} resulted in a tailing factor of 1.6. For the 0.5 mm ID column, a tailing factor of 1.8 was determined for $V_{inj} = 5\ \mu L$. For the remaining configurations, no significant effect on the peak shape of gemcitabine was observed.

Because of these observations, the determination of peak capacities was performed based on the peak widths of methotrexate, ifosfamide, cyclophosphamide, and etoposide. Since ifosfamide and cyclophosphamide are constitutional isomers and thus also isobaric compounds they require chromatographic separation even when using MS detection [25]. The comparison of R and n_p is shown in Figure 5-4.

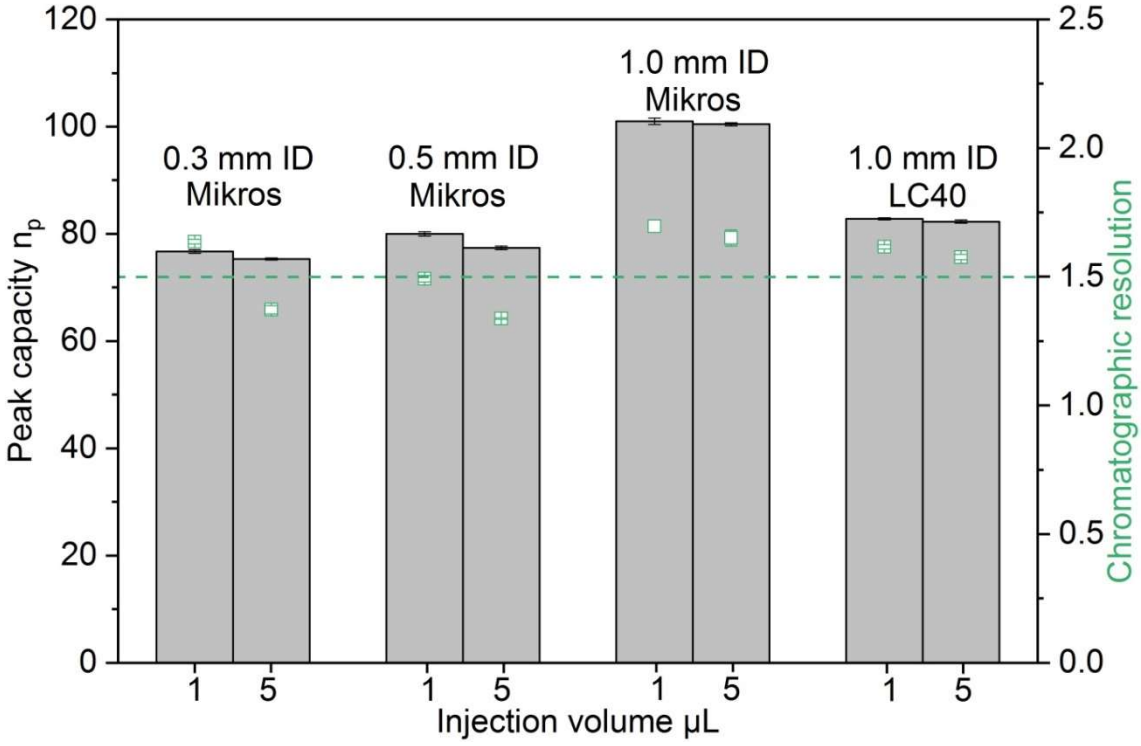

Figure 5-4: Comparison of the peak capacities achieved and the chromatographic resolution of the critical peak pair ifosfamide / cyclophosphamide for an injection volume of 1 µL and 5 µL on the configurations investigated. The dashed green line represents the necessary resolution for a baseline separated peak pair.

When comparing the investigated configurations, it can be seen that the injection volume has no influence on n_p. The highest n_p was found with approx. 100 for the 1.0 mm ID Micros coupling. The average for the other configuration was $n_p = 79.1 \pm 2.8$. When comparing the resolutions, a clear influence of the V_{dwell} can be seen. In general, baseline separation is achieved when < 1% of the peak areas overlap. In terms of chromatographic resolution, this is obtained at $R = 1.5$, represented by the green dotted line in Figure 5-4. Therefore, for all configurations, baseline separation could be achieved at $V_{inj} = 1\ \mu L$. However, only in the 1.0 mm ID Mikros configuration the resolution remained constant when the injection volume was increased to 5 µL. Furthermore, with the 1.0 mm ID LC-40 coupling the reduction of the n_p could be justified with the increased V_{post} and the associated post-column ECBB, additionally an influence of the unfavorable V_{dwell} on the performance is present. Thus, an optimization of the V_{dwell} would have to take place for the use of the 1.0 mm ID column. In the first instance, this could be achieved by reducing the volume of the static mixer.

Finally, to return to the reference in the introduction regarding miniaturization in HPLC as a green alternative, the methods were compared from an ecological point of view based on solvent consumption within 24 h. Implementing the method on the 2.1 mm ID column would represent a solvent consumption of 1,764 mL. By reducing the column ID to 1.0 mm or 0.5 mm, the solvent consumption can be cut to 400 mL or 100 mL, respectively. For the analysis on the 0.3 mm ID column, only 36 mL would be required.

5.4 Conclusion

The results of the study demonstrated that further reduction of the column ID in modern UHPLC systems based on the classical modular design with the aim to increase sample throughput, reduce the influence of frictional heating and better coupling with mass flow dependent detectors are only conditionally feasible. To effectively use 1.0 mm ID columns with UHPLC systems, a significant reduction in extra-column volume is still required.

Furthermore, it was shown that a simple comparison of the V_{eff}/V_{ex} ratio can provide a first estimate of the performance of a combination of a column and HPCL-system in isocratic mode. In addition, it was shown that the trend towards optimizing V_{post} at the expense of V_{pre} volume means that smaller column IDs can no longer be used efficiently. The resulting band broadening could be observed in both isocratic and gradient modes.

5.5 References

[1] J.W. Jorgenson, E.J. Guthrie, Liquid chromatography in open-tubular columns. Theory of column optimization with limited pressure and analysis time, and fabrication of chemically bonded reversed-phase columns on etched borosilicate glass capillaries, J. Chromatogr. A. 255 (1983) 335–348. https://doi.org/10.1016/S0021-9673(01)88293-5.

[2] M. V. Novotny, Development of capillary liquid chromatography: A personal perspective, J. Chromatogr. A. 1523 (2017) 3–16. https://doi.org/10.1016/j.chroma.2017.06.042.

[3] P. Xiang, Y. Yang, Z. Zhao, M. Chen, S. Liu, Ultrafast gradient separation with narrow open tubular liquid chromatography, Anal. Chem. 91 (2019) 10738–10743. https://doi.org/10.1021/acs.analchem.9b02190.

[4] C. Thoben, T. Werres, I. Henning, P.R. Simon, S. Zimmermann, T.C. Schmidt, T. Teutenberg, Towards a miniaturized on-site nano-high performance liquid chromatography electrospray ionization ion mobility spectrometer with online enrichment, Green Anal. Chem. 1 (2022) 100011. https://doi.org/10.1016/j.greeac.2022.100011.

[5] P.I. Napolitano-Tabares, I. Negrín-Santamaría, A. Gutiérrez-Serpa, V. Pino, Recent efforts to increase greenness in chromatography, Curr. Opin. Green Sustain. Chem. 32 (2021) 100536. https://doi.org/10.1016/j.cogsc.2021.100536.

[6] A. Gałuszka, Z. Migaszewski, J. Namieśnik, The 12 principles of green analytical chemistry and the SIGNIFICANCE mnemonic of green analytical practices, TrAC Trends Anal. Chem. 50 (2013) 78–84. https://doi.org/https://doi.org/10.1016/j.trac.2013.04.010.

[7] T. Werres, T.C. Schmidt, T. Teutenberg, The influence of injection volume on efficiency of microbore liquid chromatography columns for gradient and isocratic elution, J. Chromatogr. A. 1641 (2021) 461965. https://doi.org/10.1016/j.chroma.2021.461965.

[8] H. Wang, P. Bennett, Performance assessment of microflow LC combined with high-resolution MS in bioanalysis, Bioanalysis. 5 (2013) 1249–1267. https://doi.org/10.4155/bio.13.93.

[9] A.A.M. Heemskerk, J.M. Busnel, B. Schoenmaker, R.J.E. Derks, O. Klychnikov, P.J. Hensbergen, A.M. Deelder, O.A. Mayboroda, Ultra-low flow electrospray ionization-mass spectrometry for improved ionization efficiency in phosphoproteomics, Anal. Chem. 84 (2012) 4552–4559. https://doi.org/10.1021/ac300641x.

[10] K. Mejía-Carmona, J. Soares da Silva Burato, J.V.B. Borsatto, A.L. de Toffoli, F.M. Lanças, Miniaturization of liquid chromatography coupled to mass spectrometry: 1. Current trends on miniaturized LC columns, TrAC Trends Anal. Chem. 122 (2020) 115735. https://doi.org/https://doi.org/10.1016/j.trac.2019.115735.

[11] M. Dams, J.L. Dores-Sousa, R.J. Lamers, A. Treumann, S. Eeltink, High-Resolution Nano-Liquid Chromatography with Tandem Mass Spectrometric Detection for the Bottom-Up Analysis of Complex Proteomic Samples, Chromatographia. 82 (2019) 101–110. https://doi.org/10.1007/s10337-018-3647-5.

[12] F. Rahimi, S. Chatzimichail, A. Saifuddin, A.J. Surman, S.D. Taylor-Robinson, A. Salehi-Reyhani, A Review of Portable High-Performance Liquid Chromatography: the Future of the Field?, Springer Berlin Heidelberg, 2020. https://doi.org/10.1007/s10337-020-03944-6.

[13] D.C. Patel, M.F. Wahab, T.C. O'Haver, D.W. Armstrong, Separations at the Speed of Sensors, Anal. Chem. 90 (2018) 3349–3356. https://doi.org/10.1021/acs.analchem.7b04944.

[14] I. Halász, R. Endele, J. Asshauer, L. Pl, I. Clrwric, ultimate limits in HPLC, 2 (1975) 37–60. https://ac.els-cdn.com/S0021967300999412/1-s2.0-S0021967300999412-main.pdf?_tid=d67638cb-69fa-4491-8515-c7c7acf889f0&acdnat=1547646315_3e01e4f38af378f66e5fc8b3fabdf2f3.

[15] F. Lestremau, D. Wu, R. Szücs, Evaluation of 1.0mm i.d. column performances on ultra high pressure liquid chromatography instrumentation, J. Chromatogr. A. 1217 (2010) 4925–4933. https://doi.org/10.1016/j.chroma.2010.05.044.

[16] K. Broeckhoven, G. Desmet, Advances and Challenges in Extremely High-Pressure Liquid Chromatography in Current and Future Analytical Scale Column Formats, Anal. Chem. 92 (2020) 554–560. https://doi.org/10.1021/acs.analchem.9b04278.

[17] G. Desmet, K. Broeckhoven, Extra-column band broadening effects in contemporary liquid chromatography: Causes and solutions, TrAC Trends Anal. Chem. 119 (2019) 115619. https://doi.org/https://doi.org/10.1016/j.trac.2019.115619.

[18] K. Vanderlinden, K. Broeckhoven, Y. Vanderheyden, G. Desmet, Effect of pre- and post-column band broadening on the performance of high-speed chromatography columns under isocratic and gradient conditions, J. Chromatogr. A. 1442 (2016) 73–82. https://doi.org/10.1016/j.chroma.2016.03.016.

[19] J.J. Stankovich, F. Gritti, P.G. Stevenson, G. Guiochon, The impact of column connection on band broadening in very high pressure liquid chromatography, J. Sep. Sci. 36 (2013) 2709–2717. https://doi.org/10.1002/jssc.201300175.

[20] F. Gritti, G. Guiochon, On the minimization of the band-broadening contributions of a modern, very high pressure liquid chromatograph, J. Chromatogr. A. 1218 (2011) 4632–4648. https://doi.org/10.1016/J.CHROMA.2011.05.024.

[21] T. Werres, T.C. Schmidt, T. Teutenberg, Peak broadening caused by using different micro–liquid chromatography detectors, Anal. Bioanal. Chem. (2022) 6107–6114. https://doi.org/10.1007/s00216-022-04170-9.

[22] D. Spaggiari, S. Fekete, P.J. Eugster, J.L. Veuthey, L. Geiser, S. Rudaz, D. Guillarme, Contribution of various types of liquid chromatography-mass spectrometry instruments to band broadening in fast analysis, J. Chromatogr. A. 1310 (2013) 45–55. https://doi.org/10.1016/j.chroma.2013.08.001.

[23] T. Hetzel, C. vom Eyser, J. Tuerk, T. Teutenberg, T.C. Schmidt, Micro-liquid chromatography mass spectrometry for the analysis of antineoplastic drugs from wipe samples, Anal. Bioanal. Chem. 408 (2016) 8221–8229. https://doi.org/10.1007/s00216-016-9932-y.

[24] C. Gunnarson, T. Lauer, H. Willenbring, E. Larson, M. Dittmann, K. Broeckhoven, D.R. Stoll, Implications of dispersion in connecting capillaries for separation systems involving post-column flow splitting., J. Chromatogr. A. 1639 (2021) 461893. https://doi.org/10.1016/j.chroma.2021.461893.

[25] T. Werres, J. Leonhardt, M. Jäger, T. Teutenberg, Critical Comparison of Liquid Chromatography Coupled to Mass Spectrometry and Three Different Ion Mobility Spectrometry Systems on Their Separation Capability for Small Isomeric Compounds, Chromatographia. 82 (2019) 251–260. https://doi.org/10.1007/s10337-018-3640-z.

Chapter 6 Synthesis, characterization, and utilization of modified bead cellulose in miniaturized liquid chromatography for the analysis of small and large molecules

This chapter was adapted from: T. Werres, K. Hettrich, D. Polozij, M.D. Klassen, J. Bohrisch, T.C. Schmidt, T. Teutenberg, Synthesis, characterization, and utilization of modified bead cellulose in miniaturized liquid chromatography for the analysis of small and large molecules. submitted.

Abstract: Not only driven by current global events the field of green analytical chemistry is gaining momentum. Miniaturization and the elimination of organic solvents are cornerstones of green methods. Therefore, chromatography that avoids organic solvents and relies on other separation mechanisms will become more relevant. Pearl celluloses which are spherical polymers based on cellulose-2,5-acetate may provide such an alternative. Due to their good parameterizability and functionalizability, they are suitable for a wide range of applications. In the case of the cellulose phases for liquid chromatography described in this work, it was possible to synthesize sub 5 µm particles. A particularly narrow distribution of the particle size could be achieved by a complex clean-up. Furthermore, it was demonstrated how the pore size can be influenced by varying the initial concentration of cellulose 2,5-acetate and the use of additives such as lignin. In addition, chemical modifications were made to the particles by means of grafting to obtain a temperature responsive phase or to address bioanalytical applications. Particles were characterized by various physical methods. The columns were packed in a micro bore scale format of 50 x 0.5 mm and chromatographically characterized using small and large model compounds. With the bead cellulose phases synthesized it has been possible to separate a wide variety of substances of different polarity in purely aqueous mobile phase, avoiding the use of high temperatures.

6.1 Introduction

The principles of green chemistry defined by Paul Anastas and John Warner as early as 1998 are becoming increasingly important [1]. Miniaturization in particular can make a significant contribution to reducing resource consumption, such as the use of toxic and expensive organic solvents [2, 3]. An often-overlooked advantage of using miniaturized systems to develop new separation phases has been that significantly less phase material is required to produce a column. The development of innovative separation phases for liquid chromatographic applications that can be used with purely aqueous mobile phases is of great interest for many analytical issues. First, such materials can completely avoid the use of toxic and expensive organic solvents, which are essential for classical HPLC methods [4]. Another advantage of not having a binary phase system is the ability to utilize alternative detectors such as the refractive index detector. [5]. Also, new applications in the field of bioanalytics can be developed, since biotherapeutic agents such as monoclonal antibodies denature under the influence of organic solvents and thus lose their activity [6]. In bioanalytics, it is also often necessary to work with high salt loads to affect retention, selectivity, and dissolution. However, such conditions are not compatible with direct coupling of mass spectrometry [7-9].

Various methods exist, such as high temperature LC (HTLC) and temperature responsive liquid chromatography (TRLC), which rely on temperature instead of organic fraction to control analyte retention [10, 11]. For HTLC applications, the problem arises that the elution of hydrophobic substances with a purely aqueous mobile phase requires very high temperatures [12, 13]. Most silica-based stationary phases tend to degrade rapidly at temperatures above 100 °C [14]. TRLC, on the other hand, uses responsive polymers such as polyacrylamides to affect retention behavior and can be used at lower temperatures than HTLC [15, 16]. Furthermore, Polymeric separation phases are used to overcome the problems described by means of specific modifications. For example, as early as 2010, Kanazawa's group presented a thermoresponsive polymer separation phase based on polyhydroxymethacrylate and polystyrene to overcome the limitation of silica-based stationary phases. However, complete removal of metal ions used as reagents posesed thereby a major problem [17–19].

In contrast, cellulose beads, which were first described as cellulose pellets in 1951 in the US patent 2543928 [20], offer several advantages that favor their use. These include natural hydrophilicity, high porosity and large internal surface area, chemical stability, and ease of functionalization. One of the main disadvantages, as with other polymer phases, is the low pressure stability of the separation phases. Nowadays, cellulosic polymers are mainly used in

the medical field and are generally considered to be biocompatible. Applications include the use as a separation medium, carrier system, and as an adsorbent in extracorporeal blood purification [21–31]. In instrumental analytics it is widely used for the separation of chiral substances [4, 32]. At present, cellulose polymers are mainly used as monolithic phases or in particle sizes around 40-100 µm with a broad particle size distribution, which are rather unsuitable for use as stationary HPLC phases [33]. The method developed by Loth et al. for preparing bead cellulose on the basis of cellulose acetate with an average degree of substitution between 1.5 and 2.7 was applied in this study [23]. This green technology is characterized by the fact that no use of halogenated hydrocarbons is necessary. In this process, commercially available cellulose 2,5-acetate is emulsified in a solvent mixture. This procedure was further optimized in various studies with regard to particle size distribution and surface size [30, 31]. This experience was used to produce the cellulose microspheres for the studies presented in this paper.

Therefore, the main goal of this work was to produce bead celluloses with a narrow particle size distribution based on cellulose 2,5-acetate and to pack them into miniaturized columns with dimensions of 50 x 0.5 mm. To explore the potential of this material, the focus was on the production of some grafted bead celluloses for the organic solvent-free analysis of small molecules and the production of special phases for bioanalytical applications.

6.2 Material and Methods

6.2.1 Chemicals and Reagents

The raw material cellulose-2,5-acetate (CA) for the synthesis of the cellulose beads was obtained from Novaceta (Duesseldorf, Germany) and the protective colloid methylcellulose (MC) from Merck (Darmstadt, Germany). The solvents required for the synthesis ethyl acetate (EtOAc), methanol, ethanol, water, dichloromethane, hexane and acetone for the determination of the gradient dwell volume were purchased from Merck (Darmstadt, Germany). For grafting, N-acryloylpyrrolidine (NAP) (purity > 97%; Advanced ChemBlocks Inc.; Haywards, USA), and 2,2-dimethyl-1,3-dioxolane-4-methanamine (97%; Acros Organics, Geel, Belgium) were used. The other chemicals needed for the synthesis were sodium acetate trihydrate, Triton-X 100 (lab grade), NaOH, acetic acid, cerium (IV) ammonium nitrate (CAN) (p. A.), HNO_3, HCl, acryloyl chloride (96%), $NaHCO_3$ and Na_2SO_4 were obtained from Merck (Darmstadt, Germany). Water and acetonitrile of LC-MS grade were purchased from Th. Geyer (Chemsolute, Renningen, Germany). Ammonium acetate, acetic acid (AppliChem, Darmstadt, Germany) and phosphate buffered saline (PBS) tablets (Merck, Darmstadt, Germany) were

used to adjust the pH. Uracil, cyclophosphamide, metoprolol, carbamazepine, naphthalene, and propylparaben were purchased from Sigma Aldrich (St. Louis, USA). Bovine serum albumin lgG-free > 98% (BSA) was purchased from Carl Roth (Karlsruhe, Germany), myoglobin (MYO) ≥ 98% from Sigma-Aldrich, and Avastin (bevacizumab, BVCZ) was purchased from Roche (Basel, Switzerland).

6.2.2 Synthesis of Native Cellulose Beads

400 mL of EtOAc was placed in a flask and 36 g of cellulose-2,5-acetate solution was added while stirring. After one hour of mixing, 100 mL of methanol were added in 5 min and vigorously stirred. After mixing for 4 h, the polymer solution rested for 16 h. In a vessel, 18 g of methylcellulose in 2 L of water were dissolved within about 2 days. In a separate vessel, 10 g of sodium acetate trihydrate were dissolved in 270 mL of water. A solution of 4.8 g Triton-X 100 and 100 mL EtOAc was then prepared and mixed with the sodium acetate trihydrate solution for 10 min. With stirring, 400 mL of the cellulose-2,5-acetate solution was added to the surfactant emulsion and stirred for additional 10 min. To stabilize the emulsion, 520 mL of the methylcellulose solution were added to which 56 mL of EtOAc were added. After about 10 min of intensive mixing, the polymer emulsion was treated with an Ultraturrax® (IKA®-Werke, Staufen, Germany) at 10,000 rpm for 30 min and then placed in a rotary evaporator (Buechi, Switzerland; 20 rpm). After complete transfer of the polymer emulsion to the rotary evaporator, the water bath was heated to 34 °C. At a pressure of 205 to 235 mbar, the EtOAc was removed by distillation.

The suspension was centrifuged in a 1-L beaker at 6,000 g for 45 min. The supernatant was discarded, and the sediment was stirred and centrifuged twice with 1 L of water each time to completely wash out the methylcellulose After the last centrifugation, approximately 62 g of a 38% aqueous suspension was obtained. The acetyl groups were cleaved by an alkaline ethanol solution (9.5 g NaOH in 10 mL water and 250 mL ethanol). The bead cellulose was stirred for 3 h and left overnight. Saponification was followed by centrifugation at 6,000 g with a Cryofuge 6000i (Heraeus Sepatech, Hanau, Germany) for 60 min and redispersion in 3 L water. Subsequently, a pH value between 5 and 7 was adjusted with acetic acid and centrifugation was repeated. Finally, another washing step was performed with 3 L water and centrifugation. Approx. 40 g of sediment was obtained.

6.2.3 Preparation of the Modified Cellulose Beads

6.2.3.1 Synthesis Protocol for the Temperature-Responsive Cellulose Bead

For the synthesis of a temperature responsive modification N-acryloylpyrrolidine was chosen as monomer. The responsive polymer is known for its phase transition from hydrophilic to hydrophobic properties between 50-56 °C [34]. In a 100-mL three-necked flask, a mixture of 1.5 g bead cellulose as aqueous dispersion and in sum 28.5 g water was prepared. It was intensively purged with N_2 for 10 min. Then 0.73 g N-acryloylpyrrolidine was added and stirred for 1 h under N_2 atmosphere. Afterwards, the mixture was heated to 40 °C and 1.38 g of a 0.2 molar cerium (IV) ammonium nitrate solution in 0.2 molar HNO_3 were added. It was stirred for another 4 h at 40 °C. Then the mixture was neutralized with 1 molar NaOH and washed intensively with distilled water and filtered by a G4 frit.

6.2.3.2 Synthesis Protocol for the Diol Cellulose Bead

As monomer with protein specific diol functionality N-((2,2-dimethyl-1,3-dioxolan-4-yl)methyl)acrylamide was chosen [35,36]. For the graft monomer, 15 mL of dry dichloromethane containing 2.53 g of 2,2-dimethyl-1,3-dioxolane-4-methanamine and 4.25 mL of triethylamine were added to a 100 mL three-neck flask while stirring under N2 atmosphere at 0 °C. Dropwise, 1.79 g of acryloyl chloride were added via a septum. The mixture was then heated to room temperature and stirred for 4 h. The precipitated ammonium salt was separated via a G4 frit. The organic phase was extracted 3 times with 150 mL of saturated Na HCO3 solution and 3 times with 50 mL of water. Then it was dried over Na2SO4. After filtration, the dichloromethane was removed using the rotary evaporator. The product N-((2,2-dimethyl-1,3-dioxolan-4-yl)methyl)acrylamide (DMDOMA) was purified by column chromatography (hexane/acetic acid ethyl ester 40:60, "Geduran Si 60", Merck, 0.063 - 0.2 mm). The yield after the purification step was 65%.

For the particle, 1.5 g of bead cellulose was added to 28.5 g of water as an aqueous suspension in a 100 mL three-necked flask. It was purged intensively with N_2 for 10 min. Then 0.75 g DMDOMA were added and stirred for 1 h under a gentle stream of N_2. Afterwards, the mixture was heated to 40 °C and 1.38 g cerium (IV) ammonium nitrate was added as a 0.2 molar solution in 0.2 molar HNO_3. Stirring was continued for another 4 h at 40 °C and followed by neutralization with 1 M NaOH and the particles were washed intensively with distilled water over a G3 frit. The aqueous particle suspension was then stirred in a 100 mL flask for 5 h at 50 °C with 2 g of strongly acidic ion exchanger Dowex Marathon, H^+ form (Sigma-Aldrich, St. Louis, USA). After cooling, the ion exchanger was separated via a G1 frit.

6.2.3.3 Synthesis Protocol for the Large Pore Size Cellulose Bead

For the separation of macromolecules, a phase with larger pore size and higher surface area was synthesized according to Gabov et al. [37]. The synthesis of the large pore size cellulose beads followed the synthesis protocol described in section 2.2. After dissolving 36 g of cellulose acetate in 400 mL EtOAc, 2 g of lignin acetate (Sigma-Aldrich, St. Louis, USA) were added and dissolved by intensive mixing. After one hour, 100 mL methanol were added, and the procedure was continued as described in section 2.2.

6.2.3.4 Purification of the Cellulose Bead

The separation of the particle fraction < 2 µm, fines and fragments was achieved by multiple sedimentation of the suspension and subsequent decantation of the turbid supernatant until it remained clear. For the purification process, the suspension was adjusted to pH 9 with NaOH and stirred for 3 h at 50 °C and then decanted.

6.2.4 Experimental Setup for Particle and Chromatographic Characterization

The analysis of the particle size distribution was performed via laser diffraction with LS 13 320 particle size analyzer (Beckman-Coulter GmbH, Krefeld, Germany). Scanning electron microscope imaging of the bead cellulose was taken using JSEM 6330F (Jeol Ltd., Tokyo, Japan). Confocal laser scanning microscopy using TCS SPE (Leica Microsystems, Wetzlar, Germany) was performed to analyze the charge ratios and the morphology of the particles. Elemental analysis for determination of the C/N ratio was carried out on FlashEA 1112 CHNS/O automatic elemental analyzer with 2 autosampler MAS200R (Thermo Scientific, Waltham, USA). To determine the pore diameter distribution, specific pore surface area and specific pore volume, the Pascal 140 was used for the macropores and the pascal 440 (Thermoelectron Cooperation, Milano, Italy) for the mesopores. An InoLab pH 720 from WTW (Weilheim, Germany) was used to control the pH values.

All chromatographic experiments were done on a Nexera Mikros system (Shimadzu, Duisburg, Germany) consisting of a Nexera Mikros column oven, an SIL-30AC autosampler and a CMB 20A controller. The micro-HPLC was coupled either to the LCMS-8060 (Shimadzu, Duisburg, Germany) or to the 1260 Infinity II DAD WR (Agilent Technologies, California, USA) with a cell volume of 80 nL. The pressure stability tests were carried out with an Agilent 1200 HPLC pump.

The purified bead celluloses were packed into 50 x 0.5 mm silica lined capillaries using the slurry method. Water was used as the transport solvent and the maximum packing pressure was 30 bar. The columns were sealed with 1/16-inch unions and 0.2 µm stainless steel frits. Compared to a 50 x 0.5 mm column and assuming a column porosity of 0.7 and a density of the bead cellulose of 1.3 g/mc^3, approx. 10 mg of material are required, which corresponds to a reduction by a factor of 76. Table 6-1 summarizes the bead cellulose phases and the performed experiments.

Table 6-1: Overview of the bead cellulose phases and experiments.

Material	Size distribution	SEM imaging	Elemental analysis	Stabilty test	Plate height	Temperature	Protein Separation
Native	X	X	X	X	X	X	
Large pore		X	X		X		x
T-respon.			X		X	X	
Diol			X				X

6.2.5 UV and MS Method

Wavelengths of 210 and 354 nm were selected for the detection of small molecules. For the protein analyses a wavelength of 214 nm was used. The sampling rate was set to10 Hz.

The MS analyses were performed using multiple reaction monitoring. The following mass transitions were used: uracil *m/z* 113 → 96; ifosfamide *m/z* 261 → 233, *m/z* 261 → 182 and *m/z* 261 → 154; cyclophosphamide *m/z* 261 → 106, *m/z* 261 → 233 and *m/z* 261 → 142; metoprolol *m/z* 268 → 191; carbamazepine 237 → 194. The source parameters were chosen as follows: nebulizing gas flow 1.5 L, heating gas flow 3 L, interface temperature 100 °C, desolvation line temperature 250 °C and heating block temperature 400 °C.

6.2.6 Software and Data Processing

The micro-HPLC and the MS were controlled via LabSolutions LCMS 5.99 SP2 (Shimadzu, Duisburg, Germany). Data acquisition for the DAD was performed using Open LAB CDS Rev.C.0107.SR3 (Agilent Technologies California, USA). Further data processing was performed using OriginPro 2021 (64-bit) 9.8.0.200 (OriginLab, Massachusetts, USA).

6.3 Results and Discussion

6.3.1 Optimization of Purification

Crucial to the use of cellulose beads as a stationary phase in LC is the removal of fines or particle fragments. Both temperature and pH can be exploited to release smaller particle fragments from the pores of the material. Multiple fractionations of 28.8 g of the native bead were performed to optimize the purification process. After 5 sedimentations and separations of the supernatant it remained clear. In this procedure, the native bead was divided into a fraction < 6 h amounting to 5.3 g and a 6 - 18 h particle fraction of 7.9 g.

The < 6 h fraction was stirred at 50 °C for 3 h, fractionated and then stirred again at 30 °C and pH 9 (NaOH) for 3 h and finally purified by refractionation. The particle fraction 6 - 18 h was comparatively purified in one step. Before final fractionation, the suspension was stirred for 3 h at pH 9 (NaOH) and a temperature of 50 °C. In this way, about 7.9 g or 28% of purified and fractionated material was obtained from 28.8 g of starting material. The necessity of this additional purification step is evidenced by the fact that half of the material is lost after the first fractionation step. Both methods resulted in a significant reduction of fragments between 1 and 2 µm. In the < 6 h fraction, large particles, or aggregates between 20 and 100 µm appeared in the course of the cleaning processes, which is why parallel treatment with pH and T is preferable.

6.3.2 Particle Characterization

Figure 6-1 illustrates that the synthesis described in section 2.2 enables the reproducible production of bead cellulose with a narrow particle size distribution. On average, a D10 value of 1.87 ± 0.17 µm, a D50 value of 3.82 ± 0.21 µm, a D90 value of 6.67 ± 0.39 µm and a D90/D10 of 3.57 ± 0.33 with a yield between 11.6 and 15.8 g were obtained for the seven batches. The yield, based on the amount of cellulose 2,5-acetate used, was determined gravimetrically. If complete hydrolysis of acetate groups is achieved, it is about 98%.

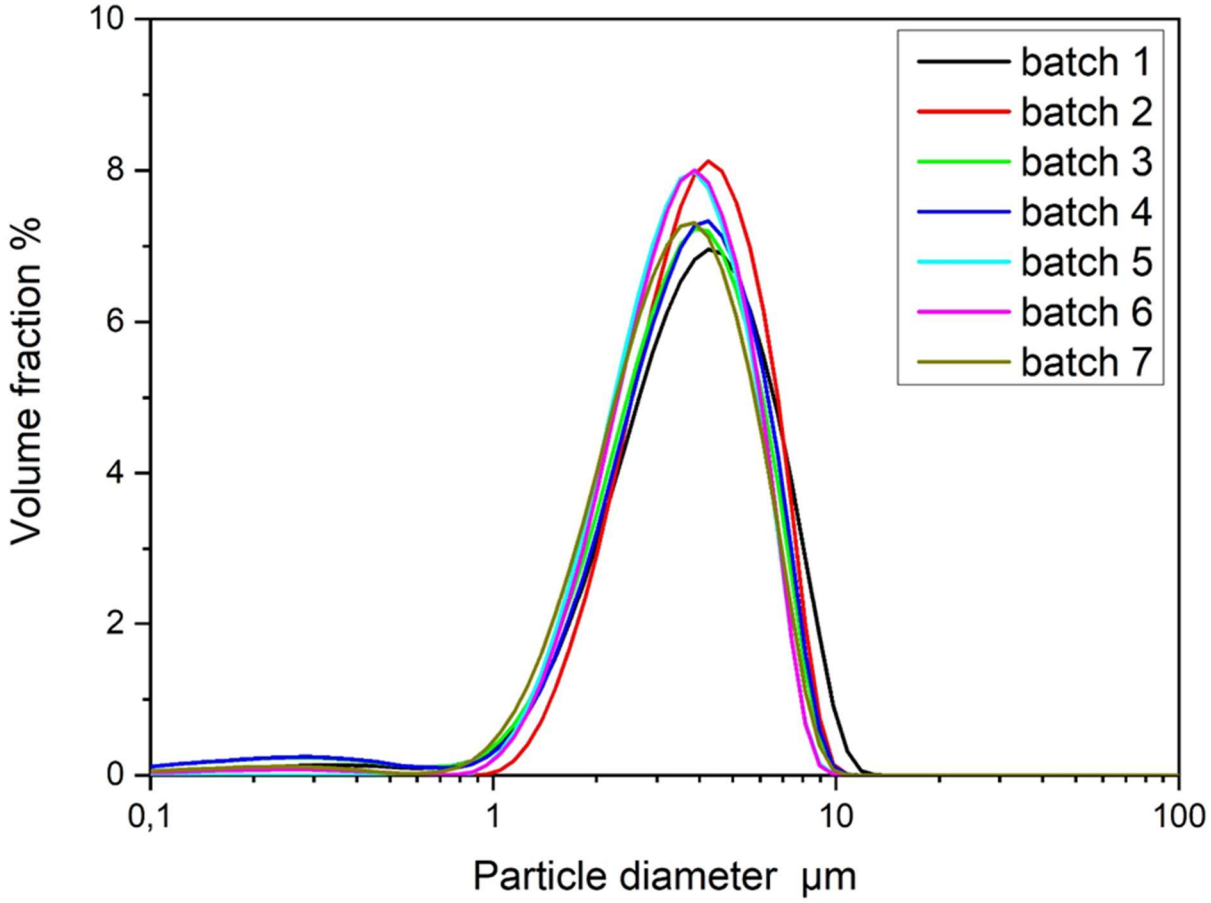

Figure 6-1: Particle size distribution of seven independently synthesised bead cellulose batches, based on the synthesis procedure before purification.

Batches 4 and 5 were merged and treated with the optimized purification process. A significantly narrower particle size distribution of D90/D10 of 2.9 was obtained. The native cellulose beads had a D10 value of 2.7 µm, a D50 value of 4.9 µm and a D90 value of 7.8 µm. The overall yield of the combined native cellulose beads after the purification was in the range of 30% resulting in 8.4 g for grafting and column packing. The results of the particle size distributions of all batches can be found in Table 6-4 of the supporting information. Generally, the material losses due to entrapped "fines" were higher with native particles compared to cellulose beads with higher porosity. With these operations, it has been possible to manufacture bead celluloses of a quality and size that has not yet been described [38].

In addition to the native cellulose phase, particles with larger pores were designed for the separation of biomolecules. The addition of lignin compounds during the preparation of the beads and subsequent leaching of the lignin leads to a modified surface and thus to higher porosities [37]. To obtain optical evidence of the morphological structure of the particles, SEM images of both unmodified particles were taken (Figure 2). Based on these images, a difference in the surface texture of the particles can be observed. In addition to the larger pore size due to

the use of lignin in the synthesis process, the surface of the particle displayed in Figure 2 b was significantly increased, which is reflected in a rougher texture.

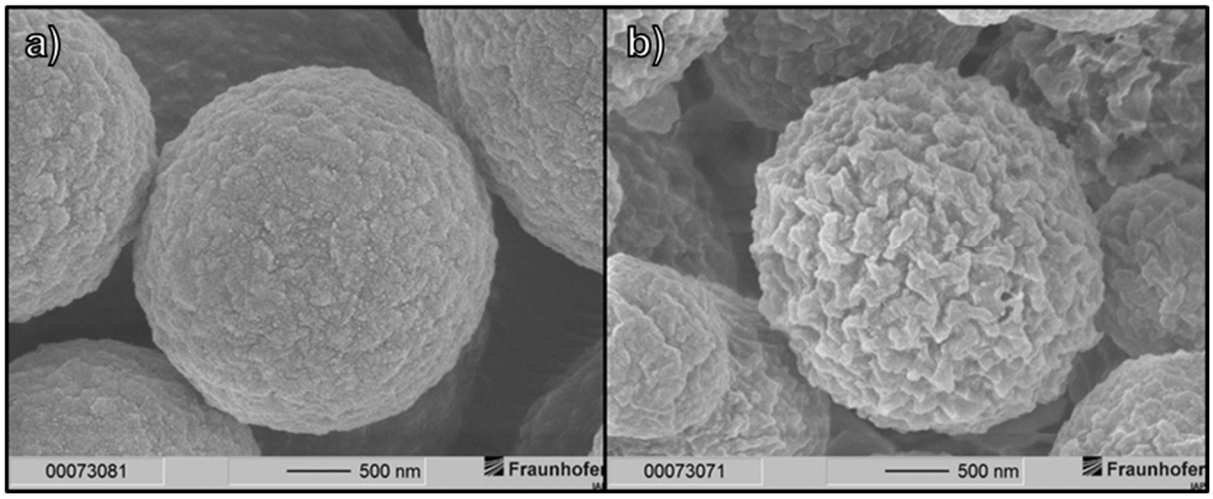

Figure 6-2: Scanning electron micrographs of the a) native cellulose bead and the b) larger pore size with high surface cellulose bead (b).

Porosimetry measurements were performed to characterize the macro- and mesopores of the two unmodified particles. A significant difference between the phases was found. For the native material, an average pore size of around 10 nm was determined with a maximum cumulative pore volume of about 100 mm^3/g. The maximum pore size was 200 nm. For the larger pore size beads, an average pore size of about 30 nm was determined with a maximum cumulative pore volume of approximately 800 mm^3/g. The maximum pore size was 500 nm. The surface area of the larger pore size material was increased by a factor of 4.4 from 18 to 80 m^2/g compared to the native material. At the same time, the porosity increased from 51% to 62%. Graphs of the pore size distribution can be found in Chapter 6.5.2. The grafting reaction with both acrylamide monomers was performed according to the synthesis protocol given in Figure 6-3.

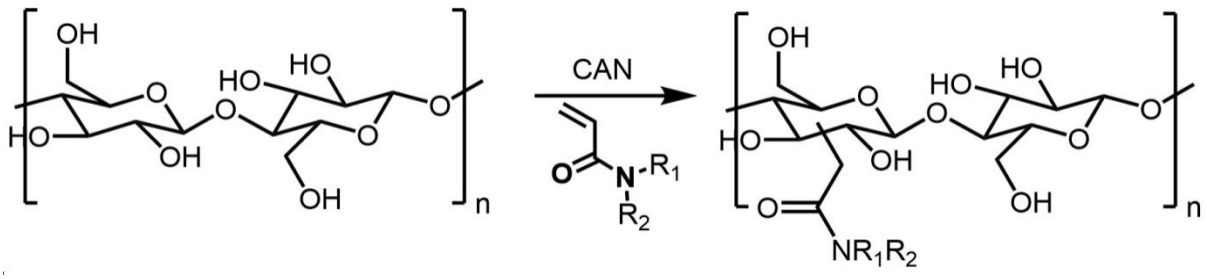

Figure 6-3: Grafting reaction on cellulose beads (general formula).

To verify the successful modification of the base cellulose beads, an elemental analysis was carried out and the C/N ratio was determined. For the N-acryloylpyrrolidine modified phase (R1, R2 = pyrrolidinyl in Figure 6-3), a degree of substitution between 0.45 and 0.60 per anhydroglucose unit was determined. Elemental analysis of the DMDOMA particles (R1 = H,

R2 = 1-(2,3-dihydroxy)propyl in Figure 6-3) gave a degree of substitution of about 0.09 per anhydroglucose unit. The results of the elemental analysis are shown in Table 6-2.

Table 6-2: Elemental analysis of the different cellulose bead modifications

Modification	C %	H %	N %	C/N	Corresponds to DS
N-acryloylpyrrolidine	46.87	6.95	2.70	17.36	0.45
DMDOMA	43.30	6.50	0.70	61.86	0.09

6.3.3 Chromatographic characterization

In preliminary tests, the pressure stability of the unmodified cellulose beads was investigated. For this purpose, the material was packed into a tube with the dimensions of 4.6 x 150 mm using the slurry method and the flow rate was increased stepwise. Up to a pressure of 55 bar, the pressure curve corresponded to the flow rate. Each further incremental increase of the flow rate eventually leads to a continuous increase of the pressure in the respective time interval until the column material finally collapses at around 50 bar.

To determine the plate height, van-Deemeter analyses were performed using uracil as a model analyte. The lowest plate height was found for the porous phase with 0.11 mm, followed by the native phase with a minimum plate height of 0.13 mm. For the temperature responsive bead, a minimum plate height of 0.28 mm was determined.

For general stability testing of the cellulose beads, a 40-fold replicate measurement was performed on the native phase. No increase in pressure, no shift in retention time and no change in peak shape were observed.

6.3.4 Example Separation using Temperature Responsive phase

The van't Hoff model was used to compare the native bead with the T-responsive bead. The corresponding equation is:

$$\ln k = -\frac{\Delta H^0}{R}\frac{1}{T} + \frac{\Delta S^0}{R} + \ln \beta \qquad \text{Equation 6-1}$$

Where k is the retention factor, ΔH^0 is the transfer enthalpy, R the general gas constant, T the absolute temperature, ΔS^0 the transfer entropy and β the column phase ratio [10].

As can be seen in Figure 6-4 a), ΔH^0 for the T-responsive beads is positive and thus an atypical progression of the van’t Hoff plot is present compared to the typical plot found for the native

beads shown in Figure 4 b). When ΔH^0 is positive, the transfer of the analyte from the stationary phase to the mobile phase is favored and thus endothermic. For the van't Hoff plot to be linear, it must be assumed that ΔH^0, ΔS^0 and β are constant over the temperature range under consideration or that the parameters influence each other in such a way that a linear relationship exists. In Figure 6-4 a) the transition from hydrophilic to hydrophobic properties was clearly demonstrated by the steep slope between 50 to 55 °C. Furthermore, there is a distinct decrease in the steepness after the change of the hydrophilicity of the phase. For comparison, the same components were tested on the native bead. Here, the retention behavior of naphthalene and propylparaben follows the expected linear van't Hoff plot with a positive slope.

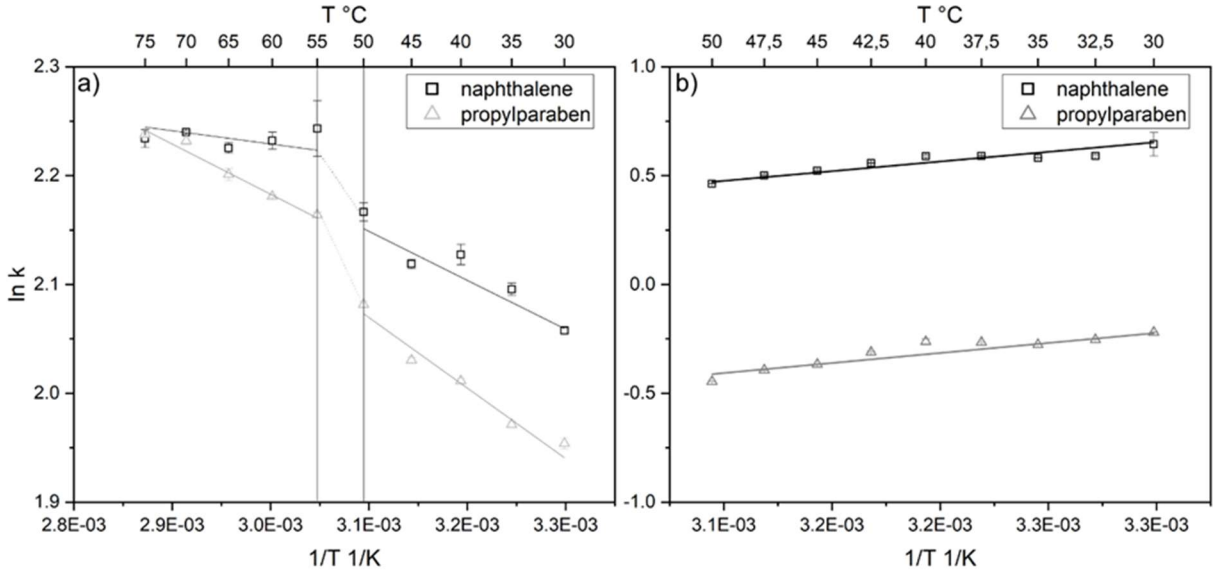

Figure 6-4: Comparison of the van't Hoff plots for naphthalene and propylparaben. a) Results for the temperature responsive stationary phase, the vertical lines mark the phase transition from hydrophilic to hydrophobic properties. b) Results for the native bead.

Figure 6-5 shows a separation of components with a broad polarity range. The temperature responsive modification of the N-acryloylpyrrolidine modified stationary phase caused a stronger retention on the material when the temperature was increased. While for metoprolol only a small shift of 0.3 min and for uracil no influence on the retention time with increasing temperature could be observed, a clear shift in retention time was observed for the two positional isomers cyclophosphamide and ifosfamide as well as carbamazepine. Although the two positional isomers could not be chromatographically resolved, the separation from uracil was significantly improved. While coelution of the three components at 40 °C is observed, the resolution was increased to R = 0.5 at 65 °C.

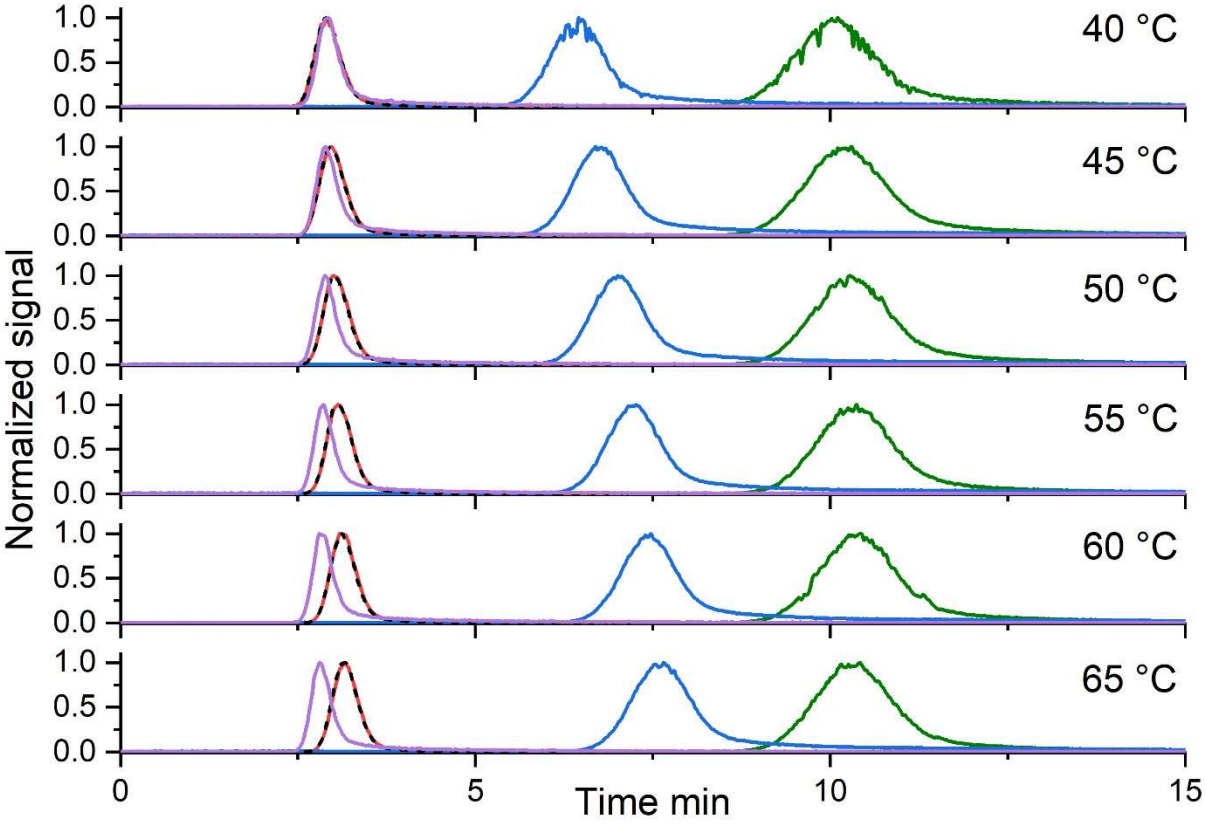

Figure 6-5: Normalized plot of elution as a function of temperature using the temperature responsive NAP stationary phase. Uracil (violet); cyclophosphamide (dotted red); ifosfamide (dotted black); carbamazepine (blue) and metoprolol (olive). Chromatograms were acquired on the Nexera Mikros; mobile phase: 10 mmol/L ammonium acetate solution; pH= 7; detection: MS 8060; flow rate: 5 µL/min; injection volume: 100 nL; column dimension: 50 x 0.5 mm.

6.3.5 Example Separation for Bioanalytical Applications

Two bead cellulose phases were developed especially for bioanalytical applications. One is the large pore material with an average pore size of 30 nm based on the porosimetry measurements (see Chapter 6.5.2), which should be suitable for chromatography of proteins with a hydrodynamic ratio of less than 6 nm [39]. The other is a medium polar phase which was loaded with the grafting monomer DMDOMA and therefore has diol functionality. The separation of the selected model proteins is shown in Figure 6-6.

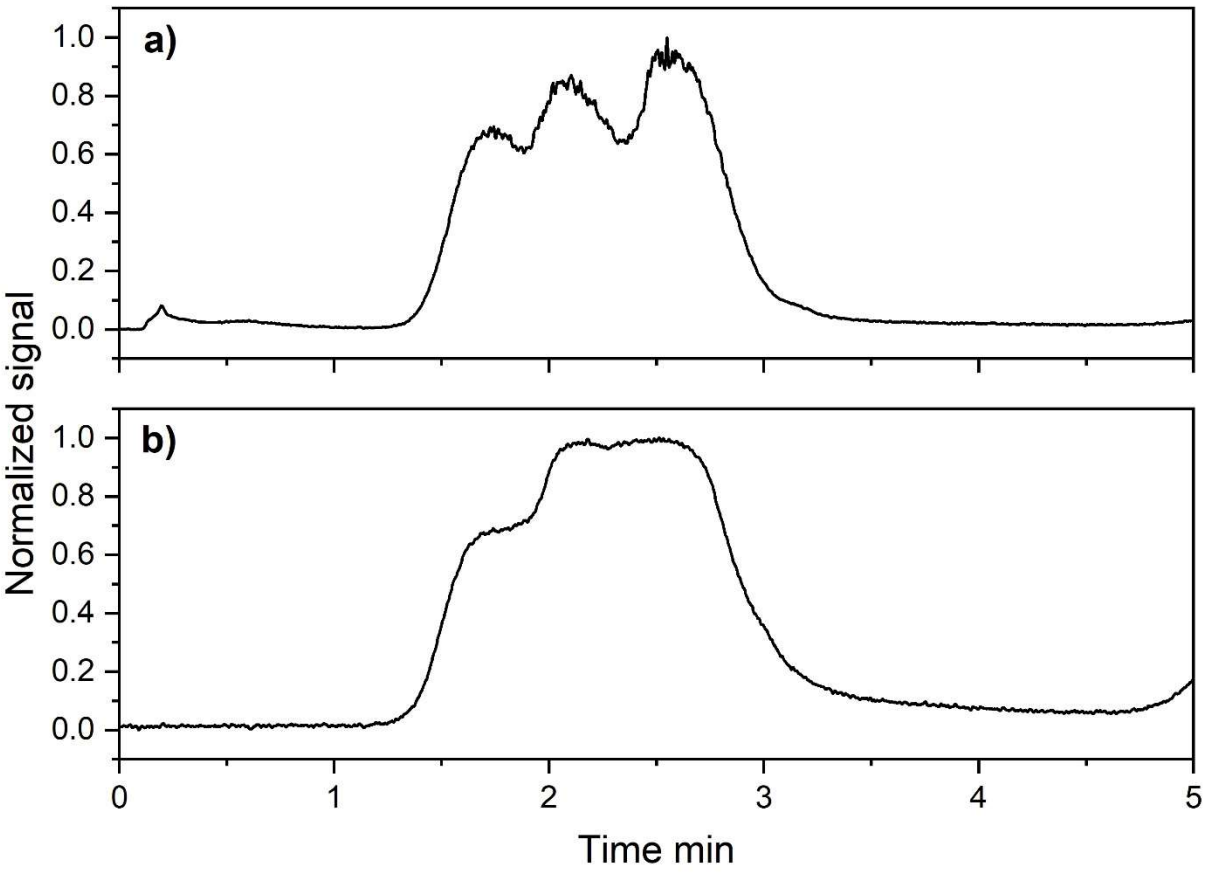

Figure 6-6: Chromatographic separation of proteins (from left to right) BSA, MYO and BVCZ (0.33 mg mL^{-1} in water each) as protein mix (1 mg mL^{-1}) on a) larger pore size bead cellulose column and b) the diol bead cellulose column. Mobile phase: PBS buffer 10 mM, temperature: 30 °C, flow rate: 5 µL min^{-1}, wavelength: 214 nm, injection volume: 1.5 µL. Column dimensions: 50 x 0.5 mm.

Both phases showed comparable theoretical resolutions between individual biomolecules based on the chromatographic deconvolution peaks, with both phases yielding comparable resolutions. Using this approach, a resolution of 0.66 was achieved for the BSA/MYO peak pair and a resolution of 0.71 was achieved for the MYO/BVCZ peak pair on the bead cellulose with larger pore size and high surface area. On the DMDOMA, a value of $R_{BSA/MYO} = 0.61$ and $R_{MYO/BVCZ} = 0.51$ was obtained. A summary of the data is shown in Table 6-3. Single injections of the analytes confirm the identical elution order on both columns. The elution of the analytes is not in order of their molecular weight. MYO (~17 kDa) elutes between BSA (~66 kDa) and BVCZ (~148 Da), therefore, a separation mechanism based on size exclusion can be ruled out. Despite the larger pore diameter, penetration of the proteins does not occur. Diffusion of the proteins into the accessible pores would be expected to increase the retention time. BSA has an isoelectric point (pI) of 4.5 to 5.0 and is negatively charged at pH 7.0 [40]. MYO is neutral at pI = 7.0, whereas BVCZ is positively charged at pH 7 with a pI = 8.3 [41, 42]. The negative charge of cellulose beads has a repulsive effect on BSA, a neutral effect on

MYO and a weak attractive effect on BVCZ. This also reflects the elution order. The native and diol cellulose bead thus have the function of a weak cation exchanger. Furthermore, this experiment demonstrated that, in contrast to the separation of the small molecules, the efficiency of the 5 cm column is not sufficient for the separation of biomolecules under isocratic conditions. Therefore, to further investigate the retention behavior of the proteins, two diol columns were connected to obtain an effective column length of 10 cm for the salt gradient experiments. The results of these experiments are shown in Figure 6-7.

Table 6-3: Peak widths, retention times and resolutions based on the deconvolution.

	Compound	Retention time min	FWHM min	Resolution
Large pore	BSA	1.69	0.33	
				0.66
	MYO	2.08	0.37	
				0.71
	BVCZ	2.60	0.50	
Diol	BSA	1.65	0.31	
				0.61
	MYO	2.03	0.42	
				0.71
	BVCZ	2.54	0.74	

In the first experiment, the proteins were separated using 22 min generic salt gradients on the coupled diol bead cellulose stationary phase (Figure 6-7 a). This increased the resolution of the peak pairs for $R_{BSA/MYO} = 6.5$ and $R_{MYO/BVCZ} = 0.9$. However, the separation is compromised by strong tailing of the analytes, which have not been observed to the same extent in the separation of small molecules. One reason for this could be the interaction of the metallic column hardware with basic proteins [33]. In addition, it should be noted that the effect of adsorption of proteins on surfaces by the introduction of two additional steel frits through the column coupling also negatively affects tailing in this case. The more basic the protein, the stronger the interactions with the stationary phase and the more pronounced the tailing. The tailing was more pronounced for BVCZ (pI = 8.3) than for MYO (pI = 7.0).

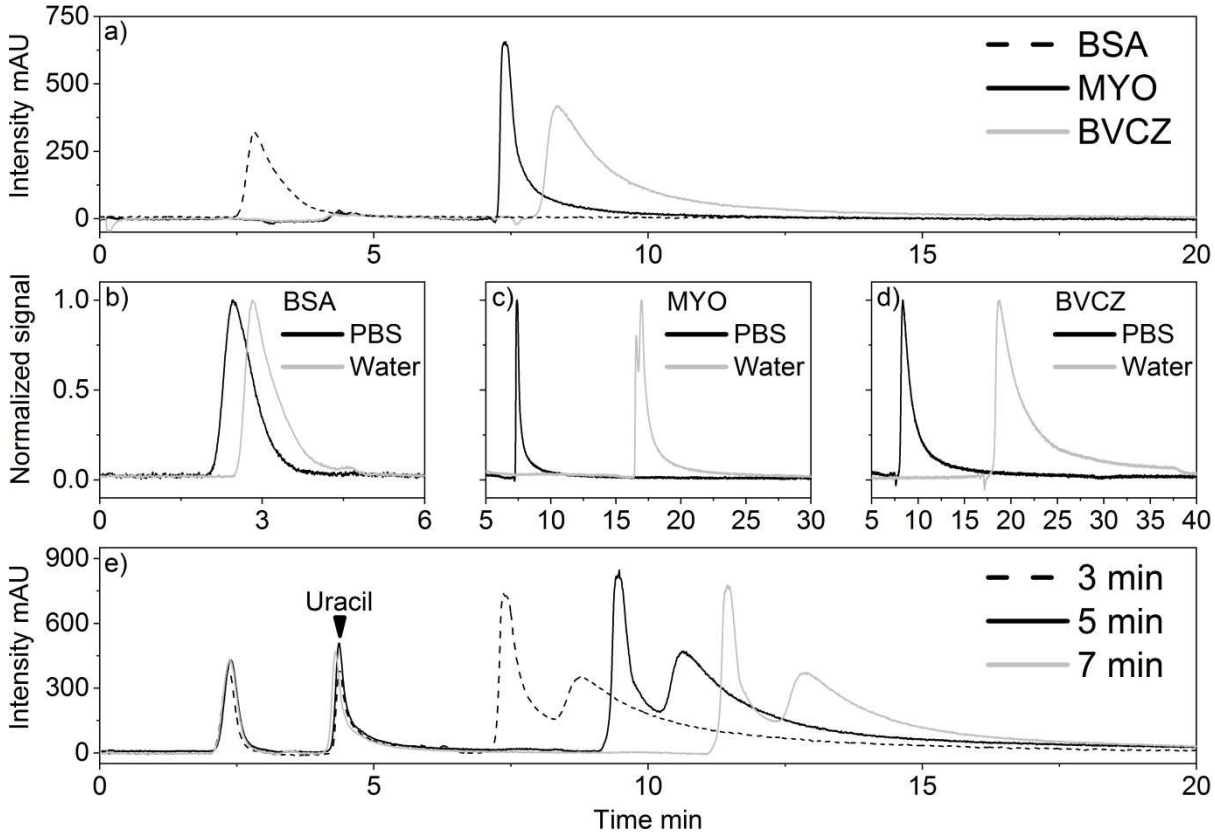

Figure 6-7: Comparison of retention behaviour of MYO, BSA and BVCZ on two coupled diol columns. a) Chromatographic separation of the three proteins using a generic salt gradient. Gradient elution: Mobile phase A: 10 mmol L^{-1} PBS pH 7.3, B: pure aqueous, 0-3 min: 0% B, 3-25 min: 100% B, 25-40 min: 0% B. Middle row: Comparison of retention behaviour under purely aqueous conditions and 10 mM PBS for b) BSA, c) MYO and d) BVCZ. E) Increase from 100% water to 100% 150 mM PBS after 3-, 5- and 7-min. Temperature: 30 °C, flow rate: 5 µL min^{-1}, wavelength: 214 nm, injection volume: 1.0 µL.

In the second experiment, it was investigated whether the phase material allows a purely aqueous elution of the proteins. Aqueous elution was possible for all components considered and led to an increase in the retention time, while the peak shape was maintained except for the anticipated band broadening. As shown in Figure 6-7 b, the retention time shift was moderate for BSA, with a 15% increase from 2.5 to 2.8 min. A comparable increase in retention time of 130% and 125% was found for MYO and BVCZ, respectively (Figure 6-7 c and d). While hydrophobic interaction chromatography uses high salt concentrations to remove the hydrate shell and expose the hydrophobic regions of the protein to achieve an increase in retention, the opposite effect is achieved using bead cellulose. This allows the previously established hypothesis to be confirmed, by reducing the salt concentration the free hydroxyl groups of DMDOMA act as a weak cation exchanger.

In the last experiment of the series shown in Figure 6-7 c, step gradients with an increase from 0% to 100% B were used to investigate a potential trap and elute function of the phases. Here, the analytes were dissolved in water and the plateau was extended from 3, to 5 and 7 min. By adjusting the injection solution to the starting conditions of the gradient, the peak shape of BSA was greatly improved. Since BSA has only a low retention on the phase, no effect of the step gradient can be observed. For MYO and BVCZ, an equivalent retention time shift corresponding to the plateau of 1.99 ± 0.05 min was observed.

Based on the experiments, the material is suitable as a stationary phase for the separation of proteins. The interactions of cellulose with the analytes are very low due to the above-mentioned cross-linking of the OH groups by hydrogen bonds. As a base material, it is significantly less polar than silica gel and is therefore ideal for applications where attractive phase interactions are not desired. Saltless elution allows direct coupling to mass spectrometry without the need for desalting steps or the use of volatile salts.

6.4 Conclusion

A synthesis method and a purification process for the reproducible production of cellulose beads in the sub-5-µm range were developed. The parameterizability of the material was demonstrated by producing different pore sizes and surface morphologies. Furthermore, the cellulose beads showed pressure stability up to 55 bar and were tested in a temperature range of 30-75 °C.

It has been shown that the native cellulose bead can be modified by various grafting reactions to make it useful for a variety of chromatographic applications. This was exemplified by modification with N-acryloylpyrrolidine for a T-responsive cellulose sphere and diol modification for bioanalytical applications. With these chemical modifications, separation and elution of nonpolar small and large molecules was achieved without the use of organic solvents or high temperatures using a mobile phase of pure water. Very low salt concentrations were sufficient for the separation of proteins, opening the possibility of new couplings with mass spectrometry.

6.5 Supplementary Information

6.5.1 Particle Size Distribution for All Batches

Table 6-4 summarizes the results of particle size distribution measurements of the seven batches of bead cellulose prepared according to the described synthesis process in the main paper. The values for the combined sample were determined after the described purification step.

Table 6-4: Results on the reproducibility of the bead cellulose preparations.

Sample	D10 µm	D50 µm	D90 µm	D90/D10	Mass atro g
Batch 1	1.9	4.1	7.4	3.9	13.1
Batch 2	2.2	4.2	7.0	3.2	15.8
Batch 3	1.7	3.7	6.7	3.9	15.2
Batch 4	1.7	3.8	6.7	3.9	13.9
Batch 5	2.0	3.7	6.3	3.1	14.0
Batch 6	1.9	3.7	6.3	3.3	11.6
Batch 7	1.7	3.6	6.3	3.7	12.2
Combined 4+5	2.7	4.9	7.8	2.9	8.4

The variation for the batches 1-7 is less than 1 µm and the distribution width varies only in a very narrow range between D90/D10 = 3.1 and 3.9. The quantities D10, D50 and D90 indicate what percentages of the total particles are below the specified diameter. The average particle size (D50) and the width of the distribution (D10, D90) thus provide good comparability with other particle phases. Thus, a previously unattained quality of the material is achieved before the fractionation and purification step. As it can be seen, after the purification the distribution was improved further.

6.5.2 Results of Pore Size and Surface Area

The method of porosimetry was used to determine the pore diameter distribution, specific pore surface area and specific pore volume. Hg intrusion was performed using Thermoelectron Cooperation (Milano, Italy) "Pascal 140" (macropores) and "Pascal 440" (mesopores) instruments. Subsequently, the resulting intrusion curves were merged and evaluated. The results for the native and large pore cellulose bead are summarized in Table 6-5.

Table 6-5: Results for cumulative volume, pore surface area and porosity for the native and the large pore cellulose bead.

Material	Cumulative volume	Pore surface area	Porosity
	mm3/g	m2/g	%
Native	571	18	51
Large pore	1371	80	62

There was a clear difference in both samples investigated. This becomes even clearer when comparing the pore size and pore surface distributions graphically. In Figure 6-8, the pore size distribution of the native cellulose bead was compared with the large pore material and Figure 6-9 compares the results for the specific surface area.

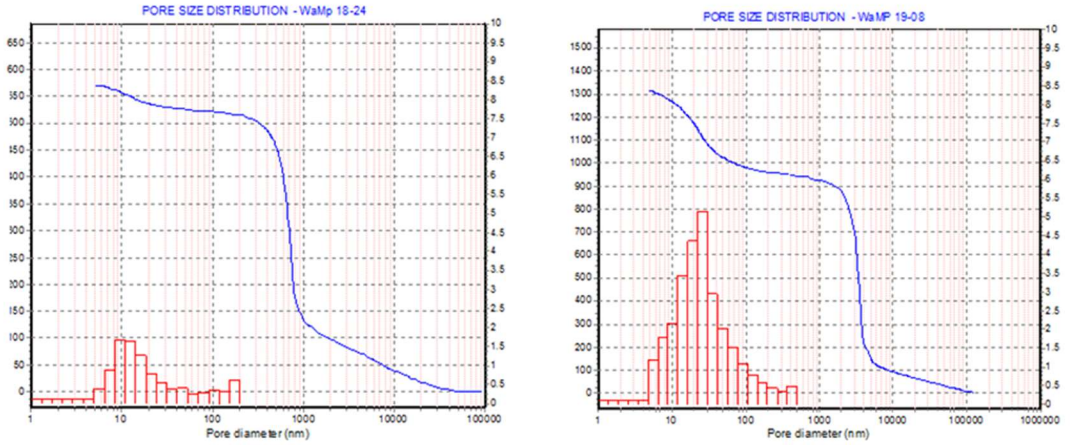

Figure 6-8: Pore size distribution of the native cellulose bead (left) and the large pore cellulose bead (right). Ordinate axis left: Cumulative pore volume, ordinate axis right: relative pore volume and the abscissa axis with pore diameter.

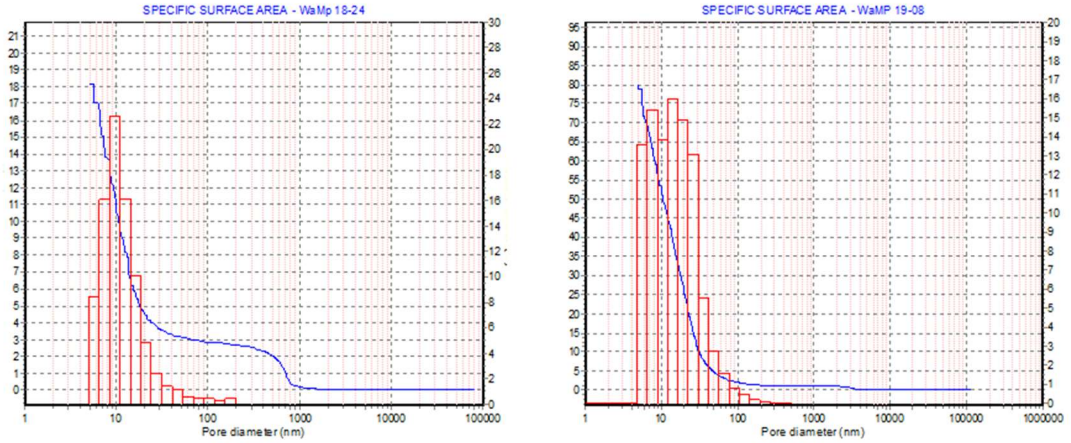

Figure 6-9: Specific pore surface area of the native cellulose bead (left) and the large pore cellulose bead (right). Ordinate axis left: Surface area, ordinate axis right: relative surface area and the abscissa axis with pore diameter.

6.6 References

[1] P. Anastas, N. Eghbali, Green Chemistry: Principles and Practice, Chem. Soc. Rev. 39 (2010) 301–312. https://doi.org/10.1039/b918763b.

[2] C. Aydoğan, F. Rigano, L.K. Krčmová, D.S. Chung, M. MacKa, L. Mondello, Miniaturized LC in Molecular Omics, Anal. Chem. 92 (2020) 11485–11497. https://doi.org/10.1021/acs.analchem.0c01436.

[3] C. Thoben, T. Werres, I. Henning, P.R. Simon, S. Zimmermann, T.C. Schmidt, T. Teutenberg, Towards a miniaturized on-site nano-high performance liquid chromatography electrospray ionization ion mobility spectrometer with online enrichment, Green Anal. Chem. 1 (2022) 100011. https://doi.org/10.1016/j.greeac.2022.100011.

[4] G. Li, X. Dai, Y. Min, L. Zhang, J. Shen, Y. Okamoto, Synthesis and characterization of cellulose derivative-based hybrid beads as chiral stationary phases for efficient chromatographic enantioseparation, New J. Chem. 45 (2021) 6432–6437. https://doi.org/10.1039/d0nj05094f.

[5] M.M. Al-Sanea, M. Gamal, Critical analytical review: Rare and recent applications of refractive index detector in HPLC chromatographic drug analysis, Microchem. J. 178 (2022) 107339. https://doi.org/https://doi.org/10.1016/j.microc.2022.107339.

[6] I.K. Ventouri, D.B.A. Malheiro, R.L.C. Voeten, S. Kok, M. Honing, G.W. Somsen, R. Haselberg, Probing Protein Denaturation during Size-Exclusion Chromatography Using Native Mass Spectrometry, Anal. Chem. 92 (2020) 4292–4300. https://doi.org/10.1021/acs.analchem.9b04961.

[7] T. Muyizere, Y. Zheng, H. Liu, J. Zhao, J. Li, X. Lu, D.E. Austin, Z. Zhang, Metal salt assisted electrospray ionization mass spectrometry for the soft ionization of GAP polymers in negative ion mode, Analyst. 145 (2020) 34–45. https://doi.org/10.1039/c9an01887e.

[8] S.P. Cleary, J.S. Prell, Liberating Native Mass Spectrometry from Dependence on Volatile Salt Buffers by Use of Gábor Transform, ChemPhysChem. 20 (2019) 519–523. https://doi.org/https://doi.org/10.1002/cphc.201900022.

[9] S. Karki, F. Shi, J.J. Archer, H. Sistani, R.J. Levis, Direct Analysis of Proteins from Solutions with High Salt Concentration Using Laser Electrospray Mass Spectrometry, J. Am. Soc. Mass Spectrom. 29 (2018) 1002–1011. https://doi.org/10.1007/s13361-018-1893-2.

[10] T. Teutenberg, Potential of high temperature liquid chromatography for the improvement of separation efficiency-A review, Anal. Chim. Acta. 643 (2009) 1–12. https://doi.org/10.1016/j.aca.2009.04.008.

[11] M. Baert, K. Wicht, A. Moussa, G. Desmet, K. Broeckhoven, F. Lynen, Implementations of temperature gradients in temperature-responsive liquid chromatography, J. Chromatogr. A. 1654 (2021) 462425. https://doi.org/https://doi.org/10.1016/j.chroma.2021.462425.

[12] C. Becker, M.A. Jochmann, T. Teutenberg, T.C. Schmidt, A nebulizer interface for liquid chromatography - Flame ionization detection: Development and validation, Talanta. 206 (2020) 120229. https://doi.org/https://doi.org/10.1016/j.talanta.2019.120229.

[13] C. Becker, A.A. Deeb, T. Teutenberg, M.A. Jochmann, T.C. Schmidt, Determination of liquid chromatography/flame ionization detection response factors for N-heterocycles, carboxylic acids, halogenated compounds, and others, Anal. Bioanal. Chem. 412 (2020) 171–179. https://doi.org/10.1007/s00216-019-02222-1.

[14] T. Teutenberg, K. Hollebekkers, S. Wiese, A. Boergers, Temperature and pH-stability of commercial stationary phases, J. Sep. Sci. 32 (2009) 1262–1274. https://doi.org/10.1002/jssc.200800712.

[15] M. Baert, K. Wicht, Z. Hou, R. Szucs, F. Du Prez, F. Lynen, Exploration of the Selectivity and Retention Behavior of Alternative Polyacrylamides in Temperature Responsive Liquid Chromatography, Anal. Chem. 92 (2020) 9815–9822. https://doi.org/10.1021/acs.analchem.0c01321.

[16] A.J. Satti, P. Espeel, S. Martens, T. Van Hoeylandt, F.E. Du Prez, F. Lynen, Tunable temperature responsive liquid chromatography through thiolactone-based immobilization of poly(N-isopropylacrylamide), J. Chromatogr. A. 1426 (2015) 126–132. https://doi.org/10.1016/j.chroma.2015.11.063.

[17] A. Mizutani, K. Nagase, A. Kikuchi, H. Kanazawa, Y. Akiyama, J. Kobayashi, M. Annaka, T. Okano, Preparation of thermo-responsive polymer brushes on hydrophilic polymeric beads by surface-initiated atom transfer radical polymerization for a highly resolutive separation of peptides, J. Chromatogr. A. 1217 (2010) 5978–5985. https://doi.org/10.1016/j.chroma.2010.07.067.

[18] A. Mizutani, K. Nagase, A. Kikuchi, H. Kanazawa, Y. Akiyama, J. Kobayashi, M. Annaka, T. Okano, Effective separation of peptides using highly dense thermo-responsive polymer brush-grafted porous polystyrene beads, J. Chromatogr. B Anal. Technol. Biomed. Life Sci. 878 (2010) 2191–2198. https://doi.org/10.1016/j.jchromb.2010.06.026.

[19] A. Mizutani, K. Nagase, A. Kikuchi, H. Kanazawa, Y. Akiyama, J. Kobayashi, M. Annaka, T. Okano, Thermo-responsive polymer brush-grafted porous polystyrene beads for all-aqueous chromatography, J. Chromatogr. A. 1217 (2010) 522–529. https://doi.org/10.1016/j.chroma.2009.11.073.

[20] J. J. O'Neil, E. P. Reichardt, Method of producing cellulose pellet, 1951. https://patents.google.com/patent/US2543928A/en

[21] J. Prentice, S.T. Evans, D. Robbins, G. Ferreira, Pressure-Flow experiments, packing, and modeling for scale-up of a mixed mode chromatography column for biopharmaceutical manufacturing, J. Chromatogr. A. 1625 (2020) 461117. https://doi.org/10.1016/j.chroma.2020.461117.

[22] H. Zhang, Z.Y. Wu, Y.Y. Yang, F.Q. Yang, S.P. Li, Recent applications of immobilized biomaterials in herbal analysis, J. Chromatogr. A. 1603 (2019) 216–230. https://doi.org/10.1016/j.chroma.2019.06.059.

[23] W. Wagenknecht, F. Loht, C. Fanter, Process for producing spherical microparticles on the basis of cellulose acetate, 99 (1996) 1–9.

[24] Y. Liu, L. Qiao, A. Wang, Y. Li, L. Zhao, K. Du, Tentacle-type poly(hydroxamic acid)-modified macroporous cellulose beads: Synthesis, characterization, and application for heavy metal ions adsorption, J. Chromatogr. A. 1645 (2021). https://doi.org/10.1016/j.chroma.2021.462098.

[25] J. Peška, J. Štamberg, J. Hradil, M. Ilavský, Cellulose in bead form. Properties related to chromatographic uses, J. Chromatogr. A. 125 (1976) 455–469. https://doi.org/10.1016/S0021-9673(00)85709-X.

[26] S. Kuga, New cellulose gel for chromatography, J. Chromatogr. A. 195 (1980) 221–230. https://doi.org/10.1016/S0021-9673(00)96813-4

[27] J.A. Kaster, W. de Oliveira, W.G. Glasser, W.H. Velander, Optimization of pressure-flow limits, strength, intraparticle transport and dynamic capacity by hydrogel solids content and bead size in cellulose immunosorbents, J. Chromatogr. A. 648 (1993) 79–90. https://doi.org/10.1016/0021-9673(93)83289-5.

[28] B. Wolf, W. Schmitz, H. Schneider, Composites of bead cellulose and hydrophilic solubilizers, Int. J. Pharm. 139 (1996) 87–94.

[29] W. De Oliveira, W.G. Glasser, Hydrogels from polysaccharides. I. Cellulose beads for chromatographic support, J. Appl. Polym. Sci. 60 (1996) 63–73. https://doi.org/10.1002/(sici)1097-4628(19960404)60:1<63::aid-app8>3.3.co;2-4.

[30] K. Thümmler, S. Fischer, A. Feldner, V. Weber, M. Ettenauer, F. Loth, D. Falkenhagen, Preparation and characterization of cellulose microspheres, Cellulose. 18 (2011) 135–142. https://doi.org/10.1007/s10570-010-9465-z.

[31] S. Fischer, K. Thümmler, B. Volkert, K. Hettrich, I. Schmidt, K. Fischer, Properties and applications of cellulose acetate, Macromol. Symp. 262 (2008) 89–96. https://doi.org/10.1002/masy.200850210.

[32] L. Loukotková, M. Rambousková, Z. Bosáková, E. Tesařová, Cellulose tris(3,5-dimethylphenylcarbamate)-based chiral stationary phases as effective tools for enantioselective HPLC separation of structurally different disubstituted binaphthyls, Chirality. 20 (2008) 900–909. https://doi.org/10.1002/chir.20585.

[33] K. Du, Ionic liquid-regenerated macroporous cellulose monolith: Fabrication, characterization and its protein chromatography, J. Chromatogr. A. 1494 (2017) 40–45. https://doi.org/10.1016/j.chroma.2017.03.004.

[34] N.A. Plate, T.L. Lebedeva, L.I. Valuev, Lower critical solution temperature in aqueous solutions of yV-alkyl-substituted polyacrylamides, Polym. J. 31 (1999) 21–27. https://doi.org/10.1295/polymj.31.21.

[35] P. Pomastowski, J. Walczak, M. Gawin, S. Bocian, W. Piekoszewski, B. Buszewski, HPLC separation of casein components on a diol-bonded silica column with MALDI TOF/TOF MS identification, Anal. Methods. 6 (2014) 5236–5244. https://doi.org/10.1039/c4ay00895b.

[36] K. Beyaz, M. Charton, A. Rouilly, E. Vedrenne, C. Vaca-Garcia, A. Benaboura, S. Thiebaud-Roux, Synthesis of graft-copolymers from palm cellulose and solketal acrylate and their characterization, Ind. Crops Prod. 97 (2017) 32–40. https://doi.org/https://doi.org/10.1016/j.indcrop.2016.12.001.

[37] K. Gabov, T. Oja, T. Deguchi, A. Fallarero, P. Fardim, Preparation, characterization and antimicrobial application of hybrid cellulose-lignin beads, Cellulose. 24 (2017) 641–658. https://doi.org/10.1007/s10570-016-1172-y.

[38] M. Gericke, J. Trygg, P. Fardim, Functional cellulose beads: Preparation, characterization, and applications, Chem. Rev. 113 (2013) 4812–4836. https://doi.org/10.1021/cr300242j.

[39] A. Murisier, S. Fekete, D. Guillarme, V. D'Atri, The importance of being metal-free: The critical choice of column hardware for size exclusion chromatography coupled to high resolution mass spectrometry, Anal. Chim. Acta. 1183 (2021). https://doi.org/10.1016/j.aca.2021.338987.

[40] H.T.M. Phan, S. Bartelt-Hunt, K.B. Rodenhausen, M. Schubert, J.C. Bartz, Investigation of bovine serum albumin (BSA) attachment onto self-assembled monolayers (SAMs) using combinatorial quartz crystal microbalance with dissipation (QCM-D) and spectroscopic ellipsometry (SE), PLoS One. 10 (2015). https://doi.org/10.1371/journal.pone.0141282.

[41] S. Kaja, J.D. Hilgenberg, E. Everett, S.E. Olitsky, J. Gossage, P. Koulen, Effects of dilution and prolonged storage with preservative in a polyethylene container on Bevacizumab (AvastinTM) for topical delivery as a nasal spray in anti-hereditary hemorrhagic telangiectasia and related therapies, Hum. Antibodies. 20 (2011) 95–101. https://doi.org/10.3233/HAB-2011-0244.

[42] S. Devineau, K.I. Inoue, R. Kusaka, S.H. Urashima, S. Nihonyanagi, D. Baigl, A. Tsuneshige, T. Tahara, Change of the isoelectric point of hemoglobin at the air/water interface probed by the orientational flip-flop of water molecules, Phys. Chem. Chem. Phys. 19 (2017) 10292–10300. https://doi.org/10.1039/c6cp08854f.

Chapter 7 Towards a miniaturized on-site nano-high performance liquid chromatography electrospray ionization ion mobility spectrometer with online enrichment

This chapter was adapted from: C. Thoben, T. Werres, I. Henning, P.R. Simon, S. Zimmermann, T.C. Schmidt, T. Teutenberg, Towards a miniaturized on-site nano-high performance liquid chromatography electrospray ionization ion mobility spectrometer with online enrichment, Green Anal. Chem. 1 (2022) 100011. https://doi.org/10.1016/j.greeac.2022.100011.

Abstract: Safeguarding water quality is resource-intensive and costly. Especially in cases of accidents or disasters, compact devices that allow quick assessment of the current situation are lacking. The objective of this work is the development of a portable measuring device for on-site detection of pollutants in water based on nano-high performance liquid chromatography (nano-HPLC) and electrospray ionization (ESI) ion mobility spectrometry (IMS). Integrated online enrichment by means of solid phase extraction (SPE) further improves sensitivity. In this work, an SPE cartridge exchange unit is presented, which was developed by additive manufacturing in a cost-effective and resource-efficient way. Prerequisites are an easy adaptation to commercially available SPE cartridges and pressure stability of up to 50 bar. In addition, a compact ESI-IMS with 75 mm drift tube length and a resolving power of R = 100 is presented that enables ionization, separation based on ion mobility and detection of analytes at a flow rate of 0.6 – 1.8 µL/min from the liquid phase. This approach also allows miniaturization of the overall system leading to a reduction in energy requirements and the amount of solvents used. For future environmentally benign systems, complete elimination of toxic solvents would be ideal. Therefore, acetonitrile and the nontoxic ethanol are compared as organic mobile phase in terms of elution and ionization efficiency. For characterization, a test mixture containing relevant target analytes, such as chlortoluron, isoproturon, pyrimethanil, mepanipyrim, cyprodinil and carbamazepine, is analyzed. In addition, the analytical greenness metric approach tool is used to evaluate the overall system in terms of its green credentials.

It was shown that ethanol can be well used as an organic solvent for the mobile phase and even exhibits better ionization than acetonitrile for the selected model analytes. Furthermore, a relatively high orthogonality of $O = 0.53$ and an effective 2D peak capacity of ${}^{2D}n_{\mathrm{eff}} = 174$ are reached. Due to the overall miniaturization and splitless coupling, the aims of green chemistry can be met, and ideally a value of 0.92 can be achieved using the AGREE tool for the presented system.

7.1 Introduction

With constantly increasing industrial requirements and regulations, the number of newly synthesized chemicals is rapidly growing and hence also the complexity of the analytical chemist's work. This fact can be exemplified by the large number of chemicals registered under the European Union regulation REACH (Registration, Evaluation, authorisation and Restriction of Chemicals) [1]. Since the regulation came into force in 2007, a total of 23,445 different substances have been registered up to the publication break on October 15, 2021. Similar laws exist in other countries, such as the USA with the Toxic Control Act or Japan's Existing Notified Chemical Substances (ENCS) list [2-4]. Each new substance can potentially also be a new contaminant, especially in cases of accidents or spills in water bodies. However, compact on-site monitoring devices that allow quick assessment are lacking. Current concepts rely on large car trailers equipped with complex and expensive high-end laboratory analytical instrumentation to ensure on-site measurement [5]. Even though these systems provide high-quality data sets, they are too complex and expensive to be available in sufficient numbers for flexible use. In addition, good access to the monitoring site and a power supply are essential for the use of these platforms.

Especially with miniaturization, the energy requirements can generally be reduced and the amount of toxic organic solvents can be minimized by downsizing peripheral equipment. Further possibilities of a more environmentally friendly system include the avoidance of extensive sample preparation steps, the complete elimination of toxic solvents and the use of compact energy-efficient analytical instruments. There is a clear trend towards the development of portable analytical instruments. Examples are portable GC–MS systems [6, 7] or the HPLC system described by Chatzimichail et al. [8]. Additional research lies in the area of further miniaturization of the pump system towards nL/min flow rates. LED-based spectroscopic detectors are often used in this application due to their compactness. This achieves a reduction in the size, energy requirements and solvent consumption of a gradient syringe pump system without compromising system performance [9-11]. The comprehensive review by Snyder et al. [12] provides a very good overview of the state of the art in miniaturized and portable MS systems. Ion mobility spectrometry is particularly suitable for on-site measurements, especially with gas chromatographic pre-separation [13-15]. In contrast to mass spectrometry, no vacuum is required for the separation of the generated ions. IMS is already a powerful separation technique used particularly at airports for identification of trace amounts of explosives and other warfare agents in the gas phase [16, 17]. In addition, IMS is becoming more and more applicable in the field of water analysis [18]. Due to the low peak capacity of IMS and the competitive

ionization of different analytes, which can extend to ion suppression, chromatographic pre-separation is often chosen [19, 20]. When using conventional HPLC systems with flow rates above > 300 µL/min, a split via a T-piece is necessary for coupling to an ESI-IMS to reduce the LC flow to a few µL/min [21, 22]. Another possibility is to create the split within the ion source area, e.g. via a T-cylinder [23]. However, the most adept way seems to be the reduction of the flow rate of the HPLC even further, thereby allowing a splitless coupling of HPLC and IMS [24, 25].

The aim of this work is therefore to develop a portable device for on-site detection of pollutants in water based on nano-high performance liquid chromatography (nano-HPLC) and electrospray ionization (ESI) ion mobility spectrometry (IMS). To further improve sensitivity, online enrichment using integrated solid phase extraction (SPE) is used. Therefore, this work presents an SPE cartridge exchange unit developed by additive manufacturing in a cost-effective and resource-efficient way. The SPE cartridge ensures separation of the analyte mixture to reduce sample complexity before ionization and separation in the IMS. Using a compact ESI-IMS for the separation based on ion mobility and the detection of analytes, a two-dimensional separation is achieved. Ideally, the complete elimination of toxic solvents should be aimed at. This consideration needs to take into account the concept of green chemistry, which is becoming increasingly important in the general consciousness. Developments in the field of green chemistry are rarely described with appropriate green metrics [26]. By default, processes and devices that are created with green chemistry in mind should also always be subjected to an evaluation procedure. Ideally, a standard assessment technique should be applied that allows the comparison of different methods and approaches across publications. The scientific community has already made various proposals. Gaber et al. have developed the HPLC Environmental Assessment Tool (HPLC-EAT), a simple approach for profiling the greenness of liquid chromatographic methods [27]. The analytical method is subdivided and evaluated in environmental, health and safety units based on the solvents used. The proposal by Płotka-Wasylka called Green Analytical Procedure Index (GAPI) is more comprehensive and allows the evaluation of the whole analytical workflow [28]. The assessment includes sample preparation, reagent and compounds used, sample collection, sample preservation, sample transport and storage, as well as instrumentation. The results can then be displayed as a pictogram. The tool used in this work proposed by Pena-Pereira et al. is based on the 12 principles of green chemistry to evaluate methods and systems presenting the results in a well-structured pictogram [29]. The user has the possibility to add weighting to the 12 principles if needed.

7.2 Material and Methods

7.2.1 Instrumental

In this work, a self-constructed compact ESI-IMS with 75 mm drift tube length and a resolving power of R = 100 is used, the detailed description of the setup can be found elsewhere [30]. The ions are generated by an electrospray ion source consisting of a metal emitter (New Objective Metal Taper Tip, DNU-MS, Berlin, Germany) with a tip inner diameter of 50 µm and a desolvation region of 50 mm length. The ion source operates at a flow rate of 0.6 – 1.8 µL min^{-1}. The ESI voltage of 2.7 – 3.3 kV is applied between the emitter and the grounded inlet of the desolvation region. This implies that the detector and the amplifier as well as the analog-to-digital converter are at high potential [31]. A tristate ion shutter not discriminating larger ions with lower mobility is used to inject the generated ions from the desolvation region into the drift region, as has been described in several IMS setups [30, 32-35]. Table 7-1 gives an overview of the relevant operating parameters of the ESI-IMS.

Table 7-1: ESI-IMS operating parameters.

Parameter	Value	Parameter	Value
Length of drift region	75 mm	Drift field strength	66 V/mm
Length of desolvation region	50 mm	Desolvation field strength	66 V/mm
Emitter-to-inlet voltage	2.7 – 3.3 kV	Liquid flow	0.6 – 1.8 µL/min
Drift gas flow rate	250 mL/min	Emitter diameter	50 µm
Drift gas dew point	-85 °C	Drift region temperature	23 °C
Drift gas	Purified dry air	Desolvation region temperature	23 °C
Pressure	1013 mbar		

The True Nano™ UHPLC (VICI AG International, Schenkon, Switzerland) is used for delivering a precise and low flow rate. The system is equipped with a binary syringe pump system capable of generating a maximum pressure of 1500 bar providing flow rates down to 10 nL min^{-1}. Loading of the sample loop is performed by an LSPone syringe pump (Advanced Microfluidics SA, Ecublens, Switzerland) using a 25 µL syringe. Sample injection onto the column was carried out by the integrated six-port-two-position valve and via a fixed sample loop of 200 nL. The comparison of the two mobile phase systems water/acetonitrile (ACN) and water/ethanol (EtOH) was performed on a YMC-Triart C18 column with a length of 50 mm

and an ID of 0.3 mm packed with fully porous 3 µm particles with a pore size of 120 Å (YMC Europe GmbH, Dinslaken, Germany). Stacked injection was used for enrichment and performed by overfilling the sample loop with a multiple of its volume. Thereafter the valve was switched, and the sample was transferred to the separation cartridge under isocratic conditions at 10% EtOH. This step was repeated until the desired enrichment factor was reached. After injection of the last enrichment volume, the measurement was started. The separation cartridges with dimensions of 10 × 0.3 mm were packed with the YMC Triart C18 1.9 µm material by Dr. A. Maisch HPLC GmbH (Ammerbuch-Entringen, Germany). Stainless steel tubing (VICI AG International) with an outer diameter of 360 µm and an inner diameter of 50 µm is used for the HPLC tubing. The 360 µm fittings from VICI AG (JR-C360NFS6) are used as connectors. A photo of the complete system with the VICI nano-HPLC pump, the open cartridge changer, including the separation cartridge, and the ESI-IMS is shown in Figure 7-1 a). Photos and a detailed description of the cartridge changer can be found in chapter 7.5.1.

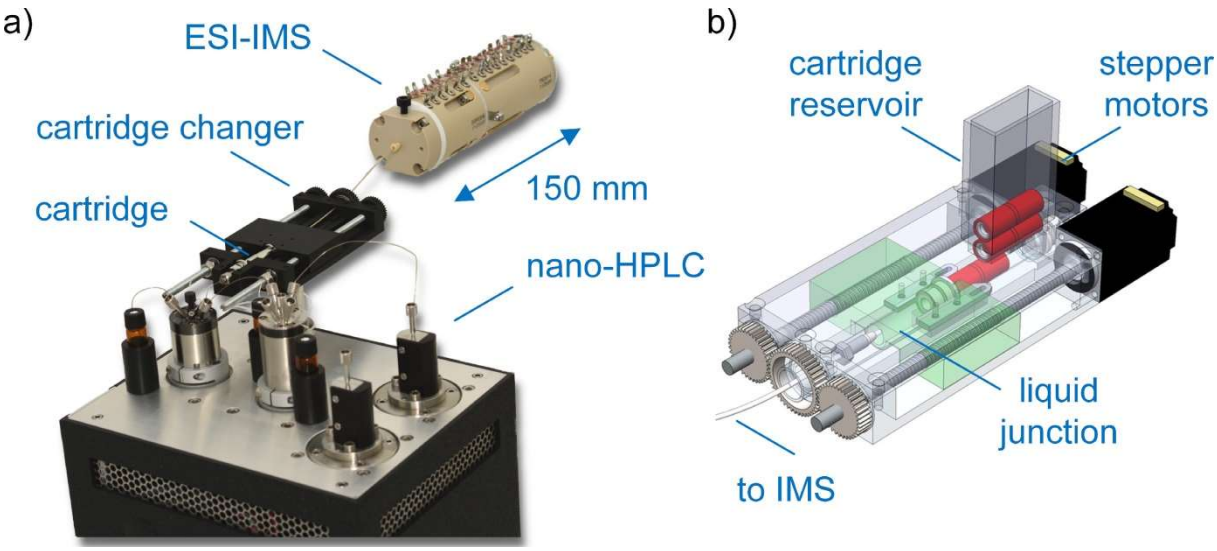

Figure 7-1: a) Photo of the complete system with the VICI nano-HPLC pump, the open cartridge changer with the separation cartridge and the ESI-IMS, and b) the CAD drawing of the cartridge changer.

The determination of the energy consumption of all current-carrying components in the system was done using the precision current clamp BENNING CM 11 (BENNING GmbH, Bocholt, Germany) and the measuring adapter Voltcraft DLA-1 L 16 (Conrad Electronic SE, Hirschau, Germany).

Prerequisites for the cartridge changer are a simple adaptation to commercially available SPE cartridges and a pressure stability up to 50 bar. The CAD files for the cartridge changer were created in SOLIDWORKS 2022 (SolidLine GmbH, Walluf, Germany), and the generated CAD drawing is shown in Figure 7-1 b). Prusa Slicer 2.3.0 (Prusa Research, Prague, Czech Republic)

was used as the slicer software. The additive manufacturing was carried out on the Prusa i3 MK3S running on the Marlin Firmware 3.10.1 equipped with an MMU2S and utilizing a nozzle size of 0.4 mm. Print setting was set to “0.15 mm quality”, the filament setting was set to “generic PLA”, and the fill was set to 50%. As filament, the Extrudr PLA NX2 black 1.75 mm (FD3D GmbH, Lauterach, Austria) was chosen. To avoid overhangs and guarantee sufficient precision, the printing parts are aligned at a 45° angle to the printing bed. The cartridge changer was clamped by means of M5 threaded rods, which are equipped with ball bearings to ensure for uniform force dissipation. This guarantees a fluid-tight connection between the cartridge and the rest of the system components. Therefore, no 3D printed parts have direct contact with the mobile phase solvents. For the reader to rebuild the cartridge changer, all required 3D files have been made available in the supplementary. The other components required and further information on production can be found in chapter 7.5.2.

7.2.2 Chemicals

LC-MS grade water, acetonitrile, ethanol and methanol (MeOH) were used as mobile phases and were purchased from Altmann Analytik GmbH & Co. KG, Germany. Cyprodinil, mepanipyrim, isoproturon, pyrimethanil, carbamazepine and chlortoluron were used as model compounds in this work and were purchased in analytical standard quality from Sigma-Aldrich Chemie GmbH, Germany.

7.3 Results and Discussion

7.3.1 Comparison of the Mobile Phase Systems

For comparison of ACN and EtOH as organic mobile phase, a model mixture of 6 substances was chosen. The 2D plots (IMS drift time versus HPLC retention time) of the gradient separations without enrichment are shown in Figure 7-2. Dimers are detected for chlortoluron (1) and isoproturon (2), and even trimers can be observed here (not marked in Figure 7-2). The chromatographic separation of the model substances remains identical, regardless of whether ACN or EtOH is used as organic modifier. When using ACN, fewer solvent peaks occur. However, the ionization of carbamazepine (6) is completely suppressed. Furthermore, the peak intensities especially for chlortoluron (1), isoproturon (2), pyrimethanil (3) and carbamazepine (6) are significantly increased when EtOH is used as the organic mobile phase. This is due to the influence of the solvent on the effectiveness of the electrospray ionization. It is well known that MeOH favours more efficient ionization in the

positive mode when compared to ACN [36]. Because EtOH has similar physico-chemical properties as MeOH, a similar improvement in ionization can be assumed here.

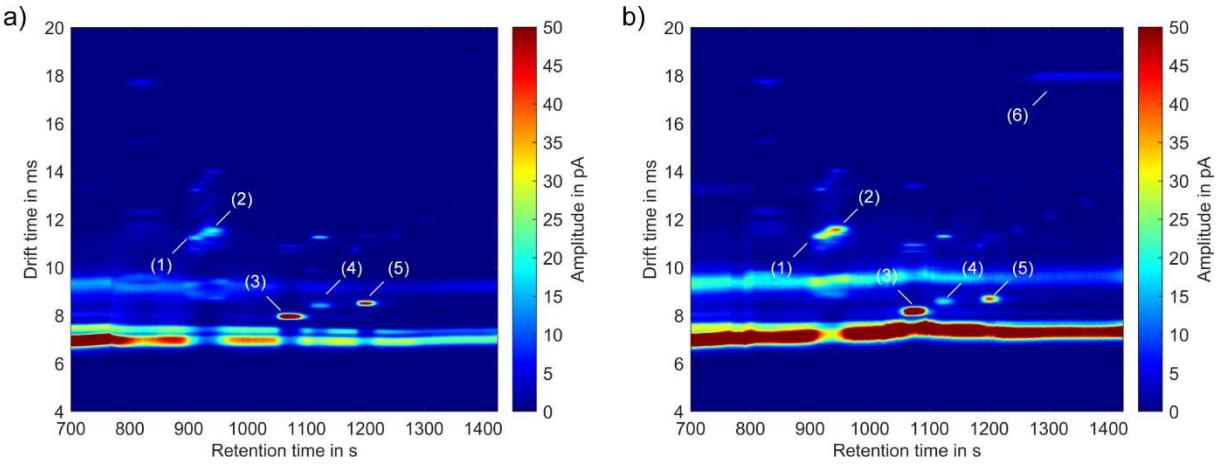

Figure 7-2: 2D plot (IMS drift time versus HPLC retention time) of a gradient separation using a YMC-Triart C18 column 50 x 0.3 mm without enrichment of the model mixture with 5 mg/L chlortoluron (1), isoproturon (2), pyrimethanil (3), mepanipyrim (4), cyprodinil (5) and carbamazepine (6) with a) A: water and B: acetonitrile and b) A: water and B: ethanol as mobile phase at a flow rate of 600 nL/min. The gradient used for each organic mobile phase is: 0–50% B in 2 s; 50–90% B in 619 s, 236 s hold 90% B, 90–50% B in 26 s and 559 s hold 50% B.

The same effects are also visible in Figure 7-3 by comparing the use of MeOH and EtOH as organic components in the solvent mixture. Here, the analysis is performed directly without pre-separation and without enrichment by using only the ESI-IMS with a syringe pump. Isoproturon with a concentration of 500 µg/L is used as the analyte in both cases. Previous studies show that in negative mode, ACN can improve ionization efficiency when compared to MeOH [37]. However, Asbury and Hill have shown that EtOH provides better signal intensity for adenosine-5-monophosphates than ACN and MeOH in negative mode [38]. Hence, EtOH is highly suitable for use as a solvent in ESI-IMS.

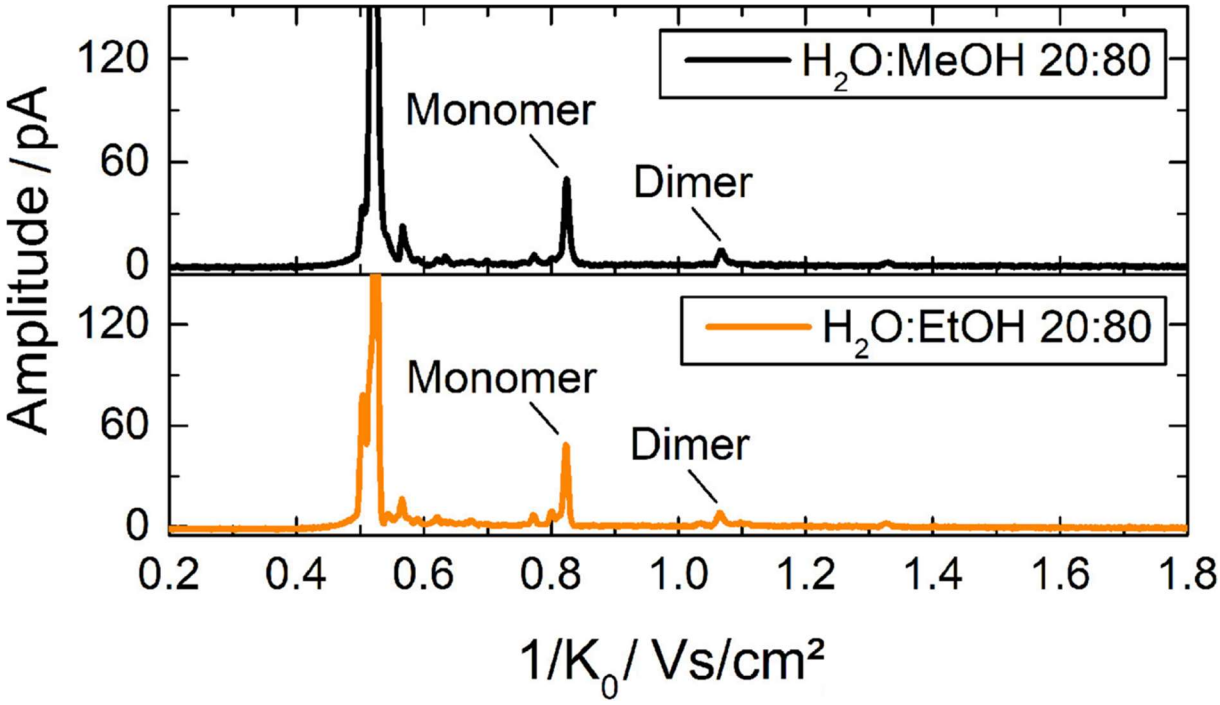

Figure 7-3: IMS spectrum of 500 µg/L isoproturon without pre-separation and without enrichment using methanol (black) and ethanol (orange) as organic solvent component, each at 80%, with a flow rate of 1000 nL/min.

Another significant difference in the operation of the nano-HPLC-ESI-IMS system is the higher pressure across the column if EtOH is used instead of ACN. The maximum pressure is 35 bar for EtOH compared to only 20 bar for ACN. Despite the higher overall pressure, the use of EtOH as an organic mobile phase appears to be practicable.

7.3.2 Enrichment Experiments

In order to further improve the sensitivity, sample enrichment is advisable. However, direct enrichment from surface waters on the analytical column is not desirable. The reason is that suspended particles can lead to clogging and thus total failure of the system. By replacing the analytical separation column by the SPE cartridge, this problem can be circumvented. In addition, by exchanging the cartridge after each sample, the washing process can be eliminated and carryover effects can be prevented. Nevertheless, it is necessary to have enough phase material available to enrich larger volumes and thus further increase the sensitivity of the entire system. To maximize the peak capacity, the particle diameter (d_p) was reduced by a factor of 1.58. Considering that the back pressure is inversely proportional to the square of d_p, the length (L) of the separation column, which is proportional to the back pressure, was reduced by a factor of 5. Thus, the d_p/L is reduced by a factor of 2. This also means that a loss in

chromatographic resolution is accepted in favor of a shorter analysis time and a reduction of the back pressure.

Therefore, in a next step, the online enrichment on the separation cartridge is considered. Here, a single injection and a sixfold stacked injection of a mixture of the herbicides isoproturon and cyprodinil are investigated. The flow rate was increased to 1800 nL/min and the total time of the method was reduced to 530 s. In this case, the system pressure increases to the maximum value of 38 bar with higher flow rate and the use of the SPE-cartridge. The comparison of the 2D plots with a) single injection and b) sixfold stacked injection is shown in Figure 7-4. The two substances can be separated and the chromatographic resolution for the monomers are $R_{s,\,HPLC} = 1.7$ for single injection and $R_{s,\,HPLC} = 1.3$ for sixfold stacked injection. In addition, the peaks in the ion mobility dimension in both cases exhibit a resolution of $R_{s,\,IMS} = 1.9$.

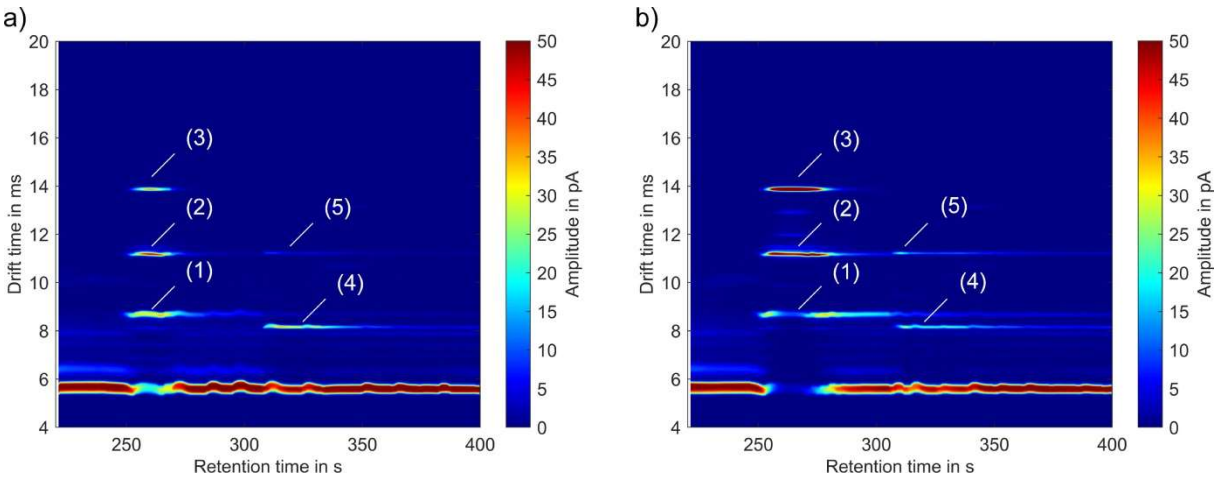

Figure 7-4: 2D plot (IMS drift time versus HPLC retention time) of a gradient separation using the separation cartridge and a concentration of 5 mg/L isoproturon and cyprodinil with a) one injection equivalent to 200 nL and b) with enrichment due to six stacked injections on the cartridge equivalent to 1200 nL with A: water and B: ethanol as mobile phase at a flow rate of 1800 nL/min. In the IMS, the isoproturon forms a monomer peak (1), a dimer peak (2), as well as a trimer peak (3), and the cyprodinil forms a monomer peak (4) and a dimer peak (5). After injection, the separation of the two herbicides is carried out on the same cartridge with the following gradient: 0–10% B in 1 s, 60 s hold 10%B, 10–50% B in 60 s, 50–90% B in 199 s, 60 s hold 90% B, 90–10% in 90 s and 60 s hold 10% B.

Furthermore, the influence of online enrichment is clearly visible, as increased multimers of the compounds are seen after enrichment. This is exemplified in Figure 7-5, looking at an ion mobility spectrum at a retention time of 225 s. With the sixfold injection, the trimer peak (3) increases threefold compared to the single injection. In this case, the monomer peak (1) decreases by the same factor.

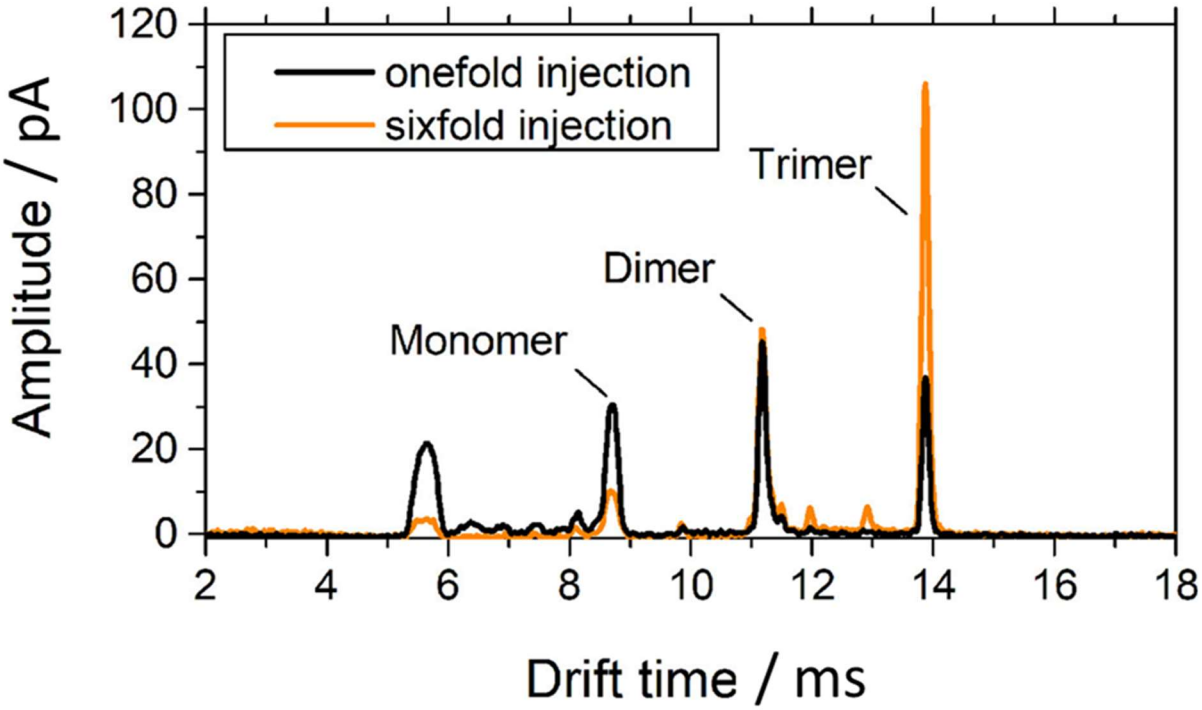

Figure 7-5: Ion mobility spectrum of the isoproturon peaks at a retention time of 225 s with single injection (black) with a corresponding on-column mass of 1 ng and sixfold stack injection with a corresponding mass loading of 6 ng on the separation cartridge (orange).

After these experiments, the model mixture of the 6 substances with a concentration of 50 µg/L was analyzed. The same gradient as described above is applied and a single injection, fivefold stacked injection and tenfold stacked injection are used and compared. As expected, the individual peak heights of the substances increase with the number of stacked injections, as can be seen in Figure 7-6. At the retention time of 200 s, an artefact can be seen that might be explained either by column bleeding or by the formation of highly charged solvent droplets, clusters, or a combination of both [39].

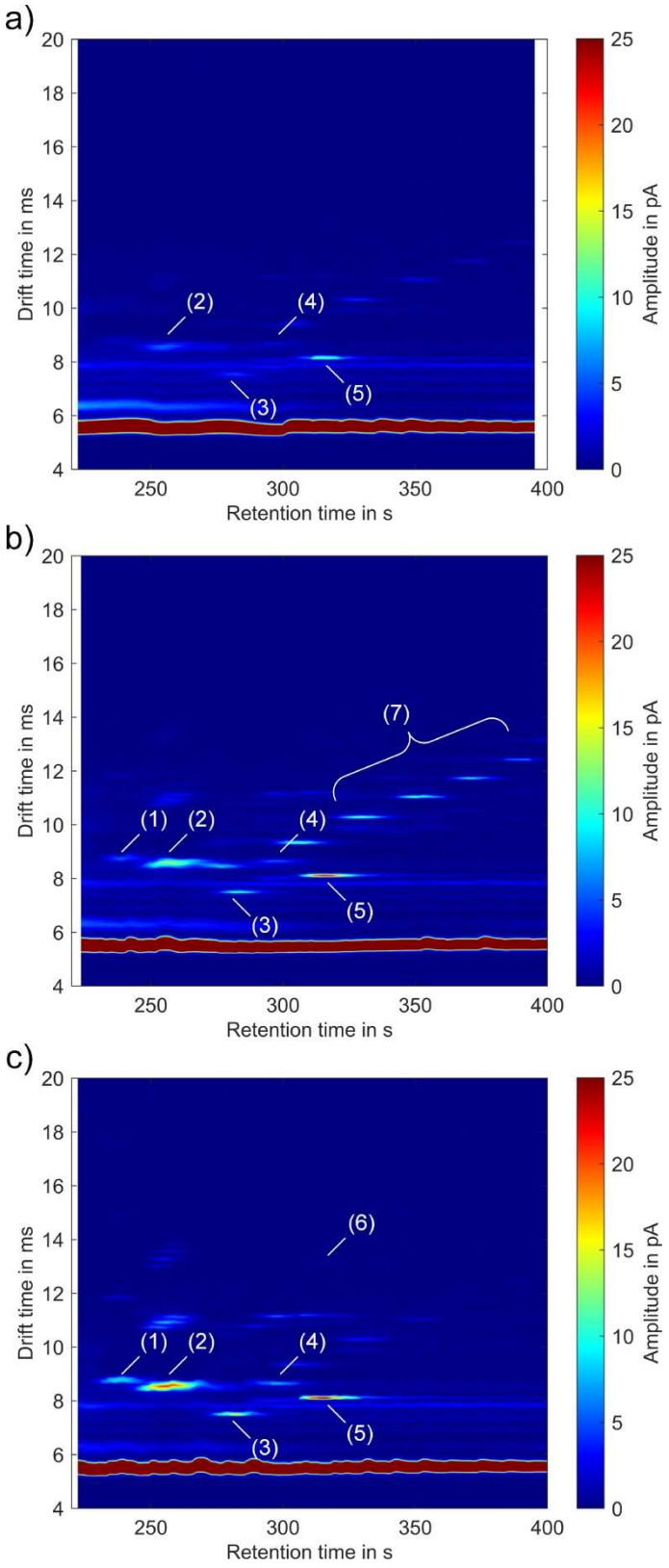

Figure 7-6: 2D plot (IMS drift time versus HPLC retention time) of a gradient separation using separation cartridge 10 x 0.3 mm of model mixture containing a concentration of 50 µg/L for each compound of chlortoluron (1), isoproturon (2), pyrimethanil (3), mepanipyrim (4), cyprodinil (5) and carbamazepine (6) with a) single injection, b) five stacked injections and c) with ten stacked injections on the cartridge with ethanol as organic mobile phase at a flow rate of 1800 nL/min.

The equidistant peaks (7) across the diagonal line, which can be clearly seen in Figure 7-6 b) for the fivefold injection, are most likely caused by the oligomer Triton [37]. Analogously, such matrix ions are also detected when using ESI-MS [40]. However, during the measurements, cartridge bleeding was observed after multiple injections. This can be attributed to the pressure spikes and the resulting shearing stress on the phase material caused by the stacked injection.

Similar to the initial separation when using the YMC-Triart C18 analytical column, a satisfactory separation is obtained on the cartridge. The adjacent peaks (1) and (2) have a resolution of $R_{s,\,HPLC} = 0.7$ in the chromatographic dimension and an $R_{s,\,IMS} = 1.0$ in the ion mobility dimension for tenfold stacked injection. For peaks (4) and (5), a resolution of $R_{s,\,HPLC} = 0.7$ and $R_{s,\,IMS} = 2.6$ can be determined in the chromatographic and ion mobility dimension, respectively.

To calculate the effective 2D peak capacities (${}^{2\mathrm{D}}n_{\mathrm{eff}}$) and orthogonality ($O$) of nano-HPLC and IMS separation, the vector-based approach of Dück et al. [41] was used. Table 7-2 shows the results for the tenfold injection. For comparison, a chip electrochromatography (ChEC)-IMS method by Hartner et al. [19] and an HPLC-IMS measurement by Zühlke et al. [23] are also listed. The calculation of the effective 2D peak capacity was performed once only considering the monomers. An orthogonality of $O = 0.53$ and an effective 2D peak capacity of ${}^{2\mathrm{D}}n_{\mathrm{eff}} = 174$ are achieved. In addition, the multimers are included in another calculation for the multimers from isoproturon. Due to the lower ion mobility of the trimers and the resulting larger drift time, a much larger orthogonality of $O = 0.77$ is achieved. This leads to a higher effective peak capacity of ${}^{2\mathrm{D}}n_{\mathrm{eff}} = 324$. However, individual substances occupy several peak sites here, which of course reduces the theoretical maximum number of separable compounds.

Since not all substances form dimers or trimers to the same extent, an estimate of the reduction is hardly possible. However, if we assume that all substances form dimers, the theoretical maximum number of separable compounds is reduced by half and thus returns to the range of the peak capacity when just observing monomers. The orthogonality obtained and the reduction in the theoretical maximum number of separable compounds due to multimers thus largely balance each other out in a rough approximation. Moreover, an increase in the number of peaks further complicates the interpretation of the measurement results. A possible solution to this problem is the use of a database, which is currently subject of research [42, 43] and makes it easier to assign the peaks to the corresponding substances. Ideally, the data should be generated for use on a comparable system, since ion mobility depends on many influencing factors.

Table 7-2: Effective 2D peak capacities and orthogonality.

	nano-HPLC-IMS	nano-HPLC-IMS	ChEC-IMS [19]	HPLC-IMS [23]
Number of compounds	6	6 (incl. multimers)	5	24
2D sep. time	199 s	199 s	100 s	20 min
Orthogonality (O)	0.53	0.77	0.50	0.56
effective 2D peak capacities ($^{2D}n_{eff}$)	174	324*	198	240

*theoretical value, the multimers reduce this value according to the occurrence frequency of the multimers.

Overall, the 2D separation based on liquid chromatography and ion mobility offers a good approach to separating complex mixtures. Not all components have to be baseline separated in one dimension, as the two separation dimensions are orthogonal.

7.3.3 Greenness Assessment of the System

Within the framework of this publication, the current status of the described system was compared to the intended field demonstrator by use of the AGREE tool. Wojnowski has made the open-source software program available on his site that can be used free of charge [44]. AGREEprep, a variation of this evaluation method specifically for sample preparation was recently published [45].

The results of the case studies with the AGREE tool are shown in Figure 7-7 and the corresponding input for creation of the pictogram is listed in Table 7-3. Equal weights have been chosen for the 12 principles (p). As described, the concept of the presented system is based on direct enrichment from surface waters on a separation cartridge. This is followed by a two-dimensional separation consisting of chromatographic and ion mobility separation. Currently the system is a laboratory setup and the sample treatment is done by off-line analysis (p 1). A maximum of up to 100 µL of surface water can be enriched on the cartridge (p 2). The analysis is currently done off-line (p 3). Only a filtration of the sample is needed to eliminate suspended particles (p 4). The entire system is miniaturized, the individual components are not yet connected via software and are therefore only partially automated (p 5). Derivatization of the analytes is not necessary (p 6). The resulting waste consists only of the enriched sample volume as well as the total volume of water and EtOH for the analytical run. In total, this amounts to 112 µL for a single analysis (p 7). In the measurements, six components could be separated in a total runtime of 400 s (p 8). The power consumption of all components was determined

individually, the total consumption per sample was 0.04 kWh (p 9). All solvents used were obtained from conventional sources (p 10). Due to the use of EtOH, the mobile phase contains no toxic solvent (p 11). Nevertheless, EtOH is considered highly flammable (p 12). Based on this evaluation, the analytical procedure achieves a value of 0.73, where 1.00 corresponds to the ideal green system.

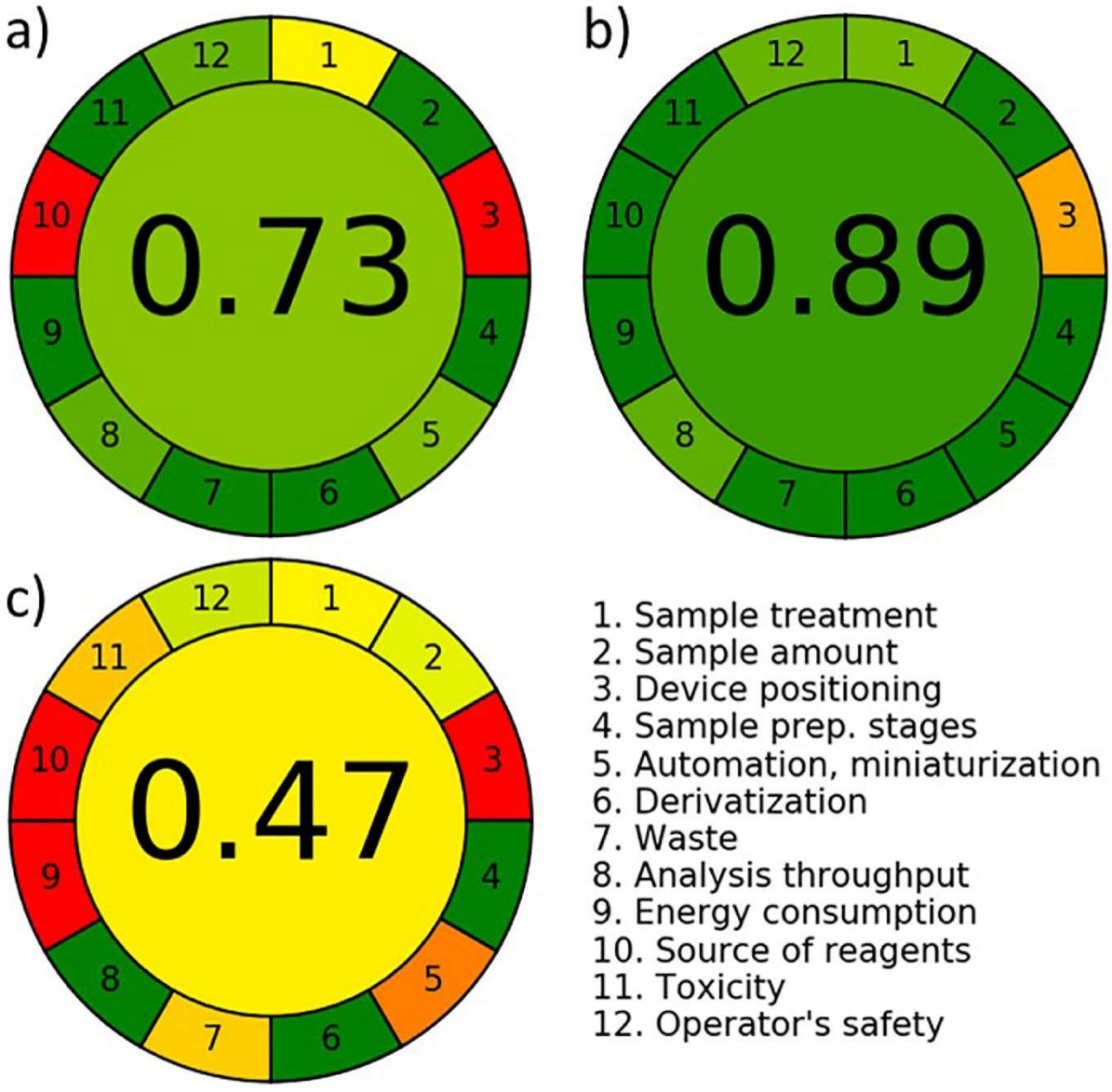

Figure 7-7: Results of the AGREE assessment for a) the current system, b) the intended system after optimization, and c) a comparable conventional method (classic laboratory analysis). The lower right corner shows the legend of the 12 criteria.

The simple evaluation of the system in the development process allows an identification of targeted optimizations in the context of the green chemistry approach. Especially the sample treatment, the device positioning and the source of reagents can be further optimized. By

integrating the nano-UHPLC, the loading pump, the cartridge changer and the ESI-IMS into one software, the system can be fully automated (p 5). The enclosure of the components and the operation of the entire system with rechargeable batteries will make the system mobile and enable sample treatment and device positioning on-line (p 1 and p 3). Furthermore, EtOH can be derived from renewable resources (p 10). However, bio EtOH is currently not processed to the extent that it would reach the desired HPLC grade purity. Based on these changes, the final value can be improved to 0.92.

In order to enable a better assessment of the results, the presented concept was compared to a classical laboratory protocol for the determination of 17 analytes in surface waters. Here, the clear influence of miniaturization on the evaluation of the entire concept can be seen. It is obvious that above all the increased amount of waste (factor 76), the use of the toxic ACN and the significantly higher energy consumption of a laboratory scale LC-MS system have a negative effect on the overall score. For the classic laboratory analysis, a score of only 0.47 is achieved.

Table 7-3: Selected variables and the resulting scores for the description of the current system, intended system and a comparable conventional method in the AGREE software. Grayed out are the intended changes of the system.

Principle	State of the current system		Intended system after optimization		Compareable classical approach	
	Variable	Score	Variable	Score	Variable	Score
1 sample treatment	off-line analysis	0.48	infield and online	0.78	off-line analysis	0.48
2 sample amount	100 µL	0.98	100 µL	0.98	2 mL	0.55
3 device positioning	off-line	0.00	on-line	0.66	off-line	0.00
4 sample prep. stages	3 or fewer	1.00	3 or fewer	1.00	3 or fewer	1.00
5 degree of automation sample preperation	semi automatic none or miniaturized	0.75	automatic none or miniaturized	1.00	semi automatic not miniaturized	0.25
6 derivatization	none	1.00	none	1.00	none	1.00
7 waste volume	112 µL	0.99	112 µL	0.99	8.5 mL	0.41
8 number of analytes sample throughput	6 6	0.82	6 6	0.82	17 5	1.00
9 energy consumption	0.04 kWh	1.00	0.04 kWh	1.00	LC-MS	0.00
10 source of reagents	none of the reagents are bio based	0.00	all of the reagents are bio based	1.00	none of the reagents are bio based	0.00
11 toxicity	no	1.00	no	1.00	yes; 2.4 mL	0.39
12 operator´s safty	highly flameable	0.80	highly flameable	0.80	highly flameble; corrosive	0.60

7.4 Conclusion

The novelty of the present work lies in the coupling of a nano-HPLC with an ESI-IMS. Herewith, a splitless setup can be achieved. An orthogonality of $O = 0.53$ and an effective 2D peak capacity of ${}^{2D}n_{\mathrm{eff}} = 174$ have been achieved. Due to the overall miniaturization, solvent consumption for operation can be significantly reduced compared to conventional methods. In addition, due to the compact design and the use of ion mobility spectrometry, the required energy demand is significantly reduced compared to a conventional LC-MS method. For example, no vacuum pumps are required for the operation of an IMS. Also, the use of ethanol as an organic mobile phase was investigated. It could be shown that ethanol can be used as

organic solvent for the mobile phase. In addition, it exhibits better ionization than ACN for the selected model analytes. Thus, it could be shown that this work can serve as a basis to develop a device as an on-site alarm unit, which can be used for example in case of accidents or disasters, in order to provide a fast and flexible response.

The AGREE tool is very well suited to evaluate new analytical protocols, to identify weaknesses already in the development step and to enable the comparison with existing methods. It is much more quantitative than the very simple HPLC-EAT tool and less complex than the GAPI method, making it an effective tool for a comprehensive qualitative benchmarking and the creation of green metrics.

7.5 Supplementary Information

7.5.1 Description of the Cartridge Changer

Figure 7-8 shows pictures of the printed and implemented cartridge changer. The magazine (1.) is used to store the cartridges. The process of changing is accomplished solely by the back-and-forth movement of the cartridge carrier (2.). In the closed position, the cartridge is firmly clamped between the changer body (3.) and the carrier (2.). The holder can be moved back by turning the threaded rods. The gears (4.) ensure an even distribution of force and prevent wedging. The cartridge is carried along via the clips (6.) and is ejected via the outlet (6.). This process allows a cartridge to be fed from the magazine to the changer body. By moving the holder forward, it is clamped again.

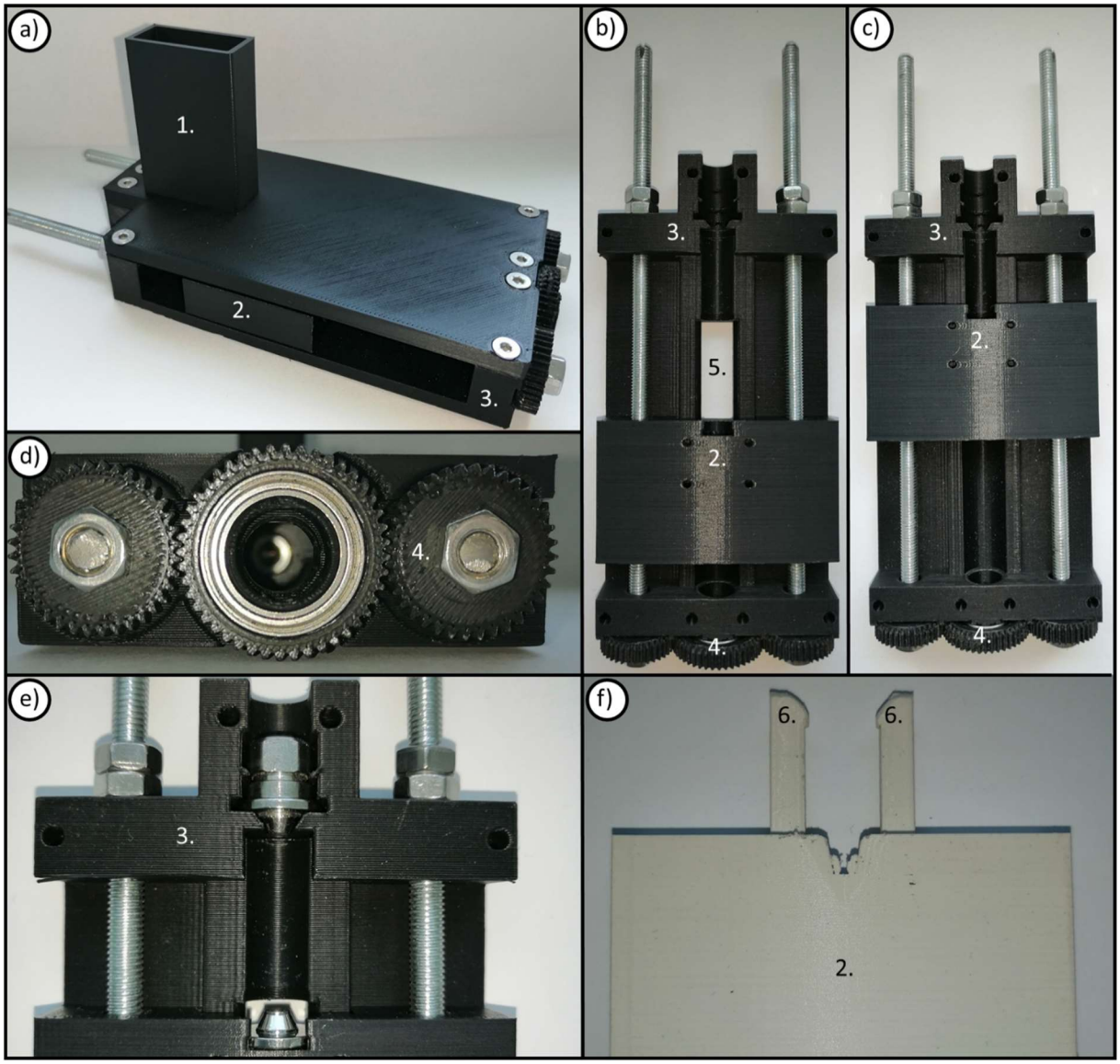

Figure 7-8: Pictures of the cartridge changer. a) View of the assembled changer. b) Changer without cover in open position. c) Changer without cover in closed position. d) Side view of the gears. e) Changer with Inserted HPLC connectors. f) Alternative cartridge carrier with clips. 1. Magazine and cover; 2. Cartridge carrier; 3. Changer body 4. Gears 5. Cartridge ejection; 6. Clips.

7.5.2 Directory of STEP and STL Files and Further Information

The files required for printing of the cartridge changer are provided as part of the supplementary and are accessible through doi.org/10.1016/j.greeac.2022.100011 under a Creative Commons license. In the provided formats, the files can be adapted to the reader's needs. The provided zip file contains the files for the gears, the changer body, the clips, the cartridge carrier, and the magazine.

To complete the assembly, two M5 threaded rods of approx. 15 cm, 6 M5 nuts, a stainless-steel ball bearing SS 6701 12 x 18 x 4 mm and two miniature thrust ball bearings F5-10M

5 x 10 x 4 mm are needed. The thrust ball bearings are placed in the recesses of the cartridge body marked in red in Figure 7-9.

Before manufacturing the cartridge changer, it is important to consider the environment in which the changer will be used to identify the appropriate material. For example, the polylactic acid (PLA) used in this work has excellent stiffness and mechanical strength, making it well suited for prototypes for the laboratory assembly. However, PLA is unsuitable for field use due to its deformability at temperatures over 50 °C and possible swelling and degradation when exposed to water or high humidity. Polyether ether ketone (PEEK) would be suitable for use in the field, because it has exceptionally good chemical resistance and good mechanical properties. However, processing by 3D printing is challenging. Acrylonitrile butadiene styrene (ABS), while less mechanical resilient than PLA, has better resistance to moisture and can also be processed with standard printers.

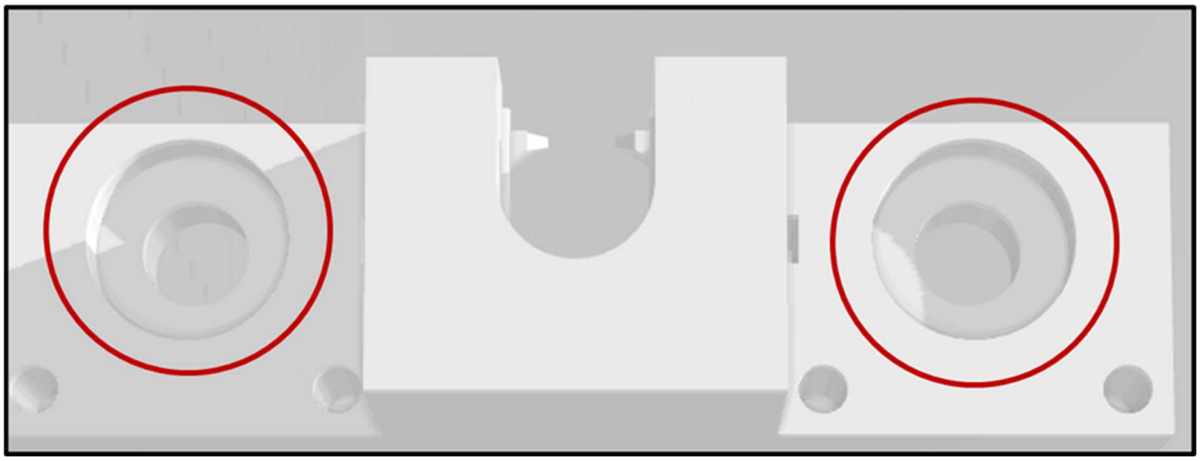

Figure 7-9: Section of the cartridge body from the STL file. Red markings show the positions for the thrust ball bearings.

7.6 References

[1] Registration, Evaluation, Authorisation and Restriction of Chemicals (REACH), n.d.

[2] Toxic Substances Control Act 1976 (TSCA), n.d.

[3] Insecticide, Fungicide, and Rodenticide Act (FIFRA), n.d.

[4] Existing Notified Chemical Substances (ENCS), n.d.

[5] M.A. Stravs, C. Stamm, C. Ort, H. Singer, Transportable Automated HRMS Platform "MS2field" Enables Insights into Water-Quality Dynamics in Real Time, Environ. Sci. Technol. Lett. 8 (2021) 373–380. https://doi.org/10.1021/acs.estlett.1c00066.

[6] M.N. Torres, N.B. Valdes, J.R. Almirall, Comparison of portable and benchtop GC–MS coupled to capillary microextraction of volatiles (CMV) for the extraction and analysis of ignitable liquid residues, Forensic Chem. 19 (2020) 100240. https://doi.org/10.1016/j.forc.2020.100240.

[7] P.E. Leary, B.W. Kammrath, J.A. Reffner, Portable Gas Chromatography–Mass Spectrometry: Instrumentation and Applications, Portable Spectrosc. Spectrom. (2021) 367–389. https://doi.org/https://doi.org/10.1002/9781119636489.ch15.

[8] S. Chatzimichail, F. Rahimi, A. Saifuddin, A.J. Surman, S.D. Taylor-Robinson, A. Salehi-Reyhani, Hand-portable HPLC with broadband spectral detection enables analysis of complex polycyclic aromatic hydrocarbon mixtures, Commun. Chem. 4 (2021). https://doi.org/10.1038/s42004-021-00457-7.

[9] S. Sharma, A. Plistil, H.E. Barnett, H.D. Tolley, P.B. Farnsworth, S.D. Stearns, M.L. Lee, Hand-Portable Gradient Capillary Liquid Chromatography Pumping System, Anal. Chem. 87 (2015) 10457–10461. https://doi.org/10.1021/acs.analchem.5b02583.

[10] Y. Li, M. Dvořák, P.N. Nesterenko, R. Stanley, N. Nuchtavorn, L.K. Krčmová, J. Aufartová, M. Macka, Miniaturised medium pressure capillary liquid chromatography system with flexible open platform design using off-the-shelf microfluidic components, Anal. Chim. Acta. 896 (2015) 166–176. https://doi.org/https://doi.org/10.1016/j.aca.2015.09.015.

[11] X. Zhao, X. Xie, S. Sharma, L.T. Tolley, A. Plistil, H.E. Barnett, M.P. Brisbin, A.C. Swensen, J.C. Price, P.B. Farnsworth, H.D. Tolley, S.D. Stearns, M.L. Lee, Compact Ultrahigh-Pressure Nanoflow Capillary Liquid Chromatograph, Anal. Chem. 89 (2017) 807–812. https://doi.org/10.1021/acs.analchem.6b03575.

[12] D.T. Snyder, C.J. Pulliam, Z. Ouyang, R.G. Cooks, Miniature and Fieldable Mass Spectrometers: Recent Advances, Anal. Chem. 88 (2016) 2–29. https://doi.org/10.1021/acs.analchem.5b03070.

[13] A.P. Snyder, C.S. Harden, A.H. Brittain, M.G. Kim, N.S. Arnold, H.L.C. Meuzelaar, Portable hand-held gas chromatography/ion mobility spectrometry device, Anal. Chem. 65 (1993) 299–306. https://doi.org/10.1021/ac00051a019.

[14] R.B. Turner, J.L. Brokenshire, Hand-held ion mobility spectrometers, TrAC Trends Anal. Chem. 13 (1994) 275–280. https://doi.org/https://doi.org/10.1016/0165-9936(94)87064-0.

[15] A. Ahrens, S. Zimmermann, Towards a hand-held, fast, and sensitive gas chromatograph-ion mobility spectrometer for detecting volatile compounds, Anal. Bioanal. Chem. 413 (2021) 1009–1016. https://doi.org/10.1007/s00216-020-03059-9.

[16] R.G. Ewing, D.A. Atkinson, G.A. Eiceman, G.J. Ewing, A critical review of ion mobility spectrometry for the detection of explosives and explosive related compounds, Talanta. 54 (2001) 515–529. https://doi.org/https://doi.org/10.1016/S0039-9140(00)00565-8.

[17] M.A. Mäkinen, O.A. Anttalainen, M.E.T. Sillanpää, Ion Mobility Spectrometry and Its Applications in Detection of Chemical Warfare Agents, Anal. Chem. 82 (2010) 9594–9600. https://doi.org/10.1021/ac100931n.

[18] M. Zarejousheghani, S. Schrader, M. Möder, T. Mayer, H. Borsdorf, Negative electrospray ionization ion mobility spectrometry combined with paper-based molecular imprinted polymer disks: A novel approach for rapid target screening of trace organic compounds in water samples, Talanta. 190 (2018) 47–54. https://doi.org/https://doi.org/10.1016/j.talanta.2018.07.076.

[19] N.T. Hartner, C.-R. Raddatz, C. Thoben, S.K. Piendl, S. Zimmermann, D. Belder, On-Line Coupling of Chip-Electrochromatography and Ion Mobility Spectrometry, Anal. Chem. 92 (2020) 15129–15136. https://doi.org/10.1021/acs.analchem.0c03446.

[20] T.J. Causon, S. Hann, Theoretical evaluation of peak capacity improvements by use of liquid chromatography combined with drift tube ion mobility-mass spectrometry, J. Chromatogr. A. 1416 (2015) 47–56. https://doi.org/10.1016/j.chroma.2015.09.009.

[21] Z. Wang, D. Kang, X. Jia, H. Zhang, J. Guo, C. Liu, Q. Meng, W. Liu, Analysis of alkaloids from Peganum harmala L. sequential extracts by liquid chromatography coupled to ion mobility spectrometry, J. Chromatogr. B. 1096 (2018) 73–79. https://doi.org/https://doi.org/10.1016/j.jchromb.2018.08.021.

[22] Y. Lu, X. Wu, L. Yuan, Y. Li, P. Wang, J. Yu, P. Tian, W. Liu, A rapid liquid chromatography-electrospray ionization-ion mobility spectrometry method for monitoring nine representative metabolites in the seedlings of cucumber and wheat, J. Sep. Sci. 44 (2021) 709–716. https://doi.org/10.1002/jssc.202000811.

[23] M. Zühlke, D. Riebe, T. Beitz, H.G. Löhmannsröben, S. Andreotti, K. Reinert, K. Zenichowski, M. Diener, High-performance liquid chromatography with electrospray ionization ion mobility spectrometry: Characterization, data management, and applications, J. Sep. Sci. 39 (2016) 4756–4764. https://doi.org/10.1002/jssc.201600749.

[24] S.K. Piendl, C.R. Raddatz, N.T. Hartner, C. Thoben, R. Warias, S. Zimmermann, D. Belder, 2D in Seconds: Coupling of Chip-HPLC with Ion Mobility Spectrometry, Anal. Chem. 91 (2019) 7613–7620. https://doi.org/10.1021/acs.analchem.9b00302.

[25] T. Werres, T.C. Schmidt, T. Teutenberg, The influence of injection volume on efficiency of microbore liquid chromatography columns for gradient and isocratic elution, J. Chromatogr. A. 1641 (2021) 461965. https://doi.org/10.1016/j.chroma.2021.461965.

[26] P.I. Napolitano-Tabares, I. Negrín-Santamaría, A. Gutiérrez-Serpa, V. Pino, Recent efforts to increase greenness in chromatography, Curr. Opin. Green Sustain. Chem. 32 (2021) 100536. https://doi.org/10.1016/j.cogsc.2021.100536.

[27] Y. Gaber, U. Törnvall, M.A. Kumar, M. Ali Amin, R. Hatti-Kaul, HPLC-EAT (Environmental Assessment Tool): A tool for profiling safety, health and environmental impacts of liquid chromatography methods, Green Chem. 13 (2011) 2021–2025. https://doi.org/10.1039/C0GC00667J.

[28] J. Płotka-Wasylka, A new tool for the evaluation of the analytical procedure: Green Analytical Procedure Index, Talanta. 181 (2018) 204–209. https://doi.org/10.1016/j.talanta.2018.01.013.

[29] F. Pena-Pereira, W. Wojnowski, M. Tobiszewski, AGREE - Analytical GREEnness Metric Approach and Software, Anal. Chem. 92 (2020) 10076–10082. https://doi.org/10.1021/acs.analchem.0c01887.

[30] C. Thoben, C.R. Raddatz, M. Lippmann, Z. Salehimoghaddam, S. Zimmermann, Electrospray ionization ion mobility spectrometer with new tristate ion gating for improved sensitivity for compounds with lower ion mobility, Talanta. 233 (2021) 122579. https://doi.org/10.1016/j.talanta.2021.122579.

[31] M. Lippmann, A.T. Kirk, M. Hitzemann, S. Zimmermann, IMS Instrumentation I: Isolated data acquisition for ion mobility spectrometers with grounded ion sources, Int. J. Ion Mobil. Spectrom. 23 (2020) 69–74. https://doi.org/10.1007/s12127-020-00260-5.

[32] F. Schlottmann, A.T. Kirk, M. Allers, A. Bohnhorst, S. Zimmermann, High Kinetic Energy Ion Mobility Spectrometry (HiKE-IMS) at 40 mbar, J. Am. Soc. Mass Spectrom. 31 (2020) 1536–1543. https://doi.org/10.1021/jasms.0c00098.

[33] A.T. Kirk, D. Grube, T. Kobelt, C. Wendt, S. Zimmermann, High-Resolution High Kinetic Energy Ion Mobility Spectrometer Based on a Low-Discrimination Tristate Ion Shutter, Anal. Chem. 90 (2018) 5603–5611. https://doi.org/10.1021/acs.analchem.7b04586.

[34] P. Kwantwi-Barima, T. Reinecke, B.H. Clowers, Increased ion throughput using tristate ion-gate multiplexing, Analyst. 144 (2019) 6660–6670. https://doi.org/10.1039/c9an01585j.

[35] C. Chen, M. Tabrizchi, H. Li, Ion gating in ion mobility spectrometry: Principles and advances, TrAC Trends Anal. Chem. 133 (2020) 116100. https://doi.org/https://doi.org/10.1016/j.trac.2020.116100.

[36] M. Jemal, D.J. Hawthorne, Effect of high performance liquid chromatography mobile phase (methanol versus acetonitrile) on the positive and negative ion electrospray response of a compound that contains both an unsaturated lactone and a methyl sulfone group, Rapid Commun. Mass Spectrom. 13 (1999) 61–66. https://doi.org/https://doi.org/10.1002/(SICI)1097-0231(19990115)13:1<61::AID-RCM451>3.0.CO;2-2.

[37] T. Reinecke, A.T. Kirk, A. Ahrens, C.-R. Raddatz, C. Thoben, S. Zimmermann, A compact high resolution electrospray ionization ion mobility spectrometer, Talanta. 150 (2016) 1–6. https://doi.org/https://doi.org/10.1016/j.talanta.2015.12.006.

[38] G.R. Asbury, H.H. Hill, Negative Ion Electrospray Ionization Ion Mobility Spectrometry, Int. J. Ion Mobil. Spectrom. 2 (1999) 1–8. https://doi.org/10.1021/ac00086a021.

[39] C. Markert, M. Thinius, L. Lehmann, C. Heintz, F. Stappert, W. Wissdorf, H. Kersten, T. Benter, B.B. Schneider, T.R. Covey, Observation of charged droplets from electrospray ionization (ESI) plumes in API mass spectrometers, Anal. Bioanal. Chem. 413 (2021) 5587–5600. https://doi.org/10.1007/s00216-021-03452-y.

[40] B.O. Keller, J. Sui, A.B. Young, R.M. Whittal, Interferences and contaminants encountered in modern mass spectrometry, Anal. Chim. Acta. 627 (2008) 71–81. https://doi.org/https://doi.org/10.1016/j.aca.2008.04.043.

[41] R. Dück, H. Sonderfeld, O.J. Schmitz, A simple method for the determination of peak distribution in comprehensive two-dimensional liquid chromatography, J. Chromatogr. A. 1246 (2012) 69–75. https://doi.org/10.1016/j.chroma.2012.02.038.

[42] X. Zheng, N.A. Aly, Y. Zhou, K.T. Dupuis, A. Bilbao, V.L. Paurus, D.J. Orton, R. Wilson, S.H. Payne, R.D. Smith, E.S. Baker, A structural examination and collision cross section database for over 500 metabolites and xenobiotics using drift tube ion mobility spectrometry, Chem. Sci. 8 (2017) 7724–7736. https://doi.org/10.1039/c7sc03464d.

[43] S. Stephan, J. Hippler, T. Köhler, A.A. Deeb, T.C. Schmidt, O.J. Schmitz, Contaminant screening of wastewater with HPLC-IM-qTOF-MS and LC+LC-IM-qTOF-MS using a CCS database, Anal. Bioanal. Chem. 408 (2016) 6545–6555. https://doi.org/10.1007/s00216-016-9820-5.

[44] dr inż. W. Wojnowski, mostwiedzy.pl/AGREE, (n.d.).

[45] W. Wojnowski, M. Tobiszewski, F. Pena-Pereira, E. Psillakis, AGREEprep – Analytical greenness metric for sample preparation, TrAC Trends Anal. Chem. 149 (2022) 116553. https://doi.org/https://doi.org/10.1016/j.trac.2022.116553.

Chapter 8 General Conclusions and Outlook

8.1 General Conclusions

The doctoral thesis was composed of a research and a development part. In the former part, the influence of the pre- and post-column volume as well as the influence of the column ID in relation to the total extra-column volume on the peak broadening was investigated. The later part capitalized on the inherent benefits of miniaturized LC for the development of new stationary phases and used the findings from the first part to develop a new miniaturized portable system. Both parts were united by the ambition to fill gaps in the literature and to use the research results to contribute to an easing of switching to cLC and therefore make the use of this technology attractive to a broader pool of users. Overall, it could be shown that many disadvantages of miniaturized LC can be minimized by simple measures, but it also became evident that for the true utilization of the intrinsic potential of the technological approach, it is inevitable to abandon the classical modular design from the sixties in favor of compact separations systems [1].

Methods normally used to evaluate the performance of LC columns, such as van Deemter analysis and kinetic plot theory, were successfully applied to investigate the influence of extra-column volumes on apparent efficiency [2]. This was done against the background that the study design should be related to real measurement conditions. In contrast to comparable studies, where individual system components are usually investigated in isolation, the most important factors for band broadening could be identified in the studies looking at the total system [3]. For example, it was shown in Chapters 3 and 5 that, contrary to the assumption that the pre-column volume is negligible in gradient elution, it has a significant influence [4]. The optimization of modern HPLC-systems to reduce the post-column volume at the expense of the pre-column volume led to the systems becoming unusable for isocratic operation, and in gradient operation strong band broadening effects for early eluting substances had to be accepted. This effect is due to the modular design of these systems. The detector comparison demonstrated that simple derivations regarding the band broadening based on the extra-column volume are not possible. Although mass spectrometry has become one of the most important detection techniques, it is not commonly used for band broadening studies, where the UV detector still dominates. To counteract this, MS was part of the investigations in Chapter 4 and the main method in Chapter 5. Chapter 4 also showed where the limits of the trend are to reduce the ID of the columns on a conventional scale to take advantage of miniaturized systems, and

again it became clear that this is only possible with compromises that do not have to be made with real miniaturization.

The second part of the work was devoted to development with the focus on the incorporation of the principles of GAC [5]. Chapter 6 demonstrated how a comprehensive characterization and development of new stationary phases based on bead cellulose, which eliminated the need for organic solvents, was successfully carried out based on a few grams of starting material. This clearly demonstrated that even in the field of stationary phase development, the use of miniaturized LC offers a significant advantage since less phase material was required per column and thus an efficient optimization process could be pursued. To complete the thesis, the findings from Chapters 3 - 5 were used in Chapter 7 to develop a miniaturized compact cLC-system for online enrichment and measurements in the field, with the purpose to offer a solution for the analysis of pollutants in surface waters. The system thus joins a series of other portable developments described in the literature which show that with the growing demand for on-site analysis, there is no way around the compact cLC [6–9]. During the engineering of the system, tools were used that enabled an evaluation based on environmental friendliness. Among other things, this resulted in the elimination of the use of toxic organic solvents [10, 11].

The quantification of the effects leading to band broadening was performed on a fully porous RP phase, which naturally raises the question to what extent the results can be transferred to other separation mechanisms or particle morphologies; further studies would be required to assess this. Another limitation was the maximum operable pressure of the cLC systems employed. Since the influences of extra-column band broadening have been extensively studied, the focus in further research could be on the stationary phase. Devices with extended back pressure could be used and the improved heat dissipation of capillary columns could be investigated in ultra-fast separations. Alternatively, the focus could be on increasing the separation speed by shorter columns and higher flow rates or increasing the separation efficiency by reducing the particle diameter. Furthermore, first efficiency studies in combination with MS detection have been performed in this thesis, but these can only be interpreted as a starting point, especially when wide flow rate ranges are investigated, ESI-MS source parameters have a significant influence on the signal intensity and should be investigated in detail. If the pendulum of scientific curiosity swings more in the direction of device development, it is recommended to start this on the basis of compact portable systems and to consider the principles of GAC already in the development process.

Regardless of whether and in what form the proposed research will be conducted in the future, the results described in this thesis hopefully help to increase the acceptance of cLC and thus pave its way as a future technology in terms of a fast, reliable alternative to conventional LC and additionally strengthen the idea of green analytical chemistry.

8.2 Short-Term Vision

As shown at several points throughout this thesis, a trend is emerging that prefers efficiency in the form of compact miniaturized LC systems to the flexibility of modular systems. The lab-on-chip approaches take this idea to the extreme but the disadvantages of such systems have already been explained in chapter 1.5. In order to address the described problems of the LOC-systems, own research work is performed using 3D printing for LOC development. This concept combines the advantages of LOC with the modular design of conventional LC. An exemplary arrangement for the mixing of two or more components, followed by a chromatographic separation and detection can be seen in Figure 8-1.

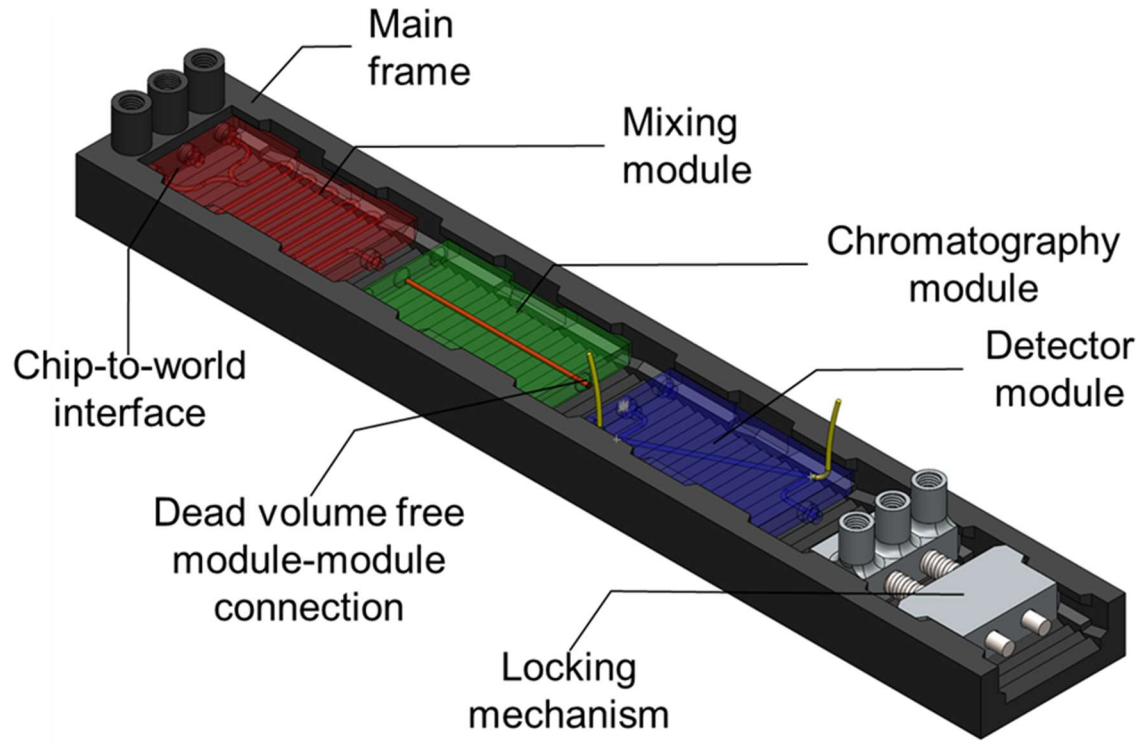

Figure 8-1: Exemplary setup of the proposed LOC system consisting of the main frame and three dedicated LOC modules. Shown in red is a meander module for mixing of two components, shown in green is the chromatography module with orange stationary phase. The detector module is shown in blue. The dedicated chip modules currently have the dimensions of 5 cm x 3 cm x 0.6 cm

The aim of this research is to create dedicated LOC modules that fulfill functions such as the mixing of components, the chromatographic separation of mixtures as well as the detection.

The modules are manufactured in PEEK by means of additive manufacturing using the material extrusion process (MEX). PEEK is mechanically very stable and resistant to most common solvents and therefore ideally suited. The individual modules can be arranged and combined on a main frame without dead volume and are thus significantly more flexible than classic LOC systems. Another advantage of the dedicated modules is that it is no longer difficult to introduce the stationary phase into the chip. If necessary, fundamental adjustments to the microfluidic structure can be made and the new module produced within one day. This considerably reduces the manufacturing time. There are also no limits to customizing the chip to world interface to the user's needs. This makes the proposed system the first truly flexible LOC system that can be used to answer analytical questions in a conventional laboratory environment without the need for complex setups.

8.3 Long-Term Vision

If one reviews all the information in the previous chapters it becomes clear that there is considerable untapped potential in the miniaturization of liquid chromatography systems. This invites philosophizing and is used in conclusion as the basis for the development of an idealized imagined wearable HPLC. Transfer capillaries are a thing of the past, but if connections between individual system components are still necessary, these can be made with the latest generation of OT columns [12, 13]. Also, the analytical separation column consists of such a several meter long coiled OT-column similar in nature to the gas chromatography counterpart [14]. Enrichment and purification of the samples can take place directly in the additively manufactured valves according to the column-in-valve principle [15]. The necessary SPE materials, like the pumps, can be integrated with optimal modification and arrangement by 3D printing [16]. Detection takes place on-column and can be carried out at different positions on the column, according to the requirements of the application [17]. In this way, the measurement time can be optimally adapted to the specific question. With the increasing expansion of the 5G network and the 6G network in the starting blocks, the evaluation and processing of the data can take place completely in the cloud [18]. This would also enable networking of all measuring devices and thus reduce the number of misinterpreted data through AI-supported comparisons of the measurement results and significantly increase the reliability of the data sets comparable to current approaches for automated predictive maintenance [19]. To adhere to the opening sentence of this sub-chapter, if in the future the scientific community succeeds in further developing the described techniques, consistently implementing them and bringing them together, we will be one step closer to developing a µTAS HPLC the size of a watch.

8.4 References

[1] S.W. Foster, X. Xie, J.M. Hellmig, G. Moura-Letts, W.R. West, M.L. Lee, J.P. Grinias, Online monitoring of small volume reactions using compact liquid chromatography instrumentation, Sep. Sci. PLUS. 5 (2022) 213–219. https://doi.org/https://doi.org/10.1002/sscp.202200012.

[2] T. Hetzel, Characterization of micro liquid chromatography - theoretical performance limits and practical aspects for routine analysis on the example of cytotoxic drugs, 2017.

[3] G. Desmet, K. Broeckhoven, S. Deridder, D. Cabooter, Review of recent insights in the measurement and modelling of the B-term dispersion and related mass transfer properties in liquid chromatography, Anal. Chim. Acta. 1214 (2022) 339955. https://doi.org/https://doi.org/10.1016/j.aca.2022.339955.

[4] K. Vanderlinden, K. Broeckhoven, Y. Vanderheyden, G. Desmet, Effect of pre- and post-column band broadening on the performance of high-speed chromatography columns under isocratic and gradient conditions, J. Chromatogr. A. 1442 (2016) 73–82. https://doi.org/10.1016/j.chroma.2016.03.016.

[5] P.I. Napolitano-Tabares, I. Negrín-Santamaría, A. Gutiérrez-Serpa, V. Pino, Recent efforts to increase greenness in chromatography, Curr. Opin. Green Sustain. Chem. 32 (2021) 100536. https://doi.org/10.1016/j.cogsc.2021.100536.

[6] Y. Li, M. Dvořák, P.N. Nesterenko, R. Stanley, N. Nuchtavorn, L.K. Krčmová, J. Aufartová, M. Macka, Miniaturised medium pressure capillary liquid chromatography system with flexible open platform design using off-the-shelf microfluidic components, Anal. Chim. Acta. 896 (2015) 166–176. https://doi.org/https://doi.org/10.1016/j.aca.2015.09.015.

[7] M.C. May, D.C. Pavone, I.S. Lurie, The separation and identification of synthetic cathinones by portable low microflow liquid chromatography with dual capillary columns in series and dual wavelength ultraviolet detection, J. Sep. Sci. 43 (2020) 3756–3764. https://doi.org/10.1002/jssc.202000767.

[8] S.C. Lam, L.J. Coates, M. Hemida, V. Gupta, P.R. Haddad, M. Macka, B. Paull, Miniature and fully portable gradient capillary liquid chromatograph, Anal. Chim. Acta. 1101 (2020) 199–210. https://doi.org/https://doi.org/10.1016/j.aca.2019.12.014.

[9] F. Rahimi, S. Chatzimichail, A. Saifuddin, A.J. Surman, S.D. Taylor-Robinson, A. Salehi-Reyhani, A Review of Portable High-Performance Liquid Chromatography: the Future of the Field?, Springer Berlin Heidelberg, 2020. https://doi.org/10.1007/s10337-020-03944-6.

[10] J. Płotka-Wasylka, A new tool for the evaluation of the analytical procedure: Green Analytical Procedure Index, Talanta. 181 (2018) 204–209. https://doi.org/10.1016/j.talanta.2018.01.013.

[11] F. Pena-Pereira, W. Wojnowski, M. Tobiszewski, AGREE - Analytical GREEnness Metric Approach and Software, Anal. Chem. 92 (2020) 10076–10082. https://doi.org/10.1021/acs.analchem.0c01887.

[12] H. Chen, Y. Yang, Z. Qiao, P. Xiang, J. Ren, Y. Meng, K. Zhang, J. Juan Lu, S. Liu, A narrow open tubular column for high efficiency liquid chromatographic separation, Analyst. 143 (2018) 2008–2011. https://doi.org/10.1039/c7an02065a.

[13] P. Xiang, Y. Yang, Z. Zhao, M. Chen, S. Liu, Ultrafast gradient separation with narrow open tubular liquid chromatography, Anal. Chem. 91 (2019) 10738–10743. https://doi.org/10.1021/acs.analchem.9b02190.

[14] A. Ali, G. Sun, J.S. Kim, Y.S. Kim, H.J. An, W.J. Cheong, Preparation and Evaluation of 2 m Long Open Tubular Capillary Columns of 50 μm Internal Diameter for Separation of Peptides in Liquid Chromatography, Chromatographia. 84 (2021) 257–266. https://doi.org/10.1007/s10337-020-04003-w.

[15] V. Pepermans, M.T. Rerick, B. Degreef, S. Eeltink, S.G. Weber, G. Desmet, Column-in-valve designs to minimize extra-column volumes, J. Chromatogr. A. 1637 (2021) 461779. https://doi.org/https://doi.org/10.1016/j.chroma.2020.461779.

[16] M.G. Moleirinho, S. Feast, A.S. Moreira, R.J.S. Silva, P.M. Alves, M.J.T. Carrondo, T. Huber, C. Fee, C. Peixoto, 3D-printed ordered bed structures for chromatographic purification of enveloped and non-enveloped viral particles, Sep. Purif. Technol. 254 (2021) 117681. https://doi.org/10.1016/j.seppur.2020.117681.

[17] M. V. Novotny, Development of capillary liquid chromatography: A personal perspective, J. Chromatogr. A. 1523 (2017) 3–16. https://doi.org/10.1016/j.chroma.2017.06.042.

[18] M.Z. Chowdhury, M. Shahjalal, S. Ahmed, Y.M. Jang, 6G Wireless Communication Systems: Applications, Requirements, Technologies, Challenges, and Research Directions, IEEE Open J. Commun. Soc. 1 (2020) 957–975. https://doi.org/10.1109/OJCOMS.2020.3010270.

[19] J. Dalzochio, R. Kunst, E. Pignaton, A. Binotto, S. Sanyal, J. Favilla, J. Barbosa, Machine learning and reasoning for predictive maintenance in Industry 4.0: Current status and challenges, Comput. Ind. 123 (2020) 103298. https://doi.org/https://doi.org/10.1016/j.compind.2020.103298.

Appendix

List of Figures

List of Tables

List of Abbreviations

µLC	micro-liquid chromatographic
µPAC	micro pillar array columns
µTAS	miniaturized total analysis systems
ABS	acrylonitrile butadiene styrene
ACN	acetonitrile
ASA	acetylsalicylic acid
BAuA	The German Federal Institute for Occupational Safety and Health
BSA	bovine serum albumin
BVCZ	Bevacizumab (Avastin)
CA	cellulose-2,5-acetate
CAL	computed axial lithography
CAN	cerium (IV) ammonium nitrate
CFD	computational fluid dynamics
ChEC	electrochromatography
cLC	capillary liquid chromatography
DAD	diode array detectors
DMDOMA	N-((2,2-dimethyl-1,3-dioxolan-4-yl)methyl)acrylamide
ECBB	extra-column band broadening
ELSD	evaporative light scattering detector
ENCS	Existing Notified Chemical Substances
ESI	electrospray ionization
EtOAc	ethyl acetate
EtOH	ethanol
FLD	fluorescence detector
FS	fused silica
FWHM	full width at half maximum
GAC	Green Analytical Chemistry
GAPI	Green Analytical Procedure Index
HILIC	hydrophilic interaction liquid chromatography
HPLC	high performance liquid chromatography system
HPLC-EAT	HPLC Environmental Assessment Tool
HTLC	high temperature liquid chromatography
ID	inner diameter
IMS	ion mobility spectrometry

KPL	kinetic plot limits
LC	liquid chromatographic
LOC	Lab-on-Chip systems
MC	methylcellulose
MeOH	methanol
MEX	material extrusion process
MIP	molecular imprinted polymers
MS	mass spectrometry
MYO	myoglobin
NAP	N-acryloylpyrrolidine
nano-HPLC	nano-high performance liquid chromatography
nLC	nano-liquid chromatographic
OT	open tubular columns
PBS	phosphate buffered saline
PDMS	polydimethylsiloxane
PEEK	polyether ether ketone
PLA	polylactic acid
PLOT	porous layer open tubular column
REACH	Registration, Evaluation, authorisation and Restriction of Chemicals
SPE	solid phase extraction
STAMP	Separation Technology for A Million Peaks
SUVOS	semiconductor ultraviolet optical sources
TTF	Title Transfer Facility
UHPLC	ultra-high performance liquid chromatography
USP	United States Pharmacopoeia
WCOT	wall coated open tubular columns
ZDV	zero-dead volume

List of Publications

Articles in peer-reviewed journals

T. Werres, J. Leonhardt, M. Jäger, T. Teutenberg, Critical Comparison of Liquid Chromatography Coupled to Mass Spectrometry and Three Different Ion Mobility Spectrometry Systems on Their Separation Capability for Small Isomeric Compounds, Chromatographia. 82 **(2019)** 251–260. https://doi.org/10.1007/s10337-018-3640-z**.**

T. Werres, T.C. Schmidt, T. Teutenberg, The influence of injection volume on efficiency of microbore liquid chromatography columns for gradient and isocratic elution, J. Chromatogr. A. 1641 **(2021)** 461965. https://doi.org/10.1016/j.chroma.2021.461965.

C. Thoben, T. Werres, I. Henning, P.R. Simon, S. Zimmermann, T.C. Schmidt, T. Teutenberg, Towards a miniaturized on-site nano-high performance liquid chromatography electrospray ionization ion mobility spectrometer with online enrichment, Green Anal. Chem. 1 **(2022)** 100011. https://doi.org/10.1016/j.greeac.2022.100011.

T. Werres, T.C. Schmidt, T. Teutenberg, Peak broadening caused by using different micro–liquid chromatography detectors, Anal. Bioanal. Chem. 414 **(2022)** 6107–6114**.** https://doi.org/10.1007/s00216-022-04170-9.

T. Werres, T.C. Schmidt, T. Teutenberg, Influence of the Column Inner Diameter on Chromatographic Efficiency in Miniaturized and Conventional Ultra-High-Performance Liquid Chromatography. Chromatographia 86 **(2023)** 143–151. https://doi.org/10.1007/s10337-023-04237-4.

Oral Presentations

T. Werres, T.C. Schmidt, T. Teutenberg, When Mass Spectrometry Fails: The Separation of Small Isomeric Species by Liquid Chromatography and Ion Mobility. 23th - 27th September 2018, 32nd International Symposium on Chromatography, Cannes-Mandelieu, France

T. Werres, T.C. Schmidt, T. Teutenberg, Experimental Investigation of the Influence of the Injection Volume on the Efficiency of Miniaturized Separation Columns. 16th - 20th June 2019, 32nd International Symposium on Chromatography, Milan, Italy

C. Thoben, T. Werres, C.-R. Raddatz, M. Lippmann, M. Hitzemann, T. Teutenberg, S. Zimmermann, Portables nano-HPLC-ESI-IMS. 17th - 19th March 2021, 8. IMS Anwendertreffen, Potsdam, Germany (virtual due to corona pandemic)

T. Werres, C. Thoben, C.-R. Raddatz, I. Henning, T.C. Schmidt, S. Zimmermann, T. Teutenberg, Development of a Portable Measuring Device for the Detection of Pollutants in Water on the Basis of Nano-Liquid Chromatography and Ion Mobility Spectrometry. 13th - 15th April 2021, International Symposium The Chemical Monitoring Station of the Future, Koblenz, Germany (virtual due to corona pandemic)

T. Werres, C. Thoben, C.-R. Raddatz, I. Henning, T.C. Schmidt, S. Zimmermann, T. Teutenberg, Development of a Portable Measuring Device for the Detection of Pollutants in Water on the Basis of Nano-Liquid Chromatography and Ion Mobility Spectrometry. 12th - 15th July 2021, 37th International Symposium on Microscale Separations and Bioanalysis, Boston, USA (virtual due to corona pandemic)

T. Werres, T.C. Schmidt, T. Teutenberg, Peak Broadening Caused by Using Different Micro Liquid Chromatography Detectors. 18th – 22nd September 2022, 33rd International Symposium on Chromatography, Budapest, Hungary

Poster Presentations

T. Werres, T.C. Schmidt, T. Teutenberg, Untersuchungen zum Einfluss des Injektionsvolumens auf die Effizienz miniaturisierter Trennsäulen. 17th - 19th March 2019, ANAKON 2019, Münster, Germany

C. Thoben, T. Werres, C.-R. Raddatz, T. Teutenberg, S. Zimmermann, Nutzung von Ethanol als organische mobile Phase für die nano-HPLC-ESI-IMS. 15th - 17th March 2022, 9. IMS Anwendertreffen, Potsdam, Germany

T. Werres, I. Henning, P. Constantinidis, T.C. Schmidt, T. Teutenberg, Towards a 3D Printed Highly Customizable Lab-on-Chip-Platform. 18th - 22nd September 2022, 33rd International Symposium on Chromatography, Budapest, Hungary

Declaration of Scientific Contribution

This thesis includes work that was published in cooperation with co-authors. My own contributions are declared in the following:

Chapter 3

T. Werres, T.C. Schmidt, T. Teutenberg, The influence of injection volume on efficiency of microbore liquid chromatography columns for gradient and isocratic elution, J. Chromatogr. A. 1641 (2021) 461965. https://doi.org/10.1016/j.chroma.2021.461965.

CRediT authorship contribution statement

Tobias Werres: Conceptualization, Investigation, Visualization, Project administration, Writing - original draft. **Thorsten Teutenberg:** Funding acquisition, Supervision, Writing - review & editing. **Torsten C. Schmidt:** Supervision, Writing - review & editing.

Chapter 4

T. Werres, T.C. Schmidt, T. Teutenberg, Peak broadening caused by using different micro–liquid chromatography detectors, Anal. Bioanal. Chem. (2022) 6107–6114. https://doi.org/10.1007/s00216-022-04170-9.

CRediT authorship contribution statement

Tobias Werres: Conceptualization, Investigation, Visualization, Project administration, Writing - original draft. **Thorsten Teutenberg:** Funding acquisition, Supervision, Writing - review & editing. **Torsten C. Schmidt:** Supervision, Writing - review & editing.

Chapter 5

T. Werres, T.C. Schmidt, T. Teutenberg, Influence of the Column Inner Diameter on Chromatographic Efficiency in Miniaturized and Conventional Ultra-High-Performance Liquid Chromatography. Chromatographia 86 (2023) 143–151. https://doi.org/10.1007/s10337-023-04237-4.

CRediT authorship contribution statement

Tobias Werres: Conceptualization, Investigation, Visualization, Project administration, Writing - original draft. **Thorsten Teutenberg:** Funding acquisition, Supervision, Writing - review & editing. **Torsten C. Schmidt:** Supervision, Writing - review & editing.

Chapter 6

T. Werres, Hettrich, K., Polozij D., Klassen, M.D, Bohrisch, J, T.C. Schmidt, T. Teutenberg, Synthesis, characterization, and utilization of modified bead cellulose in miniaturized liquid chromatography for the analysis of small and large molecules, submitted.

Tobias Werres: Conceptualization, Investigation, Visualization, Project administration, Writing - original draft. **Kay Hettrich:** Investigation, Visualization, Writing - review & editing. **Denis Polozij:** Investigation. **Martin Klaßen:** Investigation, Writing - review & editing. **Jörg Bohrisch:** Supervision, Writing - review & editing. **Thorsten Teutenberg:** Funding acquisition, Supervision, Writing - review & editing. **Torsten C. Schmidt:** Supervision, Writing - review & editing.

Chapter 7

C. Thoben, T. Werres, I. Henning, P.R. Simon, S. Zimmermann, T.C. Schmidt, T. Teutenberg, Towards a miniaturized on-site nano-high performance liquid chromatography electrospray ionization ion mobility spectrometer with online enrichment, Green Anal. Chem. 1 (2022) 100011. https://doi.org/10.1016/j.greeac.2022.100011.

Christian Thoben: Conceptualization, Investigation, Visualization, Project administration, Writing - original draft. **Tobias Werres:** Conceptualization, Investigation, Visualization, Project administration, Writing - original draft. **Ireneus Henning:** Investigation, Visualization. **Paul R. Simon:** Investigation, Visualization. **Stefan Zimmermann:** Funding acquisition, Supervision, Writing - review & editing. **Torsten C. Schmidt:** Supervision, Writing - review & editing. **Thorsten Teutenberg:** Funding acquisition, Supervision, Writing - review & editing.

Curriculum Vitae

Der Lebenslauf ist in der Online-Version aus Gründen des Datenschutzes nicht enthalten.

The Curriculum Vitae is not included in the online version for data protection reasons.

Erklärung

Hiermit versichere ich, dass ich die vorliegende Arbeit mit dem Titel

„Characterization of extra-column peak broadening in capillary high-performance liquid chromatography"

selbst verfasst, keine außer den angegebenen Hilfsmitteln und Quellen benutzt habe, alle wörtlich oder inhaltlich übernommenen Stellen als solche gekennzeichnet sind und die Arbeit in dieser oder ähnlicher Form noch bei keiner anderen Universität eingereicht wurde.

Duisburg, im Oktober 2022

Tobias Werres